



UNIVERSITÀ DEGLI STUDI
DI MILANO

FACOLTÀ DI SCIENZE DEL FARMACO

Department of Pharmaceutical Science

DOCTORATE SCHOOL IN CHEMICAL SCIENCE AND
TECHNOLOGIES

Curriculum

Pharmaceutical Sciences (XXVII Cycle)

CHIM/08

***Antifouling agents: functionalization of surfaces
to obtain novel medical devices materials
inhibiting biofilm formation***

**Silvia Carolina Dell'Orto
R09607**

Tutor: Dr. Stefania VILLA

Coordinator: Prof. Ermanno VALOTI

Academic year 2013/2014

*"If we knew what it was we were doing,
it would not be called research, would it?"*

Albert Einstein

DECLARATION

The work described within this dissertation was carried out at the University of Milan, Department of Pharmaceutical Science, between November 2011 and October 2014 under the supervision of Dr Stefania Villa. This dissertation is the result of my own work unless otherwise stated.

This work was supported by Fondazione Cariplo, grant no. 2011-0277. The funders had no role in study design, data collection and analysis, decision to publish, or preparation of the manuscript.

Silvia Carolina Dell'Orto

January 2015



**UNIVERSITÀ
DEGLI STUDI
DI MILANO**

ACKNOWLEDGEMENTS

It is a great pleasure to look back on the past years and thank many people who made this thesis possible.

First and foremost, I would like to express my sincere gratitude to my supervisors Dr. Stefania Villa and Dr. Arianna Gelain for their valuable guidance, their continuous support, encouragement and for the opportunity they gave me to carry out research in their group. To work with you has been a real pleasure to me.

I've loved this project that allowed me to learn multidisciplinary skills and to build a fundamental basis of my knowledge.

I am also thankful to Professor Daniela Barlocco for the excellent example she provided me as a successful chemist and professor.

I'd like to thank Fondazione Cariplo for funding and I wish to express my gratitude to all the people who have collaborated in the ANFOMAT project and, in particular, to Dr. Cristina Cattò who shared with me the alternating fortunes during these wonderful years.

I am very grateful to Professor David Spring for giving me the opportunity to work for six months in his chemistry lab at University of Cambridge, where I found a stimulating and fun environment in which to learn and grow. I'd also thank those who have made working and living in Cambridge such an enjoyable experience, the Spring Group and in particular Dr. Claudia De Fusco, for all the excellent help and sound advices she gave me. I am also very thankful to the best FLATmates I could ask for, Angelica and Chiara, for the unforgettable moments we had together and for their friendship.

I would also thank past and present members of the VB lab for their help in the laboratory but also for being fun, happy and friendly people to be around and making my time here unforgettable. It was a real pleasure for me to teach you all how to move in a chemistry lab, to support you in hard times and see you growing up and becoming more and more independent. I am very proud of all of you.

A special thank goes out to my mentor and my friend Dr. Daniela Masciocchi for her patience and support and for believing in me more than I believe in myself. A big thank you also goes to Dr. Federica Porta for her help and for the good times that we had together. She has been an invaluable support, day in, day out, during all these years. I have been lost without them both.

Finally, I would like to thank my parents, Laura and Enrico, my family, my wonderful nephews, Francesco and Giorgia, my friends and Dario for their eternal love, encouragement and support. I hope I made you proud. To You I dedicated this thesis.

ABSTRACT

Vascular and urinary catheters are the most frequently used indwelling medical devices in the intensive care units and, in general, in medical wards. Despite drug/device combination products and antimicrobial therapies (including systemic antibiotic prophylaxis), device-related infections are difficult to eradicate and pose a severe threat to human health and excess of medical costs. The most important factor in the pathogenesis of catheter-related infections is the formation of an adherent functional heterogenic microbial consortium, embedded in a self-produced matrix of extracellular polymeric substance (EPS), called biofilm. Biofilm formation is an important cause of illness since the biofilm lifestyle is associated with the chronic nature of infections, the evasion to the host immune-response and the enhanced resistance to medical treatments. Indeed, after bacteria become established in a biofilm, the individual cells exhibit tolerance up to 1000 folds more than their planktonic counterparts and often do not respond to antimicrobial agents. Given the less innovation in the discovery and the development of novel antimicrobial compounds over the past 20 years and the alarming incidence of recalcitrant device-related infections, the need for an innovative anti-infective material is becoming imperative. Bio-inspired molecules able to disarm microorganisms without affecting their existence, offer an elegant way to interfere with specific key-steps that orchestrate biofilm formation sidestepping drug resistance and extending the efficacy of the current antimicrobial agents.

The general goal of this applied research project is to develop an innovative antibiotic-free functionalized material able to hold out against infections of vascular and urinary catheters by means of compounds with known anti-biofilm activities. Initially, it was necessary to prepare chemically modified anti-biofilm derivatives related to zosteric acid, a natural preventive compound against device-related infections, in order to improve their affinity and retention on a surface. The antifouling performance was tested against *Escherichia coli*, selected as the model system for bacterial infections. Furthermore, affinity purification experiments of proteins from *E. coli* extracts allowed the identification of targets directly interacting with these antibiofilm compounds. Then, the methodology for grafting the modified agents to materials was developed and optimized. The new materials efficacy and their ability to increase the susceptibility of microorganisms to traditional antibiotics were tested in biofilm reactors using chemical and molecular techniques combined with microscopic investigations.

CONTENTS

DECLARATION	ii
ACKNOWLEDGEMENTS	iii
ABSTRACT	iv
CONTENTS	v
ABBREVIATIONS	x
1. Introduction	1
1.1 Biofilm: a common cause of bacterial infections	2
1.1.1 Biofilm organization	2
1.1.2 The EPS matrix	3
1.1.3 Biofilm life cycle	6
1.1.4 Quorum sensing	8
1.2 Mechanisms of biofilm resistance	12
1.3 Biofilm inhibitors	17
1.3.1 Compounds that modulate biofilm by targeting bacterial signaling pathways	17
1.3.1.1 Acyl homoserine lactones (AHLs)	17
1.3.1.2 Autoinducing peptides (APIs)	19
1.3.1.3 Autoinducer-2 (AI-2)	20
1.3.1.4 c-di-GMP	21
1.3.1.5 Indole signaling	21
1.3.1.6 Two-component systems	23
1.3.1.7 Other signaling molecules	24
1.3.2 Chemical library screening	24
1.3.3 Natural products and their analogues	27
1.3.3.1 Plant extracts	27
1.3.3.2 Halogenated furanones	29
1.3.3.3 Marine natural products and analogues	30

1.3.3.4 Zosteric acid	32
1.3.3.5 Conclusions	34
2. Research project	35
3. Section A - Design, synthesis and biological evaluation of antibiofilm derivatives	38
3.1 Project description (A)	38
3.2 General chemistry	43
3.2.1 Synthesis of (<i>E, Z</i>) zosteric acid (1, 38)	43
3.2.2 Synthesis of substituted cinnamic acid derivatives (9-11, 14, 17, 46)	43
3.2.3 Synthesis of 3-hydroxy-4-aminocinnamic acid (24)	44
3.2.4 Synthesis of ethyl cinnamate (44) and <i>cis</i> cinnamic acid (39)	44
3.2.5 Synthesis of <i>trans</i> methyl coumarate (25), <i>trans</i> methyl 4-methoxycinnamate (27) and <i>cis</i> methyl coumarate (43)	45
3.2.6 Synthesis of <i>cis</i> methyl 4-methoxycinnamate (42)	45
3.2.7 Synthesis of <i>cis</i> 4-methoxycinnamic acid (41)	46
3.2.8 Synthesis of 4-acetamidosalicylic acid (48)	46
3.3 Biological studies	47
3.3.1 Planktonic growth and cellular adhesion in the presence of DMSO	48
3.3.2 Cellular growth with zosteric acid related compounds as the sole carbon and energy source	48
3.3.3 Planktonic growth in the presence of zosteric acid related compounds	48
3.3.4 Microplate-based cell adhesion assay in the presence of zosteric acid related compounds	50
3.3.5 Biological activity of zosteric acid derivatives	51
3.3.6 Anti-biofilm performance of zosteric acid derivatives	52
3.4 Proteomic studies	54
3.4.1 WrbA protein and supposed mechanism of action of cinnamic acid derivatives	56
3.5 Discussion	59
3.6 Final remarks	63

3.7 Experimental	65
3.7.1 Chemistry	65
3.7.1.1 Materials and methods	65
3.7.1.2 Experimental procedures	66
3.7.2 Biology	73
3.7.2.1 <i>Escherichia coli</i> strain and growth conditions	73
3.7.2.2 Planktonic growth in the presence of zosteric acid related compounds	73
3.7.2.3 Cellular growth with the zosteric acid related compounds as the sole carbon and energy source	73
3.7.2.4 Microplate-based biofilm assay in the presence of zosteric acid related compounds	74
3.7.2.5 Statistical analysis	74
4. Section B - Functionalization of a surface	75
4.1 Background	75
4.2 Project description (B)	77
4.3 Passive protection of surfaces	79
4.3.1 Materials and methods	80
4.3.2 Experimental procedure	80
4.3.3 Characterization	81
4.3.3.1 Reflection Absorption Infrared Spectroscopy (RAIR)	81
4.3.4 Biological evaluation: the colony-biofilm assay	83
4.4 Active protection of surfaces	87
4.4.1 The choice of material	88
4.4.2 Pre-treatment of surfaces	90
4.4.3 Graft-polymerization process	92
4.4.4 Experimental	92
4.4.4.1 Materials and methods	92
4.4.4.2 Cleaning of PE coupons	93
4.4.4.3 Activation of PE	93
4.4.4.4 The grafting procedure: LDPE-HEMA-OH surface	94
4.4.4.5 Preparation of the LDPE-HEMA-COOH surface	94

4.4.4.6 General procedure to graft molecules to the LDPE-HEMA-COOH surface <i>via</i> amide bond formation	95
4.4.5 Characterization	95
4.4.5.1 Contact angle measurements	95
4.4.5.2 Scanning Electron Microscope (SEM) analysis	99
4.4.5.3 X-ray Photoelectron Spectroscopy (XPS) analysis	100
4.4.5.4 Attenuated Total Reflectance Infrared Spectroscopy (ATR-FTIR) analysis	103
4.4.5.5 Fluorescence Spectroscopy analysis	105
4.4.5 Biological evaluation	110
4.4.6 Antibiotic susceptibility test	113
4.5 Final remarks	116
5. Experience abroad	117
5.1 Introduction	117
5.2 Project Description (C)	119
5.3 Docking studies	120
5.4 General chemistry	124
5.4.1 Synthesis of benzyl macrocycle	125
5.4.2 Synthesis of indole macrocycle	127
5.4.3 Synthesis of the coumaric acid macrocycle	128
5.4.4 Synthesis of the urea macrocycle	129
5.4.5 Synthesis of the tetrazolone macrocycle	131
5.5 Experimental Session	132
5.5.1 Materials and methods	132
5.5.2 General procedures	133
5.5.2.1 GP1 – Amide formation	133
5.5.2.2 GP2 – CuAAC macrocyclization	133
5.5.2.3 GP3 – Metathesis macrocyclization	133
5.5.2.4 GP4 – Hydrolysis	134
5.5.2.4 GP5 – Coupling with dipeptide	134

5.5.3 Synthesis of benzyl derivatives (B1-9)	135
5.5.4 Synthesis of indole derivatives (I1-7)	140
5.5.5 Synthesis of <i>m</i> -coumaric acid derivatives (CA1-3)	145
5.5.6 Synthesis of tetrazolone derivatives (T1-3)	148
5.6 Final remarks	150
6. Appendix	151
7. References	166

ABBREVIATIONS

AHL	Acyl homoserine lactone
AI-2	Autoinducer-2
AIP	Autoinducing peptide
ANOVA	Analysis of variance
AP	Anti-biofilm performance
ATP	Adenosine triphosphate
ATR-IR	Attenuated total reflection infrared spectroscopy
Boc	<i>Tert</i> -Butoxycarbonyl
CA	Cinnamic acid
CADD	Computer-aided drug design
CDC	Center for Disease Control
c-di-GMP	Bis-(3'5')-cyclic di-guanylic acid
cDOS	Constrained Diversity Oriented Synthesis
CLSM	Confocal Laser Scanning Microscope
Cmp(s)	Compound(s)
COSY	Correlation spectroscopy
DCM	Dichloromethane
DGC	Diguanylate cyclase
DIPEA	<i>N,N</i> -diisopropylethylamine
DMF	Dimethylformamide
DMSO	Dimethyl sulfoxide
DNA	Deoxyribonucleic acid
DOS	Diversity Oriented Synthesis
DPD	(S)-4,5-dihydroxy-2,3-pentanedione
eDNA	Extracellular DNA
EHEC	Enterohemorrhagic <i>E. coli</i>
EPS	Extracellular polymeric substances
ESI	Electron spray ionisation
Et	Ethyl
FMN	Flavin mononucleotide
Fmoc	9-Fluorenylmethoxycarbonyl
FP	Fluorescence polarisation
GA	Glutaraldehyde
h	hour(s)
HAIs	Healthcare-associated infections

HATU	2-(1H-7-Azabenzotriazol-1-yl)-1,1,3,3-tetramethyl uranium hexafluorophosphate
HDPE	High-density polyethylene
HEMA	Hydroxyethyl methacrylate
HF	Halogenated furanone
HMBC	Heteronuclear multiple bond correlation
HMQC	Heteronuclear multiple quantum correlation
HPLC	High-performance liquid chromatography
HRMS	High resolution mass spectrometry
HTS	High throughput screening
Hz	Hertz
IC ₅₀	Half maximal inhibitory concentration
J	Coupling constant
K _a	Acid dissociation constant
LB	Luria-Bertani
LCMS	Liquid chromatography mass spectrometry
LDPE	Low-density polyethylene
LDPE-CA	LDPE grafted with <i>p</i> -aminocinnamic acid
LDPE-HEMA-COOH	Polyethylene grafted with hydroxyethyl methacrylate (hydroxyl groups converted into the corresponding carboxylic acids)
LDPE-HEMA-OH	Polyethylene grafted with hydroxyethyl methacrylate
LDPE-SA	LDPE grafted with <i>p</i> -aminosalicylic acid
LLDPE	Linear low-density polyethylene
log P	Partition-coefficient
m.p.	Melting point
mw	Microwaves
<i>m/z</i>	Mass-to-charge ratio
MDR	Multidrug resistance
MDT	Multidrug tolerance
Me	Methyl
MIC	Minimum inhibitory concentration
min	minute(s)
mol	Mole(s)
NMM	<i>N</i> -methylnmorpholine
NMR	Nuclear magnetic resonance
NQO	NADH:quinone oxidoreductase
OD	Optical density
OD ₆₀₀	Optical density at 600 nm

<i>p</i>	Para position
Pa	Pascal
PAS	<i>p</i> -aminosalicylic acid
PBD	Polo-box domain
PBD	Polo-box domain
PBS	Phosphate-buffered saline
PC	Polycarbonate
Pd	Palladium
PDB	Protein data bank
PDE	Phosphodiesterase
PE	Polyethylene
PEG	Polyethylene glycol
PEI	Polyethylenimine
Ph	Phenyl
Plk	Polo-like kinase
PLL-g-PEG	poly(L-lysine)-graft-poly(ethylene glycol) polymer
PPI	Protein-protein interactions
PPIase	Periplasmic <i>cis-trans</i> prolyl isomerases
ppm	Parts per million
pThr	Phospho-threonine
PVC	Polyvinyl chloride
Py	Pyridine
QAC	Quaternary ammonium compounds
QS	Quorum sensing
RAFT	Reversible addition–fragmentation chain transfer
RAIR	Reflection Absorption Infrared Spectroscopy
R _f	Retention factor
RpoS	Sigma factor sigma-38
rt	Room temperature
s	second(s)
SA	Salicylic acid
SAM	S-Adenosyl methionine
sccm	Standard cubic centimeters per minute
SEM	Scanning electron microscopy
Ser	Serine
SM	Starting material
SpT	Serine-phosphothreonine

TBT	Tributyltin
TFA	Trifluoroacetic acid
THF	Tetrahydrofurane
Thr	Threonine
Thr	Threonine
TIPS	Triisopropylsilane
TLC	Thin layer chromatography
TMS	Tetramethylsilane
tr	Retention time
TrpR	Tryptophan repressor
UV	Ultraviolet
v/v	volume/volume
w/v	Weight per unit volume (weight-to-volume ratio)
WrbA	Tryptophan [W] repressor-binding protein
XPS	X-ray photoelectron spectroscopy
ZA	Zosteric acid

1. INTRODUCTION

Despite the availability of drug-device combination products and antimicrobial therapies, device-related infections are difficult to eradicate leading high risks to human health and excess of medical costs. Regularly, traditional therapies fail without removal of the implanted device. One of the most important factor in the pathogenesis of catheter-related infections is the formation of biofilms, complex structured communities of microorganisms associated with surfaces and embedded in self-produced extracellular polymeric substances.[1] The resistance of biofilms to medical treatments is not caused by a single mechanism but by several factors acting together like diffusion limitation and non-genetic phenotypic heterogeneity.[2, 3] Biofilms are increasingly recognized as being significant in human diseases (accounting for 80% of bacterial infections in the body) which include but are not limited to: lung infections of cystic fibrosis patients, colitis, urethritis, conjunctivitis, otitis, bacterial endocarditis and periodontitis, chronic wound infections and tooth decay.[4] Given the less innovation in the field of antimicrobial discovery research and development over the past 20 years and the alarming incidence of recalcitrant device-related infections, the need for an innovative anti-infective material is becoming essential.[5] A new trend is to develop antibiofilm strategies acting by mechanisms more subtle than the simple killing activities such as those influencing the multicellular behavior, by manipulating the expression of specific phenotype that represent microbial virulence traits (e.g. binding ability, motility, cell-to-cell communication, yeast-hyphae-dimorphism). This goal can be achieved using sub-lethal concentrations of antibiofilm agents with a novel targets, unique modes of action and properties that are different from those of the currently used antimicrobials.[6] The introduction on the material surface of bio-inspired molecules, as well as pharmaceutical compounds endowed with bacteriostatic or fungistatic activity, is a promising way to interfere with specific key-steps that orchestrate biofilm formation, sidestepping drug resistance and extending the efficacy of the antimicrobials.[7] The future of treatment strategies for biofilm infections seems to rest with specifically targeting unique biofilm characteristics, either in combination with conventional antibiotic therapy and to target biofilm infections when they are most susceptible to antibiotics.

1.1 Biofilm: a common cause of bacterial infections

Biofilm plays a key role in healthcare-associated infections (HAIs), especially those related to the implant of medical devices, such as vascular and urinary catheters and orthopedic implants. Bacterial

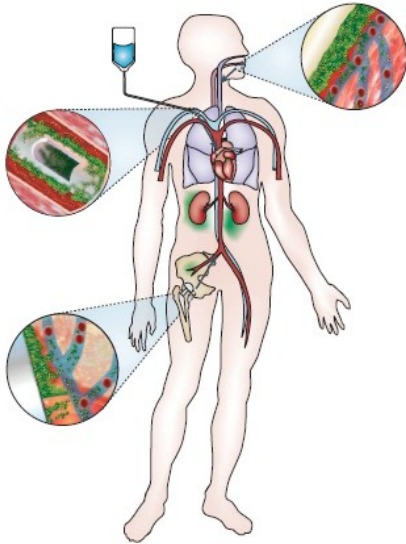


Figure 1. Three examples of possible points of entry into the body for infectious biofilms.[2]

biofilms have become recognized as a serious threat to both the medical and industrial sectors of society within the past 20 years.[8] As reported by the European Center for Disease Prevention and Control, every year approximately 4.1 million people in the EU Countries contract an infectious disease in European hospitals. The number of deaths, occurring as a direct consequence of these infections, is estimated to be at least 40000. Only in the United State, nosocomial infections account for 1.7 million infections and 99000 associated deaths each year.[9] Vascular and urinary catheters are the most frequently used indwelling medical devices in the intensive care units and in general in medical wards (Figure 1). Their wide use is associated

with an increasing risk of infectious complications that prolong hospital stay and healthcare cost. Not surprisingly, catheter-related infections are the most common cause of nosocomial infections and the duration of catheterization as well as the anatomical location are among the major risk factors.

1.1.1 Biofilm organization

Bacteria are able to switch between two different “life-styles”: single cells (planktonic mode) and biofilms (sessile mode). A biofilm is defined as a microbial community characterized by adhesion to a solid surface and by production of a matrix, which surrounds the bacterial cells and includes extracellular polymeric substances (EPS), proteins and DNA.[1] Transition from planktonic cells to biofilm is regulated by a variety of environmental and physiological cues, such as bacterial cell density, nutrient availability and cellular stress.[10] The most detrimental property of biofilms is the expression of specific features that make sessile microorganisms less susceptible to antimicrobial agents in comparison to their planktonic counterparts. Indeed, it was established that the proteome of adhered cells essentially differs from that of their planktonic forms as well as their physiology and morphology.

Within biofilm, each bacterium occupies a specific microenvironment determined by surrounding cells and closely related to the EPS matrix and channels which are responsible for pH and for the availability of nutrients and oxygen.[11] The microcolony is actually the basic structural unit of the biofilm. Depending on the species involved, it is composed of 10-25 % cells and 75-90 % EPS matrix, and often appears to be most dense in the area closest to its core. Bacterial cells within the matrix are characterized by the lack of Brownian movements and a structural analysis of many microcolonies reveals a mushroom-like shape. Although biofilms are commonly referred to as “slime”, which implies that they are not rigid structures, their mechanical stability is mainly due to the exopolysaccharides in the matrix. In addition, the cells within biofilms secrete signal molecules that regulate the expression of a panel of genes, allowing microorganisms to adapt to modified environmental conditions.

The biofilm structure and water channels, that act as a primitive circulatory system for the delivery of nutrients and the removal of metabolic waste products, turned out to be influenced by fluid flow and by intercellular small messenger molecules, or quorumones (acylated homoserine lactones, AHLs), that are used for bacterial communication (for detail see ‘Paragraph 1.1.4’). This system of nutrients and metabolic end products distribution have been observed only in peripheric regions of biofilms, since the cells within biofilms are more tightly packed. Differences in nutrients and oxygen availability within the biofilm structure affect the metabolic activity among the cells.

In general, biofilms also display viscoelastic properties. They undergo both reversible elastic responses and irreversible deformation, strongly depending on the forces acting on the EPS matrix. Elastic materials absorb stress energy through deformation and transient stress events might be resisted by reversible deformation. The result is a rearrangement of the biofilm to mitigate exposure to external shear stress. It is possible that, on an intermediate timescale, a biofilm can increase the strength of its structural matrix in response to mechanical stresses by increasing EPS production. The interaction of multivalent inorganic ions with EPS can greatly influence the mechanical properties of biofilms.

1.1.2 EPS matrix

Matrix is the extracellular material, mostly produced by the organisms themselves, in which the biofilm cells are embedded. It consists of a conglomeration of different types of biopolymers, known as extracellular polymeric substances (EPS), that form the scaffold for the three-dimensional architecture

of the biofilm and are responsible for adhesion to surfaces and for cohesion. Several functions of EPS have been determined (Table 1), proving many advantages for the biofilm mode of life.[12]

Function	Relevance for biofilms	EPS component involved
Adhesion	Allows the initial steps in the colonization of abiotic and biotic surfaces by planktonic cells, and the long-term attachment of whole biofilms to surfaces	Polysaccharides, proteins, DNA and amphiphilic molecules
Aggregation of bacterial cells	Enables bridging between cells, the temporary immobilization of bacterial populations, the development of high cell densities and cell-cell recognition	Polysaccharides, proteins and DNA
Cohesion of biofilms	Forms a hydrated polymer network (the biofilm matrix), mediating the mechanical stability of biofilms (often in conjunction with multivalent cations) and, through the EPS structure (capsule, slime or sheath), determining biofilm architecture, as well as allowing cell-cell communication	Neutral and charged polysaccharides, proteins (such as amyloids and lectins), and DNA
Retention of water	Maintains a highly hydrated microenvironment around biofilm organisms, leading to their tolerance of desiccation in water-deficient environments	Hydrophilic polysaccharides and, possibly, proteins
Protective barrier	Confers resistance to nonspecific and specific host defences during infection, and confers tolerance to various antimicrobial agents	Polysaccharides and proteins
Sorption of organic compounds	Allows the accumulation of nutrients from the environment and the sorption of xenobiotics (thus contributing to environmental detoxification)	Charged or hydrophobic polysaccharides and proteins
Sorption of inorganic ions	Promotes polysaccharide gel formation, ion exchange, mineral formation and the accumulation of toxic metal ions (thus contributing to environmental detoxification)	Charged polysaccharides and proteins, including inorganic substituents such as phosphate and sulphate
Enzymatic activity	Enables the digestion of exogenous macromolecules for nutrient acquisition and the degradation of structural EPS, allowing the release of cells from biofilms	Proteins
Nutrient source	Provides a source of carbon-, nitrogen- and phosphorus-containing compounds for utilization by the biofilm community	Potentially all EPS components
Exchange of genetic information	Facilitates horizontal gene transfer between biofilm cells	DNA
Electron donor or acceptor	Permits redox activity in the biofilm matrix	Proteins (for example, those forming pili and nanowires) and, possibly, humic substances
Export of cell components	Releases cellular material as a result of metabolic turnover	Membrane vesicles containing nucleic acids, enzymes, lipopolysaccharides and phospholipids
Sink for excess energy	Stores excess carbon under unbalanced carbon to nitrogen ratios	Polysaccharides
Binding of enzymes	Results in the accumulation, retention and stabilization of enzymes through their interaction with polysaccharides	Polysaccharides and enzymes

Table 1. Functions of extracellular polymeric substances (EPS) in bacterial biofilms.[12]

EPS have been called ‘the dark matter of biofilms’ because of the large range of matrix biopolymers and the difficulty in analyzing them.[13] They can vary greatly between biofilms, depending on the microorganisms present, the shear forces experienced, the temperature and the availability of nutrients. EPS were initially denoted “extracellular polysaccharides” but then were renamed, as it became clear that the matrix also contains proteins, nucleic acids, lipids and other biopolymers such as humic substances (Figure 2).

Polysaccharides are the major fraction of the EPS matrix. Most are long molecules, linear or branched, with a molecular mass of 0.5×10^6 Daltons to 2×10^6 Daltons.[1] Two different kinds of polysaccharides have been found: the homopolysaccharides, including the sucrose-derived glucans,

fructans and cellulose, and the heteropolysaccharides, a mixture of neutral and charged sugar residues. They can contain organic or inorganic substituents that greatly affect their physical and biological properties. Due to the presence of uronic acids, many known exopolysaccharides (including alginate, xanthan and colonic acid) are polyanionic, while intracellular adhesin is one of the polycationic exopolysaccharides. The biofilm matrix also contains a large amount of proteins. Several extracellular enzymes have been detected, many of which are involved in the degradation of biopolymers. The substrates of these extracellular enzymes include water-soluble polymers (i.e. many polysaccharides, proteins and nucleic acids), water-insoluble compounds (i.e. cellulose, chitin and lipids) and organic particles that are trapped in biofilms. Moreover, enzymes that are able to degrade EPS components makes the matrix

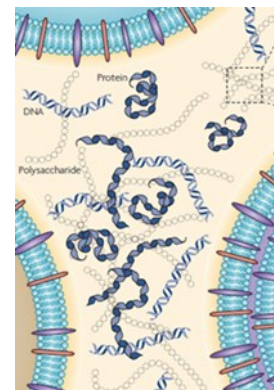


Figure 2. The extracellular polymeric substances (EPS) matrix.

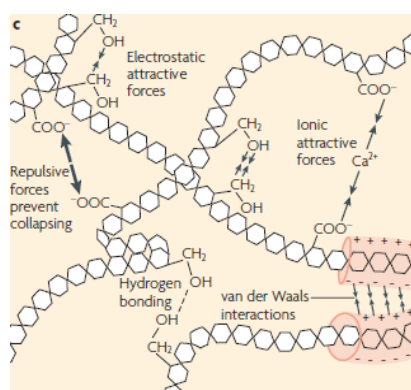


Figure 3. Classes of weak physicochemical interactions presented in the EPS matrix.

an external digestive system breaking down biopolymers to low-molecular-mass products that can be taken up and utilized as carbon and energy sources and can be involved in the degradation of structural EPS to promote the detachment of bacteria from biofilms. Other enzymes act as virulence factors in medical biofilms during infectious processes. Extracellular enzymes can be efficiently retained in the biofilm matrix by their interactions with polysaccharides. This arrangement retains the enzymatic activity close to the cell and keeps the diffusion distances of enzymatic products short, thereby optimizing their uptake by bacteria. Moreover, the interactions between enzymes and structural

exopolysaccharides enhance the thermostability of the enzymes and their resistance to proteolysis. The non-enzymatic proteins in the matrix, such as the cell surface-associated and extracellular carbohydrate-binding proteins (called lectins), are involved in the formation and stabilization of the polysaccharide matrix network and constitute a linker between the bacterial surface and extracellular EPS.

In general, EPS components are kept together by weak physicochemical interactions such as hydrogen bonds, van der Waals forces and electrostatic interactions (Figure 3).

Biofilms are also an ideal place for exchanging genetic material. Indeed, horizontal gene transfer is promoted, since the cells are maintained in close proximity to each other and can exchange genetic

information. Recently, different types of biofilm contain extracellular DNA (eDNA), whose localization can widely varied, have been found. Although eDNA was initially considered as residual material from lysed cells, it is actually an integral part of the matrix and of the biofilm mode of life.[1] Extracellular polysaccharides, proteins and DNA are highly hydrated hydrophilic molecules, but EPS can also possess hydrophobic properties, mainly due to the presence of lipids and polysaccharides-linked methyl and acetyl groups.[14]

1.1.3 Biofilm life cycle

Biofilm formation occurs as a result of a sequence of events (Figure 4).

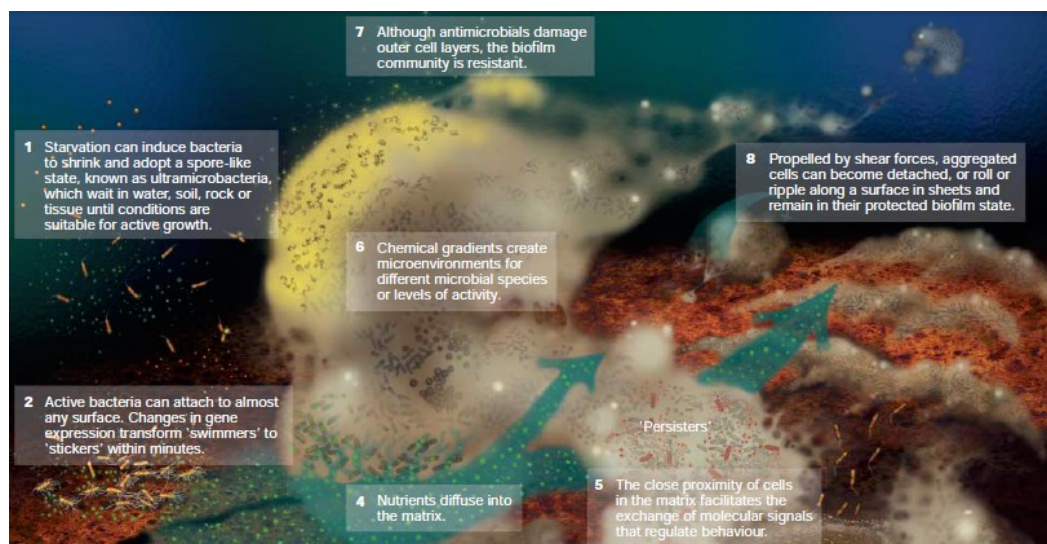


Figure 4. Conceptualization of biofilm development and dynamic behaviors. The figure was compiled from laboratory and natural observations of pure culture (both Gram-positive and Gram-negative organisms), and mixed-culture biofilms (P. Dirckx, Center for Biofilm Engineering, USA).

The formation of microbial biofilms begins with the reversible adhesion of a small number of cells to a surface. During this first stage, both organic and inorganic molecules in the bulk flow are carried toward the surface either by diffusion or turbulent flow. The adsorption of organic molecules on the surface plays a crucial role in bacterial attachment, as it may alter the physical-chemical properties of the surface. Affecting factors can include surface free energy, hydrophobicity and electrostatic charges. [15] The planktonic bacterial cells release both protons and signaling molecules as they move through the bulk fluid. If bacteria are not adjacent to any surface, these protons and molecules diffuse radially away from the floating cells. When bacterial cells found themselves next to a surface, the concentration

of both protons and signaling molecules become higher since diffusion is limited on that side. In this way bacteria can sense their proximity to a surface and elaborate species-specific behavior pattern, leading to the initial stage of adhesion and biofilm formation. Mechanisms by which bacteria are transported to a surface can include Brownian motion, sedimentation due to differences in specific gravity between the bacteria and the bulk liquid, or convective mass transport, by which cells are physically transported towards the surface by the movement of the bulk fluid.[16] In turbulent flow, the presence of multiple small turbulent eddies may drive small particles, including bacterial cells towards surfaces which may in turn override the Gibbs energy barrier required by bacteria to come into contact with a surface. The Gibbs energy barrier is the sum of the van der Waals interactions, commonly attractive and electrostatic interactions, usually negative, due to both bacteria and substratum surfaces negatively charged. Moreover, active transport, mediated by bacterial flagella activity and chemotaxis, has been considered an important mechanism enabling bacteria to interact with a surface. The presence of cell appendages such as flagella, pili, and fimbriae enhances the successful adhesion of bacteria to a surface, overcoming repulsive electrostatic forces that may exist between the cell surface and the surface of material. [17,18]

On an abiotic surface, initial attachment is governed by nonspecific interactions such as electrostatic, hydrophobic, or van der Waals forces. During this initial stage bacteria can be easily removed by fluid shear forces such as rinsing. After binding to the surface, bacterial cells begin the process of irreversible adhesion, proliferation, and accumulation as multilayered cell clusters. Then attached cells synthesize new EPS material to strengthen their adhesion to the surface and to other cells. In the transition from reversible to irreversible attachment, various short range forces are involved, including covalent and hydrogen bonding as well as hydrophobic interactions. At the end of this stage much stronger physical or chemical forces are required to remove bacteria from the surface such as scraping, scrubbing or chemical cleaners.[19] The subsequent stage is characterized by active binary division of attached cells and cell recruitment. This cell accumulation requires coordinated efforts from the microbial community to produce a well-organized structure. Once having irreversibly attached to a substratum, bacterial cells undergo phenotypic changes. Mature biofilms typically consist of differentiated mushroom-like structures of cells embedded within extracellular polymer matrix, which contains voids open to the bulk fluid to allow the transport of nutrients and oxygen from the interface to the inner parts of the biofilm and to remove metabolic wastes.

Biofilm dispersal is a naturally occurring process which may represent a mechanism to escape starvation or other negative environmental conditions within a biofilm, allowing bacterial cells the opportunity to migrate to a more favorable environment. Indeed, as biofilms grow in size, cells that reside in the inner layers of the biofilm do not have access to nutrients and suffer from accumulation of toxic waste products making their microenvironment unfavorable. In response to the adverse conditions, bacterial cells are able to detach from the biofilm getting back to the planktonic state and start a new biofilm formation cycle. In most cases, dispersal is induced by the biofilm itself due to environmental cues, such as changes in nutrient availability, fluctuation in local oxygen concentrations or increase in nitric oxide.[20] Although the exact mechanism of dispersal has not been fully elucidated, several studies highlighted that it involves the synthesis of degradative enzymes with specificity for biofilm matrix components [21], the return of motility [22], the surfactant production [23] and the cell lysis [24].

1.1.4 Quorum Sensing

Quorum sensing (QS) is a complex regulatory process based on bacterial cell density. This communication process among cells plays a pivotal role in modulating not only the expression of genes associated with the production of specific enzymes, virulence factors and metabolites but also the development of microbial communities as biofilms.[25] Indeed, QS is a regulatory mechanism that allows sessile microorganisms to respond to the needs that are related to the increasing population density through the expression of specific sets of genes, adapting to modified environment conditions such as a low availability of nutrients. During QS, bacteria communicate with each other by small diffusible signal molecules called autoinducers that are produced and secreted by bacterial cell. Although regulation by QS is highly conserved, its molecular mechanisms, as well as the chemical nature of the autoinducers and receptors, differ significantly between Gram-positive and Gram-negative bacteria.[9] The most common classes of signal molecules in Gram-negative bacteria are N-acyl homoserine lactones (AHLs) and quorum sensing mediated by AHLs represents one of the best-understood bacterial systems at the molecular level. To date, the majority of natural AHLs reported in literature share conserved structural characteristics: a homoserine lactone ring unsubstituted at the β - and γ -positions which is N-acylated at the α -position with a group derived from fatty acid biosynthesis (a fatty acyl group).[26] AHLs are able to freely diffuse in and out of bacterial cells, allowing the total

AHLs concentration to correlate to the total bacterial concentration, thus enabling population density-based control of gene expression. This cascade of events ultimately leads to the control of gene expression resulting in virulence factor production and biofilm formation and maintenance. The first AHL-based quorum sensing system was discovered in the bioluminescent marine bacterium *Vibrio fischeri*, which was observed to produce light only at high cellular densities. The quorum sensing circuit outlined in Figure 5 represents the basic paradigm for AHL-mediated signaling. AHL autoinducers are synthesized by enzymes of the LuxI family and can bind transcription regulators of the LuxR family. AHL binding to LuxR activates the transcription of QS-dependent genes.[27]

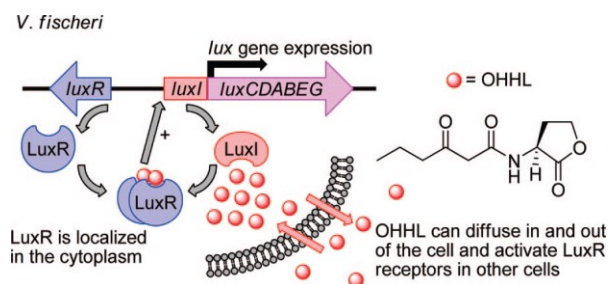


Figure 5. Schematic of LuxI/LuxR quorum sensing system in *V. fischeri*. [27]

In each bacterial cell, the enzyme LuxI (belonging to the family of signal generators) catalyzes the production of a small signaling molecule, the N-(3-oxohexanoyl)-HSL (“OHHL”), a derivative of AHL which freely diffuses within the population. Although the level of OHHL produced by a single cell is low, at high population density the signaling molecule accumulates, passes across cell membranes and binds to the transcription regulator LuxR. High cell densities are required to achieve an intracellular ligand concentration sufficient for LuxR binding. Without the OHHL ligand, the LuxR protein is unstable and rapidly degrades. Once activated, LuxR* stimulates transcription of luxICDAB cluster, leading to rapid amplification of the OHHL signal and emission of light. The complex LuxR*-OHHL further increases the expression of LuxI itself, leading to an autoinduction of the signaling molecule, which is therefore considered an autoinducer. Although, the luxI gene is not present in *Escherichia coli*, N-acyl-L-homoserine lactone must be synthesized by other microorganisms.[28, 29]

The quorum sensing signaling process that occurs in some Gram-negative bacteria is often more complex. Several bacterial species have been shown to use intricate network-type architectures for cell-cell signaling, involving two or more AHL signals, and even other types of quorum sensing pathways. For instance, *Pseudomonas aeruginosa* uses at least three types of QS signaling systems, two of these

are AHL-based.[29] There are two AHL derivatives, *N*-(3-oxododecanoyl)-L-homoserine lactone (OdDHL) and *N*-butanoyl- L-homoserine lactone (BHL) which are obtained by two separate signaling systems, each involving a LuxI-type synthase and a LuxR-type receptor. OdDHL is generated by LasI, while BHL synthesized by the synthase RhlI and detected by the RhlR protein. These AHL-dependent signaling systems are integrated with a third system that employs a chemically distinct signal molecule, 2-heptyl-3-hydroxy-4(1*H*)-quinolone (termed the *Pseudomonas* quinolone signal or PQS).

Quorum-sensing is frequently found in pathogens because it is a powerful global regulatory mechanism which allows the concomitant modulation of the expression of several genes in accordance with cell density. The simultaneous regulation (activation or repression, or both) of multiple genes acts as a biological switch that produces phenotypic modifications within the population.

In contrast to Gram-negative bacteria, Gram-positive signal molecules belong to the class of oligopeptides (short peptides of 5-50 amino acids) synthesized by ribosomes and often subjected to extensive post-translational modifications. In Gram-positive bacteria quorum sensing system the signal does not diffuse into the bacterial cell to reach cytoplasmic receptors, but binds to a two-component membrane system.[30] Binding of signaling peptides to sensor proteins in the cell membrane triggers a signal transduction cascade, which leads to phosphorylation of a response regulator and QS-dependent gene expression. A model of QS systems in Gram-positive bacteria is the *agr* (accessory gene regulation) system of *S. aureus*, where autoinducer-dependent phosphorylation of the AgrA regulator leads to transcription activation of genes encoding virulence factors (Figure 6).[31]

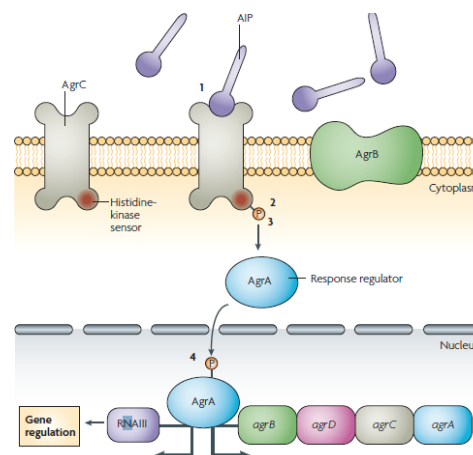


Figure 6. Quorum sensing and two-component signaling in the staphylococcal *agr* system.[32] *S. aureus* produces an autoinducing peptide (AIP) that accumulates extracellularly and activates the T-cell receptors (TCRS). The TCRS involves signal recognition by a histidine kinase (AgrC) (1), followed by histidine phosphorylation (2) and phosphotransfer to a response regulator (AgrA) (3), which then binds to the RNAIII transcript that encodes a small RNA that functions to modulate gene expression of *S. aureus* genes (4).

The quorum-sensing *agr* system consists of a two component trans-membrane transduction complex (AgrA and AgrC), a signaling peptide (AgrD) and a membrane component (AgrB), responsible for the externalization of the post-translationally modified signaling peptide. The effector molecule is a regulatory RNA, called RNAIII, whose synthesis is dependent on *agr* activation and driven by the P3 promoter. Many virulence factors of *S. aureus* are controlled by *agr*, which is thus considered a regulator of virulence. Also colonizing factors such as adhesins are regulated differently by *agr*. At the beginning of infection, when the level of signaling molecules is low, the expression of colonization factors is favored and staphylococci can establish in host tissues. When then the infection progresses, the activity of *agr* is higher and the expression of aggressive virulence factors is up-regulated in order to defeat host defenses, and allow bacteria to acquire nutrients from the impaired host tissues.[32]

In many bacterial species, QS has been shown to play a crucial role in biofilm survival and for this reason QS inhibitors and antagonists represent one of the most promising therapeutic tools for the treatment of biofilm-based infections (for detail see ‘Paragraph 1.3.1’). The different chemical nature of signal molecules and of the molecular mechanisms involved in QS would suggest that QS inhibitors can only be directed against either Gram-positive or Gram-negative bacteria.

As mentioned before, AHLs and peptides represent the two major classes of known bacterial signaling quorum sensing molecules, used by Gram-negative and Gram-positive bacteria, respectively, for intraspecies communication. Recently, a family of molecules generically termed autoinducer-2 (AI-2) has been found.[33] AI-2-based quorum sensing was first identified in the early 1990s in the Gram-negative bacterium *V. harveyi*. It was observed that an AHL-deficient strain of the bacterium remained capable of producing bioluminescence even in the absence of the natural AHL autoinducer 3-hydroxy-C4-HSL. This suggested that a second quorum sensing pathway, employing a different signaling molecule, was operating. This novel autoinducer was termed AI-2. It is produced and recognized by many Gram-negative and Gram-positive bacteria and may represent a potential tool by which different bacterial species can communicate with each other, as opposite to the intraspecies communication typically mediated by the other autoinducers discovered.[27] The gene responsible for its production is *luxS* since the enzyme LuxS is responsible for AI-2 biosynthesis. LuxS is a metalloenzyme containing a divalent metal in the active site: the type of metal cation present is presumed to vary during the course of the reaction. The substrate for the LuxS enzyme is *S*-ribosyl-L-homocysteine (SRH), which is derived from *S*-Adenosyl methionine (SAM) (Figure 7).

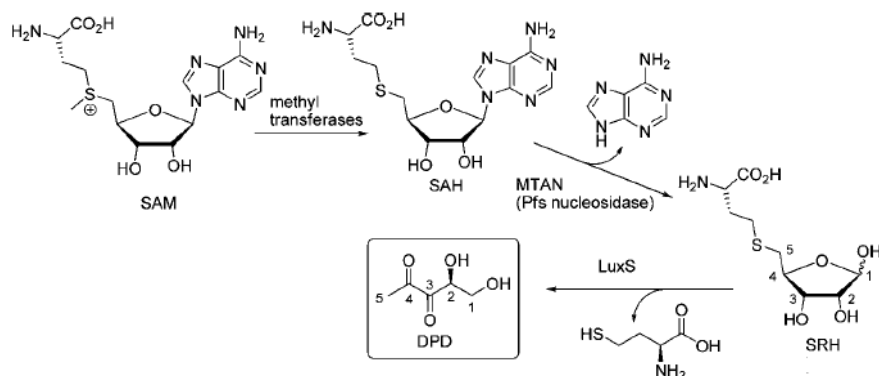


Figure 7. Enzymatic synthesis of DPD.

SAM is converted to SAH via the action of SAM dependent methyl transferases. This latter is hydrolyzed to SRH by the 5'-methylthioadenosine/*S*-adenosylhomocysteine nucleosidase (MTAN) enzyme (also known as Pfs nucleosidase). SRH is then cleaved by LuxS to form L-homocysteine (Hcy) and 4,5-dihydroxy-2,3-pentanedione (DPD) which undergoes spontaneous rearrangements to form a variety of DPD derivatives that interconvert and exist in equilibrium (known as the AI-2 pool). Different bacterial strains recognize different DPD derivatives; the interconversion of molecules within the AI-2 pool therefore presumably allows bacteria to respond to their own AI-2 and also to AI-2 produced by other bacterial species. The discovery of antagonists of AI-2 quorum sensing may provide a possible means to achieve broad-spectrum antivirulence and has thus attracted significant attention in recent years.

1.2 Mechanisms of Biofilm Resistance

Antimicrobial resistance is one of the most serious health threats. The constant increase of antibiotic resistance, coupled with the insufficient investment in antibacterial research, has led to a decline in the efficacy of the existing therapies and a paucity of novel structural classes of antimicrobial able to replace them or to complete their use. Due to the compact nature of biofilm structures, the presumed reduced rates of cellular growth and respiration of biofilm bacteria and the protection conferred by biofilm matrix, natural and synthetic agents are unable to adequately attack and destroy infectious biofilm populations.[34] Once adhered, bacteria show a profound resistance, making biofilm cells 10-

1,000 fold less susceptible to several antimicrobial agents than the same bacteria grown in planktonic (free-floating) culture.

Antimicrobial compounds are often classified according to their major modes of action:

- interference with cell-wall synthesis (β -lactams and glycopeptides);
- inhibition of protein synthesis by binding to 50S ribosomal subunit (macrolides, chloramphenicol, clindamycin, linezolid) and by binding to 30S ribosomal subunit (aminoglycosides, tetracyclines);
- interference with nucleic acid synthesis by inhibition of DNA synthesis (fluoroquinolones) and by inhibition of RNA synthesis (rifampin);
- inhibition of metabolic pathway (sulfonamides and folic acid analogues);
- disruption of bacterial membrane structure (polymyxins and daptomycin).

Some of these agents, such as those that inhibit cell-wall construction actively bring about bacterial cell death are termed bactericidal. Other agents, such as the tetracyclines, which inhibit protein synthesis, are referred to as bacteriostatic, as they simply prevent the growth of the bacteria. Some antibacterial agents are effective only against a narrow spectrum of bacteria, for example, the glycopeptides display activity against Gram-positive organisms, whereas others, such as the β -lactams that target processes

that are common across species are classified as broad-spectrum antibacterial agents.

Bacteria may manifest resistance to antibacterial drugs through a variety of mechanisms.[35] Firstly, the organism may acquire genes encoding enzymes, such as β -lactamases, that destroy the antibacterial agents before they could have an effect. Then efflux pumps, able to extrude the antibacterial agents from the cell before they can reach the target site and exert their effect, may be gained. Moreover, bacteria may acquire several genes for a metabolic pathway, which ultimately produces altered bacterial cell walls that no longer contain the binding site of the

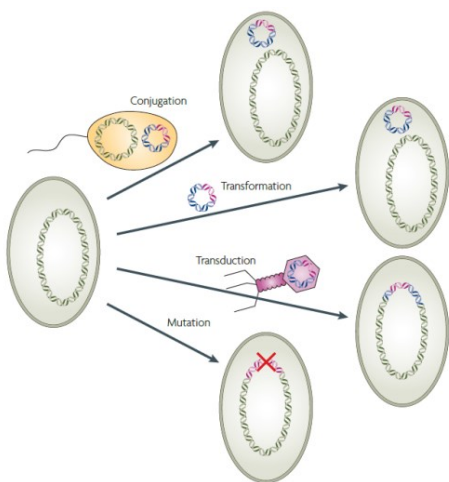


Figure 8. Mechanisms of resistance acquisition.[34]

antimicrobial agent, or mutations that limit access of antimicrobial agents to the intracellular target site *via* down-regulation of porin genes. Microorganisms also develop resistance through the acquisition of new genetic material from resistant strains of bacteria. This is termed horizontal evolution and may

occur between strains of the same or different species. Mechanisms of genetic exchange include conjugation, transformation or transduction (Figure 8). [36] During the conjugation process, a bacterium transfers plasmid-containing resistance genes to an adjacent bacterium by means of an elongated structure known as pilus which joins the two microorganisms. The conjugation frequency appears to be higher in bacteria growing in the sessile mode than in the planktonic mode. Transduction occurs when the resistance genes are transferred from one bacterium to another *via* bacteriophage while transformation is the process where microorganisms acquire and incorporate DNA segments from another ones that have release their DNA complement into the environment after cell lysis. Mutation and selection, together with the mechanisms of genetic exchange, enable bacterial species to adapt quickly to the introduction of antibacterial agents into the environment.

Treatment of biofilms with antibiotics often results in an ineffective therapy. Several factors have been suggested to account for the extraordinary resistance of biofilm bacteria [4, 9]:

- a) the reduced metabolic and growth rates. Different concentrations of the key metabolic substrates within the biofilm proved that surface-bound communities contain cells at all phases of bacterial growth and cells at the different activity levels (Figure 9). This leads to microbial population heterogeneity.

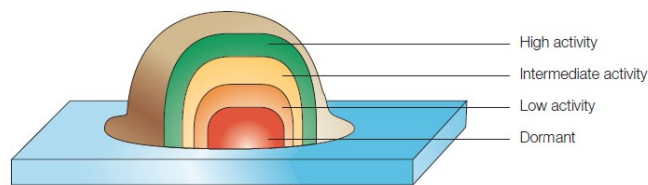


Figure 9. Metabolic activity in a biofilm cell cluster is a function of depth within the biofilm and is influenced by nutrient transport.

Better access to nutrients and oxygen in the periphery region of biofilm promotes metabolic activity of cells. In this part of biological layer the bacteria are able to proliferate. On the contrary, in the deeper part of biofilm the metabolic

potential of bacteria is limited by the worse diffusion process of nutrients. Since most of biocides killing metabolically active bacteria, it has been proposed that bacteria at the dormant growth phase in the deeper region of biofilm are less susceptible to antimicrobial agents which are active against growth factors in planktonic bacteria.[37]

- b) the EPS matrix, able to decrease the amount of antibacterial agents available to interact with biofilm cells (additionally, the biofilm structure might physically reduce the penetration of antimicrobial agents by walling off access to regions of the biofilm). Furthermore, the aggregation of bacteria into the EPS-coated biofilm might make them less susceptible to

phagocytosis. The process of disaggregation of biofilm cells is of considerable interest as a means of increasing the antibiotic sensitivity of biofilm bacteria.[38]

- c) biofilm cells are physiologically distinct from planktonic bacteria and express specific protective factors, such as multidrug efflux pumps and stress response regulators. Differences between planktonic and sessile bacteria involved physiological alterations following the attachment to a surface which result in biofilm bacteria that are morphologically and biochemically distinct from their free-floating counterparts. Bacterial efflux pumps are implicated in the multidrug resistance (MDR) phenotype combined with other more specific resistance systems, including target mutation and enzymatic modification of antimicrobial agents. The identification of a unique biofilm phenotype and genes that could contribute efflux system-mediate resistance of bacterial biofilms is a crucial point to identify new targets for controlling bacterial infections.[39]
- d) the inability of antibiotics to penetrate to all areas of the biofilm. Resistant biofilm bacteria become susceptible to antimicrobial agents following dispersion or disaggregation of biofilm. One promising solution to this problem has emerged from the manipulation of electrical fields that surround bacteria in a biofilm. This bioelectric effect alters the configuration of the EPS matrix and perhaps also enhances the penetration of antimicrobial agents across the bacterial-cell envelope. Using alternating-current densities of less than 100 micro-Amperes per cm^2 , it has been found that the antibiotic concentrations required to kill biofilm cells are greatly reduced in comparison with untreated biofilm bacteria. These concentrations, however, were still higher than those needed to kill planktonic bacteria of the same species.[40]
- e) the presence of sub-populations of cells referred to as “persister”. These cells neither grow nor die during exposure to bactericidal agents exhibiting multidrug tolerance (MDT) that shut down the antibiotic targets and their formation is dependent on the bacteria growth state and not on bactericidal agents exposure. Only the persister fraction is responsible for survival of the whole sessile population. Indeed, persister cells are responsible for biofilm regrowth when the antibiotics concentration decrease or when the treatment is discontinued. The phenomenon of tolerance to antimicrobial agents has also been linked with programmed cell death (PCD) system.[41]

- f) the production of stress-response proteins, conferring increase resistance to the environmental conditions such as immune attack and antibiotic treatment. The general stress response acts both as a rapid emergency response and as a long-term mechanism, that enables the cell adaptation to nutrient deprivation and other environmental stresses that cause changes in cellular metabolism. Activation of the general stress response in the cells, immobilized in biofilm matrix, may results in increasing resistance to biocides action.[42]

In this context, a new antimicrobial-free strategy might be designed to reduce consumption of antimicrobial agents, ensuring the prudent use of these fragile strategies, protecting and empowering antibiotics that are critically important for human and animal health and wellbeing.

1.3 Biofilm inhibitors¹

As most pathogenic bacteria exist as biofilm communities, the discovery and development of agents able to limit biofilm formation or even wipe out established biofilms, could enhance the efficacy of antibiotics that are ineffective against biofilm bacteria. First of all, it is essential to recognize molecular scaffolds having the ability to affect biofilm development through non-microbicidal mechanisms from their microbicidal counterparts, as the resistance to compounds that are not microbicidal will be significantly reduced compared to the conventional bactericidal entities.[44]

This Chapter provides an overview of the several approaches that have been applied to the discovery of small molecules that have been shown to have an anti-biofilm behaviour in a non-bactericidal manner.[43] These approaches are grouped into:

- the identification and development of small molecules that target one of the bacterial signaling pathways involved in biofilm regulation (included quorum sensing inhibitors);
- chemical library screening for compounds with anti-biofilm activity;
- the identification of natural products that possess anti-biofilm activity, and the chemical manipulation of these natural compounds to obtain analogues with increased activity.

1.3.1 Compounds that modulate biofilm by targeting bacterial signaling pathways

Quorum sensing pathways considerably influence biofilm formation as well as the production of virulence factors. As mentioned before (see ‘Paragraph 1.1.4’), there are different classes of autoinducers, based upon on shared molecular features, which represent potential targets: the acyl homoserine lactones (AHLs), the autoinducing peptides (AIPs) and the autoinducer-2 (AI-2). Therefore, an extensive research in this area has led to the discovery of several analogues with the ability to modulate QS-dependent enzymes.

1.3.1.1 Acyl homoserine lactones (AHLs)

Gram-negative bacteria predominantly employ N-acyl homoserine lactones (AHLs) as autoinducers, and more than 70 species of bacteria communicate via AHL-mediated QS with specificity modulated

¹ This Chapter is a summary of the review published by Villa and coworkers.[43]

by variation in the length and oxidation state of the acyl side chain (Figure 10).[45] Native AHLs, found in bacteria, are L-isomers, while the D-isomers are known to have no biological activity.

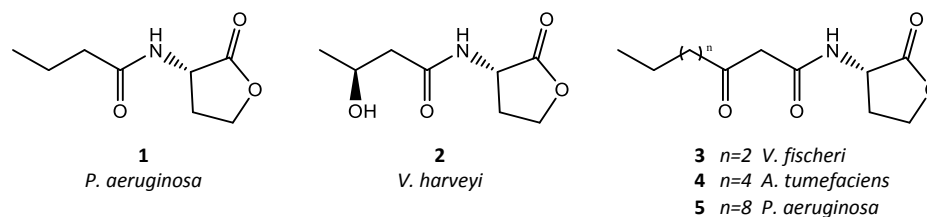


Figure 10. AHLs utilized by Gram-negative bacteria for quorum sensing.

AHLs has been one of the primary scaffolds studied over the past thirty years for the design of potential biofilm inhibitors (Figure 11). The AHL analogues are compounds that contain a carbon chain (of any functionality or substitution) or an aryl group linked to an amide group whose nitrogen atom is in general directly bound to a ring system at a chiral carbon.

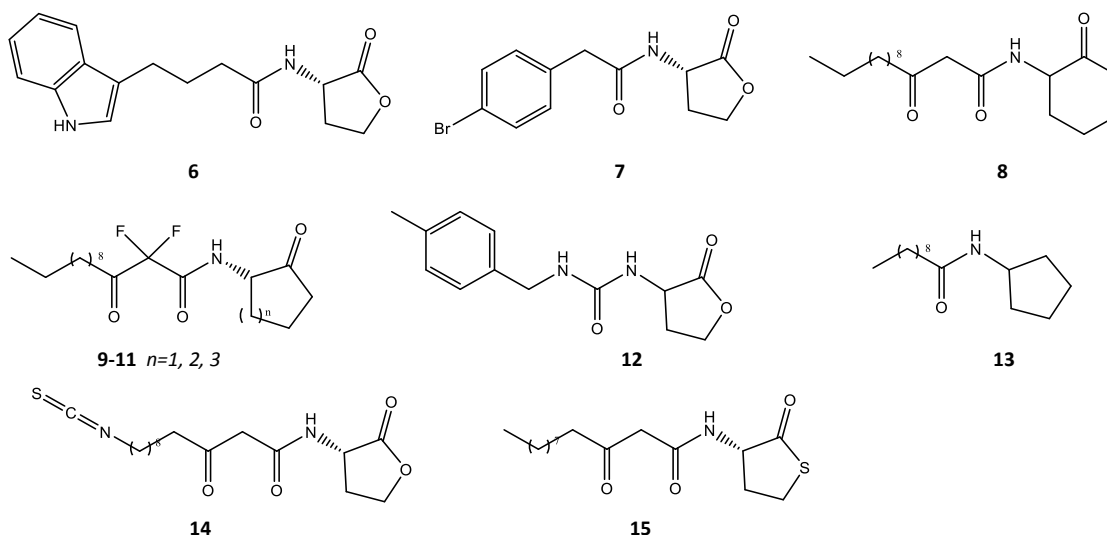


Figure 11. Derivatives of the AHL scaffold that possess biological activity.

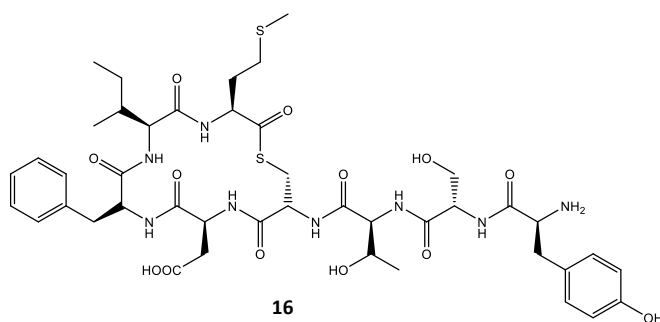
Significant inhibition of biofilm formation was observed for all these derivatives. Blackwell group has demonstrated that two of their most active synthetic AHLs (**6**, **7**) could retard biofilm formation in *P. aeruginosa* PA01.[46] Other studies about the modification of AHLs to evaluate their effects on quorum sensing and biofilm formation in *P. aeruginosa* includes that of Suga and Spring. The work by Suga *et al.* [47] involved the synthesis of a 96-member library, constructed through solid phase protocols, to mimic AHLs by replacing the homoserine lactone moiety with a variety of functionalities. Noteworthy, among the compound identified within this study, the AHL derivative **8** had no effect on

biofilm growth. Spring *et al.*'s research investigated analogues of *P. aeruginosa* AHLs in which the lactone functionality was replaced by a ketone, with additional difluorination between the β -keto amide positions (**9-11**).[48]

Other analogues have been reported involving ureas, thiolactones, sulfonamides and N-acylated cyclopentylamides as viable modifications of AHLs to drive QS inhibition and thereby affect biofilm formation (e.g. **12-13**). Moreover, a series of inhibitors bearing electrophilic functional groups including isothiocyanates, bromoacetamides and chloroacetamides, were designed. The lead compound **14** was also shown to inhibit biofilm formation by wild type PA01 by almost 50% at a concentration of 50 μ M.[45] Furthermore, homoserine lactones themselves are notoriously prone to hydrolysis at physiological pH and the ring-opened product is QS inactive. In order to avoid the problem of lactone hydrolysis, the thiolactone AHL analogues have been investigated.[49] The half-life of a representative active analogue **15** was shown to be almost double that of its parent AHL in bacterial growth medium. Although these analogues have not yet been tested for their activity as inhibitors of biofilm formation, the thiolactone could be a promising scaffold for the development of stable modulators of QS controlled biofilm formation.

1.3.1.2 Autoinducing peptides (AIPs)

QS in Gram-positive bacteria is predominantly mediated by autoinducing peptides (AIPs), though it has been shown that bacteria do not use only peptide signaling molecules for communication but also small molecules known as γ -butyrolactones that have been identified in some species of *Streptomyces*. Many AIPs possess hydrophobic domains, which have been found to be essential for activity. These motifs play a crucial role in promotion of hydrophobic interactions influencing receptor activation. Moreover, the agr QS systems in *S. aureus* regulate a number of virulence phenotypes, including biofilm formation.



Additional studies using peptides and peptidomimetics as potential quorum sensing probe have identified the analogue of *S. aureus* AIP-1 **16** that can also influence QS pathways in *S. aureus*. Truncated peptides such as compound

17 have been found to be potent QS antagonists while the peptidomimetic **18** has been shown to promote biofilm formation in *S. aureus* (Figure 12).

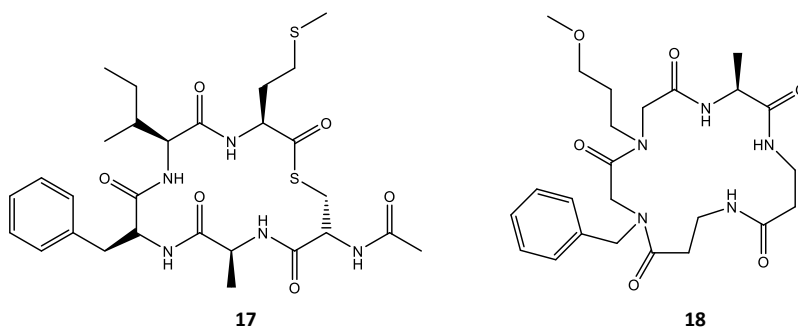


Figure 12. Peptide derived molecules with activity against *S.aureus*.

1.3.1.3 Autoinducer-2 (AI-2)

One of the QS mechanisms shared by both Gram-negative and Gram-positive bacteria involves the production of a small molecule termed autoinducer- 2 (AI-2). All AI-2 molecules are derived from the precursor molecule (S)-4,5-dihydroxy-2,3-pentanedione (DPD) **19**.

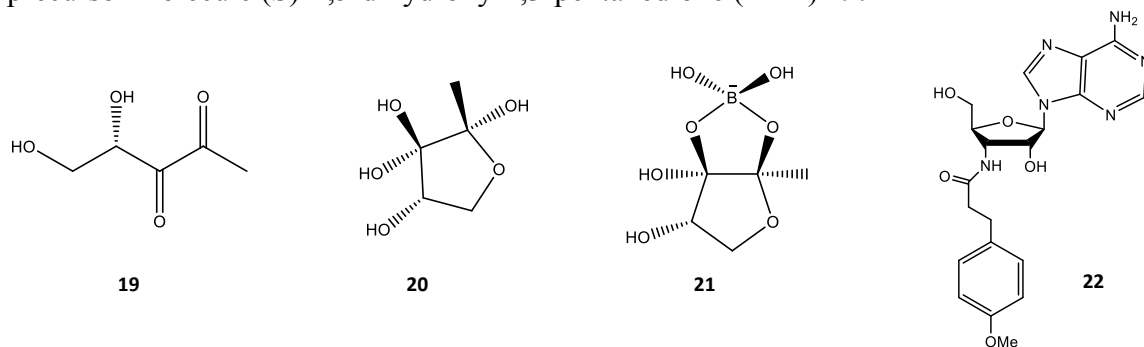
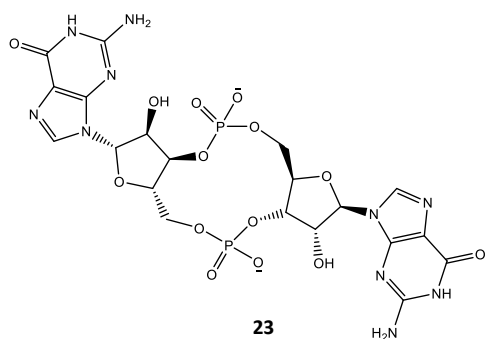


Figure 13. DPD and AI-2 molecules isolated from *S. typhimurium* and *V. harveyi* and SAM analogue **22**.

Two AI-2 molecules are shown in Figure 13: **20** has been isolated and characterized from *Salmonella typhimurium* and **21** from *Vibrio harveyi* as a borate diester, resulted from the high concentrations of boron in the natural marine water habitat of this bacterium. To define their effects on QS, the synthesis of a small number of DPD analogues has been performed. As the biosynthesis of DPD begins from SAM, the screening of a small library of nucleoside analogues has also been investigated. The adenosine analogue **22** has been found to block AI-2-based QS without interfering with bacterial growth.

1.3.1.4 c-di-GMP

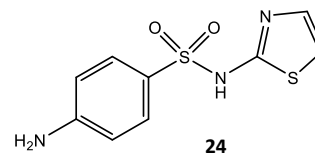
Bis-(3'5')-cyclic di-guanylic acid (c-di-GMP) **23** is a second messenger signaling molecule that is



ubiquitous in bacteria. Diguanilate cyclases (DGCs) and phosphodiesterases (PDEs) are responsible for the synthesis and the degradation of c-di-GMP, respectively. These proteins are highly regulated by various environmental and intracellular signals such as oxygen, light and small molecules. c-di-GMP is also involved in biofilm dispersion. A *P. aeruginosa* mutant, showing elevated c-di-GMP levels, has exhibited defective

detachment in response to environmental signals that typically elicit biofilm dispersion, such as changes in nutrient availability. It has been demonstrated that c-di-GMP levels may be high in order to promote the initial stages of biofilm formation, where motility is required, but then they decrease to allow biofilm maturation. Since QS and c-di-GMP signaling pathways likely regulate some of the same complex processes in bacteria, (e.g. biofilm formation), it is possible that the two signaling pathways could be linked.

Interfering with c-di-GMP signaling is an attractive target for control of biofilm formation by means of c-di-GMP analogues or with small molecules that interfere with the synthesis or degradation of c-di-GMP. A screening of a 1120 compounds library with known biological activities against diguanilate cyclase DGC identified sulfathiazole **24** as promising for *E. coli* DGC activity inhibition (IC₅₀ = 5.8 μM).



1.3.1.5 Indole signaling

Indole is another intercellular signal molecule that plays an important role in the control of many bacterial behaviours such as antibiotic resistance, virulence and biofilm formation. It has been shown to decrease biofilm formation in *E. coli* in a non-toxic manner and in several bacterial species it is immediately converted by oxygenases to various oxidized indole derivatives, such as hydroxyindoles **25–27**, isatin **28**, and isoindigo **29** (Figure 14).

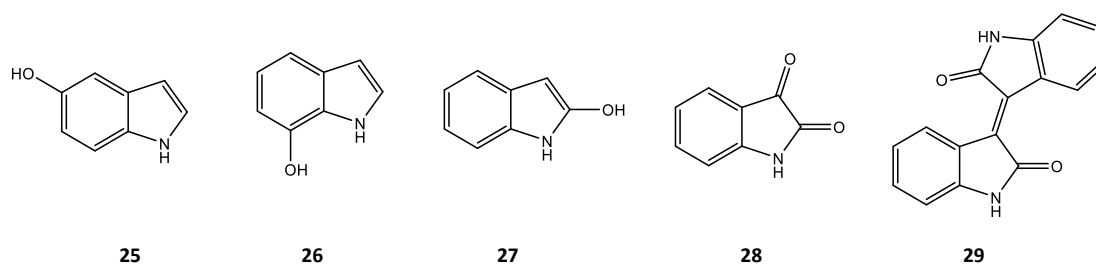


Figure 14. Indole derivatives that affect biofilm formation.

Screening of these compounds for the ability to inhibit biofilm formation by a strain of enterohemorrhagic *E. coli* (EHEC) have revealed that 5-hydroxyindole **25** and 7-hydroxyindole **26** are able to inhibit biofilm formation at the concentration of 1 mM. Moreover, 2-hydroxyindole **27** at the same concentration had no effect on biofilm formation, while isoindigo **29** (at a concentration of 250 μ M, which is the limit of its solubility) has no effect. Finally, isatin **28** has increased biofilm formation in a dose-dependant manner. As many pathogenic bacteria rapidly degrade indole into some of its various metabolites, the ability of indole derived plant secondary metabolites to modulate bacterial biofilm formation has also been investigated. The most active derivatives for suppression of biofilm formation by this *E. coli* strain have been 3-indolylacetonitrile (IAN) **30** and indole-3-carboxyaldehyde (I3CA) **31** (Figure 15).

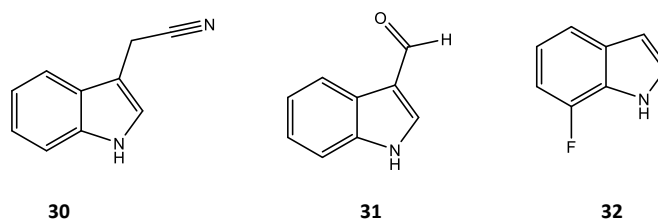


Figure 1. Indole derivatives that affect biofilm formation.

In a further study aimed to discover novel indole compounds with an increased anti-virulence activity compared to IAN **30**, the synthetic 7-fluoroindole (7FI) **32** has been identified as the most active derivative since was able to reduce biofilm formation at 1 mM concentration. Indeed, it was demonstrated that **32** suppresses swarming motility, protease activity, and extracellular polymeric matrix production in *P. aeruginosa* and furthermore reduces the production of QS-regulated virulence factors.

1.3.1.6 Two-component systems

Two-component signal transduction systems (TCS) are a class of regulatory systems found mainly in bacteria, though some have been identified in a small number of eukaryotic organisms, and consist of a histidine kinase and a response regulator. In response to an extracellular signal, the histidine kinase undergoes autophosphorylation at a conserved histidine residue. The histidine kinase then transfers the phosphate group to a conserved aspartate residue on the response regulator, resulting in activation of an effector domain, which then leads to the response. This typically involves the control of gene expression by binding of the phosphorylated response regulator to a DNA upstream regulatory region. TCS are activated by a variety of environmental factors including pH, nutrient level, redox state, osmotic pressure, quorum signals and the presence of antibiotics. The role of TCS in the regulation of biofilm formation and maintenance makes them potential targets for the development of anti-biofilm compounds, which have been underexploited to date. Indeed, it has been shown that both the histidine kinase and response regulator of TCS are targetable by small molecules (Figure 16).

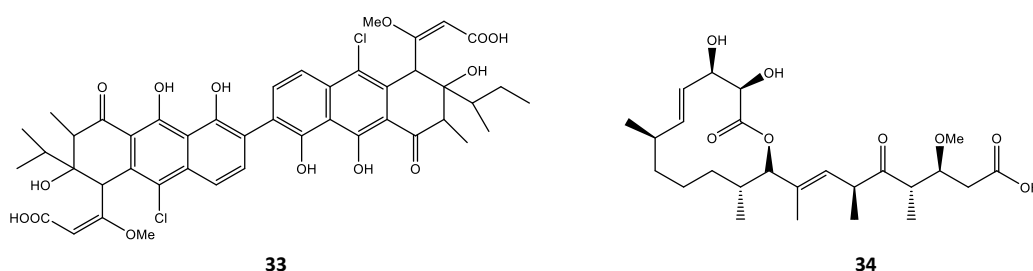
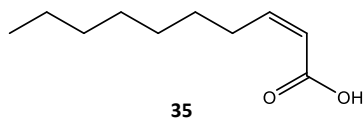


Figure 16. TCS inhibitors walkmycin C 33 and carolacton 34.

Walkmycin C **33** is a known histidine kinase inhibitor isolated from a screening performed on *Bacillus subtilis*. In addition, at levels below the minimum inhibitory concentration (MIC), walkmycin C resulted in the formation of abnormal biofilms and a reduction in biofilm mass. The bacterial secondary metabolite carolacton **34**, affects the viability of *S. mutans* biofilms at nanomolar concentrations. This compound has only minor effects on planktonic bacteria growth but kills bacterial cells within a biofilm state. Although the ability of carolacton to modulate *S. mutans* biofilms is not through a strictly non-microbicidal mechanism, the fact that this compound does not affect planktonic growth represents an alternative strategy for the small molecule control of biofilms and further validates targeting of TCS as a means of controlling bacterial biofilms.

1.3.1.7 Other signaling molecules

A fatty acid signaling molecule, cis-2-decenoic acid **35**, produced by *P. aeruginosa* during growth, has been shown to inhibit biofilm development. It induces the dispersion of established biofilms formed by a number of bacteria including *E. coli*, *Klebsiella pneumoniae*, *B. subtilis*, and *S. aureus* at low nanomolar concentrations, as evidenced by microcolony disaggregation and measurement of the number of cells released into the bulk biofilm culture medium.



In addition, some D-amino acids, which are produced by bacteria during stationary phase, turned out to be a native signal for biofilm dispersion in *B. subtilis* and able to inhibit biofilm formation. The inhibitory activity of the D-amino acids is a consequence of disruption of the connection between the extracellular matrix protein and the bacterial cell. Against *B. subtilis*, D-tyrosine, D-leucine, D-tryptophan, and D-methionine inhibit biofilm formation while the analogous L-amino acids, and other D-amino acids, including D-alanine and D-phenylalanine, are inactive. The individual amino acids have showed inhibitory activity at concentrations from low micromolar (D-tyrosine) to millimolar (D-leucine). Nevertheless, the combination of the four amino acids led to a significant increase of activity compared to any alone.

1.3.2 Chemical library screening

Due to the lack of knowledge about the molecular scaffolds able to interfere with biofilm formation at sub-lethal concentration, High Throughput Screening (HTS) of compound libraries has been used as an effective tool for the identification of novel antibiofilm molecules. The screening of 13,000 compounds carried out by Wood and co-workers [50] revealed that ursolic acid **36** inhibited *E. coli* biofilm formation at concentrations as low as 22 μ M without affecting growth. DNA microarrays analyses demonstrated that ursolic acid had no effects on quorum-sensing, but it induced chemotaxis in *E. coli* and ensured cells to remain too motile for a proper biofilm formation. Among the naturally occurring ursolic acid derivatives (Figure 17), compound **37** has shown an antibiofilm activity at sub-lethal concentrations against the *P. aeruginosa* PA01 biofilm.

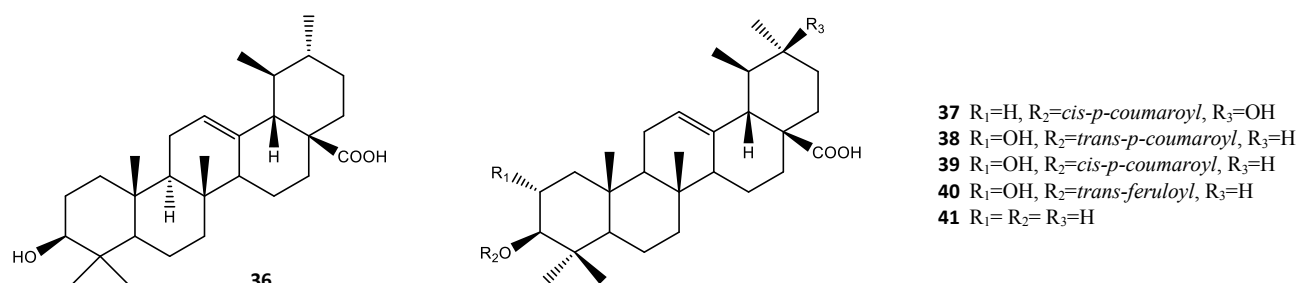
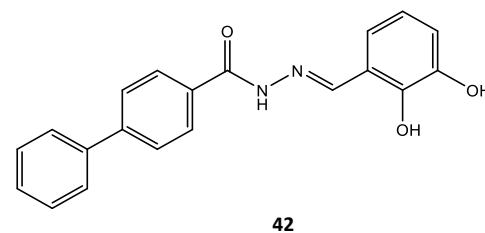
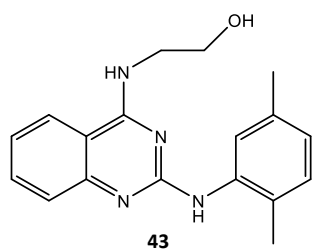


Figure 17. Compounds with an antibiofilm activity identified by HTS.

Clardy and Junker reported a comprehensive HTS, in which they sought to identify novel small molecules that inhibited and dispersed PA01 biofilms.[51] A total of 66095 molecules, derived from libraries containing known bioactive compounds, natural products, and commercially available entities, were screened using a luminescence-based assay. Among these, compound **42** was found to be one of the most active biofilm modulators ever disclosed against either Gram-positive or Gram-negative bacteria ($IC_{50} = 530$ nM).

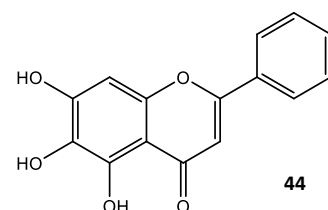


An HTS of 8000-compound chemical library identified several molecules that inhibited *Vibrio cholerae* motility without exhibiting toxicity.[52] The lead compound, the quinazoline-2,4-diamino analogue **43**, showed inhibition of biofilm formation at the sub-lethal concentration of 10 $\mu\text{g/mL}$.



Also computer-aided drug design (CADD) techniques have been employed in the search for new biofilm modulators. One such study involved the investigation of 51 active compounds derived from traditional Chinese medicines, whose antibacterial properties had been previously documented.[53] The

most active compound, baicalein **44**, a flavonoid that is speculated to play a role in apoptosis and to also inhibit lipid peroxidation, had no remarkable effect on bacterial growth but when dosed together with an antibiotic a significant synergistic effect has been seen. In a recent study, 147 recognized drugs and natural compounds has been selected from the SuperNatural and SuperDrug databases on the basis of their two-dimensional (2D) structural similarity to the following quorum-sensing inhibitors: furanone C30 **45**, patulin **46**, the



P. aeruginosa LasR natural ligand (3-oxo-C12-AHL **47**) and a known quorum-sensing receptor agonist TP-1 **48** (Figure 18).[54]

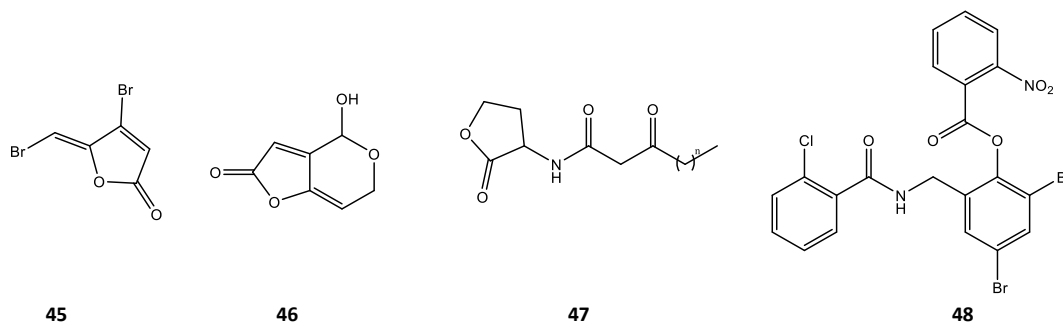


Figure 18. Structures of furanone C30, patulin, 3-oxo-C12-AHL and TP-1.

This screening led to the discovery of three compounds, salicylic acid **49**, nifuroxazide **50** and chlorzoxazone **51**, which significantly inhibit the quorum sensing-regulated gene expression at concentrations at which they do not affect bacterial growth (Figure 19). In addition biofilms treated with these compounds appear thinner and less structured than control biofilms and the total biofilm mass is reduced.

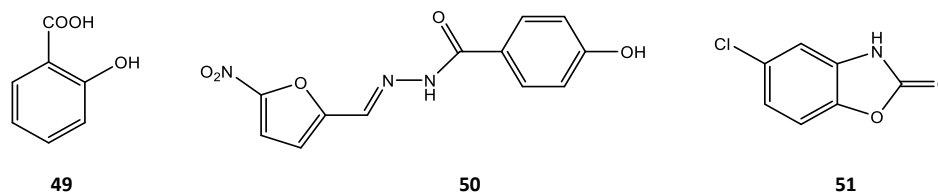


Figure 19. Structures of salicylic acid, nifuroxazide and chlorzoxazone.

A high-throughput epifluorescence microscopy imaging based HTS has been developed for the identification of small molecule inhibiting biofilm formation in *V. cholerae*. Among the number of compounds that reduced biofilm formation without altering bacterial cell viability, the two lead compounds **52** and **53** (Figure 20), analogues of the antimalarial drug mefloquine, have been identified.[55]

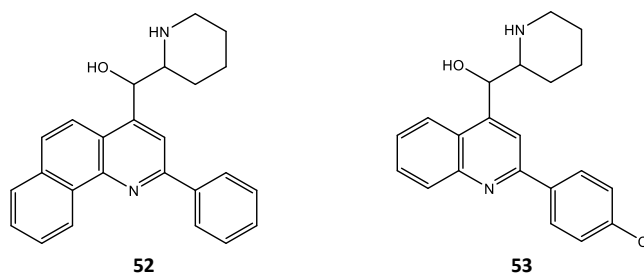


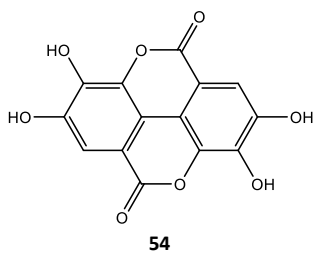
Figure 20. Structures of mefloquine analogues.

1.3.3 Natural products and their analogues

Nature has been proven to be an outstanding source for new and innovative antibiofilm compounds active at sub-lethal concentrations. Plants and microbes of terrestrial and marine origin are known to produce small molecules offering chemical diversity with structural complexity and biological potency. Some of these molecules exhibit novel biological activities that make them indispensable tools in biomedical research and unique prototypes for the development of innovative therapies. A number of natural products that possess the ability to inhibit or disperse bacterial biofilms have been used as the starting points for the design of more efficacious compounds through modifications of their scaffolds.

1.3.3.1 Plant extracts

Studying natural products derived from plant sources for the discovery of new biologically active compounds is not uncommon as many traditional medicines use plant extracts for the treatment and cure of disease symptoms. For instance, extracts from *Rubus ulmifolius*, rich in the polyphenol ellagic acid **54** and glycosylated derivatives, showed an inhibitory effect on *S. aureus* biofilm formation at concentrations below those required to limit bacterial growth.[56] Meanwhile, a number of flavonoids found in citrus species, including naringenin **55** and quercetin **56** (Figure 21), which are antagonists of homoserine lactone and AI-2-mediated cell-cell signaling are able to inhibit biofilm formation by *V. harveyi* and *E. coli* in a dose-dependent manner.[57]



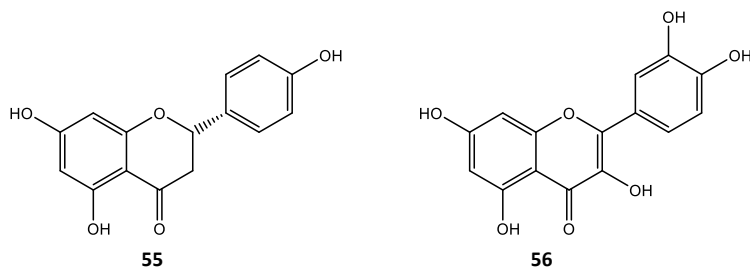
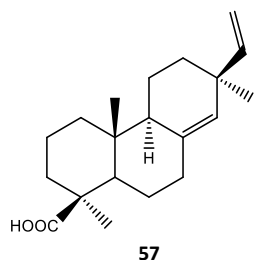


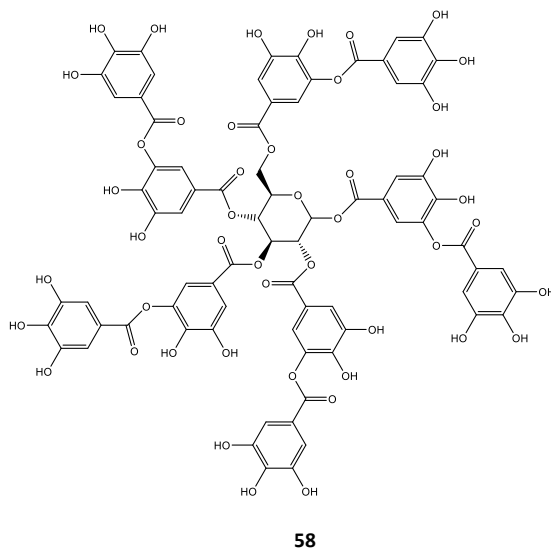
Figure 21. Structures of molecules isolated from plants.

Another plant derived natural product, recently identified as potential biofilm formation inhibitor, is 4-*epi*-pimaric acid **57** isolated from *Aralia cachemirica*. It inhibites biofilm formation by *S. mutans* at sub-MIC concentrations and was shown by confocal microscopy to inhibit clumping and attachment.[58]



Tannic acid **58**, the main component of the extract of *Quercus infectoria* G. Olivier nutgalls (a traditional Thai medicinal plant) shows the same MIC (0.13-0.50 mg/mL) of the whole extract against methicillin-resistant *S. aureus* suggesting that it might be the active component of the herb extract influencing bacterial cell surface hydrophobicity that is involved in antibiofilm mechanisms.

At sub-MIC only antibiofilm activity and not bacterial growth is inhibited.[59]



1.3.3.2 Halogenated furanones

Comprehensive research reports have detailed the biological activities and effects that halogenated furanones (HFs) have on bacterial QS. These small molecules are natural products native to the marine red algae *Delisea pulchra* and primarily serve as a defense mechanism by acting as natural chemical deterrents. Several studies have shown that natural HFs isolated from the algae possess the ability to prevent biofilm formation and swarming in *E. coli* and *B. subtilis*. It is possible to evidence several structural similarities between HFs and AHLs such as the presence of a non-polar aliphatic carbon chain linked to a relatively polar group. As seen in AHLs, the length of the carbon chain linked to the furanone ring is varied in addition to the presence of hydroxyl or acyl functionalities. Besides, the presence of bromine atoms in these small molecules is one of the most significant structural differences between HFs and AHLs.

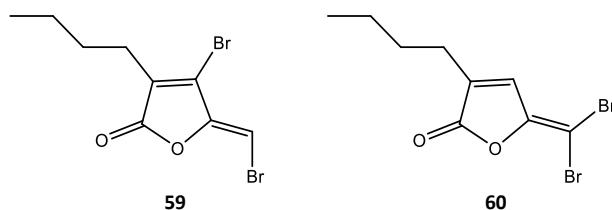


Figure 22. Structure of natural halogenated furanones.

Starting from the natural furanones **59** and **60** (Figure 22), the influence of the number and the position of bromine atoms on the activity have been explored. Compounds **61** and **62** (Figure 23) at 224 μM concentration reduce *E. coli* biofilm formation by 75% and 63% respectively, while the tetrabromo derivative **63** at 141 μM concentration causes a reduction of biofilm formation by 80%. [60]

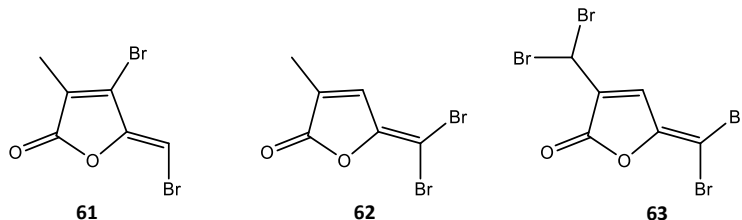


Figure 23. Synthetic halogenated furanones bearing in their structure some bromine atoms.

Nevertheless, other synthetic furanones **64-68** (Figure 24), lacking bromine atoms but bearing an exocyclic ester functionality, are able to inhibit *P. aeruginosa* biofilm formation. [61]

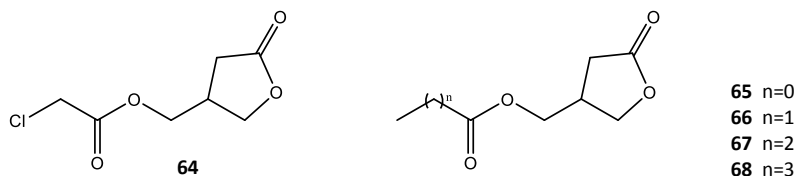
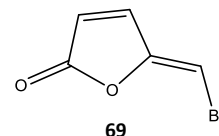


Figure 24. Synthetic halogenated furanones bearing in their structure an exocyclic ester functionality.

Moreover, 5-bromomethylene-5H-furan-2-one **69**, lacking a side chain but bearing a vinyl bromide moiety, was able to penetrate *P. aeruginosa* biofilm and interfere with QS without any associated microbicidal properties.[62] To date, the halogenated furanones cannot be used for human treatment therapies since they are characterized by toxicity, carcinogenic properties, and instability under aqueous conditions.



1.3.3.3 Marine natural products and analogues

Nowadays, some of the most active discovered anti-biofilm compounds have been based on the molecular scaffolds of marine natural products. Oroidin **70** and Bromoageliferin **71** (Figure 25) are alkaloids produced by the sponge *Agelasidae* as chemical anti-feeding defense mechanism against predator. They are structurally characterized by the presence of 2-aminoimidazole (2-AI) subunits.

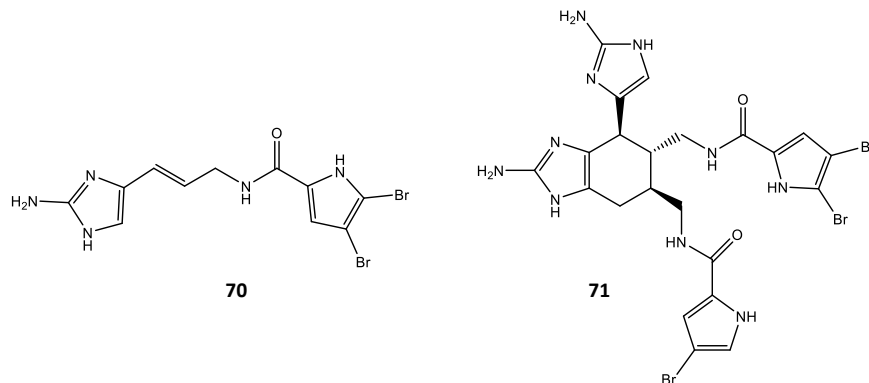


Figure 25. Structures of oroidin and bromoageliferin.

The simplification of bromoageliferin structure has led to the couple of analogues TAGE (*trans*-bromoageliferin) **72** and CAGE (*cis*-bromoageliferin) **73** (Figure 26) showing a biofilm formation inhibition against *P. aeruginosa* PA01 and PA14. In details, TAGE inhibits PA01 and PA14 biofilm formation with IC_{50} values of 100 μ M and 190 μ M respectively, similarly to CAGE.[63]

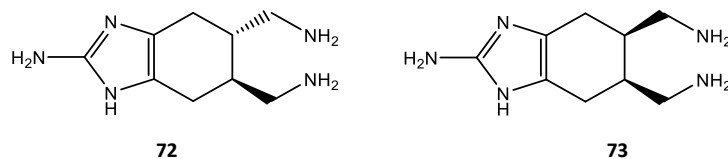
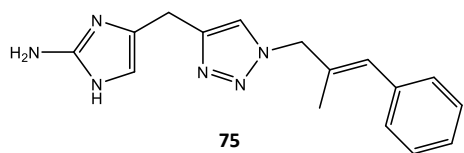
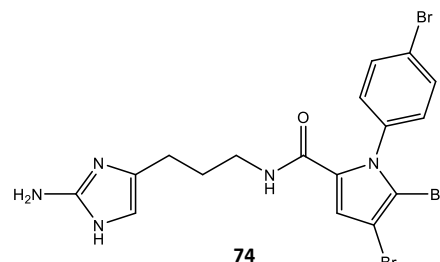


Figure 26. Structures of TAGE and CAGE.

Since Oroidin shows a similar activity to TAGE and CAGE on *P. aeruginosa* ($IC_{50} = 190 \mu\text{M}$ and $IC_{50} = 166 \mu\text{M}$ against PA01 and PA14 respectively), structure–activity–relationships (SARs) for anti-biofilm activity have been investigated. In order to delineate which structural features of the molecule could be required for biological activity, three regions within the oroidin template have been systematically varied: the pyrrole tail group, the linker chain, and the 2-AI head group. These studies have revealed that any modifications to the 2-AI head of the molecule completely abolish the activity. Among these, the most active molecule discovered was dihydrosventrin (DHS) **74**.^[64] In addition, derivatives presenting the reversed amide bond have been synthesized. In particular, compounds bearing an aliphatic chain have shown the inhibition of biofilm development by PA01 and PA14 at low micromolar concentration and their potency is directly related to chain length. Moreover, the introduction of a triazole moiety has



been explored. In particular, 2-aminoimidazole-triazole (2-AIT) **75** shows a broad spectrum inhibitory activity against both Gram-positive and Gram-negative bacteria.^[65] Further efforts to increase the activity of **75** through modification of

the aryl moiety were carried out through the use of Suzuki–Miyaura coupling. A number of these compounds were found to be effective biofilm dispersion agents against *A. baumannii*. Moreover, the effect of different substituents to modulate biofilms has been investigated through a synthetic approach involving Grignard addition to α -amino Weinreb amides. The introduction of alkyl substituents at the 1-position of the 2-AI ring also modulates the activity: in general short chain substituents led to a decrease of activity, while the most active analogues against *P. aeruginosa* biofilm formation are those possessing an alkyl chain of intermediate length.

Also the 2-aminopyrimidine (2-AP) scaffold has been investigated and the obtained derivatives exhibit a lower activity in comparison with 2-AI compounds against the Gram-negative bacteria. Among the

most active derivatives, **76** and **77** have been found to inhibit biofilm formation with an IC_{50} value of 72 μ M and 67 μ M respectively (Figure 27).[66]

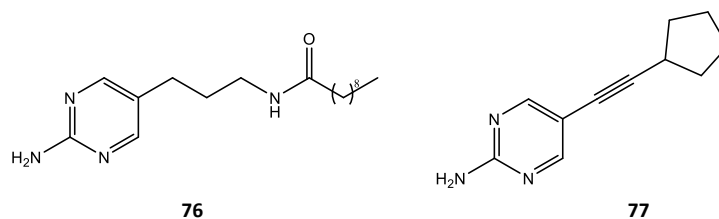


Figure 27. Structures of 2-AP derivatives.

1.3.3.4 Zosteric acid

Seagrasses, a group of about 60 species of flowering plants, live completely submerged in marine waters and form the most widespread coastal systems in the world. Several studies on marine plants highlighted a lack of correlation between antimicrobial activities and abundance of surface-associated microorganisms, suggesting that chemical defences may function by mechanisms more subtle than the simple killing activities, like those influencing the multicellular behaviour by manipulating the expression of specific phenotypes that represent different stages of the biofilm process.[67] In this context, sub-lethal concentration represents one mechanism by which the host minimizes the risk of counter adaptation which would be likely to occur if secondary metabolites were toxic.[68] Zosteric acid (ZA, **1**), the natural extract from *Zostera marina* or eelgrass, has shown to prevent biofouling from some bacteria, algae, barnacles and tubeworms at non-toxic concentrations.[69] The chemical name of zosteric acid is *p*-(sulpho-oxy) cinnamic acid (Figure 28).

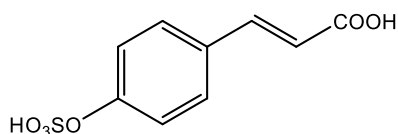


Figure 28. Zosteric acid formula.

Recently, the efficacy of zosteric acid sodium salt as inhibitor of biofilm formation was evaluated against two bacteria (*Escherichia coli* and *Bacillus cereus*) and two filamentous fungi (*Aspergillus niger* and *Penicillium citrinum*).[70] The anti-biofilm activity of ZA sodium salt was species-specific, and the reduction in microbial adhesion ranged from 23 % to 99 %, depending on the environmental

conditions. Previously studies demonstrated that zosteric acid also possesses the ability to significantly reduce, at sublethal concentrations, both bacterial and fungal adhesion and to successfully counteract the effects of colonization-promoting factors like temperature, time and pH. It was found that ZA is not a chemorepellent but it is able to stimulate individual *E. coli* cell motion by increasing the production of flagella, causing the bacteria to wander away from the surface instead of adhering firmly and developing biofilm. In addition, this anti-biofilm compound retards *E. coli* biofilm development with a significant decrease in biofilm biomass and thickness, plays a role in shaping biofilm architecture, in thwarting budded-to-hyphal-form transition, in extending the performance of antimicrobial agents and shows cytocompatibility towards soft and hard tissue. A deeper proteomic investigation highlights that this anti-biofilm compound leads to global stress on bacterial cells promoting the expression of several protective proteins and the synthesis of flagella to escape from unfavourable conditions.[71]

To date, the mode of its antifouling action has not yet been fully elucidated. Stanley and coworkers [72] hypothesized that the reason of the antifouling effect of zosteric acid lies in the high affinity for water due to its sulfate group. As a result, its antifouling capability could be attributed to the free-floating molecules that interact with bacteria. Moreover, it was hypothesized that zosteric acid molecules in aqueous environment can block the surface interaction sites of the organisms, thus preventing their attachment to a surface. A recent study demonstrated that the antifouling agent did not affect cell surface wettability of both bacterial and fungal cells but increased by 40% bacterial swimming motility. [71] The hyper-motile phenotype observed in the zosteric acid sodium salt-treated samples, suggested that zosteric acid sodium salt impacts the transition between motile and sessile lifestyle by causing *Escherichia coli* to wander across the surface instead of firmly adhering and developing biofilm. Whole cell proteome of *E. coli* was analysed to study protein patterns expressed by the surface-exposed planktonic cells without and with the zosteric acid sodium salt. Two principal groups of proteins, energy metabolism related and stress-associated proteins, were differently expressed in presence of zosteric acid sodium salt (Figure 29).

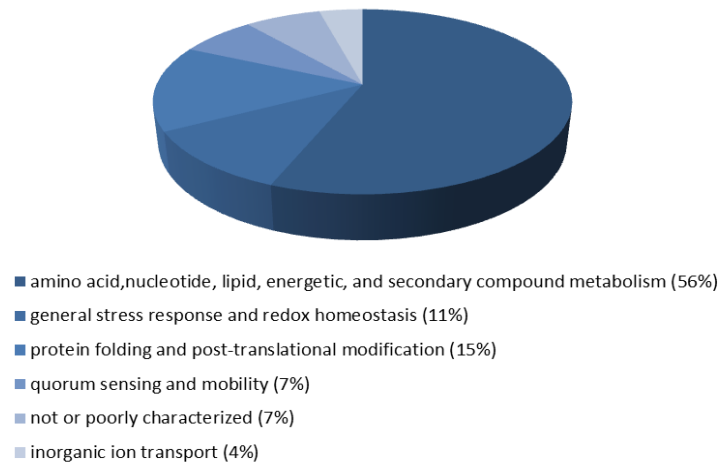


Figure 29. Functional classification of proteins modulated in *E. coli* cells treated with zosteric acid sodium salt. This chart shows the different groups to which the 27 identified proteins with a known or predicted function can be assigned.

In summary, the interaction of zosteric acid sodium salt with *E. coli* cells seems to involve complex cross-talk regulating various genes. This indicates that it may target key-steps involved in biofilm formation by modulating the threshold level of AI-2 and inducing a hypermotile phenotype unable to firmly adhere on surfaces. In addition, it is possible that the antifouling action of zosteric acid sodium salt is caused by cell envelope defects leading to modifications of physicochemical properties of cell surface and thus changes in bacterial adhesion to abiotic surfaces. The presence of zosteric acid sodium salt acts as environmental cue leading to a global stress on *E. coli* cells, increasing the ability to express various protective proteins, the production of AI-2 and the synthesis of flagella to escape from adverse conditions.

1.3.3.5 Conclusions

Nature represents an immense source of new bioactive substances with unrivalled structural diversity and complexity. Plants have adaptively developed fascinating strategies over millions of years to prevent harmful bacterial colonization on their living tissues in response to an ever-present pathogen pressure. These natural strategies have inspired anti-biofilm strategies and could be a promising starting point for novel therapeutic approaches. In this context, zosteric acid has been found to be suitable for implementation as a preventive or integrative approach against biofilm formation.

2. RESEARCH PROJECT

The aim of my research project is the development of an innovative antibiotic-free functionalized material to resist infections of vascular and urinary catheters using compounds with known anti-biofilm activities. The search of suitable non-toxic, active plant-derived compounds to incorporate into the antifouling coating could be a successful approach for the prevention of biofilm-related infections. This new perspective is based on the concept of using sub-lethal doses of bio-inspired molecules to interfere with the key-steps that orchestrate biofilm formation (like surface sensing process and/or cell-to-cell signaling pathways), thus infection cascade might be hampered. In addition, as this approach do not directly kill cells or prevent their growth, there is presumably a less evolutionary pressure for the development of resistance than with traditional antimicrobial agents.

This project began from the investigation of zosteric acid or *p*-(sulfo-oxy) cinnamic acid, a secondary metabolite produced by the seagrass *Zostera Marina*, which turned out to be suitable for implementation as a preventive or integrative approach against device-related infections. With the aim to identify the essential requirements for zosteric acid antifouling activity, several derivatives were synthesized and submitted to biological assays in order to evaluate both their planktonic growth inhibition and their anti-adhesion properties.

This thesis is divided into two main sections. Within each section, I firstly provided a basic outline of the concepts under discussion. In the first one, I included some observations about the structure-activity relationships (SARs) exhibited by a small library of molecules (45 compounds), whose chemical structures are related to the scaffold of zosteric acid. Moreover, also two derivatives of salicylic acid were taken into account in this first stage, since salicylic acid, whose antimicrobial activity is well-known in biological world, was used in the subsequent section as reference compound to evaluate the efficiency of cinnamic acid functionalized surface. Initially, it was necessary to prepare chemically modified anti-biofilm compounds. The anchorage of these compounds to the polymeric material, used for the preparation of medical devices, was performed functionalizing these derivatives with chemical groups able to allow their binding to reactive positions on the polymer by an opportune spacer. The chemical modifications have conserved the parts of molecule responsible for the antifouling activity. The obtained results prove to be valuable in the rational design of the next generation chemical tools, with an improved activity and selectivity, to study and modulate bacterial adhesion. In addition, the

identification of the cellular target of zosteric acid analogues constituted a crucial step in understanding their true mode of action and for the structure-led design and improvement of any potential therapeutic compound and material. Then, a further goal of this work was to understand the molecular mechanism by which zosteric acid and its derivatives affected the biofilm formation in *E. coli*, by identifying the target proteins bound by the antibiofilm compounds using an affinity pull-down approach.

The second branch of this thesis was focused on the functionalization of materials with molecules, selected from the previous biological evaluation, showing interesting antifouling properties, with the aim to hinder biofilm formation. In literature, various synthetic approaches based on immobilization or release of bactericidal substances were extensively explored to produce antibacterial coatings. Although providing encouraging results, these approaches suffer from the use of active agents which may be associated with side-effects such as cytotoxicity, hypersensitivity, inflammatory responses or the progressive alarming phenomenon of antibiotic resistance.

In this context, a bio-inspired method devoted to the development of an antibiofilm surface using derivatives which mechanisms of action are different from that of the traditional antimicrobial compounds can be a promising approach to prevent biofilm formation.

In this second section, two different strategies were employed to achieve this purpose:

- a physical coating or passive coating, that consists in depositing an antifouling layer on the material surface (lacking of long-termed activity);
- a covalent linkage of molecules to the surface, which offers better stability.

Advantages were conferred with the covalently linkage of selected bioactive molecule to the surface of a material in a way to expose the active moiety to the cellular target. Indeed, in this approach, no molecule were leached from the surface, sidestepping the problem of the compound kinetics release, providing a long-term protection against bacterial colonization and reducing the risk of developing resistant microbial strains, as the concentration of the anti-biofilm agents were constantly below the lethal concentration.

Finally, in this dissertation I also inserted a brief description of the work I performed during my six months experience in the Department of Chemistry at the University of Cambridge (UK), under the supervision of Professor David Spring, involving the design and the synthesis of potential Plk1 macrocyclic inhibitors.

This project was founded by Cariplo Foundation and the scientific background of involved researchers includes:

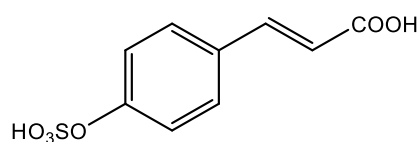
- 1) competence in biocide-free antifouling strategies and biofilm analysis (DEFENS-UNIMI: Dr. Cristina Cattò, Dr. Federica Villa, Dr. Francesca Cappitelli*);*
- 2) competences in the immobilization of enzymes on inorganic and organic surfaces (ICRM-CNR: Dr. Francesco Secundo);*
- 3) enzyme modification with polymer or with small hydrophobic molecules (isoprenylation, acylation) (ICRM-CNR, DEFENS-UNIMI: Dr. Francesco Secundo, Dr. Federica Villa, Dr. Francesca Cappitelli*);*
- 4) functional studies about the activity of antifouling molecules and redox-cycling agents based on comparative proteomics (DEFENS-UNIMI: Dr. Cristina Cattò, Dr. Fabio Forlani, Dr. Alberto Vitali);*
- 5) chemical modification of molecules with well-known antifouling activity and clear mechanism of action by reaction through the available functional group or, if necessary, introducing new reactive groups to link them directly or by a spacer to the material surface (DISFARM-UNIMI: Dr. Silvia Dell'Orto, Dr. Stefania Villa, Dr. Arianna Gelain);*
- 6) functionalization of the polymer surfaces which are employed for production of the medical devices (DISFARM-UNIMI: Dr. Silvia Dell'Orto, Dr. Stefania Villa, Dr. Arianna Gelain).*

** Project Coordinator*

3. SECTION A: DESIGN, SYNTHESIS AND BIOLOGICAL EVALUATION OF ANTI-BIOFILM DERIVATIVES

3.1. Project Description (A)

Zosteric acid (ZA, **1**), a natural product extracted from the seagrass *Zostera Marina*, has been shown to deter, at non-toxic concentrations, fouling by marine bacteria, algae, barnacles and tubeworms.[69] It turned out to be a powerful antibiofilm agent able to significantly reduce, at sublethal concentrations, both bacterial and fungal adhesion (for details see ‘Paragraph 1.3.3.4’).

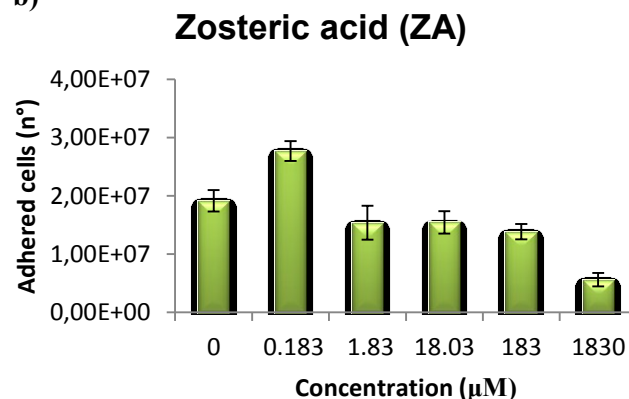


ZOSTERIC ACID (ZA, **1**)

a)

	% Reduction	
	Planktonic growth ^a	Cells adhesion ^b
<i>E.coli</i> (treated with 1.83 mM of zosteric acid)	1.21	-70.56

b)



Since zosteric acid has shown antifouling properties only at 1.83 mM, a series of derivatives related to its structure were designed and synthesized in order to understand the structural requirements essential for the antifouling activity.

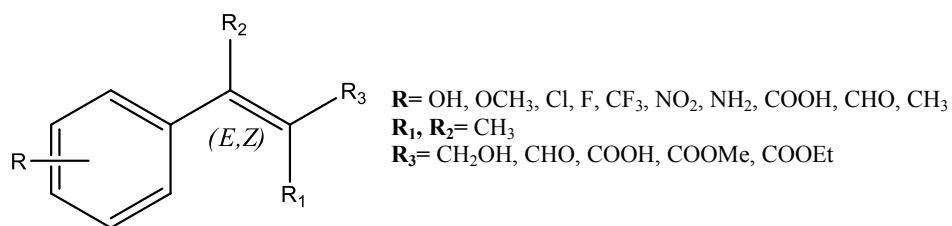


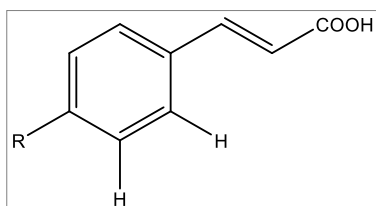
Chart 1. Cinnamic acid derivatives (1-45)

In detail, the performed modifications are summarized in Chart 1 and consist of:

- the introduction of substituents, characterized by different steric and electronic features, at various positions on the phenyl ring;
- several side chains modifications, such as the removal of the unsaturation;
- the insertion of a methyl group in *alfa* or *beta* position of the carboxylic acid;
- the replacement of the carboxylic moieties with an aldehyde, an alcohol or ester functionalities.

Several compounds were purchased from Sigma-Aldrich, some others were prepared following slightly modified literature procedures.[73, 74, 75] The zosteric acid analogues were divided in six groups according to the structural changes made on zosteric acid scaffold:

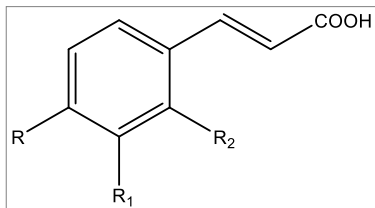
- Group 1:** molecules bearing different substituents at the *para* position on the phenyl ring, maintaining unchanged the carboxylic function and the *trans* configuration of the double bond.



Group	Cmp		R	E/Z
1	1	ZOSTERIC ACID	OSO ₃ H	E
1	2	COUMARIC ACID*	OH	E
1	3	CINNAMIC ACID*	H	E
1	4	4-METHOXYCINNAMIC ACID*	OCH ₃	E
1	5	4-NITROCINNAMIC ACID*	NO ₂	E
1	6	4-CHLOROCINNAMIC ACID*	Cl	E
1	7	4-AMINOCINNAMIC ACID HYDROCHLORIDE*	NH ₃ ⁺ Cl ⁻	E
1	8	4-AMINOCINNAMIC ACID *	NH ₂	E
1	9	4-CYANOCINNAMIC ACID	CN	E
1	10	(4-TRIFLUOROMETHYL)CINNAMIC ACID	CF ₃	E
1	11	4-CARBOXYCINNAMIC ACID	COOH	E
1	12	4-FORMYL CINNAMIC ACID*	COH	E
1	13	4-FLUOROCINNAMIC ACID*	F	E
1	14	4-METHYL CINNAMIC ACID	CH ₃	E

*commercially available

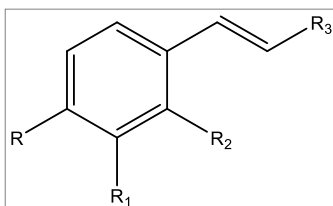
- Group 2: molecules bearing different substituents at *ortho* and *meta* position on the phenyl ring, maintaining unchanged the carboxylic function and the *trans* configuration of the double bond.



Group	Cmp		R	R ₁	R ₂	E/Z
2	15	2-HYDROXYCINNAMIC ACID*	H	H	OH	<i>E</i>
2	16	3-HYDROXYCINNAMIC ACID*	H	OH	H	<i>E</i>
2	17	2-CHLOROCINNAMIC ACID	H	H	Cl	<i>E</i>
2	18	3-CHLOROCINNAMIC ACID*	H	Cl	H	<i>E</i>
2	19	2-METHOXYCINNAMIC ACID*	H	H	OCH ₃	<i>E</i>
2	20	2-CHLORO-4-FLUOROCINNAMIC ACID*	F	H	Cl	<i>E</i>
2	21	2,4-DICHLOROCINNAMIC ACID*	Cl	H	Cl	<i>E</i>
2	22	3,4-DICHLOROCINNAMIC ACID*	Cl	Cl	H	<i>E</i>
2	23	CAFFEIC ACID*	OH	OH	H	<i>E</i>
2	24	3-HYDROXY-4-AMINO CINNAMIC ACID	NH ₂	OH	H	<i>E</i>
2	46	3-HYDROXY-4-NITRO CINNAMIC ACID	NO ₂	OH	H	<i>E</i>

*commercially available

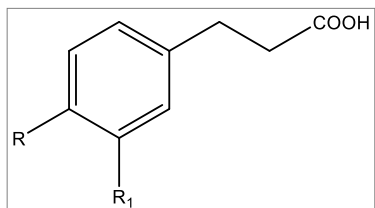
- Group 3: molecules whose carboxylic acid was replaced by different functionalities.



Group	Cmp		R	R ₁	R ₂	R ₃	E/Z
3	25	METHYL COUMARATE*	OH	H	H	COOCH ₃	<i>E</i>
3	26	METHYL CINNAMATE*	H	H	H	COOCH ₃	<i>E</i>
3	27	METHYL 4-METHOXYCINNAMATE	OCH ₃	H	H	COOCH ₃	<i>E</i>
3	28	ETHYL CINNAMATE*	H	H	H	COOCH ₂ CH ₃	<i>E</i>
3	29	ETHYL β-METHYLCINNAMATE*	H	H	H	COOCH ₂ CH ₃	<i>E</i>
3	30	ETHYL 2-HYDROXYCINNAMATE*	H	H	OH	COOCH ₂ CH ₃	<i>E</i>
3	31	CINNAMALDEHYDE*	H	H	H	COH	<i>E</i>
3	32	α-METHYLCINNAMALDEHYDE*	H	H	H	COH	<i>E</i>
3	33	CINNAMYL ALCOHOL*	H	H	H	CH ₂ OH	<i>E</i>

*commercially available

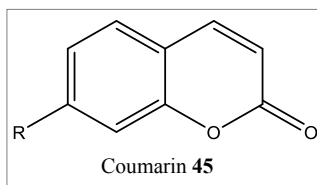
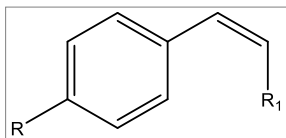
- Group 4: molecules characterized by a saturated side chain.



Group	Cmp		R	R ₁	E/Z
4	34	3-PHENYLPROPIONIC ACID*	H	H	<i>E</i>
4	35	3-(4-HYDROXY)PHENYLPROPIONIC ACID*	OH	H	<i>E</i>
4	36	3-(4-METHOXY)PHENYLPROPIONIC ACID*	OCH ₃	H	<i>E</i>
4	37	(3,4-DIHYDROXY)HYDROCINNAMIC ACID*	OH	OH	<i>E</i>

*commercially available

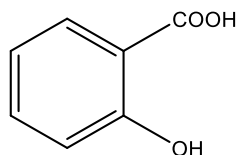
- Group 5: molecules characterized by the side chain in *cis* configuration.



Group	Cmp		R	R ₁	E/Z
5	38	ZOSTERIC ACID	OSO ₃ H	COOH	Z
5	39	CINNAMIC ACID	H	COOH	Z
5	40	COUMARIC ACID*	OH	COOH	Z
5	41	4-METHOXYCINNAMIC ACID	OCH ₃	COOH	Z
5	42	METHYL 4-METHOXYCINNAMIC ACID	OCH ₃	COOCH ₃	Z
5	43	METHYL COUMARATE	OH	COOCH ₃	Z
5	44	ETHYL CINNAMATE	H	COOCH ₂ CH ₃	Z
5	45	COUMARIN*	H	-	Z

*commercially available

Subsequently, besides cinnamic acid analogues, another different class of molecules, which derived from the structure of the natural compound salicylic acid (SA), has been investigated. To date, salicylates are known to be powerful antifouling agents against a wide range of fungi and bacteria [44] and they are able to prevent bacterial adhesion on medical devices. [76]

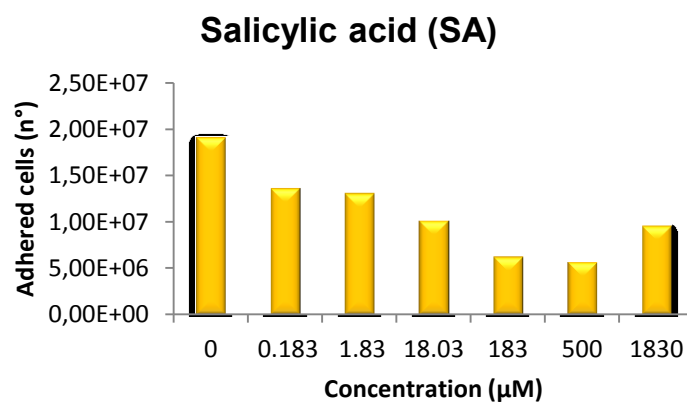


SALICYLIC ACID (SA)

a)

	% Reduction	
	Planktonic growth	Cells adhesion
<i>E.coli</i> (treated with 183 μM of salicylic acid)	-0.18	-67.42

b)



In this case, I focused my attention only on the substitution at the *para* position since it was the most interesting for the subsequent grafting to the polymeric support (Chart 2).

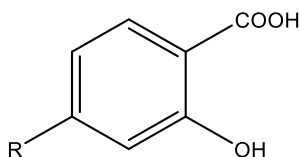


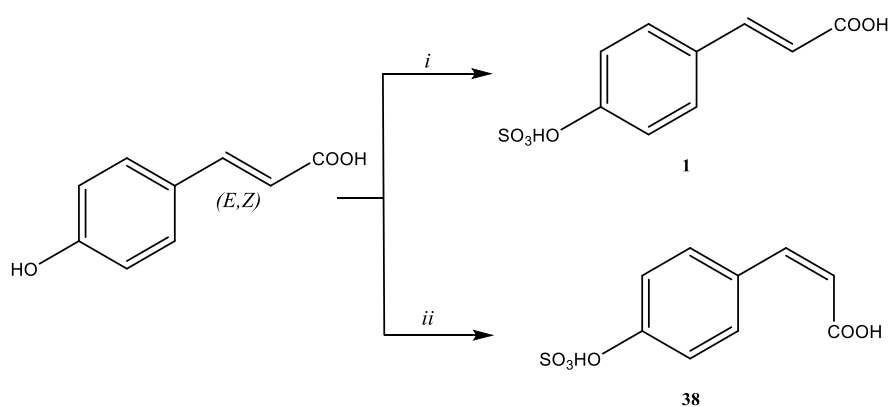
Chart 2. Salicylic acid derivatives (47, 48)

R= NH₂, NHCOCH₃

3.2 General chemistry

3.2.1 Synthesis of (*E*, *Z*) zosteric acid (1, 38)

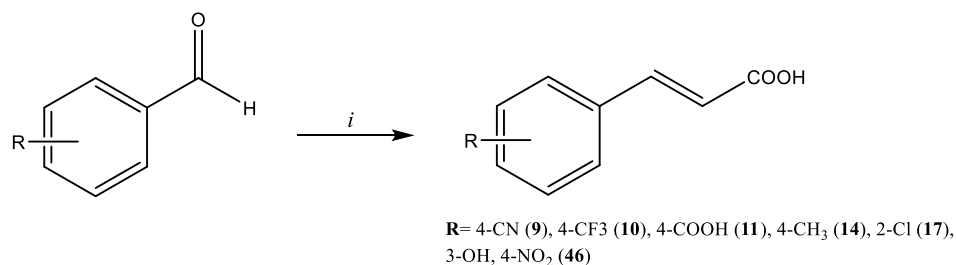
Zosteric acid was synthesized either in conventional conditions, as already described in a previous work [69], or under microwave irradiation. In this latter case, the yield is comparable to that obtained by conventional method but the reaction time is greatly reduced. The *cis* isomer **38** was obtained starting from *cis* 4-hydroxycinnamic acid **40** under microwave irradiation in the presence of sulphur trioxide pyridine complex in dry acetonitrile. The final products were isolated as sodium salts (Scheme 1).



Scheme 1. Reagents and conditions: *i*) Py·SO₃, dry DMF, 120 °C, 25 min, mw. *ii*) Py·SO₃, dry CH₃CN, 120 °C, 25 min.

3.2.2 Synthesis of substituted cinnamic acid derivatives (9-11, 14, 17, 46)

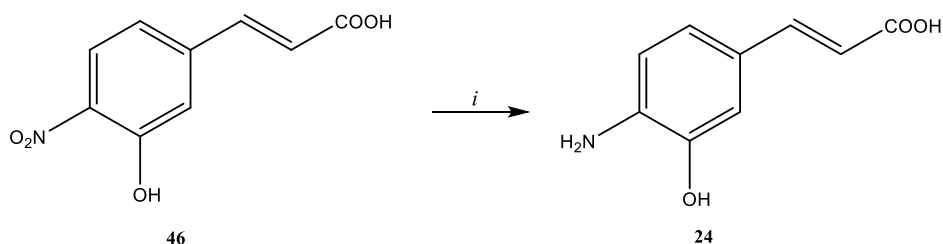
The majority of the substituted cinnamic acid derivatives were prepared in very good yield (> 90%) by Knoevenagel-Doebner procedure.[73] In detail, compound (9-11, 14, 17, 46) were obtained through a one-pot reaction between the suitable substituted benzaldehyde and malonic acid in refluxing pyridine to induce decarboxylation (Scheme 2). The *trans* geometries of the ethenyl π -bonds were confirmed by proton-proton coupling constants.



Scheme 2. Reagents and conditions: *i*) malonic acid, Py, piperidine (cat.), reflux, 80-180 min.

3.2.3 Synthesis of 3-hydroxy-4-aminocinnamic acid (24)

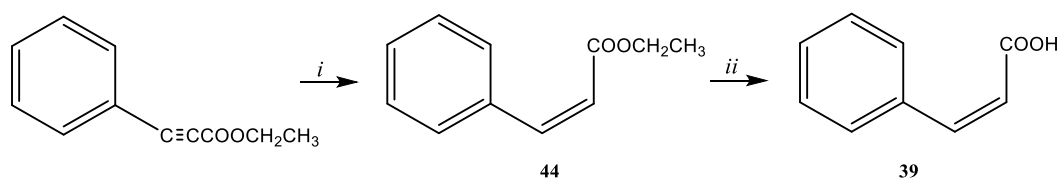
The 3-hydroxy-4-aminocinnamic acid **24** was prepared starting from the corresponding nitro derivative **46** by tin (II) chloride reduction in concentrated hydrochloric acid (Scheme 3).



Scheme 3. Reagents and conditions: *i*) SnCl_2 , conc. HCl, 80 °C, 4 h; 1 M NaOH up to pH = 4.6.

3.2.4 Synthesis of ethyl cinnamate (44) and *cis* cinnamic acid (39)

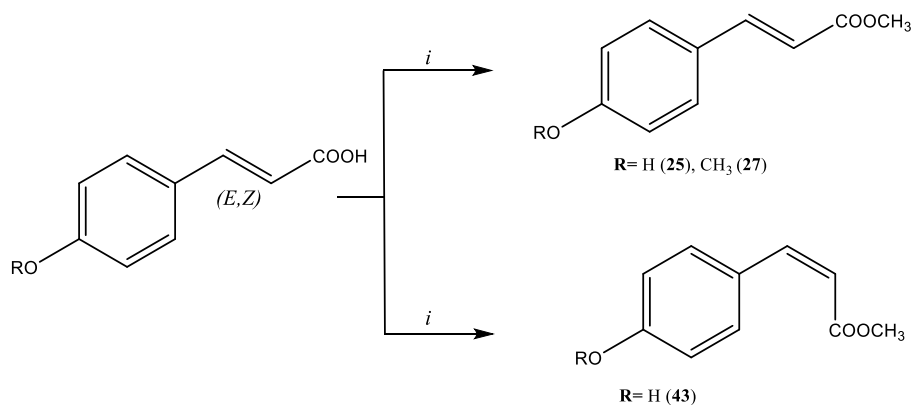
Cis cinnamic acid was synthesized from the commercially available ethyl phenylpropiolate. The subsequent hydrogenation of alkyne, in presence of Lindlar catalyst and pyridine in methanol, led to the corresponding *cis*-alkene **44**. The ester group was then hydrolyzed under alkaline condition to provide the *cis* cinnamic acid **39** (Scheme 4).[74]



Scheme 4. Reagents and conditions: *i*) Lindlar catalyst, H_2 , Py, MeOH, rt, 16 h; *ii*) 1 M NaOH, EtOH/THF (1:1), rt, 12 h.

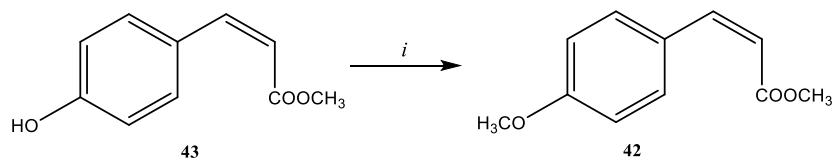
3.2.5 Synthesis of *trans* methyl coumarate (25), *trans* methyl 4-methoxycinnamate (27) and *cis* methyl coumarate (43)

Esters of cinnamic acid derivatives in *trans* (25, 27) or *cis* configuration 43 were prepared by Fischer esterification of the carboxylic group of the suitable starting material in methanol with sulfuric acid as catalyst (Scheme 5).



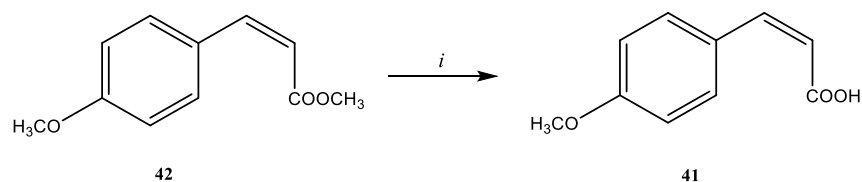
3.2.6 Synthesis of *cis* methyl 4-methoxycinnamate (42)

The protection of the hydroxyl group as methyl ether in the presence of iodomethane in dry *N,N*-dimethylformamide provided compound 42 (Scheme 6).[75]



3.2.7 Synthesis of *cis* 4-methoxycinnamic acid (**41**)

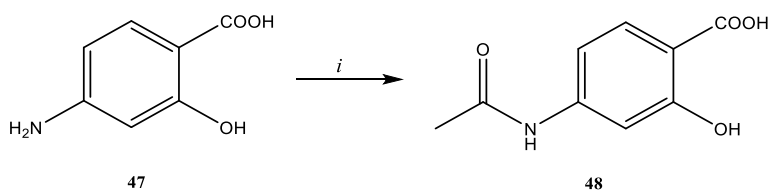
Hydrolysis of ester was performed in alkaline conditions to afford compound **41** (Scheme 7).



Scheme 7. Reagents and conditions: *i*) 1 M NaOH, EtOH, reflux, 2 h.

3.2.8 Synthesis of 4-acetamidosalicylic acid (**48**)

The commercially available 4-aminosalicylic acid **47** was protected at the amino function with acetic anhydride obtaining compound **48** (Scheme 8).



Scheme 8. Reagents and conditions: *i*) acetic anhydride, EtOH, 40 °C, 30 min.

3.3 Biological studies

All the molecules were submitted to biological assays using *Escherichia coli* as a model system for bacterial infections. They were tested at different concentrations starting from 1830 μM which was figured out as the best concentration at which zosteric acid performed its anti-biofilm activity.[69] The derivatives were tested in order to evaluate their ability to affect both planktonic growth and surface cell adhesion (**Appendix 1**). With the aim to identify common behaviors related to the biological activity of molecules with different structural features (TRENDS), planktonic growth and cells adhesion data were grouped to obtain a global picture of the anti-biofilm activity of each ZA related compound at the different concentrations (**Appendix 2**). Compounds showed:

- i) no biological activity (no reduction of the number of adhered cells and no planktonic growth effect);
- ii) anti-biofilm activity (reduction of the number of adhered cells and no planktonic growth effect);
- iii) increased biofilm formation (increase of the number of adhered cells and no planktonic growth effect);
- iv) transition from planktonic to biofilm mode of life (no reduction or increase of the number of adhered cells and planktonic growth effect);
- v) biocidal effect (reduction of the number of adhered cells and planktonic growth effect).

Each ZA related compound was also associated to a global anti-biofilm performance value (**Appendix 3**), considering the occurrence that ZA related compounds induced a different bacterial response depending on their concentration and the positive or negative contribution of each single concentration. A reduction of adhered cells was considered a positive contribution to the anti-biofilm performance value, while both the increase of the adhered cells and the decrease of planktonic growth were considered negative contributions.

3.3.1 Planktonic growth and cellular adhesion in the presence of DMSO

As DMSO was necessary to dissolve molecules in the aqueous medium, its impact on *E. coli* as possible carbon and energy source and on growth and cell adhesion was assessed. 3 % DMSO was not a carbon and energy source for the microorganisms. In addition, no significant differences among the number of planktonic and adhered cells with or without 3 % DMSO were observed (Table 2).

DMSO concentration	Planktonic growth (OD600/min) ($\times 10^3$)	Cells adhesion (No. adhered cells) ($\times 10^7$)
0 %	1.33 \pm 0.01 ^a	2.02 \pm 0.39 ^a
3 %	1.28 \pm 0.03 ^a	1.92 \pm 0.18 ^a

Table 2. Planktonic growth and cells adhesion with and without 3 % DMSO. According to post hoc analysis (Tukey's HSD, $p < 0.05$), data sharing the same letter indicates no significant difference.

3.3.2 Cellular growth with zosteric acid related compounds as the sole carbon and energy source

The ability of *E. coli* to grow with zosteric acid related compounds at 1830 μ M as the sole carbon and energy source was tested and compared with a positive control with glucose at the same concentration. *E. coli* in the positive control did not grow and showed a 600 nm optical density (OD600) lower than 0.05 after 48 h of incubation.

The minimum glucose concentration in a mineral medium that supported *E. coli* growth was 10 mM (OD600 = 0.201 \pm 0.007). Consequently, *E. coli* with glucose 10 mM was used as a positive control.

E. coli did not grow in the presence of each zosteric acid related compounds as the sole carbon and energy source and it showed a OD600 lower than 0.05 after 48 h of incubation with each molecules. All derivatives were submitted to further biological assays in order to evaluate their ability to affect both planktonic growth and surface cell adhesion.

3.3.3 Planktonic growth in the presence of zosteric acid related compounds

E. coli maximum specific growth rates in the presence of each zosteric acid related compounds at 0.183, 1.83, 18.3, 183 and 1830 μ M were calculated and compared with a negative control grown without the molecules by ANOVA statistic test (**Appendix 1**).

Molecules able to reduce the maximum specific growth rate respect to the negative control less than 10 % (0) were considered not affecting *E. coli* planktonic growth, between 10 % and 20 % (-) were

considered weakly affecting *E. coli* planktonic growth, between 20 % and 30 % (- -) were considered fairly affecting *E. coli* planktonic growth and more than 30 % (- - -) were considered highly affecting *E. coli* planktonic growth.

At the concentration of 0.183 μ M and 1.83 μ M no molecules were considered affecting *E. coli* growth since they showed any maximum specific growth rate values significantly different to the negative control ($p < 0.05$) and a percentage reduction of planktonic growth rate under 10 %.

At the concentration of 18.3 μ M forty-two molecules were considered not affecting *E. coli* planktonic growth. Among them:

- thirty-four molecules did not show growth rate values significantly different to the negative control ($p < 0.05$);
- six molecules (**2, 3, 8, 37, 42, 44**) showed maximum specific growth rate values significantly different to the negative control with a reduction of planktonic growth rate less than 10 % and therefore could be considered not affecting *E. coli* planktonic growth too;
- only compound **4** showed a reduction of planktonic growth rate between 10 % and 20 % and was considered weakly affecting *E. coli* planktonic growth.

At the concentration of 183 μ M thirty-three molecules were considered not affecting *E. coli* planktonic growth.

Among them:

- twenty-nine molecules did not show growth rate values significantly different to the negative control ($p < 0.05$);
- four molecules (**4, 5, 19, 24**) showed maximum specific growth rate values significantly different to the negative control but they presented a reduction of planktonic growth rate less than 10 % and therefore were considered not affecting *E. coli* planktonic growth too;

Ten molecules showed planktonic growth rate statistically different to the control and differently affected *E. coli* planktonic growth:

- nine molecules (**3, 6, 13, 25, 27, 30, 41, 43, 44**) showed a reduction of planktonic growth rate between 10 % and 20 % and were considered weakly affecting *E. coli* planktonic growth;
- compound **42** showed a planktonic growth rate reduction between 20 % and 30 % and was considered fairly affecting *E. coli* planktonic growth.

Finally, at the concentration of 1830 μ M, four molecules were considered not affecting *E. coli* planktonic growth.

Among them:

- compound **40** did not show growth rate values significantly different to the negative control ($p < 0.05$);
- three molecules (**24, 37, 38**) showed maximum specific growth rate values significantly different to the negative control but it presented a reduction of planktonic growth rate less than 10 % and therefore was considered not affecting *E. coli* planktonic growth too.

The remaining thirty-nine molecules showed a planktonic growth rate statistically different to the negative control and differently affected *E. coli* planktonic growth:

- nine molecules (**13, 16, 17, 20, 23, 27, 29, 35, 44**) showed a reduction of planktonic growth rate between 10 % and 20 % and were considered weakly affecting *E. coli* planktonic growth;
- eleven molecules (**2, 4, 5, 9, 12, 15, 18, 19, 21, 36, 41, 45**) showed a planktonic growth rate reduction between 20 % and 30 % and were considered fairly affecting *E. coli* planktonic growth;
- nineteen molecules (**3, 6-8, 10, 13, 14, 22, 25, 26, 28, 30-34, 39, 42, 43**) showed a planktonic growth rate reduction more than 30 % and were considered highly affecting *E. coli* planktonic growth.

3.3.4 Microplate-based cell adhesion assay in the presence of zosteric acid related compounds

The number of adhered cells in the presence of each zosteric acid related compound at 0.183, 1.83, 18.3, 183 and 1830 μ M was assessed quantitatively using fluorochrome labeled cells and compared to a negative control in the absence of any molecules by the ANOVA statistic test (**Appendix 1**).

Molecules able to reduce the number of adhered cells respect to the negative control less than 20 % (0) were considered not affecting *E. coli* cell adhesion, between 20 % and 30 % (-) were considered weakly affecting *E. coli* cell adhesion, between 30 % and 40 % (- -) were considered moderately affecting *E. coli* cell adhesion and more than 40 % (- - -) were considered highly affecting *E. coli* cell adhesion. Molecules that are able to increase the number of adhered cells respect to the negative control more than 20 % were coded +.

3.3.5 Biological activity of zosteric acid derivatives

With the aim to identify specific trends, planktonic growth and cells adhesion data were combined together to obtain an overall view of the biological activities of ZA derivatives at the different concentrations (**Appendix 2**).

Compounds showed five different behaviors related to their biological activities:

a) TREND 1

Five molecules (**5, 9, 19, 20, 36**) induced no biological activity at low and middle concentrations and transition from planktonic to biofilm mode of life (**19, 20, 36**) or biocidal effect at the maximum concentration (**5, 9**).

b) TREND 2

Eight molecules (**27, 29, 31-35, 45**) showed no biological activity at middle concentrations and transition from planktonic to biofilm mode of life (**27, 29, 35, 45**) or biocidal effect at the maximum concentration (**31-34**), but at the lowest concentration they promoted biofilm formation.

c) TREND 3:

Seventeen molecules (**2, 3, 6-8, 10, 11, 13-16, 18, 22, 23, 25, 26, 28**) had no biological activity at low concentration, showed an anti-biofilm activity at middle concentrations since significantly reduced the number of adhered cells without affecting planktonic growth and induced biocidal effect (**2, 3, 6-8, 10, 13-15, 18, 23, 25, 28**) or transition from planktonic to biofilm mode of life (**11, 16, 22, 26**) at the maximum concentration.

Among these:

- six molecules (**2, 10, 11, 13, 14, 23**) displayed an excellent anti-biofilm activity with a percentage reduction of adhered cells respect to the negative control more than 40 % (**14** maximum reduction = 75.4 %);
- seven molecules (**6, 8, 15, 16, 18, 25, 28**) displayed a moderate anti-biofilm activity with a percentage reduction of cell adhesion between 30 % and 40 %;
- two molecules (**22, 26**) showed a weak anti-biofilm activity.

Moreover, compound **4** showed a good anti-biofilm activity only at 1.83 μ M (maximum reduction = 39.1 %), since highest concentrations led to transition from planktonic to biofilm mode of life and biocidal effect.

At the lowest and the highest concentration only few molecules displayed a biological activity. At the concentration of 0.183 μM only two molecules (**3**, **12**) showed an interesting anti-biofilm activity with a percentage reduction of adhered cells more than 30 % (**3** maximum reduction at 1.83 μM = 38.8 %; **12** maximum reduction at 1.83 μM = 61.9 %), while at the concentration of 1830 μM only compound **37** showed anti-biofilm activity with a percent reduction of 63.3 %.

Molecules bearing different substituents at the *para* position on the phenyl ring (**2**, **3**, **4**, **6**, **7**, **8**, **10**, **11**, **12**, **13**, **14**) showed the best biological profile with an excellent or good activity in a wide range of concentrations. In any case, the reduction of adhered cells respect to the negative control was more than 37 % depending on the nature of the substituents (minimum reduction: 37.9 % in the presence of **8** at 18.3 μM ; maximum reduction: 75.4 % in the presence of **14** at 1.83 μM).

d) TREND 4

Nine molecules (**1**, **17**, **21**, **24**, **30**, **41-44**) showed a promising biological activity at middle concentrations but at the lowest concentration they promoted biofilm formation. Moreover, some of these molecules at the highest concentration induced the transition from planktonic to biofilm mode of life (**41**, **42**, **44**), biocidal effect (**30**) or both of them (**17**, **21**, **43**).

e) TREND 5

Compounds **38**, **39** and **40** showed particular behaviors and cannot be included in the previously trends. As for **38**, biofilm formation was promoted in a wide range of concentrations as well as for compound **39**. This latter showed an anti-biofilm activity only at 18.3 μM , while at the maximum concentration induced the transition from planktonic to biofilm mode of life. At last, molecule **40** showed a biological activity at the lowest concentration, had no anti-biofilm activity at middle concentrations and promoted biofilm formation at 1830 μM .

3.3.6 Anti-biofilm performance of zosteric acid derivatives

Beside the anti-biofilm activity, the global anti-biofilm performance of each compounds was also evaluated (**Appendix 3**). The anti-biofilm performance value was calculated as:

Anti-biofilm Performance = (sum of cell adhesion codes of all concentrations) - (sum of planktonic growth code of all concentrations)

This value included:

- i) the occurrence that ZA related compound induced a different bacterial response depending on the concentration;
- ii) the positive contribution of concentrations that reduce the number of adhered cells;
- iii) the negative contributions of concentrations that enhance the number of adhered cells;
- iv) the negative contribution of concentrations that reduce planktonic growth.

Molecules with an anti-biofilm performance:

- i) = 0 were considered globally lacking of anti-biofilm performance;
- ii) < 0 were considered globally able to exert an anti-biofilm activity (-1: low anti-biofilm performance; -2: moderate anti-biofilm performance; \leq -3: optimal anti-biofilm performance);
- iii) > 0 were considered globally able to improve biofilm performance (+1: slight improvement of biofilm performance; +2: moderate improvement of biofilm performance; \geq +3: optimal improvement of biofilm performance).

In details:

- four molecules (**5, 9, 16, 40**) presented anti-biofilm performance equal to 0;
- twenty molecules presented anti-biofilm performance < 0 (-1: **21**; -2: **4, 13, 15, 18, 25, 28**; \leq -3: **1, 2, 3, 6, 8, 10-12, 14, 17, 23, 24, 37**);
- twenty molecules presented anti-biofilm performance > 0 (+1: **20, 26, 33, 43, 44**; +2: **22, 29, 30, 35, 36, 45**; \geq +3: **19, 27, 31, 32, 34, 38, 39, 41, 42**).

3.4 Proteomic studies¹

Consistently with biological evaluation, the natural compounds, cinnamic acid and salicylic acid (used as reference compound), can be considered promising agents for preventive or integrative approach against biofilm formation and for the development of a new generation of anti-biofilm derivatives. Since the mechanism of action and the cellular target involved in their biological activity are still unknown, in this study an affinity chromatography proteomic approach coupled with a mass spectrometry analysis was employed to scan the entire *Escherichia coli* proteome with the aim to identify the molecular targets that interact with these molecules. In order to capture proteins of interest by affinity, this approach was based on a covalent immobilization on a pre-activated matrix (Sepharose 4 Fast Flow matrix, prepared with 6-aminohexanoic acid spacer arm and activated by esterification with N-hydroxysuccinimide) of 4-aminocinnamic **8** and 4-aminosalicylic acid **47** by an amidic covalent coupling. The functionalization of the solid support was demonstrated by fluorescence analysis. The mass spectrometry analysis of SDS-PAGE-resolved pull-down proteins (Figure 30) was used for target identification and revealed that both cinnamic acid and salicylic acid directly interact with the same protein WrbA (P0A8G6) in *E. coli* (Table 3). In addition, protein FkpA (P45523) and Tdh (P07913) were also identified as possible additional targets for salicylic acid (Table 3).

¹ An in-depth analysis and ‘Materials and methods’ are included in Cristina Cattò (DEFENS-UNIMI research unit) PhD thesis, entitled “New strategies based on natural compounds for controlling biofilm formation” (December, 2014).

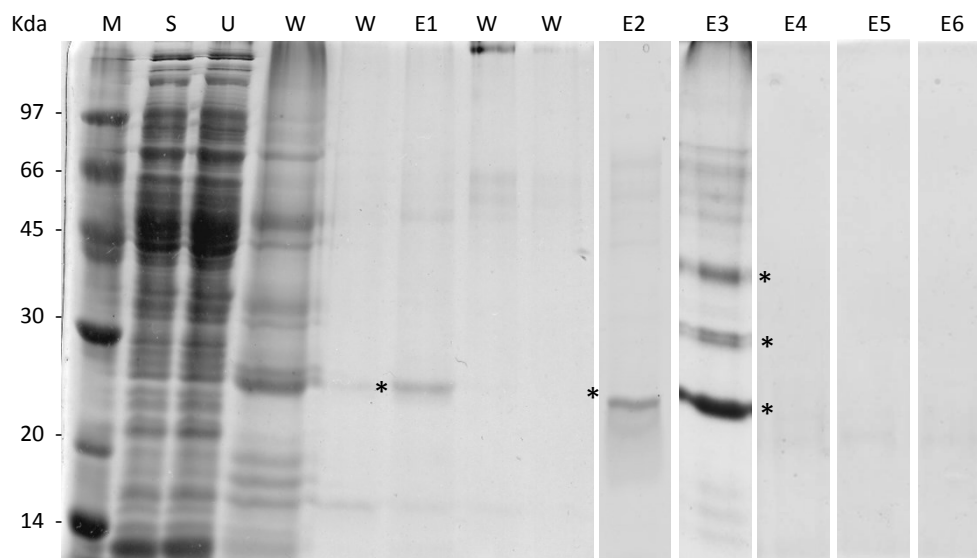


Figure 30. SDS-page analysis of the affinity chromatography of *E. coli* protein extract. Each gel is representative of three independent replicates. M: molecular mass marker; S: total soluble proteins from *E. coli* extract; U: proteins unbound; W: washing fraction; E: proteins bound to *p*-aminocinnamic acid/matrix and eluted with cinnamic acid (E1) and zosteric acid (E2), proteins bound to *p*-aminosalicylic acid/matrix and eluted with salicylic acid (E3), proteins bound to control matrix and eluted with cinnamic acid (E4), proteins bound to control matrix and eluted with zosteric acid (E5), proteins bound to control matrix and eluted with salicylic acid (E6).

Matrix ^a	Cmp ^b	Accession number ^c	Gene name ^d	Protein ^e	Score ^f	Coverage ^g
<i>p</i> -aminocinnamic acid/matrix	CA	P0A8G6	<i>wrbA</i>	NAD(P)H quinone dehydrogenase	189.78	70.2
<i>p</i> -aminocinnamic acid/matrix	ZA	P0A8G6	<i>wrbA</i>	NAD(P)H quinone dehydrogenase	684.32	71.72
<i>p</i> -aminosalicylic acid/matrix	SA	P0A8G6	<i>wrbA</i>	NAD(P)H quinone dehydrogenase	1079.55	71.72
<i>p</i> -aminosalicylic acid/matrix	SA	P45523	<i>fkpA</i>	FKBP-type peptidyl-prolyl <i>cis-trans</i> isomerase	156.99	43.33
<i>p</i> -aminosalicylic acid/matrix	SA	P07913	<i>tdh</i>	L-threonine 3-dehydrogenase	521.32	59.53

Table 3. Proteins identified by mass spectrometry analysis. a) the matrix from which the protein was eluted; b) the competitor used in the elution step; c) the alphanumeric unique protein sequence identifier; d) the gene name; e) the protein name provided by UniProtKB protein knowledgebase; f) the protein identification's SEQUEST HT Score; g) percentage of protein sequence covered by identified peptides (Coverage).

3.4.1 WrbA protein and supposed mechanism of action of cinnamic acid derivatives

WrbA-like proteins (tryptophan [W] repressor-binding proteins) are widely distributed flavoproteins and supposed to be implicated in defence against oxidative stress. Crystallographic studies reported that *E. coli* WrbA is characterized by a tetrameric quaternary structure with a hydrophobic active site pocket that provides an ideal stacking environment for aromatic moieties [77], indeed well adapted to accommodate compounds such as cinnamic acid and salicylic acid (Figure 31).

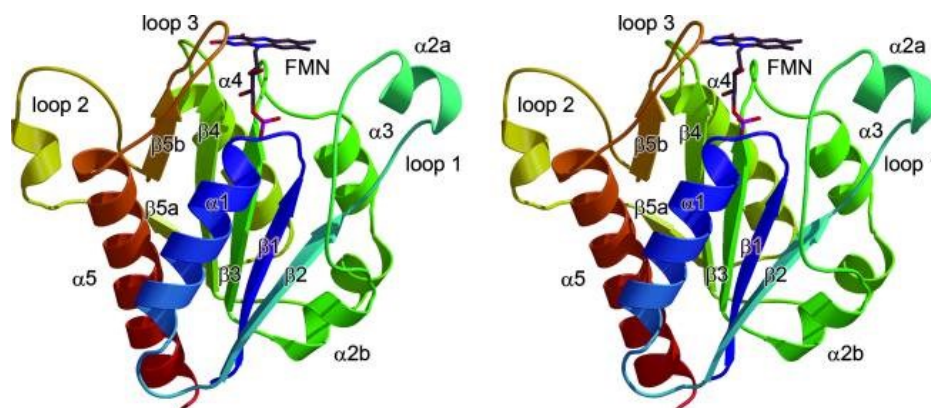


Figure 31. Cartoon representation of the WrbA monomer from *E. coli*. The stereo image of the protein chain shows the N terminus in blue and the C terminus in red. Strands of the central, parallel β -sheet and the surrounding α -helices are numbered according to their occurrence in the protein sequence. The flavin mononucleotide (FMN) cofactor is bound peripherally at the C-terminal end of the β -sheet. Protein Data Bank identifier [PDB ID] 3B61. [77]

WrbA is endowed with the NADH:quinone oxidoreductase (NQO) activity involved in the maintaining quinones in a fully reduced state.[78] Quinones are compounds generally tethered to the plasma membrane or freely traversing the lipid bilayer. Although these compounds are essential for normal electron transport by cycling between the oxidized (hydroquinone) state and the two-electron reduced (hydroquinol) state, it has been demonstrated that quinonoids also participate in deleterious redox cycling through direct interactions with single-electron acceptors such as O_2 , leading to the accumulation of reactive oxygen species (ROS) such as superoxide, hydrogen peroxide, and the hydroxyl radical responsible of devastating consequence in the cells.[79] In order to guard against the production of ROS from one-electron redox cycling, cells have evolved NQOs to maintain quinones in a reduced state as a measure of protection against oxidative stress. A previous study [71] demonstrated that zosteric acid makes *E. coli* cells more prone to accumulate ROS leading a stress condition to which bacterium responds by activating defensive mechanisms against oxidative damage.

Indeed, although further studies will be necessary, it can be hypothesized that cinnamic acid scaffold may negatively modulate the oxidoreductase activity of WrbA leading to a ROS accumulation inside cells affecting biofilm formation. Furthermore, recent data proved the ability of ROS to modulate quorum sensing and showed their important role in biofilm formation.[80] Finally, the upset of ROS level caused by the cinnamic acid scaffold might interfere with the quorum sensing signal destabilizing the biofilm formation.

In the past *E. coli* WrbA was reported to promote complex formation between the tryptophan repressor (TrpR) and its DNA operator sequences.[81] Subsequent experiments demonstrated that WrbA did not specifically bind to DNA and its involvement in transcription regulation was revoked. Anyway, although a direct connection to tryptophan repressor was retracted, a role in the tryptophan metabolism was considered possible especially related to the indole production. Indole is known as a metabolite of tryptophan which has recently been proved to participate in various aspects of bacterial life including virulence induction, cell cycle regulation, stress resistance, genetic stability, controlling metabolic feedback and it is also proposed to be a quorum sensing signal with an important role in biofilm formation process.[44, 82] It is generated by the hydrolyses of tryptophan due to the activity of the cytoplasmic enzyme tryptophanase. This reaction occurs exclusively in bacteria and in *E. coli* is catalysed by TnaA.[83] In particular, sigma factor sigma-38 (RpoS), a 37.8 kD protein in *E. coli*, appears to promote tryptophan degradation by inducing the tryptophanase gene *tnaA*, which results in the production of indole, and by stimulating expression of the WrbA protein, which might strengthen negative regulation of the *trp* biosynthetic operon by an unknown mechanism.[84, 85]

Moreover, it is reported that either high and low levels of indole can abolish the ability to increase biofilm formation, in a dose dependent manner and with a strain specific activity. In a previous study [71], it was found that *E. coli*, grown in the presence of zosteric acid, exhibited an enhanced tryptophanase activity and an increased amount of indole. Therefore, it can be hypothesized that cinnamic acid derivatives interacts with WrbA with subsequent consequences on the indole production. The blast search assay inside Bacteria and Fungi databases revealed that WrbA sequences exist in a diversity of microorganisms with a high percentage of identity, suggesting a potential role in the microorganism life, probably associated to the response against environmental stresses. Indeed, in support of these results, recent studies demonstrated that ZA is able to significantly reduce *Pseudomonas spp* biofilm [86] and *Candida albicans* biofilm [70].

Only related to salicylic acid, other two proteins were identified as possible molecular targets. In details, FkpA is a peptidyl-prolyl isomerase that in the *E. coli* periplasm was found to work in cooperation with other three proteins (PpiA, PpiD, and SurA) known as periplasmic *cis-trans* prolyl isomerases (PPIase) that facilitate the proper protein folding by increasing the rate of transition of proline residues between the *cis* and *trans* states. It is reasonable to suppose that salicylic acid may interact with FkpA altering the PPIase and/or chaperone activity and resulting in incorrect assembling of pili with consequences on biofilm formation.[87] The second protein by which salicylic acid seems to exert its anti-biofilm activity is Tdh, an L-threonine 3-dehydrogenase that catalyses the first step in the L-threonine degradation pathways in both prokaryotes and eukaryotes.[88] Threonine has been shown to have an observable effect on the *E. coli* motility, significantly promoting swimming and twitching motility at low concentrations and significantly inhibiting biofilm formation at higher concentration.[89]

Since salicylic acid interacts with different proteins, it probably has different cell targets. This is in line with the amount of researches present in the literature that report various effects of SA on bacterial biofilm, suggesting the presence of complex and overlapping regulatory networks controlling quorum sensing, motility and biofilm formation.

3.5 Discussion

Our studies involved the preparation and the biological evaluation of zosteric acid analogues characterized by substitutions at different position on the phenyl ring as well as a variety of side chains. This investigation highlighted features that could be useful for the design of a new generation of derivatives, with the aim to find compounds endowed with a better antifouling activity compared to zosteric acid.

As for biological evaluation, all the tested compounds showed a non-linear response pattern in which the best anti-biofilm activity of the cinnamic acid derivatives in the range of sub-lethal concentrations was obtained at a specific threshold level. The results showed that the most common and generally applicable dose–response model is the hormetic U-shaped biphasic model rather than the linear one.[90] This dose-response behavior has been demonstrated by several published studies [91, 92, 93] and followed a parabola-like shape profile in which the minimum point of the response corresponds to the minimum number of adhered cell and thus to the best activity for each compound.

In line with the obtained results, derivatives showed different biological activities depending on their concentration. At the highest concentrations, it was found that most molecules inhibited biofilm formation and drastically reduced planktonic growth. Therefore, it was reasonable to suppose that the suppression of biofilm formation was a result of the inhibition of bacterial growth rather than from specific anti-biofilm effects of the substances. Other molecules at the highest concentrations enhanced biofilm formation and also reduced bacteria planktonic growth. In this case the transition to the sessile mode of life was assumed as a protective response to survival in hostile environments. Moreover, the movement of cells toward surfaces could be considered the step immediately before the killing effect as a kind of protecting way against hard stress condition.[94] At the lowest concentrations, an increase of biofilm formation was also observed for many of the molecules investigated. Low concentrations of small molecules released as exudates by plants can act as chemical signals inducing bacteria to colonize specific plant areas developing a complex biofilm that positively interacts with the plant itself. Since the present work highlighted that the zosteric acid sulfate ester was not essential for its antifouling properties, the cinnamic acid scaffold was identified as fundamental for the anti-biofilm activity.

Indeed, cinnamic acid **3**, a natural compound obtained by cinnamon (well-known in literature for its various pharmacological activities, including antimicrobial properties), has shown an interesting anti-

biofilm activity at a 1000-fold lower inhibitory concentration (sub-lethal concentration) than zosteric acid with a mechanism of action not directly related to quorum sensing (for detail see ‘Paragraph 3.8’). The substitution pattern of the phenyl ring and the nature of the substituents were found to have a significant effect on the biofilm inhibitory activity. In the first instance, a broad variety of substituents with different electronic and steric properties were introduced at position 4 on the phenyl ring: compounds (**2**, **4**, **6**, **8**, **10-14**) showed an interesting activity (Trend 3) compared to the unsubstituted cinnamic acid **3**, meanwhile the presence of nitro **5** and cyano **9** groups caused a loss in activity (Trend 1). Comparing the derivatives bearing a hydroxyl group (**2**, **16**), as well as the chlorine atom (**6**, **18**), respectively at position 4 and 3 on the phenyl ring, highlighted that the substitution at the *para* position was preferred (**2** and **6** were more active than **16** and **18**) although following the same trend. On the contrary the substitution at position 2 was not well tolerated. Indeed, as for the *m*-chloro derivative **17**, the activity was reduced 10-fold compared to the **6**, while in the other cases the biological activity was almost completely abolished. To determine whether the introduction of a second substituents on the phenyl ring would enhance activity, a series of disubstituted derivatives (**20-24**) were synthesized. In general, each disubstituted compound was found to have a different behavior and a less anti-biofilm activity compared to the corresponding monosubstituted. This effect was most evident for the 3,4-dichlorocinnamic acid **22**, whose activity was 10-fold lower than the monosubstituted counterpart **6**. Following on from this, the side chain modifications were also explored. In general, the unsubstituted compounds having the carboxylic function protected as esters (**26**, **28**) showed lower activity in comparison with cinnamic acid **3**, and in particular the ethyl ester **28** was less active than methyl ester **26**. Besides, among the *para*-substituted cinnamic acid esters (**25**, **27**), the presence of a hydroxyl group **25** seemed to be important for the antibiofilm activity, since the corresponding 4-methoxy derivative **27** was inactive. Moreover, derivatives bearing an aldehyde (**31**, **32**) or an alcohol (**33**) in replacement of the carboxylic functionality were inactive (Trend 2) confirming that the carboxylic moieties was essential for a good anti-biofilm activity. To investigate the importance of the configuration of the double bond, *cis* derivatives (**38-44**) were synthesized and the majority of these were found to have a different behavior (Trend 4) compared to the *trans* counterparts. Interestingly, exceptions to this rule were the *cis* isomers of zosteric acid **38** and cinnamic acid **39**, that had lost their anti-biofilm activity (Trend 5). Additionally, specific concentrations of **38** and **39** seemed to enhance the biofilm formation.

Similarly, some saturated derivatives (**34-37**) were chosen to investigate the role of the double bond. All the compounds exhibited the same trend (Trend 2) except for compound **37**, a catechol derivative, that did not follow this general behavior (Trend 3) probably due to a different mechanism of interaction (as compound **23**).

Finally, coumarin **45**, which could be considered the cyclic derivative of **3**, was unable to inhibit the biofilm growth, confirming the essential role of the side chain in *trans* configuration.

It is noteworthy that growth curve analysis revealed that in most cases compounds have a broad range of concentrations in which they exhibited anti-biofilm activity (not due to a bactericidal effect). Therefore, the evaluation of the anti-biofilm performance could be a useful tool to draw some additional observations.

Generally, cinnamic acid derivatives followed the same behaviors described for the anti-biofilm activity, with some exceptions:

- derivatives **4** and **13**, which have a methoxy group and a fluorine atom in the *para* position on the phenyl ring respectively, showed anti-biofilm performances slightly lower than that of the cinnamic acid **3**, which was still a positive result;
- compound **17** anti-biofilm performance turned out to be better than that of the corresponding analogue **6**, in which the chlorine atom was at position 4 on the phenyl ring. However, the general trend, according to which the substitution at position 2 was not well tolerated, was confirmed;
- the antibiofilm performance of the disubstituted halogen derivatives (**20-22**) was in general lower than that of the monosubstituted counterparts as well as its anti-biofilm activity. The same was not observed for compounds (**23**, **24**), which were characterized by electron donating substituents, whose monosubstituted analogues showed a decreased anti-biofilm performance;
- the esters **26** and **28** showed the opposite behavior, since the methyl ester **26** showed an anti-biofilm performance lower than that of the ethyl ester **28**;
- the majority of *cis* derivatives (**38-44**) were found to have a global anti-biofilm performance promoting biofilm formation.

Among the tested molecules, six molecules (**2**, **3**, **10**, **11**, **23**) had the most interesting antibiofilm performance by showing antibiofilm activity in a wide range of concentrations with maximum at micromolar level and with no effect on planktonic growth.

Therefore, in the light of all aforementioned considerations, at physiological conditions (pH = 7.4 used for biological assays), inhibition of cell adhesion appeared to be the result of molecules negative charge. An overall view of the obtained results highlighted that compounds typically containing a carboxylate anion in a conjugated system, showed the best anti-biofilm activity. Derivatives with *para* substituents on the phenyl ring displayed different degrees of *E. coli* inhibition. Since the strength of a carboxylic acid depends mainly on the extent of its ionization, analogues **5** and **9** with strong electron-withdrawing groups on the phenyl ring (nitro and cyano groups, respectively), reduced the nucleophilic character of the oxygen atoms, leading to loss of activity. Similarly, compounds bearing moderate and strong electron-releasing groups enhance the negative charge and exhibited good values of inhibition. Moreover, it was demonstrated that also the position of the anionic charge was crucial: compounds in which the conformation of the double bond was varied (*trans/cis* isomers), as well as saturated derivatives, decreased the ability to inhibit biofilm formation probably due the impairment of the conjugated aromatic system in delocalizing the negative charge that not allow electrons to move freely.

3.6 Final remarks

The ability to inhibit biofilm formation of a series of cinnamic acid related derivatives was evaluated in order to identify the structural requirements essential for their activity and to select the best candidates for the subsequent grafting to a polymeric materials.

An exhaustive biological evaluation pointed out that the synthesized compounds are endowed with different behaviors depending on their concentrations. In most cases, the tested compounds were found to be more active than zosteric acid at lower concentrations. In summary, the carboxylic acid moiety conjugated to a double bond in *trans* configuration is an essential requirement for the inhibition of the biofilm growth. Side-chain modifications led to derivatives showing a lower activity by comparison with the reference compound suggesting that the side chain has a key-role for the biological activity. Moreover, the anti-biofilm activity of the tested compounds in general decrease by the introduction of substituents at different position on the phenyl ring: only the substitution at the *para* position is well tolerated and could be considered a good point for the coupling to the polymer. It is also interesting to observe the different effect of electron donating and electron withdrawing groups on the phenyl ring, indicating that the electron density of the carboxylate may be important for the interaction with the target.

Finally, in order to identify targets that directly interact with cinnamic acid derivatives and salicylic acid, affinity purification experiments of proteins from *E. coli* extracts were performed. Mass spectrometry analysis of SDS-PAGE-resolved pull-down proteins reveal that both cinnamic acid and salicylic acid in *E. coli* directly interact with the same protein WrbA, which is involved in the biofilm formation process, leading to an altered production of both indole and ROS. Moreover, protein FkpA and Tdh were also identified as possible target for salicylic acid, suggesting the presence of complex and overlapping regulatory networks controlling quorum sensing, motility and biofilm formation. Many interpretations about the effect of interaction of cinnamic acid and salicylic acid with these proteins are possible and further experiments are necessary to clarify this question.

In conclusion, the cinnamic acid scaffold can be considered the starting point for the development of a new generation of derivatives characterized by improved activity to study and modulate bacterial adhesion.

In particular, two terms (**8**, **47**), able to significantly reduced biofilm formation, were selected as the best candidates to obtain a novel anti-biofilm material, due to the presence of an amine at the *para* position on the phenyl ring (which allowed the covalent linkage to the polymeric surface), although some derivatives (**11**, **12**, **14**) had shown a better anti-biofilm activity compared to them.

3.7 Experimental

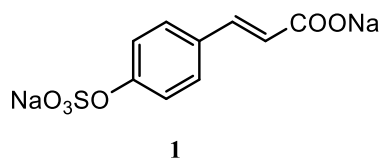
3.7.1 Chemistry

3.7.1.1 Materials and methods

All the reagents including solvents were purchased from Sigma-Aldrich and were used without any further purification. The reactions involving air-sensitive reagents were performed under nitrogen atmosphere and anhydrous solvents were used when necessary. The Biotage-Initiator microwave synthesizer was used. The course of the reaction was monitored by thin layer chromatography (TLC) analysis on aluminium-backed Silica Gel 60 plates (0.2 mm, Merck) and were visualized under a UV lamp operating at wavelengths of 254 and 365 nm. Visualization was aided by opportune staining reagents. Intermediates and final compounds were purified by flash chromatography using Merck Silica Gel 60 (70-230 mesh). The purity of final compounds were determined by HPLC analysis and were > 95 %. ^1H and ^{13}C NMR spectra were recorded at room temperature on a Varian 300 MHz Oxford instrument. CDCl_3 , CD_3OD , D_2O , acetone- d_6 and DMSO- d_6 were used as deuterated solvents for all spectra run. Chemical shifts are expressed in ppm from tetramethylsilane resonance in the indicated solvent (TMS: 0.0 ppm) and coupling constants (J-values) are given in Hertz (Hz). ^1H NMR data are reported in the following order: ppm, multiplicity (s, singlet; d, doublet; t, triplet; q, quartet; m, multiplet; br, broad), and number of protons. Melting points and NMR data are consistent with literature data. The ionization constants and lipophilicity parameters of zosteric acid were determined at 25°C by potentiometric titration with the GlpK_a apparatus (Sirius Analytical Instruments Ltd., Forest, Row, East Sussex, UK).

3.7.1.2 Experimental procedures

Synthesis of *trans* zosteric acid sodium salt **1** under microwave irradiation



In a microwave vessel, to a solution of *trans* coumaric acid **2** (50 mg, 0.30 mmol) in dry pyridine (1.5 mL), sulphur trioxide pyridine complex $\text{Py}\cdot\text{SO}_3$ (145 mg, 0.91 mmol) was added under an inert atmosphere. The resulting mixture was irradiated in a microwave synthesizer at 300 Watts at the temperature of 125°C for 25 minutes. After cooling, the solvent was evaporated under reduced pressure. Then 1N NaOH was added dropwise to pH=7. The resulting mixture was extracted with dichloromethane (3 x 2 mL) and the aqueous phase was evaporate to dryness. The residue was treated with methanol (5 mL) and the undissolved material filtered out. The evaporation of solvent provided compound **1**.

Yield: 90 %. Old-rose solid. $^1\text{H NMR}$ (D_2O): 6.33 (d, 1H, CH, $J=16.2$), 7.16 (d, 2H, ArH, $J=8.8$), 7.22 (d, 1H, CH, $J=16.2$), 7.48 (d, 2H, ArH, $J=8.8$). $^{13}\text{C NMR}$ (D_2O): 121.7, 121.8, 124.0, 129.1, 129.2, 133.1, 140.1, 152.0, 175.4.

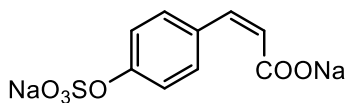
Physiochemical profiling

A weighted sample of **1** (10-25 mg) was supplied manually whereas the diluent and all the other reagents were added automatically. Zosteric acid was solubilized in water and acidified with 0.1 M HCl to pH =1.8. The solutions were then titrated with standardized 0.1 M KOH up to a pH of 12.2. Bjerrum difference plots were deduced from each titration and used to calculate precise pK value. To obtain lipophilicity parameters, separate titrations of the compounds were carried out using various volumes of n-octanol. In the presence of n-octanol, the pK value shifts as a consequence of the partitioning of the substance into the organic phase, allowing a new p_oK constant to be determined. These shifts in the pK values were used to determine log P. All measurements were performed in triplicate.

pK_a (20 °C): 4.261 ± 0.18

log P (20 °C): 0.250 ± 0.081

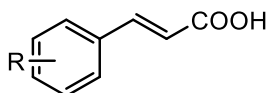
Synthesis of *cis* zosteric acid sodium salt **38** under microwave irradiation

**38**

In a microwave vessel, to a solution of *cis* coumaric acid **40** (100 mg, 0.61 mmol) in dry acetonitrile (1.5 mL), sulphur trioxide pyridine complex $\text{Py}\cdot\text{SO}_3$ (194 mg, 1.22 mmol) was added under an inert atmosphere. The resulting mixture was irradiated in a microwave synthesizer at 300 Watts at the temperature of 120°C for 25 minutes. After cooling, the solvent was evaporated under reduced pressure. Then 1N NaOH was added dropwise to pH=7. The resulting mixture was extracted with dichloromethane (3 x 2 mL) and the aqueous phase was evaporate to dryness. The residue was treated with methanol (5 mL) and the undissolved material filtered out. The evaporation of solvent provided compound **38**.

Yield: 50 %. Brown solid. $^1\text{H NMR}$ (CD_3OD): 6.44 (d, 1H, CH, $J=12.4$), 7.30 (d, 2H, ArH, $J=8.8$), 7.44 (d, 1H, CH, $J=12.4$), 7.52 (d, 2H, ArH, $J=8.8$). $^{13}\text{C NMR}$ (DMSO-d_6): 121.1, 125.3, 128.7, 131.2, 139.0, 154.8, 170.9. **HPLC**: Ascentis RP (15 cm x 4.6 mm, 2.7 μm) $\text{H}_2\text{O}-\text{CH}_3\text{CN}$ (0.1 % trifluoroacetic acid) 70-30, 1 mL min^{-1} , 254 λ , $t_{\text{R}} = 1.603$ (starting material **40**: $t_{\text{R}} = 2.407$). **LCMS** (ESI+) $m/z = 289$ $[\text{M}+\text{H}]^+$.

General procedure A for the synthesis of substituted cinnamic acids (**9-11, 14, 17, 46**)



R= 4-CN (**9**), 4- CF_3 (**10**), 4-COOH (**11**), 4- CH_3 (**14**),
2-Cl (**17**), 3-OH, 4- NO_2 (**46**)

To a solution of the suitable substituted benzaldehyde (1 mmol) in pyridine (1 mL), malonic acid (2.20 mmol) and piperidine (0.2 mmol) were added. The reaction mixture was stirred under reflux for a period of time different from each substrates (80-180 min) and then cooled to room temperature. The solution was poured into 2 N ice-cold aqueous HCl (2 mL) and the precipitate was collected by filtration, washed with water and dried under vacuum.

4-cyanocinnamic acid 9. Yield: 60 %. White solid. **TLC**: DCM/MeOH (9:1) $R_f = 0.37$. **M.p.**: 245-249 °C. $^1\text{H NMR}$ (DMSO-d₆): 6.70 (d, 1H, CH, J=16.2), 7.62 (d, 1H, CH, J=16.2), 7.83-7.90 (m, 4H, ArH). $^{13}\text{C NMR}$ (DMSO-d₆): 112.8, 119.3, 123.5, 129.5, 133.4, 139.5, 142.6, 167.8.

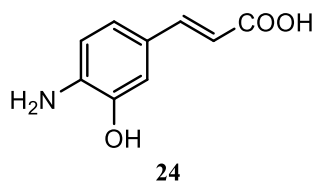
4-trifluoromethylcinnamic acid 10. Yield: 66 %. White solid. **TLC**: DCM/MeOH (9:1) $R_f = 0.38$. **M.p.**: 202-205 °C. $^1\text{H NMR}$ (DMSO-d₆): 6.67 (d, 1H, CH, J=15.9), 7.65 (d, 1H, CH, J=15.9), 7.75 (d, 2H, ArH, J=8.4), 7.91 (d, 2H, ArH, J=8.4). $^{19}\text{F NMR}$ (DMSO-d₆): -62 (s, 3F). $^{13}\text{C NMR}$ (DMSO-d₆): 122.8, 126.3, 129.5, 130.7, 139.0, 142.7, 167.8.

4-carboxycinnamic acid 11. Yield: 75 %. White solid. **TLC**: DCM/MeOH (9:1) $R_f = 0.12$. **M.p.**: 250-260 °C. $^1\text{H NMR}$ (DMSO-d₆): 6.62 (d, 1H, CH, J=15.9), 7.62 (d, 1H, CH, J=15.9), 7.78 (d, 2H, ArH, J=8.1), 7.93 (d, 2H, ArH, J=8.1). $^{13}\text{C NMR}$ (DMSO-d₆): 122.5, 128.9, 130.4, 132.5, 139.0, 143.3, 167.5, 168.0.

4-methylcinnamic acid 14. Yield: 70 %. White solid. **TLC**: DCM/MeOH (9:1) $R_f = 0.52$. **M.p.**: 196-198 °C. $^1\text{H NMR}$ (DMSO-d₆): 2.29 (s, 3H, CH₃), 6.45 (d, 1H, CH, J=15.9), 7.19 (d, 2H, ArH, J=7.8), 7.53 (d, 2H, ArH, J=7.8), 7.54 (d, 1H, CH, J=15.9), 12.33 (br s, 1H, COOH). $^{13}\text{C NMR}$ (DMSO-d₆): 21.7, 118.8, 128.8, 130.2, 132.2, 140.8, 144.6, 168.4.

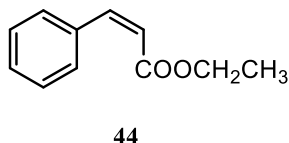
2-chlorocinnamic acid 17. Yield: 50 %. White solid. **TLC**: DCM/MeOH (9:1) $R_f = 0.53$. **M.p.**: 207-209 °C. $^1\text{H NMR}$ (CDCl₃): 6.46 (d, 1H, CH, J=15.9), 7.27-7.38 (m, 2H, ArH), 7.44 (dd, 1H, ArH, J=1.5, J=6.9), 7.65 (dd, 1H, ArH, J=1.5, J=6.9), 8.22 (d, 1H, CH, J=15.9). $^{13}\text{C NMR}$ (DMSO): 123.0, 128.5, 129.0, 130.6, 132.4, 132.5, 134.2, 139.4, 167.8.

3-hydroxy-4-nitrocinnamic acid 46. Yield: 72 %. Yellow solid. **TLC**: DCM/MeOH (9:1) $R_f = 0.45$. **M.p.**: 246-247 °C. $^1\text{H NMR}$ (CD₃OD): 6.62 (d, 1H, CH, J=15.9), 7.28 (d, 1H, ArH, J=8.7), 7.36 (s, 1H, ArH), 7.63 (d, 1H, CH, J=15.9), 8.10 (d, 1H, ArH, J=8.7). $^{13}\text{C NMR}$ (DMSO-d₆): 119.2, 119.5, 123.8, 137.6, 141.5, 142.3, 153.0, 167.7.

Synthesis of 3-hydroxy-4-aminocinnamic acid 24

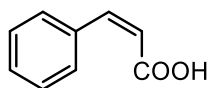
To 3-hydroxy-4-nitrocinnamic acid **46** (500 mg, 2.39 mmol) in 37 % HCl was added SnCl₂ (1.360 g, 7.17 mmol) and then the mixture was stirred at 80°C for 4 hours. The precipitate was filtered off, washed with cold EtO₂ (3 x 1 mL) and dried. Therefore, the aqueous layer was basified with 30 % NaOH (up to pH = 4.5) and then extracted with ethyl acetate (6 x 3 mL). The organic layer was dried over anhydrous Na₂SO₄, filtered and concentrated under reduced pressure to give compound **24**.

Yield: 83 %. Brown solid. **TLC**: DCM/MeOH (9:1) $R_f = 0.21$. **¹H NMR** (CD₃OD): 6.13 (d, 1H, CH, J=15.9), 6.67 (d, 1H, ArH, J=7.8), 6.88 (d, 1H, ArH, J=7.8), 6.93 (s, 1H, ArH), 7.50 (d, 1H, CH, J=15.9). **¹³C NMR** (DMSO-d₆): 112.9, 113.4, 114.1, 122.8, 123.0, 140.9, 144.4, 145.9, 168.9.

Synthesis of *cis* ethyl cinnamate 44

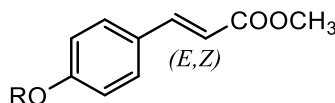
To a stirred solution of the commercially available ethyl phenylpropiolate (300 mg, 1.72 mmol) in methanol (4 mL) were added Lindlar catalyst (5 % Pd on CaCO₃ poisoned with lead) and pyridine (0.15 mL, 1.72 mmol). The reaction mixture was hydrogenated at room temperature for 3 hours. At the end of the reaction, the catalyst was filtered off through a Celite pad and the solvent was concentrated under reduced pressure. The crude was purified by column chromatography (cyclohexane/ethyl acetate 95:5) to afford compound **44**.

Yield: 51 %. Colourless oil. **TLC**: cyclohexane/ethyl acetate (9.5:0.5) $R_f = 0.39$. **¹H NMR** (CDCl₃): 1.25 (t, 3H, CH₃, J=7.2), 4.19 (q, 2H, CH₂, J=7.2, J=14.1), 5.97 (d, 1H, CH, J=12.6), 6.96 (d, 1H, CH, J=12.6), 7.34-7.36 (m, 3H, ArH), 7.58-7.59 (m, 2H, ArH). **¹³C NMR** (CDCl₃): 14.4, 60.5, 120.1, 128.2, 129.2, 130.0, 135.1, 143.3, 166.5.

Synthesis of *cis* cinnamic acid 39**39**

To a stirred solution of *cis* ethyl cinnamate **44** (100 mg, 0.57 mmol) in ethanol (1 mL) and tetrahydrofuran (1 mL), 1 M aqueous solution of NaOH (1 mL) was added. The solution was stirred at room temperature for 12 hours. The reaction was monitored by TLC until completion, then the solvent was evaporated and water (2 mL) was added. The aqueous layer was acidified to pH = 1 with 2 N HCl and then extracted with ethyl acetate (3 x 1 mL). The combined organic layers were washed with brine, dried over anhydrous sodium sulfate and the solvent was evaporated under reduced pressure. The crude was purified by flash chromatography eluting dichloromethane/methanol (9.5:0.5) to afford compound **39**.

Yield: 93 %. Colourless oil. **TLC**: DCM/MeOH (9.5:0.5) $R_f = 0.18$. **$^1\text{H NMR}$** (CDCl_3): 5.98 (d, 1H, CH, $J=12.6$), 7.08 (d, 1H, CH, $J=12.6$), 7.36-7.39 (m, 3H, ArH), 7.60-7.64 (m, 2H, ArH). **$^{13}\text{C NMR}$** (CDCl_3): 118.9, 128.3, 129.6, 130.2, 134.6, 145.9, 170.1.

General procedure B for the esterification of cinnamic acid derivatives (25, 27, 43)

R = H (*trans* **25**, *cis* **43**), CH_3 (*trans* **27**)

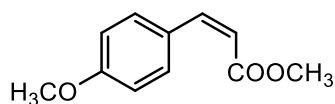
The suitable cinnamic acid (1 mmol) was dissolved in methanol (1 mL) and 96% H_2SO_4 (0.13 mL) was added dropwise. The obtained solution was refluxed for 1 hour. Then, the solvent was removed, the residue was diluted with ethyl acetate (1 mL), washed with water (1 x 2 mL) and a saturated solution of sodium hydrogencarbonate (1 x 2 mL). The organic layer was dried over anhydrous Na_2SO_4 and concentrated *in vacuo*.

trans methyl coumarate **25**. Quantitative yield. White solid. **TLC**: DCM/MeOH (9.5:0.5) $R_f = 0.62$. **M.p.**: 139-140 °C. **$^1\text{H NMR}$** (CDCl_3): 3.81 (s, 3H, CH_3), 6.30 (d, 1H, CH, $J=16.2$), 6.87 (d, 2H, ArH, $J=8.7$), 7.41 (d, 2H, ArH, $J=8.7$), 7.65 (d, 1H, CH, $J=16.2$). **$^{13}\text{C NMR}$** (CDCl_3): 55.1, 114.9, 116.2, 127.0, 130.3, 145.4, 158.5, 168.8.

trans methyl 4-methoxycinnamate 27. Quantitative yield. White solid. TLC: cyclohexane/ethyl acetate (7:3) $R_f = 0.55$. M.p.: 88-90 °C. $^1\text{H NMR}$ (CDCl_3): 3.80 (s, 3H, CH_3), 3.84 (s, 3H, CH_3), 6.31 (d, 1H, CH, $J=16.2$), 6.90 (d, 2H, ArH, $J=8.7$), 7.47 (d, 2H, ArH, $J=8.7$), 7.65 (d, 1H, CH, $J=16.2$). $^{13}\text{C NMR}$ (CDCl_3): 51.5, 55.8, 114.0, 115.2, 127.1, 130.0, 145.3, 161.7, 169.1.

cis methyl coumarate 43. Quantitative yield. White solid. TLC: DCM/ethyl acetate (8:2) $R_f = 0.58$. M.p.: 86-88 °C. $^1\text{H NMR}$ (CDCl_3): 3.80 (s, 3H, CH_3), 5.32 (br s, 1H, OH), 6.30 (d, 1H, CH, $J=16.2$), 6.85 (d, 2H, ArH, $J=8.5$), 7.43 (d, 2H, ArH, $J=8.5$), 7.64 (d, 1H, CH, $J=16.2$). $^{13}\text{C NMR}$ (DMSO-d_6): 51.9, 114.6, 116.4, 125.7, 131.0, 145.4, 160.5, 167.7.

Synthesis of *cis* methyl 4-methoxycinnamate 42

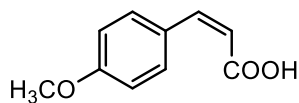


42

To a solution of the required methyl coumarate **43** (500 mg, 2.80 mmol) in dry *N,N*-dimethylformamide (1.5 mL), anhydrous potassium carbonate (580 mg, 4.20 mmol) and iodomethane (0.26 mL, 4.20 mmol) were added under an inert atmosphere. The reaction mixture was stirred at reflux for 1.5 hours. After the evaporation of *N,N*-dimethylformamide, the resultant residue was extracted with ethyl acetate (3 x 2 mL) and washed with brine (1 x 2 mL). The collected organic phase was dried over anhydrous sodium sulfate, filtered and the solvent was evaporated under reduced pressure. The crude was purified by flash chromatography (cyclohexane/ethyl acetate 7:3) to provide compound **42**.

Yield: 94 %. White solid. TLC: cyclohexane/ethyl acetate (7:3) $R_f = 0.54$. $^1\text{H NMR}$ (CDCl_3): 3.79 (s, 3H, CH_3), 3.83 (s, 3H, CH_3), 6.31 (d, 1H, CH, $J=16.2$), 6.90 (d, 2H, ArH, $J=8.7$), 7.47 (d, 2H, ArH, $J=8.7$), 7.65 (d, 1H, CH, $J=16.2$). $^{13}\text{C NMR}$ (CDCl_3): 51.5, 55.8, 114.0, 115.2, 127.1, 130.0, 145.3, 161.7, 169.1.

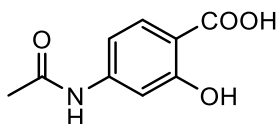
Synthesis of *cis* 4-methoxycinnamic acid **41**

**41**

To a stirred solution of *cis* methyl 4-methoxy cinnamate **42** (500 mg, 2.60 mmol) in ethanol (1mL), 1 M aqueous solution of NaOH (1 mL) was added. The solution was stirred at reflux for 2 hours. The reaction was monitored by TLC until completion, then the solvent was evaporated and water (2 mL) was added. The aqueous layer was acidified to pH = 1 with 2 N HCl and then extracted with ethyl acetate (3 x 1 mL). The combined organic layers were washed with brine, dried over anhydrous sodium sulfate and the solvent was evaporated under reduced pressure. The crude was purified by flash chromatography eluting with dichloromethane/methanol (9:1) to afford product **41**.

Quantitative yield. White solid. **TLC**: DCM/MeOH (9:1) $R_f = 0.46$. **M.p.**: 64-66 °C. **¹H NMR** (CDCl₃): 3.85 (s, 3H, CH₃), 6.33 (d, 1H, CH, J=16.2), 6.93 (d, 2H, ArH, J=8.5), 7.51 (d, 2H, ArH, J=8.5), 7.75 (d, 1H, CH, J=16.2). **¹³C NMR** (CDCl₃): 115.2, 126.4, 130.5, 147.1, 162.1, 172.9.

Synthesis of 4-acetamidosalicylic acid **48**

**48**

A suspension of 4-aminosalicylic acid **47** (1 g, 6.53 mmol) in ethanol (10 mL) and acetic anhydride (0.62 mL, 6.58 mmol) was stirred at 40 °C for 30 min and then allowed to cool at room temperature. The mixture was then concentrated *in vacuo* and extracted with ethyl acetate (3 x 2 mL). The organic phase was dried over Na₂SO₄, filtered and then concentrated under reduced pressure. The crude product was purified by flash column chromatography using dichloromethane/methanol (9:1) as eluent to afford the final product **48**.

Yield: 48 %. Brown solid. **TLC**: DCM/MeOH (9:1) $R_f = 0.52$. **M.p.**: 230-231 °C (decomp). **¹H NMR** (DMSO-d₆): 6.40 (dd, 1H, ArH, J=1.2, J=8.1), 6.87 (d, 1H, ArH, J=8.1), 7.02 (t, 1H, ArH, J=8.1), 7.16 (s, 1H, OH), 9.30 (s, 1H, NH), 9.76 (s, 1H, COOH). **¹³C NMR** (CD₃OD): 22.7, 107.2, 111.0, 129.3, 139.8, 157.7, 170.4.

3.7.2 Biology

3.7.2.1 *Escherichia coli* strain and growth condition

The well characterized *E. coli* ATCC 25404 was used as a model system for bacterial biofilms. The strain was stored at $-80\text{ }^{\circ}\text{C}$ in suspensions containing 20 % glycerol and 2 % peptone, and was routinely grown in Luria-Bertani broth (LB, Sigma-Aldrich) at $30\text{ }^{\circ}\text{C}$ for 16 h.

3.7.2.2 Planktonic growth in the presence of zosteric acid related compounds

Planktonic growth of *E. coli* in LB medium supplemented with 0 (negative control), 0.183, 1.83, 18.3, 183 and 1830 μM of the synthesized molecules and 3 % of DMSO were carried out in 384-well microtiter plates. Growth curves at 30°C were generated using the PowerWave XS2 microplate reader (Biotek). Growth was followed by measuring the optical density (OD) at 600 nm (OD₆₀₀) every 10 min for over 24 h in wells inoculated with 3 μl (3 % v/v) of an overnight culture (10^7 cells mL^{-1}). OD-based growth kinetics were constructed by plotting the OD of suspensions minus the OD of the non-inoculated medium against incubation time. The polynomial Gompertz model was used to fit the growth curves to calculate the maximum specific growth rate μm , using GraphPad Prism software (version 5.0, San Diego, CA, USA). Six biological replicates of each treatment were performed. Obtained data were normalized to the negative control and reported as the mean of these. Percentage reduction in comparison with the control was also calculated.

3.7.2.3 Cellular growth with the zosteric acid related compounds as the sole carbon and energy source

The ability of bacteria to grow with each compound as the sole carbon and energy source was tested using a mineral medium (KH_2PO_4 30 g/L, Na_2HPO_4 70 g/L, NH_4Cl 10 g/L, pH = 7) supplemented with 1830 μM of each synthesized molecule and 3 % of DMSO. Bacteria were added 10^7 cells/mL and grown at $30\text{ }^{\circ}\text{C}$ for 72 h. The positive control was the mineral medium supplemented with glucose at both 1830 μM and 10,000 μM concentration. Microbial growth was followed by measuring the optical density (OD) at 600 nm (OD₆₀₀). All the experiments were repeated three times.

3.7.2.4 Microplate-based biofilm assay in the presence of zosteric acid related compounds

Biofilm was assessed quantitatively using fluorochrome labeled cells in hydrophobic 96-well black-sided plates. Briefly, 200 μL of phosphate buffered saline (PBS, 0.01 M phosphate buffer, 0.0027 M potassium chloride pH = 7.4, Sigma-Aldrich) containing 10^7 cells supplemented with 0 (negative control), 0.183, 1.83, 18.3, 183 and 1830 μM of each synthesized molecule and 3 % of DMSO was placed in microtiter plate wells. Cells were incubated 18 hours at 30 $^{\circ}\text{C}$. The microtiter plate wells were washed two times with 200 μL PBS and adhered cells were stained using 10 $\mu\text{g}/\text{mL}$ 4,6-diamidino-2-phenylindole (Sigma-Aldrich) in PBS for 20 min in the dark at room temperature. Fluorescence intensity was measured using the fluorometer VICTOR™ X Multilabel Plate Readers (Perkin Elmer) at excitation wavelength of 335 nm and emission wavelength of 433 nm. A standard curve of fluorescence intensity versus cell number was determined and used to quantify the anti-biofilm performance of the zosteric acid related compounds. Four measurements were performed for each condition. Obtained data were normalized to the negative control and reported as the mean of these data. Percentage reduction in comparison to the control was also calculated.

3.7.2.5 Statistical analysis

Analysis of variance (ANOVA) test via a software run in MATLAB (Version 7.0, The MathWorks Inc, Natick, USA) was applied to statistically evaluate any significant differences among the samples. Tukey's honestly significant different test (HSD) was used for pairwise comparison to determine the significance of the data. Differences were considered significant for $p < 0.05$.

4. SECTION B: FUNCTIONALIZATION OF A SURFACE

4.1 Background

Infection of polymers used for medical devices is one of the major clinical complications causing a high rate of mortality and morbidity thereby significantly increasing healthcare costs.[95] Bacterial adherence to implant surfaces occurs in two phases. Firstly, bacteria compete with host cells for binding to the extracellular matrix or plasma proteins on the device surfaces; this is described as “race for the surface”.[96] Then, adherent bacteria proliferate and cluster in multilayers of exopolysaccharides within biofilms, which have a low metabolism without toxin production. The introduction of an implant into the body increases susceptibility to biomaterial-centered infections, due to the damage caused to epithelial and mucosal barriers upon implantation. Further the presence of the implant, and the resulting extracellular matrix protein adsorbed, favors the bacteria colonization leading to a surface that become persistent and refractory to antibiotics. The scientific world view is that the etiology of device-related infections is associated with the biofilm mode of growth that offers protection against hydrodynamic forces, evasion to the host immune-response and enhanced resistant to medical treatments and for these reasons, regularly, traditional therapies fail.[97] Successful treatment requires multistep procedures, e.g. removal of the infected surface, intravenous and oral therapy with antibiotics for weeks or months and re-implantation of a new device. Therefore, a new approach to defeat biofilm-related infections of indwelling device becomes imperative, and a serious change in our prospective is necessary.

To date, approaches that were employed to provide medical polymers with anti-infective properties mainly consist of:

- (a) mixing antibacterial reagents in bulk polymers;[98]
- (b) copolymerization of antibacterial reagents with monomer for polymers;[99]
- (c) surface modification to control the physicochemical interactions between the bacteria and polymeric surface.[100]

Many efforts have focused on catheter surface modification in order to create a drug-based material for reducing infections incidence.[101] The coating of medical devices with antimicrobial substances or

entrapping them within the polymeric material are the most used approaches to obtain devices with different antimicrobial spectra and durations of the antimicrobial effect.[102] Up to now, they have primarily been based on agents of known bacteriostatic/bactericidal activity already in use as disinfectants or antibiotics. Indeed, central venous and urinary catheters coated or impregnated with both antibiotic and antiseptic combinations have been approved and commercialized by Food and Drug Administration.[103] Even though the idea to combine materials in use with approved antimicrobial substances appears simple and straightforward, low drug release from bioactive materials contributes to the serious phenomenon of multidrug resistance spreading.[104] Due to the constant release of active compounds from the implanted device, that cannot be monitored or quantified, this approach became less attractive for a medical application.

Instead of fighting biofilm with antimicrobial/device combination products, the efforts should be directed towards developing an innovative anti-infective material, targeting microbial virulence traits (like binding and cell-to-cell communication) and in which active substance would not be leached from the surface avoiding the problem of the compound kinetics release and providing long-term protection against bacterial colonization.

4.2 Project Description (B)

In the light of the aforementioned observations, this section is focused on the functionalization of polyethylene, one of most common polymers employed in biomedical applications, with *p*-aminocinnamic acid **8** and *p*-aminosalicylic acid (PAS) **47** (used as reference), selected from the previously biological investigation (for detail see ‘Section A’ of this thesis) as the best candidates to form a covalent linkage with the polymeric support. These compounds not only showed a good antibiofilm activity against *E. coli*, the bacterial model system that has been taken into account, but also have an amino groups at the *para* position that allowed the subsequent grafting with the activated polymeric material.

In literature, different approaches to combine antimicrobial agents to polymers were described and can be generally attributed to two main strategies: the passive protection of surface or physical coating, obtained by spreading a solution of the anti-biofilm compounds on the material, and the active coating or chemical coating, achieved by a covalent linkage between the supporting material and the bioactive substances. While the passive approach is characterized by the lack of long term stability and non-uniform distribution of compounds within the material, a covalent attachment of active molecules offers a better stability and uniformity, avoiding the possible limitations due to the release of active agents (e.g. toxicity due to the high dose released or the production of endotoxins or other byproducts by bacteria which may elicit an inflammatory or another adverse effects).

Since this project is a part of a multidisciplinary research that involves different work units, at first the choice of the material and the polymers used as linkers was made in analogy with the work carried out by some colleagues about the surfaces functionalization with enzymes having antibacterial activity. The initial step of my work was the passive coating of polycarbonate (PC) membranes with polymers such as branched polyethylenimine (PEI) and glutaraldehyde (GA), used as linkers between the surface of the materials, and selected anti-biofilm derivatives, in order to set up the coating procedure and to obtain preliminary results about the interaction between molecules and a polymeric surface. The PC membranes were coated with an aqueous solution of PEI and subsequently with different concentrations of aqueous solutions of glutaraldehyde. To detect the presence of the coating on the surfaces, Reflection Absorption Infrared Spectroscopy (RAIR) analyses were carried out. The colony-biofilm culturing system was used to explore the anti-biofilm performance of the modified surfaces. In

particular, colony biofilms of *E. coli* were grown on semipermeable untreated and treated membranes resting on agar plates.

Afterwards, in the light of the previously considerations about the differences between passive and active coating, the next step was the covalent grafting of the selected compounds on a solid support. Various synthetic routes have been developed for the covalent binding of species onto surfaces (e.g. grafting to and grafting from techniques).[105] Polymer brushes, random or block copolymers prepared with these methods result in a long term stability with a broad range of chemical functionalities.[106]

To obtain an efficient immobilization, some requirements need to be satisfy such as:

- the linkage should be a covalent bond in order to avoid displacement by biological media and to be stable enough for all the duration of the intended application;
- the binding site of the active molecules should be situated far from the biologically active area;
- the active sites of compounds should face the biological medium;
- the active molecules should not change configuration upon binding;
- the grafting reaction should only involve specific groups on the bioactive molecules.[107]

In my work, the Low Density Polyethylene (LDPE) coupons were grafted with hydroxyethyl methacrylate (LDPE-HEMA-OH) by means of O₂ plasma pre-treatment and then the hydroxyl groups were converted into the corresponding carboxylic acids (LDPE-HEMA-COOH) which were used for covalent immobilization. Effect of different parameters, such as the plasma treatment time, the monomer concentration and the time of graft-polymerization process were investigated.

Finally, the anti-biofilm performances of the modified materials were tested by using an *in vitro* system aimed at replicating hydrodynamic flow conditions normally found *in vivo*. The Center for Disease Control (CDC) biofilm reactor was able to reproduce *Escherichia coli* biofilm under continuous liquid shear to simulate conditions to which medical devices were subjected to during their use.

Unfortunately, the final characterization of the new material was not so easy as expected due to the physical properties of polyethylene coupons (e.g. thickness, density). All the techniques used to provide information about the characteristics of the samples in each stages of the functionalization process are here reported but they are not exhaustive. Further analysis to obtain the whole characterization as well as to analyse the stability of the new material will be necessary.

4.3 Passive protection of surfaces

The passive protection of the surface is obtained by spreading the polymer and then the solution of the anti-biofilm compounds on the material (Figure 32). Poly(ethylene glycol) (PEG) systems have been extensively studied, and PEG functionalized surfaces have been demonstrated to drastically reduce bioadhesion (protein adsorption, bacterial and cell adhesion) due to the formation of an interfacial layer, which prevents direct contact between the surface and the proteins.[108]

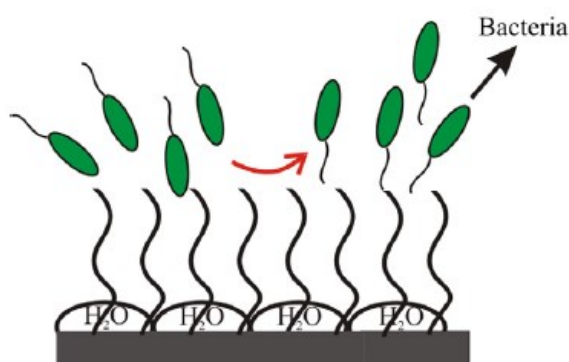


Figure 32. Passive protection of surfaces to prevent contact, and thereby protein adsorption and bacterial colonisation, of the surface.

One limitation of PEG based systems is the lack of long term stability often observed, which reduces their usefulness as surface coatings. Indeed, PEG coatings are subjected to oxidative degradation and chain cleavage, thus resulting in loss of surface functionality in terms of hydrophilicity and resistance to non-specific adsorption. However, a detrimental aspect of biopassive surfaces is their tendency to the production of defect-free coatings to completely prevent bacterial adhesion across the

whole surface, which is not easy to achieve. Thus, the initial adhesion of the bacteria is reduced but then the onset of defects and deterioration of the coating in physiological media lead to the potential colonization of the implant.

This passive approach is also exploited in ship hulls covering in order to protect themselves from damages related to marine biofouling and to reduce the maintenance costs. Since 2003, antifouling paints were loaded with tributyltin (TBT) as biocide. Although TBT anti-fouling paints are the most effective, TBT-derived leachates are highly toxic and damage the marine environment. Nowadays, paints include less toxic biocides such as copper-based compounds and metal-free compounds that are able to prevent or slow down the growth of algae and marine organisms on the hull. Their antifouling activity is exerted by a slow leaching of the biocide included in soluble or insoluble matrices into the seawater surrounding the vessel.[109] Enzymes, in particular hydrolytic enzymes such as glycosidases and proteases, have been envisaged as alternative additives in antifouling paints. The rationale is that immobilization of enzyme environmentally friendly at the surface of polymeric films led to materials displaying bacterial growth inhibiting properties.[110]

4.3.1 Materials and methods

Polycarbonate filter circles (25 mm Dia, Black Nuclepore Polycarbonate, 0.2 μm Pore Size) were purchased from GE Healthcare. Branched poly(ethylenimine) (average $M_w \sim 25,000$ by LS, average $M_n \sim 10,000$ by GPC), glutaraldehyde solution (Grade I, 50 % in H_2O , specially purified for use as an electron microscopy fixative), cinnamic acid, coumaric acid, *p*-aminosalicylic acid and *p*-aminocinnamic acid were purchased from Sigma Aldrich and used without any further purification. Zosteric acid was synthesized and characterized as reported in ‘Paragraph 3.7.1’.

4.3.2 Experimental procedure

The passive coating process for polycarbonate membranes is shown in Figure 33. Polycarbonate was

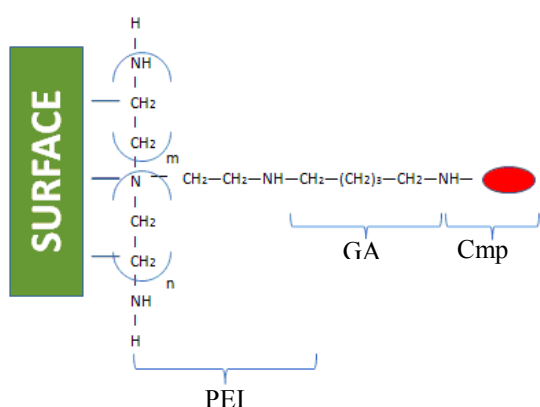


Figure 33. Passive protection of polycarbonate membranes

firstly immersed in a 3 % w/v solution of branched polyethylenimine for 24 hours obtaining a surface functionalized by amino groups resulting from the physisorption of PEI on the surface. The membranes were dried in air overnight. Then, aqueous solutions of glutaraldehyde with different concentrations (0.005 M, 0.05 M) were spread on the PEI-coated membranes which are subsequently dried in air

overnight. It was proved that high concentration of glutaraldehyde (more than 10 % w/v) caused membrane rupture. Finally, the treated samples were exposed to a 1.83 mM aqueous solution of the selected anti-biofilm compounds (zosteric acid, cinnamic acid, coumaric acid, *p*-aminosalicylic acid and *p*-aminocinnamic acid).

Since the passive coating was only a preliminary technique to study the interactions of these molecules with a surface, I have used the same concentration that was found to be the best for zosteric acid inhibitory activity.

4.3.3 Characterization

4.3.3.1 Reflection Absorption Infrared Spectroscopy (RAIR)

To order to ensure the presence of the passive coating on the membranes, Reflection Absorption Infrared Spectroscopy (RAIR) analyses were carried out.

Reflection Absorption Infrared Spectroscopy is a sensitive spectroscopic technique that can directly detect the presence of molecules at solid/air interface. This technique analyzed the infrared radiations

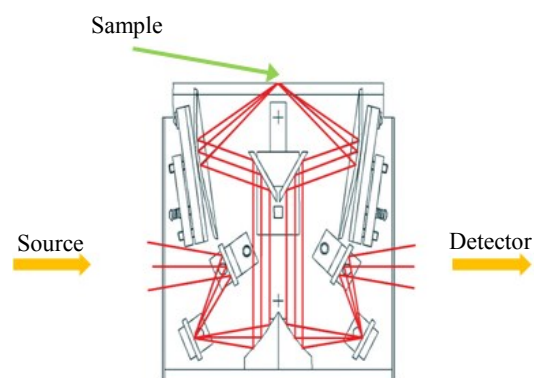


Figure 34. Proprietary beam path within the VeeMax II Specular Reflectance accessory.

reflected by sample surfaces. Nevertheless, the application of IRRAS techniques to acquire structural information from monolayers at the air-water interface presents three main problems.[111] First, IR transition moments are relatively weak. Infrared extinction coefficients are typically 20- to 1000-fold less intense than their electronic counterparts. Second, the IR reflectivity of water is poor. Finally, the intense bands of both liquid water and water vapor tend to interfere in some spectral regions of interest.

Unfortunately for these reasons, the results obtained using this technique are not comprehensive, but could be considered the starting point to find a way to study the functionalized material.

Materials and methods

RAIR technique was used to generate spectra of monolayers on a polycarbonate membrane. FT-IR spectra were collected using a Perkin Elmer (MA, USA) FTIR Spectrometer “Spectrum One” in the 4000 and 450 cm^{-1} spectral region fitted with a VeeMAX II (Pike technologies) variable angle attachment. Samples, were analyzed by reflectance technique. Prior to data acquisition, a clean polycarbonate membrane was used as background.

Results and discussion

In the graphs below the spectra of the polycarbonate membranes coated with PEI (Figure 35 A) and with PEI and different concentrations of glutaraldehyde are shown (Figure 35 B).

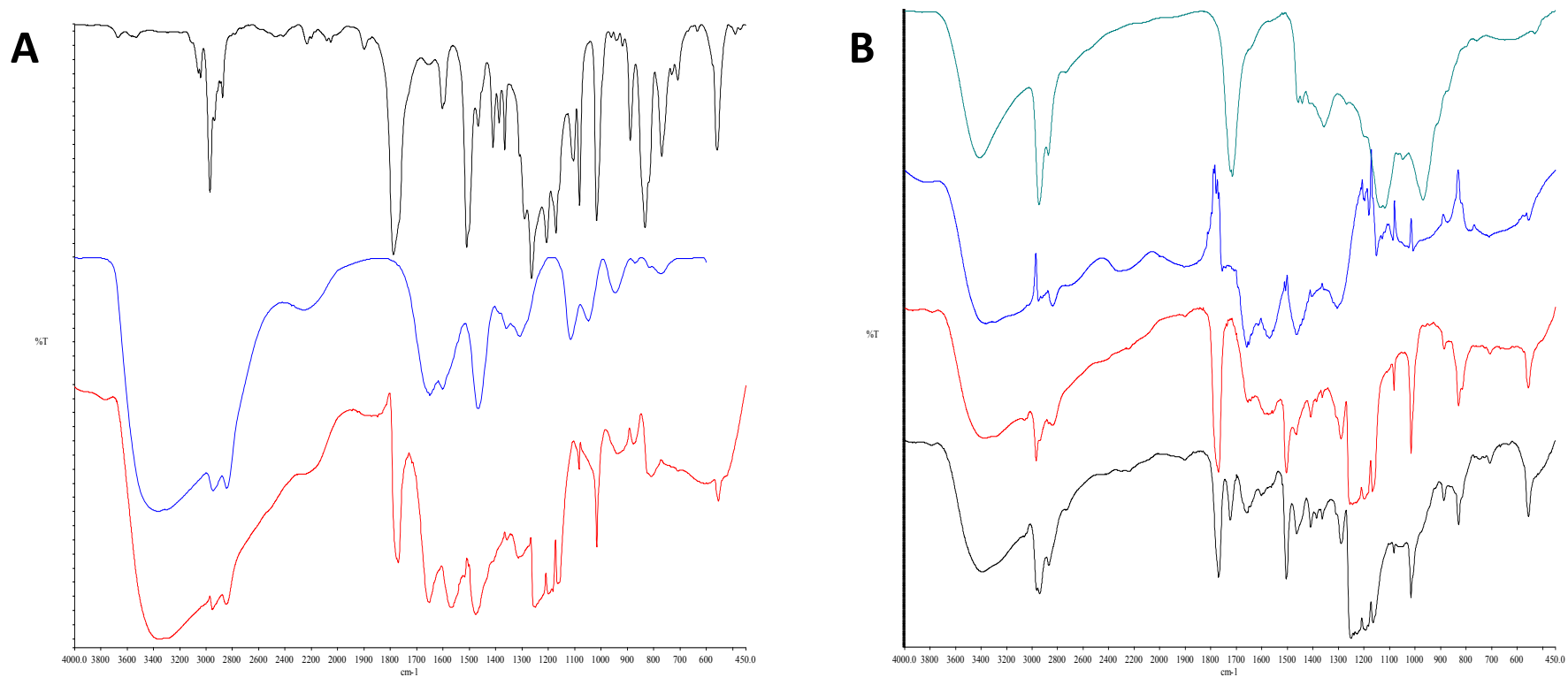


Figure 35. A) Polycarbonate membrane coated with 3 % PEI: PC (black), 3 % PEI (blue), PC + 3 % PEI (red); B) Polycarbonate membrane coated with 3 % PEI and different concentrations of glutaraldehyde: 10 % GA (green), 3 % PEI + 0.05% GA (blue), 3 % PEI + 1 % GA (red), 3 % PEI + 10 % GA (black).

As for the original membrane, despite the presence of a carbonyl group at 1774 cm^{-1} , the strongest infrared absorptions in polycarbonate are due to the C-O single bond stretches. Intense signals appear at 1165 , 1194 and 1228 cm^{-1} . Additional C-O related peaks are found around 1000 cm^{-1} , with the strongest of these at 1016 cm^{-1} . Among the aromatic ring breathing modes, only the 1506 cm^{-1} peak is significant. While the methyl stretch at 2970 cm^{-1} is weak, it is well appreciable due to the absence of other peaks in this region of the spectra. The data obtained are consistent with those reported in literature.[112] To ensure the presence of PEI and detect the interactions between PEI and polycarbonate, IR spectra were also collected on PC-PEI surfaces. The major changes have been observed in the spectrum of PC-PEI surface by comparing the spectral differences between polycarbonate and polyethyleneimine. As shown in Figure 35 A, the representative peaks between $3000\sim 2800\text{ cm}^{-1}$ corresponding to $\nu(\text{NH})$ and $\nu(\text{CH})$ stretching vibrations can be clearly observed in the IR of PC-PEI samples, which were consistent with those of pure PEI. The NH bending vibration was also discernible at 1570 cm^{-1} . Moreover, the band at 1774 cm^{-1} , which can be assigned to carbonyl groups of polycarbonate, was clearly observed confirming no chemical interactions between the supporting material and the polymer.

As for the coated membranes with PEI and different concentration of the glutaraldehyde, the obtained IR spectra are shown in Figure 35 B for comparison. Unfortunately, it was found that concentrations of glutaraldehyde lower than 10 % w/v were not detected by the instrument. On the PC-PEI samples with higher loading of glutaraldehyde ($\geq 10\%$), a weakened peak at 1670 cm^{-1} , which can be attributed to the C-O stretching vibration, suggested the presence of the cross-linking agent.

The IR spectra of membranes passively coated with the selected molecules were not recorded since the concentration of molecules was lower than the detection limit of the instrument.

4.3.4 Biological evaluation: the colony-biofilm assay

The colony-biofilm culturing system was used to explore the anti-biofilm performance of the coated

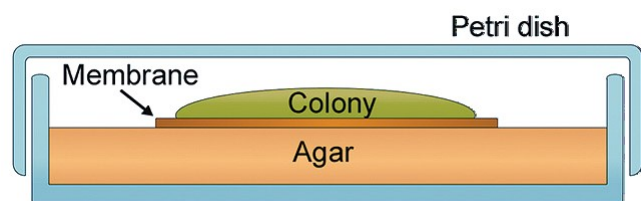


Figure 36. Side view of a biofilm-colony assay.

membranes. In particular, it was evaluated if these coated membranes were able to hinder the *E. coli* growth by themselves. This static biofilm system was particularly useful for the examination of the early stages of biofilm formation, including initial

adherence to the surface and microcolony formation and to monitor cell death in biofilms treated with antimicrobial agents.

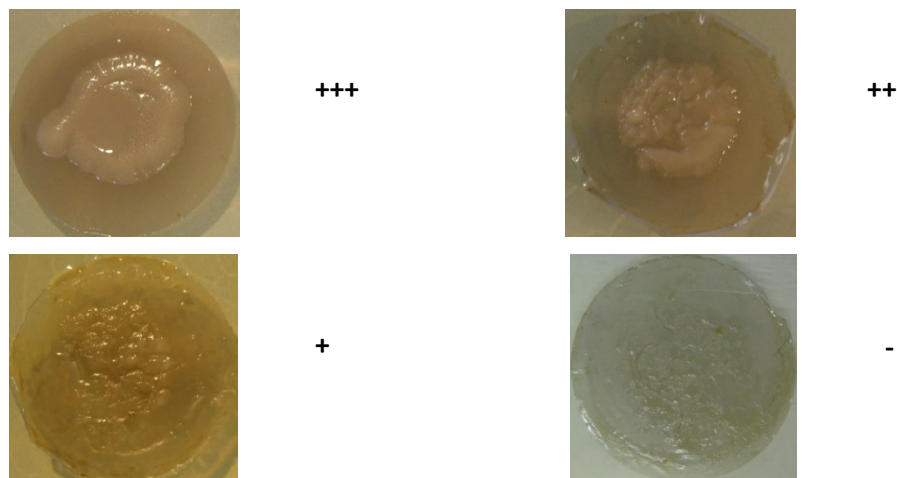
This assay was performed by growing a colony biofilm on a semipermeable membrane that sits on an agar plate (Figure 36). A new supply of nutrients can be given to bacteria just by relocating the membrane-grown cells to a fresh agar plate. Therefore it can easily change the carbon source or type of drug treatment avoiding the need to wash the cells. The biofilm formed is derived from clonal growth of the original population of bacteria deposited on the filter, whereas in liquid media, motile bacteria may be able to “invade” an aggregation of cells. Likewise, in this technique bacteria have limited ability to detach and migrate or drift away from the biofilm formed. The stable and spatially restricted nature of this system makes the colony biofilm especially useful for observing the effects of antimicrobial agents, as changes in cell number can be more easily attributed to inhibition of biofilm formation rather than detachment. It is important to ensure that each membrane receives an equal amount of cells and that there is only a single point of inoculation in the centre of the membrane.

Materials and methods

E. coli ATCC25404 was used as a model system for bacterial biofilms. The strain was stored at -80 °C in suspensions containing 20 % glycerol and 2 % peptone, and was routinely grown in Luria-Bertani broth (LB, Sigma-Aldrich) at 30 °C.

Colony biofilms of *E.coli* strains were prepared following the method reported by Anderl *et al.*[113] Briefly, 20 µl of cell suspension containing 10⁵ cells were used to inoculate functionalized and non-functionalized membranes (negative control) resting on Tryptic Soy Agar (TSA, Sigma Aldrich) culture medium. The plates were inverted and incubated at 30 °C for 24 hours. After 24 hours biofilm grown on functionalized membranes were compared with biofilm grown on non-functionalized membrane. Membranes with a biofilm growth comparable with the negative control were coded +++, membrane with a limited reduction in biofilm growth were coded ++, membrane with a considerable reduction in biofilm growth were coded + and membrane with no biofilm growth were coded -.

In order to make more clear the discussion, pictures showing the evaluation of biofilm colony growth on a membrane are here reported:



Results and Discussion

The obtained results are presented in Table 4.

POLICARBONATE MEMBRANES	
SAMPLES	GROWTH
UNTREATED MEMBRANE	+++
PEI 3%	+++
GLUTARALDEHYDE 0.005 M	+++
GLUTARALDEHYDE 0.05 M	+++
PEI 3% + GLUTARALDEHYDE 0.005 M	+++
PEI 3% + GLUTARALDEHYDE 0.05 M	+++
ZOSTERIC ACID 1.83 mM	+++
ZOSTERIC ACID 1.83 mM + GLUTARALDEHYDE 0.005 M + PEI 3%	+
ZOSTERIC ACID 1.83 mM + GLUTARALDEIDE 0.05 M + PEI 3%	+
COUMARIC ACID 1.83 mM	+++
COUMARIC ACID 1.83 mM + GLUTARALDEIDE 0.005 M + PEI 3%	++
COUMARIC ACID 1.83 mM + GLUTARALDEIDE 0.05 M + PEI 3%	-
CINNAMIC ACID 1.83 mM	+++
CINNAMIC ACID 1.83 mM + GLUTARALDEHYDE 0.005 M + PEI 3%	++

CINNAMIC ACID 1.83 mM + GLUTARALDEHYDE 0.05 M + PEI 3%	+
<i>p</i> -AMINOSALICYLIC ACID 1.83 mM	+++
<i>p</i> -AMINOSALICYLIC ACID 1.83 mM + GLUTARALDEHYDE 0.005 M + PEI 3%	++
<i>p</i> -AMINOSALICYLIC ACID 1.83 mM + GLUTARALDEHYDE 0.05 M + PEI 3%	+
<i>p</i> -AMINOCINNAMIC ACID 1.83 Mm	+++
<i>p</i> -AMINOCINNAMIC ACID 1.83 mM + GLUTARALDEHYDE 0.005 M + PEI 3%	++
<i>p</i> -AMINOCINNAMIC ACID 1.83 mM + GLUTARALDEHYDE 0.005 M + PEI 3%	+

Table 4. Evaluation of biofilm colony growth on treated and untreated membranes.

The biological investigation showed that polyethylenimine and different concentration of glutaraldehyde did not significantly affect *E.coli* growth, while the coating with these two linkers and the selected molecules generally led to a reduction of biofilm formation. Interestingly, the direct coating of polycarbonate membranes with the aqueous solution of compounds was ineffective since molecules were too close to the surface and were not able to interact with their target. Moreover, the best results in terms of bacterial growth inhibition were obtained by using a 0.05 M aqueous solution of glutaraldehyde as linker, probably due to the increase of functional groups available for the subsequent interaction.

These preliminary results were useful to confirm the importance of using appropriate linkers to distance the bioactive molecules from the polymeric surface in order to obtain a new functionalized material able to interfere with biofilm growth.

4.4 Active protection of surfaces

An alternative strategy for the prevention of biomaterial infection is based on the covalent attachment of an antimicrobial agent to the surface of the polymer (Figure 37). The most widely explored

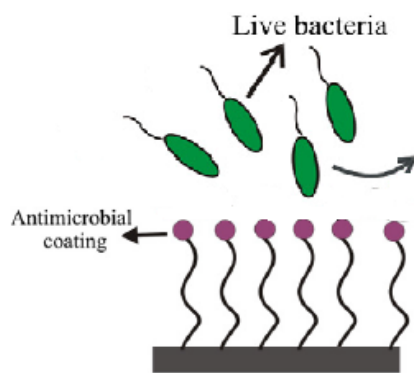


Figure 37. Active protection of surfaces.

polymeric antimicrobial coatings are based on quaternary ammonium compounds (QAC) to actively kill any bacteria that adhere to the surface.[114] Numerous studies have revealed that the minimum requirements of these systems for antimicrobial activity against bacteria is a cationic group and an apolar alkyl chain. Additionally the cationic group needs to be immobilized via a spacer, typically PEG, to ensure the mobility of the group is retained.[115] The synthesis of well defined PEGylated polymers with tertiary amines from commercially available monomers, such

as 2-(dimethylamino)ethyl methacrylate and oligo(ethylene glycol) methyl ether methacrylate was achieved by reversible addition–fragmentation chain transfer polymerization (RAFT). The resulting tertiary amines were quaternized to generate cationic polymers with different chemical functionalities (such as alkyl, primary alcohol, primary amine and carboxylic acid). The antimicrobial activity of the polymers was shown to be influenced by both the length of the alkyl spacer and the chemical functionality. Among all of these polymers with alkyl, primary alcohol, primary amine and carboxylic acid functionalities with fixed propyl spacer, that one characterized by an alkyl group had the highest antimicrobial activity.

Another approach to prepare antimicrobial materials is to incorporate the furanones, which interfere with bacterial quorum sensing systems, and its derivatives which have been shown to inhibit growth of both Gram-positive and Gram-negative bacteria.[116] Furanones covalently bound to catheters either by a copolymerization with a styrene polymer, or with plasma-1-ethyl-3-(dimethylaminopropyl) via carbodiimide reaction reduced the adhesion and colonization of *S. epidermis in vitro*. Furanones, incorporating bromine atoms, have also been covalently attached to poly(L-lysine)-graft-poly(ethylene glycol) (PLL-g-PEG) polymers and the surfaces prepared via self-assembly of the PLL-g-PEG were exposed to *S. epidermis*. [117] The grafted furanone did not reduce bacterial adhesion compared to surfaces functionalized with PLL alone. This indicates that the biopassive properties of the PLL-g-PEG

had been abolished by the presence of the furanone and further highlighted the necessity, in this instance, of free furanone for an antimicrobial effect. The main limitation of this approach is that once the bioactive compounds are grafted to a surface, they can lose much of their mobility and, being unable to penetrate in the cells, becoming inactive. Indeed, covalent immobilization of the active substance can lead to reduced activity, due to steric hindrance or inability to interact with intracellular targets.

A possible solution is to link the antimicrobial agents to a long, flexible polymeric chain anchored covalently to the surface of the material. Although this limitation can be partially resolved employing long linkers, the number of antimicrobial substances suitable for immobilization is limited to those which do not need to enter the cytoplasm to be active.

4.4.1 The choice of material

The development of an efficient antimicrobial coating is one of the major current challenges, since the presence of biofilms on the surfaces of materials is a serious medical and economical problem. Microbial adhesion depends strongly on the physico-chemical properties of the materials constituting the medical devices. The main materials currently employed to manufacture catheters are polyethylene (PE), polyvinyl chloride (PVC) and silicone. However, it is widely recognized that these polymeric materials do not escape microbial colonization leading to device-associated infections.[118] The tendency of microorganisms to adhere to surfaces and form biofilms in several environments is certainly related to the selective advantages that a surface association offers. First, surfaces provide a space to be occupied and a degree of stability in the growth environment and then, biofilm structures offer protection from a wide range of environmental injuries like UV exposure, dehydration, phagocytosis and against the action of several antimicrobial agents (for details see ‘Paragraph 1.2’).

In the passive approach, the membranes which underwent to the coating process was made of polycarbonate, since it was proved that it did not affect *E. coli* growth. As for the active coating, the polymeric material which I have used was low-density polyethylene (LDPE). Similarly to PC, it was found that LDPE itself did not affect bacterial growth.

Polyethylene is a thermoplastic polymer consisting of long hydrocarbon chains and it is produced by the polymerization of ethylene. It is classified into several different classes based mostly on the density,

the type of branching and molecular weight. As for the degree of polymerization, the most important polyethylene grades are:

- HDPE (High-density polyethylene): the density of high-density polyethylene can range from 0.93 to 0.97 g/cm³.
- LDPE (Low-density polyethylene): it is defined by a density range of 0.910–0.940 g/cm³.
- LLDPE (Linear low-density polyethylene)

Although the density of HDPE is slightly higher than that of low-density polyethylene, HDPE has few branching, giving it stronger intermolecular forces and tensile strength than LDPE. On the contrary, LDPE has more branching (on about 2 % of the carbon atoms) than HDPE, so its intermolecular forces (instantaneous-dipole induced-dipole attraction) are weaker, its tensile strength is lower, and its resilience is higher.

LDPE is produced under high pressures (81-276 MPa) and high temperatures (130-330 °C) with a free-radical initiator, such as peroxide or oxygen. The choice of initiator is made on the basis of the type of reactor, the residence time in each zone, the desired reaction temperature, and initiator cost. The main factor in choosing an initiator is its half-life indeed long half-life of the initiator led to high degree of polymerization, but also to high peroxide cost. The polymerization mechanism is a free-radical reaction that leads to the formation of long-chain branches, which can be as long as the main polymer backbone. The free-radical mechanism also leads to the formation of short-chain branches, typically one to five carbon atoms long. These short-chain branches normally presented in LDPE include 1,3-diethyl and 2-ethylhexyl side chains as well as the most common butyl branches. LDPE also contains small amounts of amyl branches while hexyl branches are rare. Most of the methyl branches occur when propylene is added to the reactor as a chain-transfer agent. The polymerization is carried out in tubular or stirred autoclave reactors.[119]

PE is used in many biomedical application mainly as packaging material for storage of physiological fluids, implants or as support for cell growth.[120] It is also characterized by very low wetting properties in aqueous media and high resistance against a wide range of reagents, showing an excellent resistance to diluted and concentrated acids and bases. This latter was an essential property for the next use, since this material underwent to chemical modifications to become suitable to link anti-biofilm compounds.

For all the aforementioned properties, I choose this polymer for the active coating described in this dissertation. It should be noted that up to now, the functionalization of material was performed only on polymeric films, whose thickness was around few nanometers. In this pioneering proposal, 1.6 mm thickness polyethylene coupons were used, leading to a more difficult characterization of the final surface since the conventional analysis methods did not work.

4.4.2 Pre-treatment of surfaces

Polymeric materials used in medical devices often do not possess the needed physical or chemical properties to allow grafting with antibiofilm molecules and require surface modifications.[120]

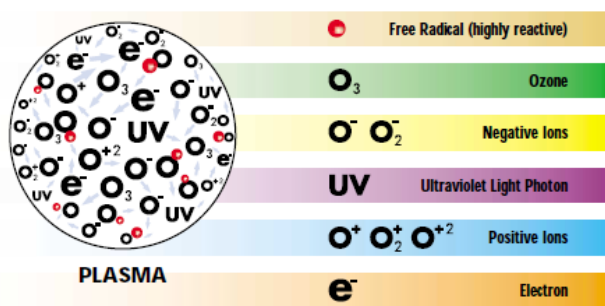


Figure 38. Active species present in an oxygen plasma.

Recently, there has been a rapid exploration of low-temperature plasma technology to improve the surface properties of polymeric materials leading to physical and chemical modifications of the first few molecular layers of the surface without changing their bulk properties. Plasma surface modification involves the interaction of the plasma-generated excited species with a solid interface. Gas phase plasma is an electrically neutral mixture of electrons, ions, radicals, photons, recombination products and neutrals created by the application of energy, such as radio frequency (RF), to a source gas contained within a vacuum chamber. Free electrons are responsible for the beginning of the process. Indeed, the exposure of the free electrons to the external energy source allows the electrons to gain sufficient kinetic energy, therefore their collision with another atom or molecule results in the formation of ions and radicals. The reactive radical species are capable of chemical reactions where the ionized atom and molecular species are capable of physical interactions through sputtering. Photon emission within a plasma is a result of the excited neutrals, ions and free radicals formed in the plasma losing their excess energy. The wavelength of the emission is sufficient to break chemical bonds, and it can be useful when treating polymeric materials.[121] Plasma surface activation employs gases (such as oxygen, nitrogen, hydrogen) which, when exposed to the plasma, dissociate and react with the surface, creating different chemical functional groups.[122] Thus, it is possible the insertion or the substitution of chemical functionalities into an otherwise non-reactive surface or to create radicals for

cross-linking or subsequent grafting. Indeed, in an oxygen plasma, the resulted hydroperoxy groups can be used as initiators in the subsequent surface graft-polymerization.[123] The most important components of a low-pressure plasma system are the vacuum chamber, the vacuum pump and a high-frequency generator for plasma creation (Figure 39).

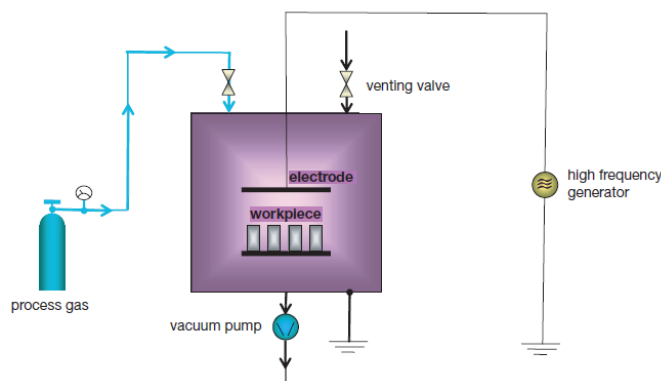


Figure 39. Low-pressure plasma system.

Due to the low surface energy of untreated material, plasma pre-activation of PE films was found to be necessary for a successful graft-polymerization, which fails in the absence of such pretreatment.[58, 124] To understand the complex reaction between the plasma and the polymer surface, it is important to understand the plasma parameters and their effects on the surface modification. Plasma technique offers several advantages since the process is solvent-free, extremely controllable and the consumption of reagents is low. However, one of the major limitations of plasma technology is the diversity of functional groups produced by the chemical reactions that occur in the plasma. Moreover, plasma polymers also have irregular, non-repeatable polymer structures with much branching and crosslinks.[125]

This technology is based on ecological, clean and dry processes suitable for industrial applications without the use of chemicals.[126]

In this study, polyethylene coupons were submitted to two different plasma treatments, using a plasma cleaning oxygen system and a oxygen plasma reactor, in order to modify the surface of samples and to compare the different results obtained kept unchanged the parameters of the other functionalization steps. The plasma reactor system has significant advantages over the cleaning one, such as a better

surface modification in terms of uniformity and number of exposed functional groups in a shorter processing time.

4.4.3 Graft-polymerization process

Plasma treatment can be also used to introduce functional groups through deposition of a polymerized thin layer of a second polymer. While the attachment of this second layer of the substrate polymer is not well defined, the product is in effect functionally modified in a useful way.[128] The substrate is firstly immersed in a solution containing the monomer, an initiator and a crosslinking agent. After the removal of the excess of the solution, the substrate is exposed to plasma. In the case of an unsuccessful plasma pretreatment, the failure of the graft-polymerization step can be occurred. In fact, when solvent evaporates from the surface of untreated material after immersion in monomer solution, the monomer tends to concentrate in the liquid phase and agglomerates in small drops instead of covering the PE surface with a uniform thin film. Moreover, no monomers remains on the surface after washing.[129, 130] Finally, the substrate is washed and dried. This method can be called plasma-induced graft-polymerization and is evidently of considerable practical interest.

In this work plasma-induced graft-polymerization of hydroxyethyl methacrylate (HEMA) was performed on polyethylene coupons. In particular, I focused my attention on the optimization of plasma and solution parameters that regulate the graft-polymerization process such as pre-treatment time for surface activation, monomer concentration and treatment time. Indeed, The chemical composition of plasma treated surface depends mainly on the gas used and the experimental conditions applied. The activation process, as well as the graft-polymerization that occurred on the PE, were followed by the characterization of the surface by means of contact angle measurements, attenuated total reflection infrared (ATR-IR) spectroscopy, X-ray photoelectron spectroscopic (XPS) and scanning electron microscopy (SEM) analyses.

4.4.4 Experimental

4.4.4.1 Materials and methods

Polyethylene used in this study was low-density polyethylene (LDPE) purchased from Alfa Aesar as sheets (300 x 300 x 1.6 mm). Samples were prepared in the form of 1.6 mm (0.063 in) thick round

shape coupons ($d=1.27\text{cm}$). Hydroxyethyl methacrylate (97 %, contains ≤ 250 ppm monomethyl ether hydroquinone as inhibitor), *p*-aminocinnamic acid and *p*-aminosalicylic acid were purchased from Sigma Aldrich and used as-received without any further purification.

4.4.4.2 Cleaning of PE coupons

Polyethylene coupons were washed with a 3 % w/v aqueous solution of a neutral detergent efficient in removing greasy residues (AUSILAB 101, Carlo Erba Reagents) and then with a 1 M aqueous solution of HCl. They were subsequently purified by extraction with acetone overnight and dried prior each plasma treatment.

4.4.4.3 Plasma activation of PE¹

Low density polyethylene coupons were exposed to a low-pressure oxygen plasma for the process of surface activation. In particular, oxygen plasma treatment, followed by exposure to the air, was used to introduce new carbon-oxygen functionalities to the polymer surface. A brief description of the low-

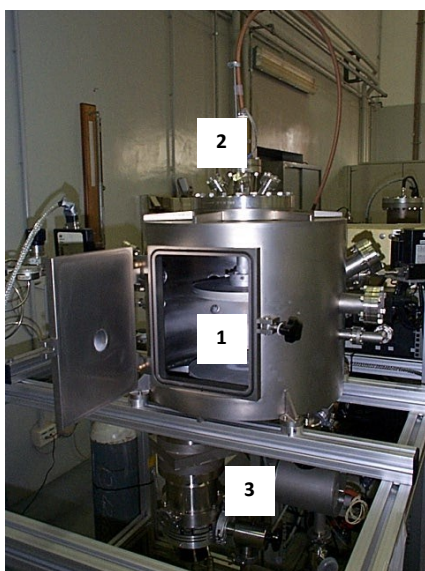


Figure 40. R2000 plasma reactor:

- 1) Process reactor
- 2) RF power
- 3) Vacuum line

pressure plasma system was given in ‘Paragraph 4.4.2’. The apparatus used for this study consists of a parallel-electrodes, capacitive-coupled plasma enhanced chemical vapor deposition (PECVD) system, made up of a cylindrical stainless steel vacuum chamber of 25 cm inner diameter with an asymmetric electrode configuration (Figure 40). The powered electrode is connected to a 13.56 MHz power supply, associated to an automatic impedance matching unit, while the other electrode is grounded and works as sample holder. The treatment was performed for 60 s at a total plasma process pressure of about 15 Pa, kept constant by balancing the incoming oxygen flux with the system pumping speed. Commercially (99.998% purity) available oxygen was supplied into the discharge vessel through a mass flow controller. The total gas

pressure was measured by a capacitive vacuum gauge. Plasma treatment was performed as a function of RF power of 100 W. At first low pressure was created in the process reactor by means of a turbo-

¹ performed at the Institute of Plasma Physics «Piero Caldirola», National Research Council (CNR), Milan (Dr. Espedito Vassallo)

molecular pump combined with a rotary pump. At a pressure of 0.026 mbar oxygen was fed into the chamber (O_2 flow= 15 sccm). When the working pressure was achieved, the generator was switched on and the process gas was getting ionized. Samples of commercial LDPE, previously washed and inserted into the vacuum chamber, were exposed to the plasma.

4.4.4.4 The grafting procedure: LDPE-HEMA-OH surface

In the graft-polymerization process, monomers were introduced into the vacuum chamber as a layer on the plasma pre-treated surface. In details, PE samples were immersed for 10 s in a solution of HEMA in ethanol. Concentration of HEMA solutions was varied from 0.05 M to 1 M that seemed to be the best range of concentrations found in literature.[129] Indeed, samples prepared with low concentration of the monomer led to PE surface that was only partially covered, while with high monomer concentrations the failure in the graft-polymerization step was observed.

PE samples, previously immersed in HEMA solution, were completely dried in air and then oxygen plasma treated in order to promote the graft-polymerization of the monomer. Using the plasma cleaner system, O_2 pressure and treatment time were varied to optimize the process while for the plasma reactor system, input power was kept constant at 100 W as well as the grafting treatment time (60 s), in order to prevent damaging of substrates.[131] The samples were finally ultrasonically washed in ethanol for 5 minutes in order to remove the ungrafted macromolecules and dried in air at room temperature.

4.4.4.5 Preparation of the LDPE-HEMA-COOH surface

The LDPE-HEMA-COOH film was obtained by treatment of the LDPE-HEMA-OH film with succinic anhydride. Thus, in a conical flask the LDPE-HEMA-OH coupons were immersed in 10 mL of dichloromethane, containing also dry pyridine (2.5 eq). Succinic anhydride (2.5 eq) dissolved in 10 mL of THF was added to the reaction mixture. The suspension was allowed to proceed at room temperature for 24 h. The film was washed with copious amounts of dichloromethane (10 x 10 mL) prior to dry in air.

Since it was not possible to define exactly the equivalent of hydroxyl groups introduced on polyethylene due to the difficulty of analysis, a general estimate of the number per unit area was made on the basis of literature data.[129]

4.4.4.6 General procedure to graft molecules to the LDPE-HEMA-COOH surface *via* amide bond formation

The carboxylic functionalities of LDPE-HEMA-COOH coupons (1 eq) were activated by dipping the surfaces into a dichloromethane solution (10 mL) of *N*-hydroxysuccinimide (1.2 eq) and *N,N*-dicyclohexylcarbodiimide (1.2 eq) under a nitrogen atmosphere at room temperature for 20 min. Then the suitable compound* (1.2 eq) was poured into the suspension and the resulting mixture was stirred at room temperature for 16 h. Then the coupons were filtered off and washed with copious amounts of dichloromethane (10 x 5 mL). Additional washes with DMF (3 x 5 mL) were necessary to remove completely the dicyclohexylurea from the surfaces. Finally the coupons were dried *in vacuo* to allow analytical analysis.

Similarly to the LDPE-HEMA-OH coupons, the equivalent of carboxylic functionalities introduced on the surface was not precisely determined, thus the subsequent grafting was performed using an excess of all reagents to ensure the amide bond formation.

* *p*-aminocinnamic acid or *p*-aminosalicylic acid respectively, selected from the previously biological investigation (see ‘Section A’ of this thesis).

4.4.5 Characterization

4.4.5.1 Contact angle measurements

Contact angle measurements are generally used for estimating the extent to which a solid surface will be wetted. When a drop is totally spread on solid surface and the contact angle is close to 0 degrees, the complete wettability of the surface is achieved. However, in many cases only a partial wettability occurs. Wettability can be defined as the degree to which a solid is wetted and can be expressed as relative strength of cohesion (liquid/liquid) and adhesion (solid/liquid) forces. If the contact angle of water is 90 degrees or more the polymeric surface may be considered hydrophobic. This relates with poor wettability, low surface energy and weak adhesion of the polymer. On the other side, drop with a small contact angle relates to hydrophilic surface, that causes better wettability, adhesion and higher surface energy of the investigated material.

In the present study, the sessile drop technique was used under ambient atmospheric conditions. Samples processed at different plasma treatment times and at graft-polymerization process were

evaluated by measuring the water contact angles, both before and immediately after the coating deposition to evaluate changes to the surface hydrophilicity resulting from the presence of a polymer layer.

Materials and methods

Contact angle measurements were performed *via* sessile drop method using a CAM 200 Instrument (KSV Ltd), which utilizes a video capture and a subsequent image analysis. Deionized water was used, and its purity was confirmed by correlating the measured surface tension based on the pendant drop shape to the literature values for pure water (72 mN/m at 25 °C).

Results and discussion

The water contact angles of polyethylene coupons treated with oxygen plasma at different times are reported in Table 5. Similarly, water contact angles of polyethylene coupons after graft-polymerization with different HEMA concentration are shown in Table 6. These changes in contact angles measurements are here discussed.

Data represents the average of repeated measurements at two different observation points on three sample replicates.

Polyethylene samples		Aging process (hours)		
		0	24	48
Plasma treatment time (min)	0	99,33 ± 0,78	93,93 ± 0,54	88,83 ± 1,15
	2'	46,43 ± 8,63	51,18 ± 0,93	72,25 ± 2,10
	10'	48,88 ± 11,98	72,51 ± 13,94	76,18 ± 17,05
	20'	33,13 ± 4,09	45,20 ± 1,44	58,91 ± 1,44
	30'	26,95 ± 3,87	46,60 ± 1,14	36,46 ± 2,60

Table 5. Water contact angle measurements at different plasma treatment times.

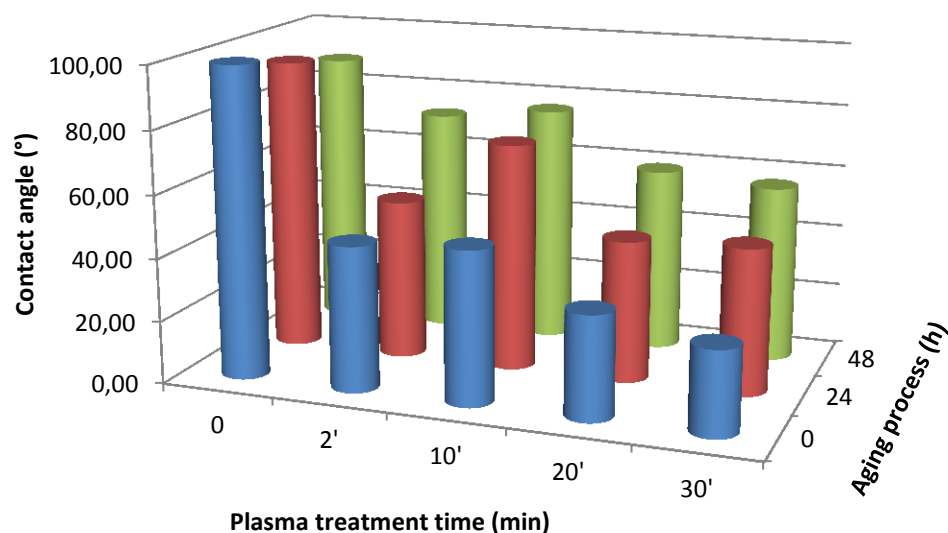


Figure 41. Plots of water contact angles of untreated and plasma treated samples and corresponding aging process.

The results confirmed that the water contact angles of the untreated LDPE achieved the highest values because, as aforementioned, it is a polymer with hydrophobic nature and chemical inert surface (Figure 41). As it can be observed, the contact angles of the untreated surface were reduced after the oxygen plasma treatment even for a short exposure time. This situation indicates that the plasma treatment considerably enhances the formation of polar species on the LDPE surface acquiring a more hydrophilic nature. These polar groups that consists mainly of carboxyl, carbonyl and hydroxyl groups resulted from the interaction between the surface and the O₂ plasma. The oxidation of a non-polar unreactive polymer such as polyethylene usually leads to a material characterized by high energy and thus, high wettability. However, the activated material is also thermodynamically unstable compared to the original lower energy hydrophobic polyethylene (in fact the surface activation by the plasma treatment is not permanent). This indicates that the plasma treated surface undergoes an aging process that can be attributed to a re-arrangement of the hydrophilic groups obtained during the O₂ plasma exposure. This result is not surprising because the aging of plasma treated surfaces is a well-known phenomenon with a rate dependent on the characteristics of the material, plasma and surrounding environment. Activated surfaces may have a shelf-life of hours or days.[132]

The hydrophilic characteristics of the surface was also evaluated after the graft-polymerization process with hydroxyethyl methacrylate (Table 6). Concentrations of HEMA and treatment time were varied in

order to optimize the process while the input power and the pressure of the plasma reactor were kept constant.

Polyethylene samples		Aging process (hours)		
		0	23	46
HEMA Concentration (M)	0	14,41 ± 2,32	43,44 ± 5,33	43,70 ± 4,36
	0,05	14,10 ± 0,65	38,20 ± 12,61	54,88 ± 3,20
	0,1	13,77 ± 5,27	26,07 ± 5,42	38,64 ± 3,54
	0,5	15,36 ± 0,02	28,45 ± 1,48	31,75 ± 7,13
	1	16,49 ± 1,39	44,80 ± 16,50	51,68 ± 8,08

Table 6. Water contact angle measurements of samples grafted with different HEMA concentration and exposed for 20 minutes to O₂ plasma to induce polymerization. The 0 M HEMA concentration refers to samples submitted only to the activation process.

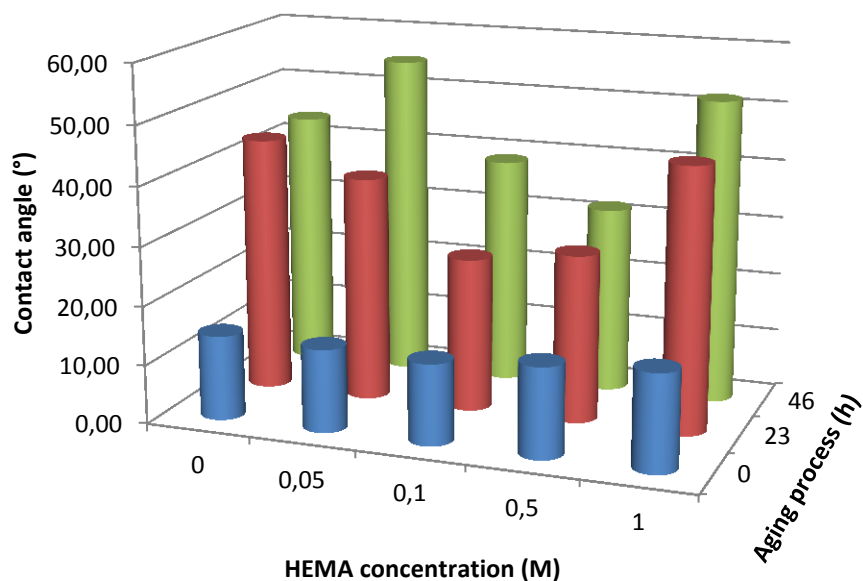


Figure 42. Plots of water contact angles of samples treated with different HEMA concentrations and corresponding aging process.

Data showed that the decrease of contact angle observed in case of surface covered with HEMA was not substantial compared with samples activated by O₂ plasma (Figure 42). Indeed, all the samples

exhibited similar contact angles values after the graft-polymerization process, providing that this range of concentrations did not significantly affect the hydrophilicity of the substrate.

In the light of these results, 0.1 M HEMA concentration and 20 minutes graft-polymerization time process were conventionally selected as the best conditions to activated polyethylene using a plasma cleaner system, while using a plasma reactor system, the best time for both the activation and graft-polymerization process is 60 s, as reported in literature [131]. Moreover, it was found that the aging process occurred also after graft-polymerization, since most of the polar groups changed their orientation towards the bulk, thus reducing the hydrophilic nature of the treated surface. In detail, samples prepared with 0.1 M and 0.5 M HEMA concentration showed a contact angle aging lower than the samples covered with higher (1 M) and lower (0.05 M) HEMA concentrations.

Obtained data suggested that it was necessary to perform the reaction for the conversion of hydroxyl groups into the corresponding carboxylic functionalities (and obviously, the subsequent linkage with bioactive molecules) immediately after the graft-polymerization treatment to ensure the highest yield of the complete material functionalization.

4.4.5.2 Scanning Electron Microscope (SEM) analysis¹

The changes of morphology of the samples prepared after activation with oxygen plasma was evaluated by low-vacuum-SEM analysis. This analysis allowed to compared SEM images of different samples prepared using both a plasma cleaning system and a plasma reactor for the activation process.

Materials and methods

Surfaces of the oxygen plasma activated polyethylene was examined with a Leo 1430 scanning electron microscopy (Zeiss, Oberkochen, Germany) to gather data on the overall physical organization of the polymer network.

Results and discussion

The clearly visible surface morphology changes obtained at different plasma treatments were evident from SEM images (Figure 43). The topology and the roughness of the originally smoothed surfaces of the original substrates were dramatically changed after plasma treatment. In particular, considerable

¹ performed at the Interdepartmental Centre for Advanced Microscopy, University of Milan (Dr. Nadia Santo, Dr. Benedetta Sacchi)

modifications of the surface roughness were detected in the oxygen-plasma-treated samples both activated by a plasma cleaning system and by plasma reactor. Using a plasma cleaning treatment, a wavy surface was obtained, while by means of the plasma reactor system the resulting polyethylene was characterized by small holes that covered uniformly all the surface. It is well-known that cleaning plasma treatment is considerably less aggressive than oxygen plasma reactor, therefore significantly activation was achieved only if an extended treatment (20 min) was performed. Conversely, the plasma reactor treatment for 60 s produced a noticeable increase of polyethylene roughness. Moreover, in this latter same structures were clearly visible also in different parts of the studied sample surfaces reflecting high reproducibility and homogeneity of the applied plasma treatment.

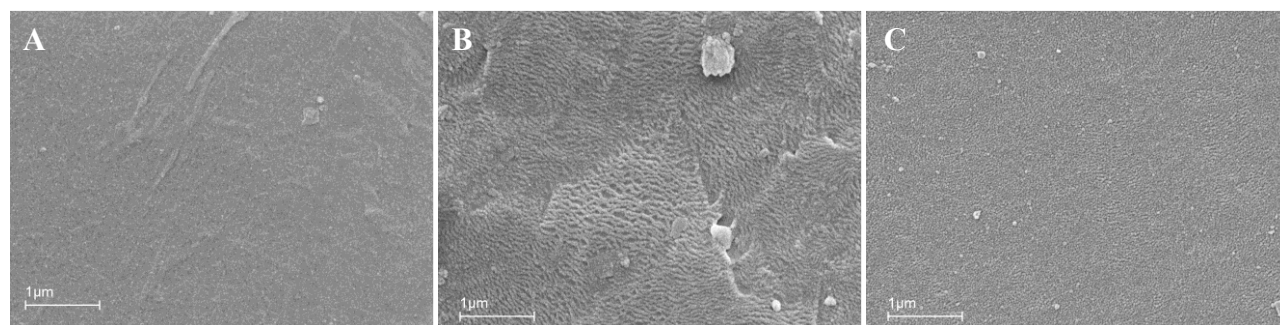


Figure 43. SEM images of coupons subjected to different treatments. A) clean polyethylene; B) PE after plasma cleaning treatment; C) PE after plasma reactor treatment.

In the light of the obtained results, among the two employed systems, plasma reactor seemed to be most relevant for the activation process, since sample surfaces turned out to be more uniform than using the plasma cleaning system in a shorter time.

4.4.5.3 X-ray Photoelectron Spectroscopy (XPS) analysis¹

The most common technique used to characterize polymeric surfaces is the X-ray photoelectron spectroscopy (XPS). In general, this technique allows the identification of chemical groups on materials and their quantification.

In this study, C, O and N at the surface of treated samples were detected using the XPS spectroscopy. The qualitative information resulted from XPS analysis of the oxidized surface after plasma treatment,

¹ performed at the Nobil Bio Ricerche S.r.l, Milan (Dr. Marco Morra)

which contained at least carbon and oxygen, and of the functionalized surface composed of an undefined amount of carbon, nitrogen and oxygen.

Only coupons functionalized with *p*-aminocinnamic acid (LDPE-CA) were submitted to this analysis, since it was reasonable to suppose that coupons grafted with *p*-aminosalicylic acid (LDPE-SA), which underwent to the same functionalization process, might show the same results.

Materials and methods

Measurements were carried out using a Perkin Elmer PHI 5400 ESCA System equipped with a monochromatic X-ray source (Mg K_a anode) operating at 10 kV and 200 W. Analyzed volume was given by the diameter of the photon beam at the sample surface (5 mm) and by the depth of analysis of about 8-10 nm. The base pressure was kept at 10⁻⁸ Pa. Curve fitting and quantification of elements were accomplished using the software and the sensitivity factors supplied by the manufacturer.

Results and discussion

The surface composition detected from XPS analysis of plasma activated polyethylene and PE functionalized with the selected molecule is shown in Table 7.

Samples	O	N	C	Si	Al
1	16.9	-	76.4	2.0	4.7
2	17.9	2.7	75.9	-	3.5
3	20.7	9.2	70.1		

Table 7. Surface composition obtained from XPS analysis of the analyzed samples. 1) plasma activated PE; 2) PE functionalized with *p*-aminocinnamic acid; 3) Theoretical composition of the graft molecule calculated from molecular formula without H atoms.

Typically, the XPS analysis of activated polyethylene yielded surface concentration values of 60-70 % carbon, 20-30 % oxygen and < 10 % nitrogen. An increase of the nitrogen content after the coupling was observed from XPS analysis of functionalized PE (LDPE-CA), as shown in Figure 44. It should be noted that the oxidized layer could be, and in general is, non-homogenous in the vertical direction, with a decreasing concentration of oxygen in relation with an increased depth. However, the error introduced by the assumption of a non-homogeneous distribution of carbon and oxygen is negligible.

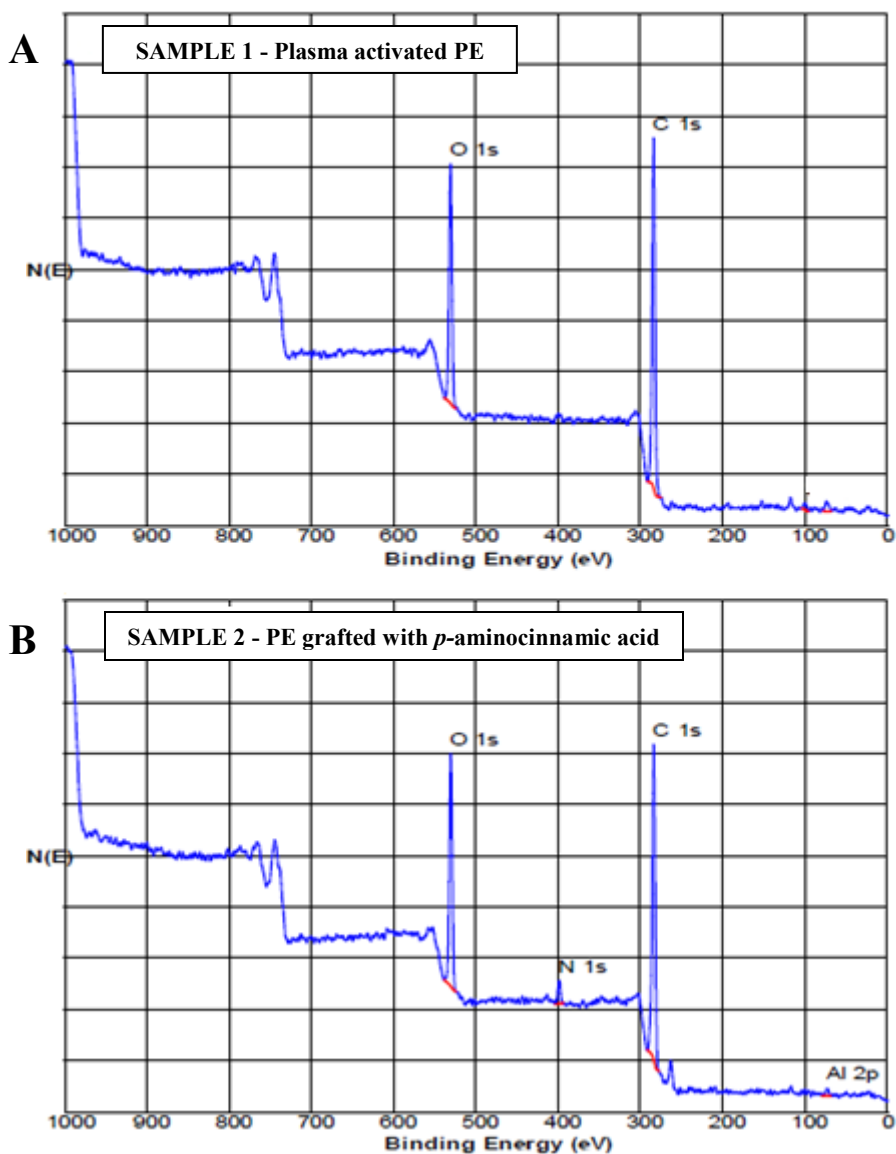


Figure 44. XPS wide scan spectra of oxygen plasma activated polyethylene (Sample 1) and polyethylene functionalized with *p*-aminocinnamic acid (LDPE-CA) (Sample 2).

According to the obtained data, some observations could be drawn:

- the surface composition of **Sample 1** (Figure 44, Panel A) was in agreement with the results expected for a polyolefin which underwent oxygen plasma treatment. The signal concentration value of oxygen peak (O1s, ~17 %) indicates a remarkable introduction of oxygen functionalities on the surface, as confirmed from the detailed analysis of carbon peak (C1s, ~77 %).

- the graph of **Sample 2** (Figure 44, Panel B) showed a well-defined nitrogen peak (N1s, ~3 %) in addition to the others peaks detected for **Sample 1**. The analysis of N1s peak revealed that the binding energy of the main component was closed to 400 eV. This results indicated that the nitrogen was not oxidized (absence of nitrite or nitrate groups). As for quantitative analysis, the calculated concentration was less than the theoretical one, but it was worth reminding that the depth of samples analysis was around few nanometers, in particular about 8-10 nm in the case of polymers. Differently, the monolayer made of linker and molecule was less than 1 nm. Therefore, the contribution of signal is almost completely due to the polymer rather than to the chemical agents although the signal did not decay linearly from the outside layers to the internal ones and the major contribution was due to the external layers.
- in both samples, some elements (Si, Al) were detected at low concentrations (≤ 5 %), most likely due to some contaminants left on the samples upon the processing techniques.

In conclusion, it was very difficult to perform reliable evaluation on the surface coverage with the selected molecules. The evaluation of quantitative parameters able to provide indications on the reaction yield in terms of surface functionalization per unit was not easy and required assumptions that were difficult to define. However, the composition data indicated that the immobilization of *p*-aminocinnamic acid led to an increase of O/C ratio and obviously of N/C ratio (as expected from the compounds elemental composition) and it was obtained in high yield.

4.4.5.4 Attenuated total reflectance infrared spectroscopy (ATR-FTIR) analysis¹

In order to detect the presence of the anti-biofilm compounds grafted on the polymeric surface, Attenuated total reflectance (ATR) infrared spectroscopy analyses were carried out, considering that plasma surface modifications are confined only to few nanometers below the surface.

FTIR spectroscopy in attenuated total reflection (ATR) mode is one of the main methods used to obtain finer surface information.[133] This technique was used to characterize the polymer surface and the spectra of the treated and the untreated samples were compared to observe the changes.

¹ performed at the Department of Pharmaceutical science, Pharmaceutical Technology Section, University of Milan (Dr. Chiara Gennari, Dr. Francesco Cilurzo)

Materials and methods

FTIR measurements were performed using a SpectrumOne spectrophotometer (Perkin-Elmer, USA), by placing the polyethylene samples on a diamond crystal mounted in ATR cell (Perkin-Elmer, USA). The spectra were collected over the wavenumber region 4000–650 cm^{-1} at 4 cm^{-1} resolution and 128 scans. The FTIR-ATR measurements provide mostly qualitative information on the chemical changes of the near-surface region. The measured thickness of the layer was limited to 4 μm . Experiments were carried out under ambient conditions.

Results and discussion

The spectrum of the untreated LDPE is a typical polyethylene spectrum with a small number of characteristic peaks (Figure 45).

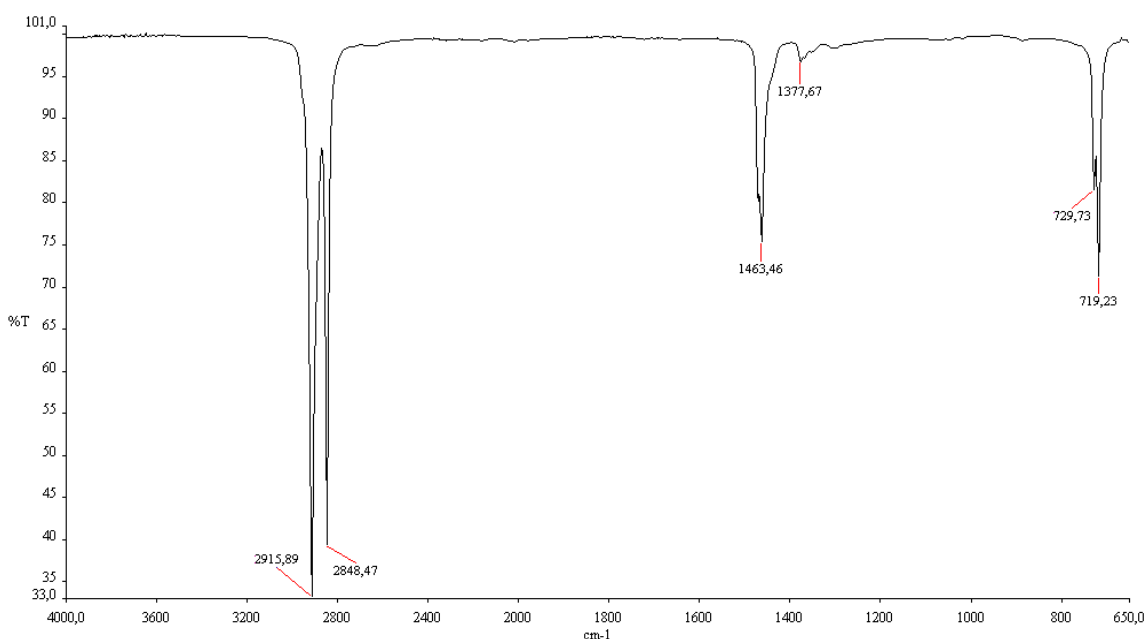


Figure 45. ATR-FTIR spectrum of LDPE coupons.

After plasma exposure of the original material, the characteristic functional groups containing oxygen were introduced and therefore significant changes in the measured spectrum should have been observed. These changes should have been caused by the incorporation of some hydroxy or peroxy groups after the plasma treatment of LDPE with the appearance of two broad peaks between 3.600–3.050 cm^{-1} and 1.800–1.520 cm^{-1} respectively since carbonyl stretching is one of the easiest

absorptions to recognize in an infrared spectrum and it usually has a very intense band. Unfortunately, according to the recorded spectra, no –OH or –OOH peaks were seen for any of the analyzed samples. This was probably due to the low concentration of the polar species upon the surface. Moreover, no changes are also observed for LDPE-HEMA-OH grafting as well as after the subsequent oxidation to carboxylic acid.

Unexpectedly, after the covalent linkage with *p*-aminocinnamic acid and *p*-aminosalicylic acid the shape of the spectrum changed, as shown in Figure 46.

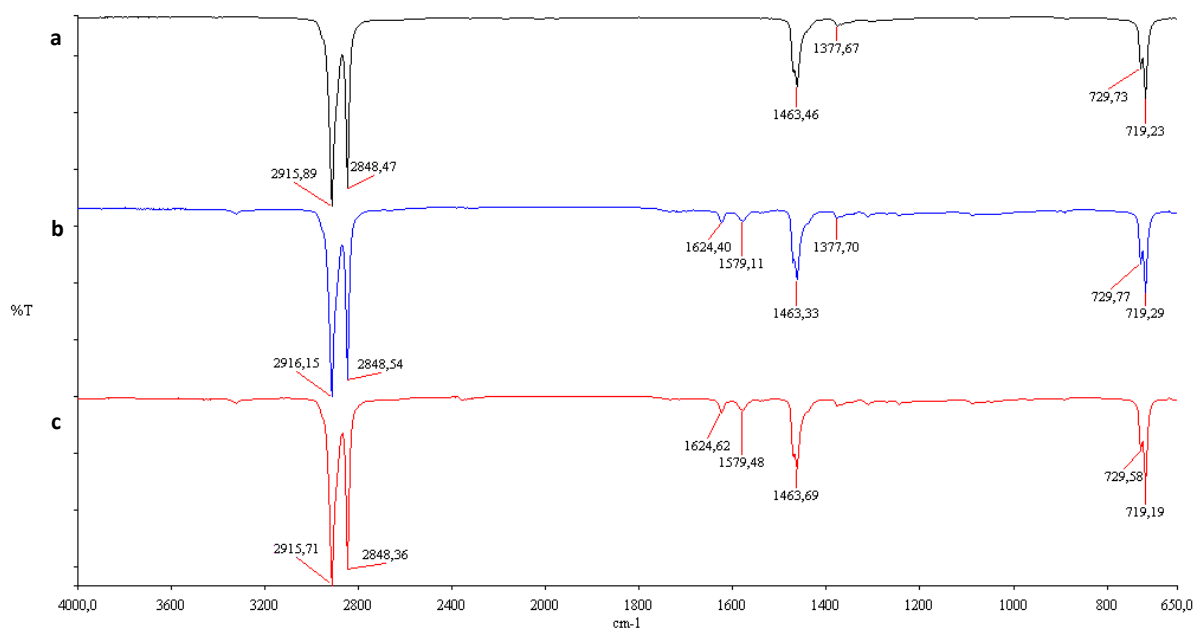


Figure 46. ATR-FTIR spectra of treated and untreated samples. The typical peaks of the amide bond confirmed the presence of a covalent bond between *p*-aminosalicylic acid (b) and *p*-aminocinnamic acid (c) to the supporting material after graft-polymerization (a).

These changes are significant especially in the infrared-region between 1.600-1.800 cm^{-1} (C-O stretching, N-H bending), suggesting that the treated samples are characterized by the typical peaks of the amide bond and confirming the presence of a covalent bond between the antibiofilm molecules and the supporting material.

4.4.5.5 Fluorescence Spectroscopy analysis

Fluorescence spectroscopy analyses were performed in order to prove the polyethylene functionalization with *p*-aminocinnamic acid and *p*-aminosalicylic acid. Firstly, the intrinsic fluorescence of these two molecules free in solution was evaluated and then it was used to estimate

their presence on the surface. The auto-fluorescence of cinnamic acid and salicylic acid immobilized scaffold was evaluated to verify the surface functionalization by Confocal Scanning Laser Microscopy (CLSM). A comparison between coupons activated with plasma cleaning system and plasma reactor was carried out.

Material and methods

Fluorescence spectra of *p*-aminocinnamic acid and *p*-aminosalicylic acid in solution were acquired in a Perkin-Elmer LS 50B spectrofluorometer. Emission spectra were recorded over the 250-600 nm range with emission and excitation slit widths set at 3.0 nm. Spectra were recorded by dissolving 2.6 mM of *p*-aminocinnamic acid and 5.0 mM *p*-aminosalicylic acid in 0.4 M NaHCO₃, 1 M NaCl, 3% DMSO buffer (pH = 8.3) (dilution buffer).

Untreated and functionalized coupons were visualized using a Leica SP5 Confocal Laser Scanning Microscope (CLSM) (405 nm laser excitation line, blue channel) before and after 10-fold used. Images were captured with a 40x, 0.8 NA water immersion objective and analysed with the software Imaris (Bitplane Scientific Software, Zurich, Switzerland). The experiments were repeated two times.

Results and discussion

When they were in solution, *p*-aminosalicylic acid, excited at 325 nm, showed an emission peak at 395 nm, while *p*-aminocinnamic acid, excited at 380 nm, showed an emission peak at 443 nm (Figure 47).

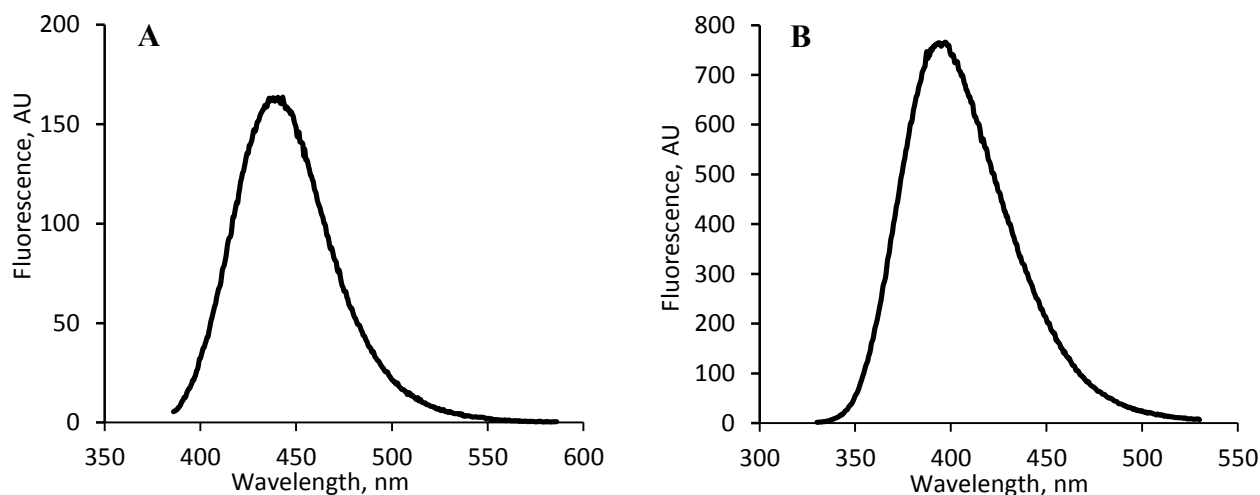


Figure 47. Fluorescent emission spectra of molecules in solution. A) *p*-aminocinnamic acid (λ_{ex} 380 nm); B) *p*-aminosalicylic acid (λ_{ex} 325 nm).

In the light of these results, both of the two compounds can be considered intrinsic fluorescent probes and can be used to prove the functionalization process. The best results were obtained using coupons activated by a plasma reactor system.

Acquired pictures of LDPE, LDPE-HEMA-OH and LDPE-HEMA-COOH control samples revealed a completely black background with absence of fluorescence (Figure 48, line 1). On the contrary, acquired images of LDPE-CA and LDPE-SA samples revealed the presence of an intense fluorescence signal that, since no fluorescence was detected in the control samples, could be attributable to the cinnamic acid and salicylic acid moieties, immobilized on the surface, demonstrating the successful of the functionalization process (Figure 48, line 2).

To prove the retention and the stability of the functionalized material, the CSLM analysis was repeated on 10-fold used coupons. Images of LDPE, LDPE-HEMA-OH and LDPE-HEMA-COOH 10-fold used control coupons revealed a completely black background with the absence of fluorescence. Pictures of LDPE-CA and LDPE-SA 10-fold used coupons still revealed the presence of an intense fluorescence signal comparable to that obtained from the not-used corresponding ones, confirming that coupons were not altered by their usage and that cinnamic acid and salicylic acid were successfully retained by the surface (Figure 48, line 3).

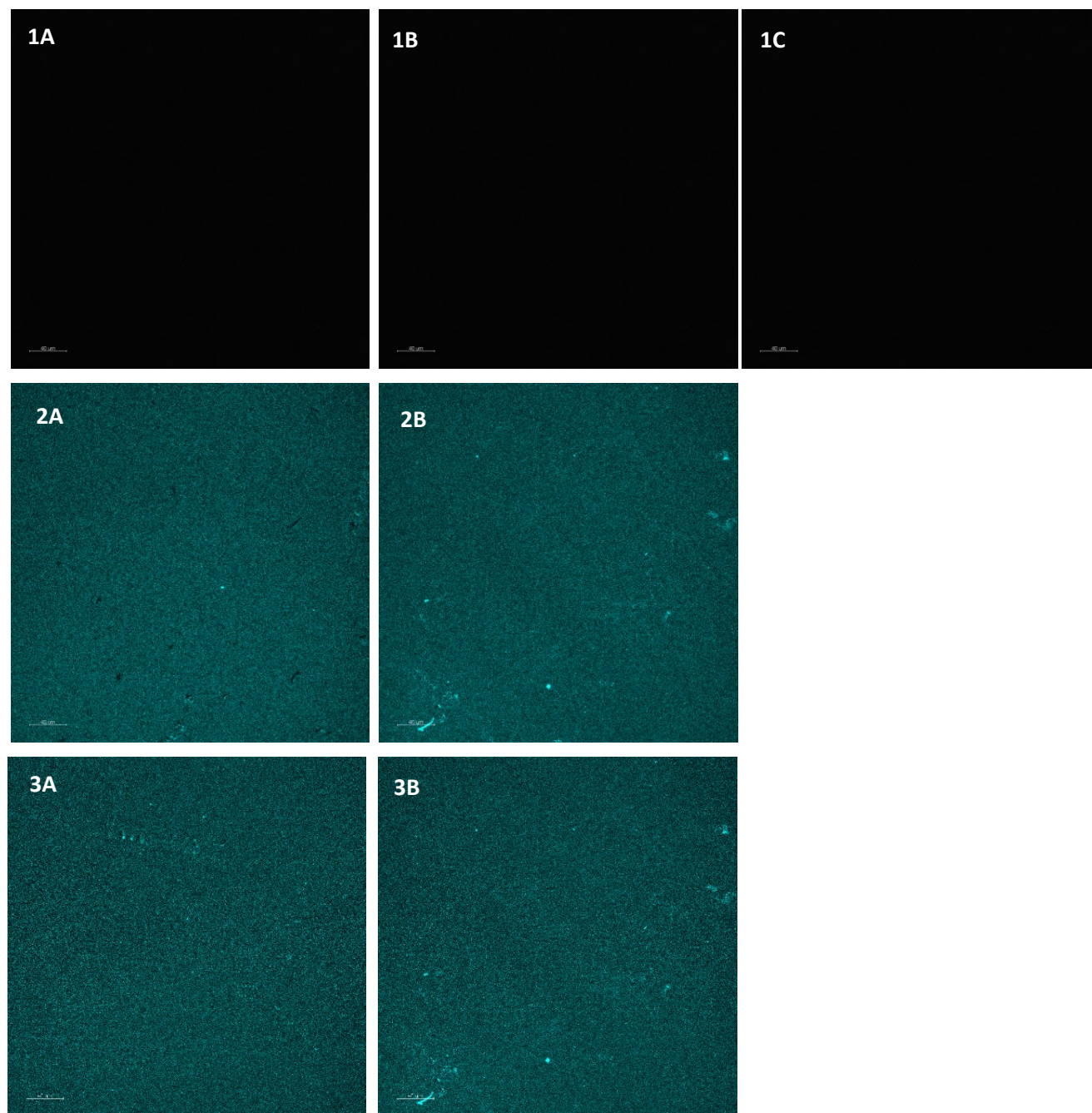


Figure 48. Representative CLSM images of unused and 10-fold used functionalized and non-functionalized polyethylene surfaces activated using plasma reactor (405 nm laser excitation line; 40 \times , 0.8 NA water immersion objective). Blue fluorescence corresponds to the molecule presence on the surface. First line (not-used coupons): 1A) LDPE; 1B) LDPE-HEMA-OH; 1C) LDPE-HEMA-COOH. Second line (not-used coupons): 2A) LDPE-SA; 2B) LDPE-CA. Third line (ten-fold used coupon): 3A) LDPE-SA; 3B) LDPE-CA. Scale bar = 40 μ m.

Also coupons activated and functionalized using a plasma cleaning system were submitted to confocal scanning laser microscopy analysis. The inadequate activation of plasma process led to coupons that showed a weak fluorescence signal probably due to a poor functionalization of the surface. Acquired pictures of LDPE, LDPE-HEMA-OH and LDPE-HEMA-COOH control samples revealed a grey background with absence of fluorescence (Figure 49, line 1), while acquired pictures of LDPE-CA and LDPE-SA samples revealed the presence of a weak non uniform fluorescence signal, confirming that plasma reactor led to a better polyethylene functionalization (Figure 49, line 2).

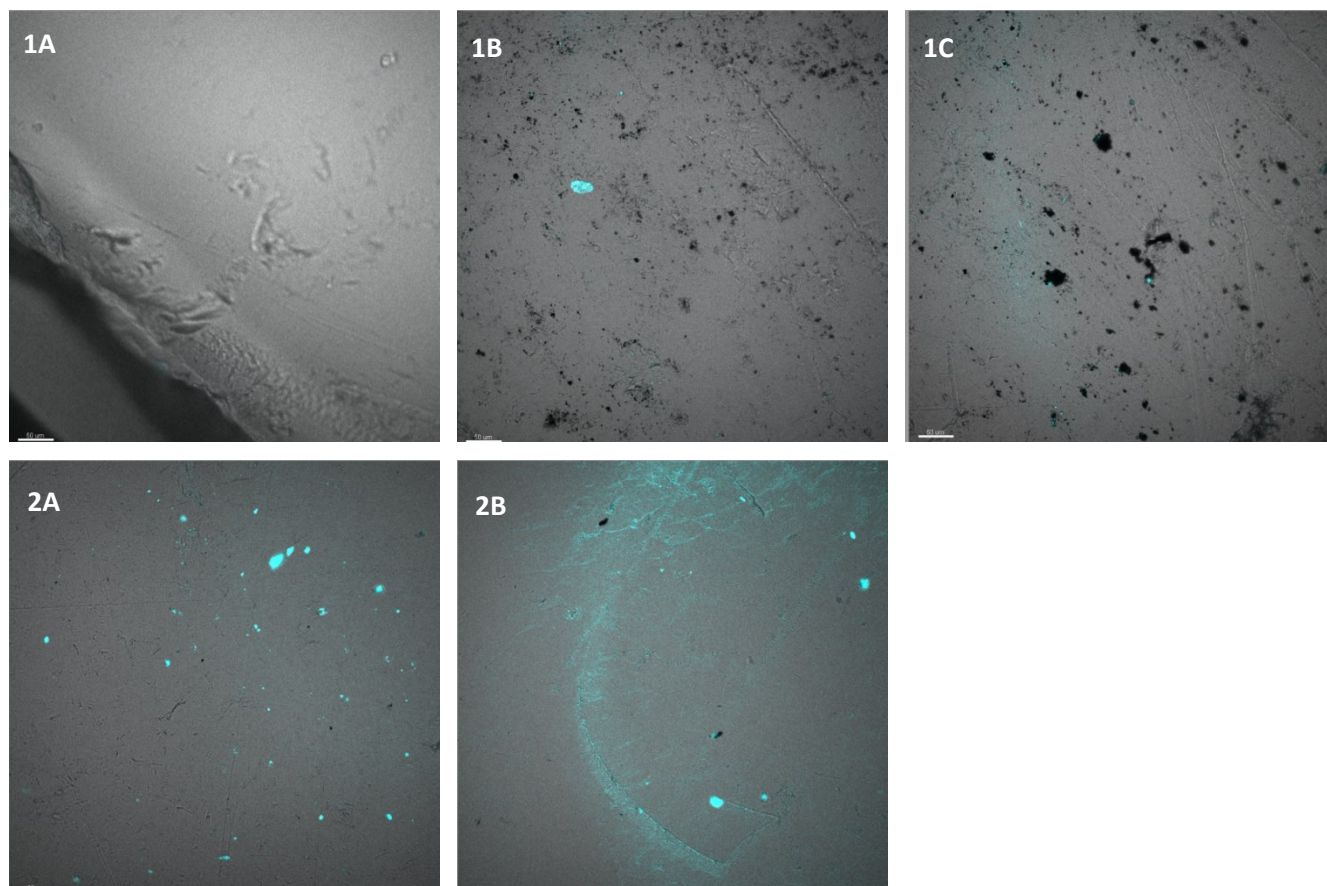


Figure 49. Representative CLSM images of unused functionalized and non-functionalized polyethylene surfaces activated using plasma cleaner (405 nm laser excitation line; 40×, 0.8 NA water immersion objective). Blue fluorescence corresponds to the molecule presence on the surface. First line: 1A) LDPE; 1B) LDPE-HEMA-OH; 1C) LDPE-HEMA-COOH. Second line: 2A) LDPE-SA; 2B) LDPE-CA.

4.4.5 Biological evaluation

In order to evaluate the antibiofilm properties of the modified material and to verify the effect of the grafting, the new surfaces were tested by using an *in vitro* system replicating the hydrodynamic flow conditions normally encountered *in vivo*. The Center for Disease Control (CDC) biofilm reactor was used to reproduce *Escherichia coli* biofilms under continuous liquid shear to simulate conditions to which medical devices could be subjected during their use.

Materials and methods

E. coli MG1655 was used as a model system for bacterial biofilms. The strain was stored at -80°C in suspensions containing 20 % glycerol and 2 % peptone, and was routinely grown in Luria-Bertani broth (LB, Sigma-Aldrich) at 37°C . *E. coli* biofilm was grown at 37°C on functionalized and non-functionalized coupons in the Center for Disease Control Bioreactor (CDC reactor, Biosurface Technologies, Bozeman, MT, USA). Inoculum of the bioreactor was prepared by inoculating 400 mL of sterile LB medium with an overnight culture of *E.coli* MG1655 strain and growing this culture at 37°C with continuous stirring for 24 hours. After the 24 hours adhesion phase, the peristaltic pump was started and sterile 10 % LB medium was continuously pumped into the reactor at a rate of 8.3 mL/min for 48 hours.

After 48 hours of dynamic phase, functionalized and non-functionalized coupons were removed, gently washed with PBS and processed to be analyzed. Biofilm grown on both functionalized and non-functionalized coupons was stained using 1x commercial solution of CellMask plasma membrane orange stain (Molecular Probes-Life Technologies) in sterile PBS. CellMask orange staining allowed to visualize total cell mass. Biofilms were incubated for 30 min in the dark at room temperature and then rinsed with sterile PBS.

Coupons without biofilm were also stained with the dyes in order to exclude any false positive signals. Biofilm samples were visualized using a Nikon Eclipse E800 epifluorescent microscope with excitation at 581 nm and emission at 644 nm for the red channel. Images were captured with a 60x, 1.0 NA water immersion objective and analyzed via MetaMorph 7.5 software (Molecular Devices, Sunnyvale, CA, USA). Percent area threshold of stained cells was performed by calculating at least ten random images for each sample for at least three coupons per experiment. The efficacy of the anti-biofilm material was calculated as percentage reduction in stained cells threshold area respect to the control images.

ANOVA test, via a software run in MATLAB environment (Version 7.0, The MathWorks Inc, Natick, USA), was applied to statistically evaluate any significant differences among the samples. Tukey's honestly significant different test (HSD) was used for pairwise comparison to determine the significance of the data. Statistically significant results were depicted by p-values < 0.05.

Results and discussion

Epifluorescence microscopic techniques were used to provide image analysis and quantification of bacterial cells *in situ*.

Direct microscopic visualization of the total biofilm biomass on functionalized and non-functionalized coupons is shown in Figure 50, where *in situ* biofilms have been stained with the CellMask plasma membrane orange stain. Pictures analysis showed significant differences in the percentage area threshold of stained cells between the control LDPE and the functionalized LDPE-CA and LDPE-SA materials (percentage threshold area of total cells: LDPE 91.04±3.88 %; LDPE-CA 29.96±6.06 %; LDPE-SA 35.45±4.54 %). No significant differences were detected in the threshold area of stained cells between the LDPE control sample and the LDPE-HEMA-OH and LDPE-HEMA-COOH linker control samples (percentage threshold area of total cells: LDPE-HEMA-OH 87.40±3.73 %; LDPE-HEMA-COOH 92.76±1.00 %), confirming that the used linker does not affect biofilm biomass (Figure 51). The analysis of the images revealed that cinnamic acid and salicylic acid functionalized material reduced biofilm biomass by 73.7 % and 61.06 % respectively, compared to the control LDPE (Figure 51). Coupons without biofilm and stained with the same dye did not produce detectable fluorescence suggesting that false positive signals were not produced (data not shown).

The two different activation processes, one using the plasma cleaning system and the other one by plasma reactor, provided two different results confirming that this first step was fundamental for the efficiency of the final conjugate.

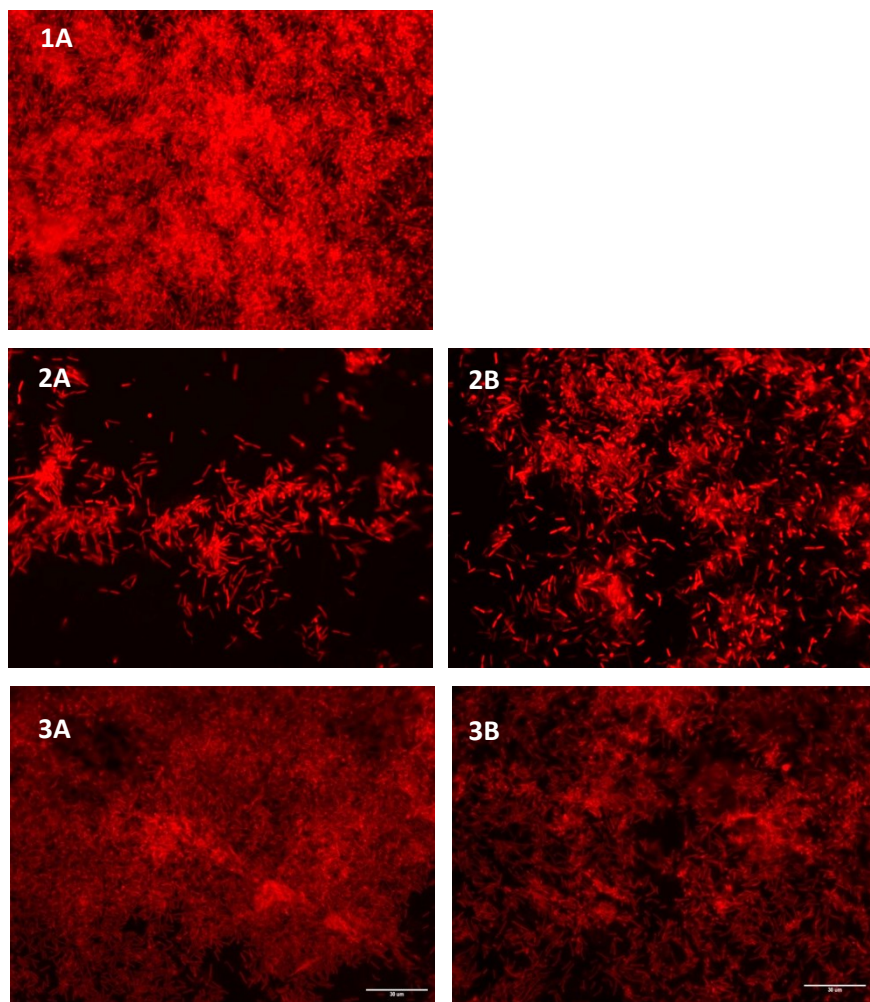


Figure 50. Representative epifluorescence microscope images of *E. coli* biofilm stained with CellMask plasma membrane orange and grown on functionalized and non-functionalized polyethylene surfaces (60x, 1.0 NA water immersion objective). First line: 1A) LDPE. Second line (coupons submitted to plasma reactor treatment): 2A) LDPE-CA; 2B) LDPE-SA. Third line (coupons submitted to plasma cleaning treatment): 3A) LDPE-CA; 3B) LDPE-SA. Red fluorescence corresponds to *E. coli* cells. λ_{ex} : 554 nm and λ_{em} : 567. Scale bar = 20 μm .

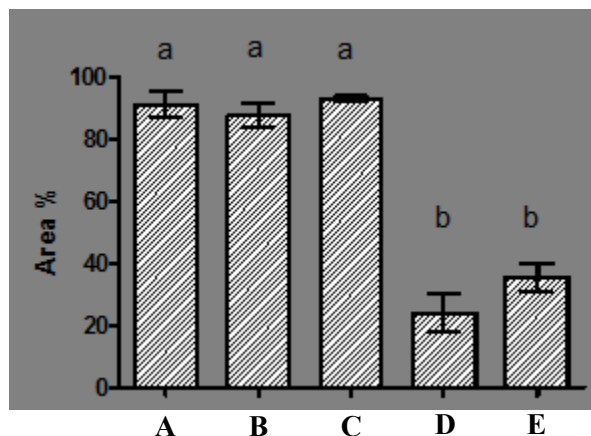


Figure 51. Percentage area threshold of CellMask plasma membrane orange stained cells on functionalized and non-functionalized polyethylene surfaces. A) LDPE; B) LDPE-HEMA-OH; C) LDPE-HEMA-COOH; D) LDPE-CA; E) LDPE-SA. Error bars display the honestly significant difference (HSD) intervals using Tukey multiple comparison with a 95 % confidence level (Tukey's HSD, $p < 0.05$). According to post-hoc analysis, means sharing the same letter are not significantly different from each other. Values are based on results from at least three separate experiments.

4.4.6 Antibiotic susceptibility test

Materials and methods

Biofilm on functionalized and non-functionalized coupons were soaked in 15 mL of 100 $\mu\text{g/mL}$ Ampicillin (Amp, Fisher Scientific) for respectively 24 h. Functionalized and non-functionalized coupons were also soaked in 15 mL of PBS for 24 h as a negative control. After the treatment, coupons were soaked in distilled water for 10 min in order to neutralize the antimicrobial agent. Collected coupons were transferred to 5 mL PBS. Sessile cells were removed from the coupon surface by 30 s vortex mixing, 2 min sonication (Branson 3510, Branson Ultrasonic Corporation, Dunbury, CT) followed by other 30 s vortex mixing. Using this procedure, all the cells were dislodged from the coupons. Dispersed cells in the bulk liquid were washed by centrifugation at 8,000 g for 30 min and suspended in PBS. Serial dilutions of the resulting cell suspensions were plated on Tryptic Soy Agar (TSA, Fisher Scientific) and incubated overnight at 37 °C. CFUs were determined by standard colony counting method. Obtained data were expressed as \log_{10}/cm^2 survived bacteria. The antimicrobial efficacy percentage was also calculated as $(\text{no. of viable cells from bulk liquid} \times 100) / (\text{no. of viable cells from bulk liquid} + \text{no. of viable cells from the remaining biofilm})$. All antimicrobial experiments were conducted in triplicate.

Results and discussion

To evaluate the susceptibility of *E. coli* biofilm to 100 µg/mL ampicillin on control LDPE, LDPE-CA and LDPE-SA functionalized surfaces, viable cells in both the biofilm and the bulk liquid were quantified by plate count analysis.

The treatment with ampicillin did not significantly affect the number of viable cells in biofilm grown of LDPE surface, since the number of viable cells in biofilm treated with ampicillin did not show significant differences respect to the biofilm grown on the same surface but treated with PBS (viable adhered cells: LDPE/PBS $7.05 \pm 0.07 \log_{10}$ CFU/cm²; LDPE/Amp $6.87 \pm 0.18 \log_{10}$ CFU/cm²) (Figure 50). On the contrary, the treatment with ampicillin drastically decreased the number of viable cells within the biofilm grown on both LDPE-CA and LDPE-SA functionalized surfaces, in comparison to the corresponding negative control treated with PBS (viable adhered cells: LDPE-CA/PBS $6.75 \pm 0.11 \log_{10}$ CFU/cm²; LDPE-CA/Amp $5.64 \pm 0.01 \log_{10}$ CFU/cm²; LDPE-SA/PBS $6.70 \pm 0.05 \log_{10}$ CFU/cm²; LDPE-SA/Amp $5.71 \pm 0.08 \log_{10}$ CFU/cm²) (Figure 52). The enhanced susceptibility of the biofilm grown on functionalized surfaces to ampicillin was also confirmed by the antimicrobial efficacy percentage that appeared significantly higher on LDPE-CA and LDPE-SA surfaces respect to LDPE surface (ampicillin efficacy percentage: LDPE/Amp 47.56 ± 7.13 %; LDPE-CA/Amp 85.59 ± 0.84 %; LDPE-SA/Amp 85.47 ± 1.92 %) (Figure 52). The combination of both LDPE-CA and LDPE-SA with ampicillin resulted in 96.2 % and 95.5 % biofilm biomass reduction respectively.

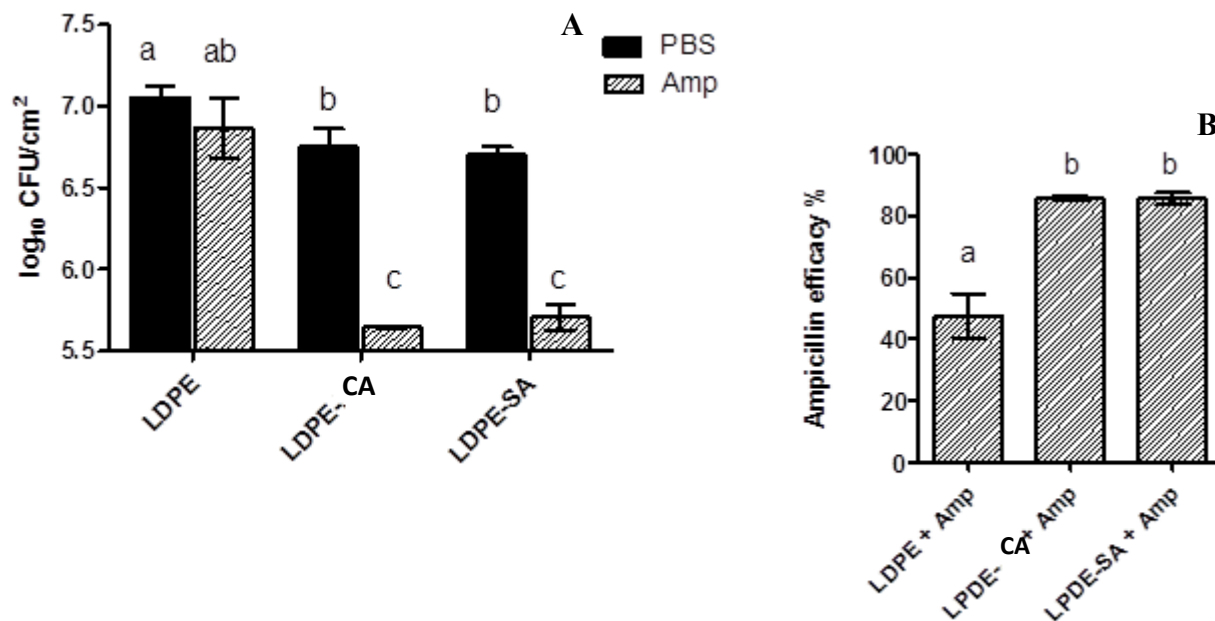


Figure 52. Ampicillin susceptibility test against *E. coli* biofilm pre-grown on functionalized and non-functionalized polyethylene surfaces. A) Biofilm growth after 24 h treatment with 100 $\mu\text{g}/\text{mL}$ ampicillin and PBS (negative control). B) 100 $\mu\text{g}/\text{mL}$ ampicillin efficacy percentage. Error bars display the honestly significant difference (HSD) intervals using Tukey multiple comparison with a 95 % confidence level (Tukey's HSD, $p < 0.05$). According to post-hoc analysis, means sharing the same letter are not significantly different from each other.

4.5 Final remarks

In this section of my research project, I carried out the functionalization of low-density polyethylene coupons with molecules selected from a formerly biological investigation, having known antibiofilm activities, with the aim to obtain a new material able to hinder the formation of the biofilm.

Before performing the covalent linkage of these compounds to a polymeric surface, also the passive coating approach was explored.

Preparing a polymer surface for the immobilisation of biologically active molecules often required a multi-step process. A low-pressure plasma reactor system was used for an efficient activation of the polymeric surfaces as well as for the grafting-polymerization process. Several analytic techniques used to characterize each step of the functionalization process were described and the obtained data reported. As for the biological evaluation, results showed that the changes made on the polyethylene due to the process of graft-polymerization did not affect the *E. coli* growth, while the grafting with *p*-aminosalicylic acid and *p*-aminocinnamic acid led to a significant decrease of biofilm biomass ($\geq 80\%$). Moreover, biofilm formed on the functionalized coupons was structurally weakened and disorganized, as confirmed from the subsequent treatment with a broad-spectrum antibiotic that completely removed bacteria from the surface.

In conclusion, as result of my research project I have obtained two new materials by the covalent linkage of molecules able to inhibit biofilm formation. Although the final characterization of these surfaces was quite difficult, due to the physical features of polyethylene coupons (e.g. thickness, density), the biological evaluation highlighted that these materials are able to resist to bacterial adhesion showing excellent anti-biofilm properties.

5. EXPERIENCE ABROAD

Constrained Diversity Oriented Synthesis for protein-protein interaction inhibitors: macrocyclic phosphopeptido-mimetics as Plk1 inhibitors targeting the Polo-box Domain and the tyrosine pocket.

During my PhD I had the opportunity to spend six months in the Department of Chemistry, University of Cambridge, under the guidance of Prof. David Spring, where I improved my skills and my knowledge on synthetic organic chemistry and chemical biology methodologies.

The work I performed was focused on the synthesis of inhibitors of the Polo-like kinase 1 (Plk1), a serine/threonine-protein kinase which has been found constitutively activated in a broad spectrum of cancer cell lines and human tumors.

5.1 Introduction

Protein-Protein Interactions (PPIs) play a central role in a broad range of essential biological processes such as intercellular communication, cellular growth and DNA replication.[134] Therefore, it is unsurprising that many human diseases can be traced to aberrant PPIs, or interactions that occur at an unsuitable time or location.[135] Hence the ability to understand and modulate their function is highly desirable. PPIs have historically been thought of as difficult to modulate with small molecules and were consequently referred to as "undruggable". This is because of the large, hydrophobic surface usually involved in the interaction and the absence of a natural small ligand to mimic. Indeed, current small molecule libraries have proven largely inadequate at addressing this target class. Despite the absence of a well-defined binding pocket it has been demonstrated that the majority of binding energy in the interaction between proteins derives from confined regions of space on the protein surface termed as "hot spots".[136] Disrupting PPIs with small molecules has particular relevance in cancer-related processes, where the functions of the aberrantly expressed proteins are manifested by their ability to communicate with their protein partners.[137] For this reason cancer-triggering PPIs have become promising therapeutic targets.

The Polo-like kinase 1 (Plk1) is a serine/threonine kinase which is essential for cell cycle progression and genomic stability.[138] It is vastly over-expressed in a range of human tumours and is associated with poor prognosis. Interference with Plk1 functions induces apoptosis in most tumour cells, but not in normal cells and the enzyme is widely considered to be a promising target

for cancer drug development.[139] A number of small molecules have been developed as ATP-competitive inhibitors of Plk1.[140] However, targeting the catalytic site incurs the problem of poor selectivity due to the high conservation of the binding site among the several kinases. Hence, there is a growing need for the development of specific Plk1 inhibitors with novel modes of action.

Plk1 engages its protein substrates via a Polo-box domain (PBD), a phosphopeptide binding module that is unique to the Plk family.[141] The phosphopeptide-driven PBD interactions mediate the correct localization of Plk1 and regulate Plk1 kinase activity.[142] There are several high-resolution crystal structures of the PBD in both unliganded and phosphopeptide substrate-bound forms.[143, 144] Substrate recognition via phospho-Ser or phospho-Thr is predominantly mediated by an extensive, water bridged hydrogen-bond network in the binding cleft. The large number of solvent-mediated contacts, in addition to direct interactions, may allow Plk1 to engage via distinct "priming" phosphorylation with a wide variety of different substrates to mediate several cellular processes.

In turn, this offers possibilities for selective inhibition of Plk1 via small molecules. Small molecules that can bind to the Plk1-PBD may disrupt recruitment of substrates by the enzyme (and/or interfere with other PBD-dependent PPIs required for normal Plk1 activity). This may provide a means of therapeutic intervention against Plk1-mediated cancers that avoids the selectivity and resistance issues associated with targeting ATP-competitive sites. We term this strategy "allo-targeting", because it bypasses the active site.

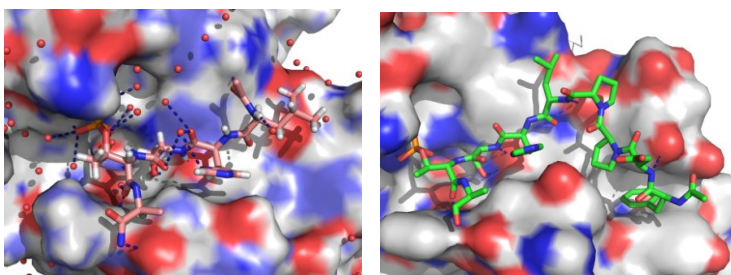


Figure 53. *Left:* Crystal structure of LHSpTA bound to the PBD (3FVH); *right:* crystal structure of FDPPLHSpTA bound to the PBD and the tyrosine pocket (3P37).

The minimal binding phosphopeptide LHSpTA has been identified from studies with the Plk1 substrate PBIP1, showing that the serine-phosphothreonine (SpT) motif makes a key contribution to the binding energy (Figure 53, *left*).[145] In later studies a cryptic pocket was discovered, known as the tyrosine pocket,

which can accommodate a hydrophobic aromatic residue (Figure 53, *right*).[146] Knowledge of these peptidic ligands and their binding modes combined with structural information about the protein surface and the hot spots involved have formed the basis for the rational design of the inhibitors described in this proposal.

5.2 Project Description (C)

The designed molecules were based on a macrocyclic core since macrocycles should be able to span more efficiently the extended binding interface associated with PPIs, allowing their functional groups to access more "hot spots" distributed across the binding surface. Their cyclic pre-organization means they have less conformational freedom in respect to their linear analogues and so suffer less entropic penalty upon binding their target.[147] In recent years interest has grown in the potential of macrocycles for drug discovery, since they combine high affinity and selectivity in structures with drug-like properties.[148, 149] In order to increase the likelihood of finding allo-inhibitors of Plk1 (that is, compounds that can bind to the Plk1-PBD), a diverse series of structures were prepared and evaluated. In this context, Diversity Oriented Synthesis (DOS) represents an excellent tool for the synthesis of diverse and structurally-complex new chemical entities. The overall aim of DOS - defined as the efficient, simultaneous synthesis of structurally diverse compounds - is to generate libraries with the greatest possible structural and functional variability through the most efficient path, thus interrogating the widest chemical space.[150]

In this project a further advance of this diversity driven approach was also evaluated. The library was constructed within preselected criteria in order to incorporate features expressly prescribed for a defined target, an approach termed constrained DOS (cDOS). Indeed, knowledge of the structure of the binding groove and the binding mode of several Plk1-PBD natural partners has facilitated the computer-assisted rational design of a cDOS library with a high potential of producing inhibitors of PPIs required for normal Plk1 activity.

Structural information about the target allowed to design complex molecules with a macrocyclic

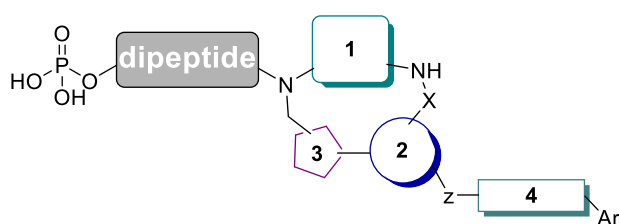


Figure 54: General skeleton of the proposed compounds

core presenting the chemical features to match PBD binding surface. The general structure is shown in Figure 54. The incorporation of the key serine-phosphothreonine motif (dipeptide) is envisioned to drive the binding towards the desired position while an aromatic ring spaced with an opportune linker (*building block 4*)

designed to occupy the hydrophobic tyrosine pocket could also improve the binding affinity. The combination of various building blocks allowed to introduce diversity in the features and the position of functional groups that are envisioned to bind the PBD, so to have more chances to find promising hits. Indeed, the modular nature of the synthesis provides access to a large number of

compounds in few steps. The subsequent coupling with the previously prepared phosphodipeptide SpT building block furnished the final compounds. Solid phase strategies were used to accomplish this goal, therefore cleavage from the resin and deprotection of the amino acid protecting groups occurred at the same time. Moreover, docking calculations to predict the ability of the planned molecule to bind the target were performed (the crystal structure of Plk1 with the opened tyrosine pocket was used).

5.3 Docking studies

The designed molecules were docked into the crystal structure of Plk1 (3RQ7) with the opened tyrosine pocket in order to predict their ability to bind the target, which is quantified by the docking score consisting of Van Der Waals, lipophilic, hydrogen bonding and metal interaction components, along with non-hydrogen bonding polar interactions in hydrophobic sites. On this basis the phosphopeptidomimetic compounds which would justify synthetic effort were selected.

All calculations were performed by the Schrödinger small-molecule drug discovery suite. The Schrödinger knowledge base (schrodinger.com/kb/639) states that a docking score of < -8 might be very good. Output data were inspected and analysed using Maestro (version 9.1-9.3) visualisation interface.[151] Grid generation is based upon the PBD-FDPPLHSpTA (3RQ7) crystal complexes and was generated in Glide.[152] The protein was prepared with the Protein Preparation Wizard (default settings).[153] The ligand was deleted and the binding site centroid specified by selection of the amino acid residues and water molecules that formerly surrounded the ligand. The chemical structures of the designed molecules were imported from an sdf file and processed initially using LigPrep (OPLS_2005 force field)[154] and then ConfGen (fast mode, default settings, OPLS_2005 force field) which generated the conformations used in the docking. [155] Glide (standard precision, default settings, OPLS_2005 force field) was used to dock ligands flexibly into the receptor grid and perform post-docking energy minimisation.[153]

The most suitable docking pose was recorded for the indole macrocycle since the presence of a side chain able to occupy the hydrophobic tyrosine pocket had improved binding affinity.

One particular conformation of this derivative (Figure 55) was an example of a ‘good’ docking pose (docking score = -12.207). The side chain was positioned correctly to interact with the residues of tyrosine pocket since the phenyl ring was lodged inside.

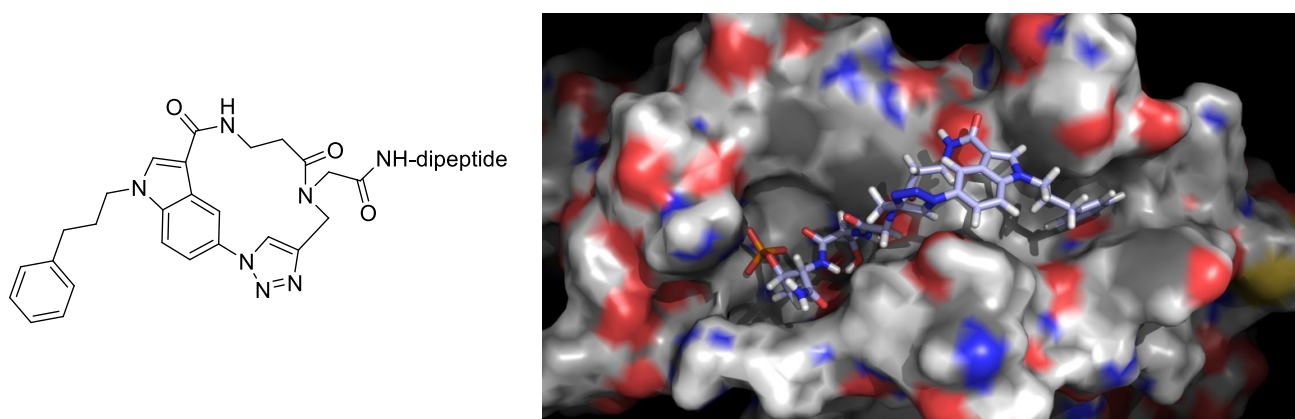


Figure 55. Docking pose for the indole macrocycle with side chain.

Also the dimer, obtained from the attempt to synthesize the indole macrocycle (for detail see ‘Paragraph 5.4’), was submitted to docking studies but it showed a bad docking score probably due to the large size of the molecule that could not reach and interact with the target.

The removal of the side chain was expected to make a significantly difference to binding affinity because it was predicted not to be interacting with the key tyrosine pocket. Actually, the docking score found for the benzyl derivative is slightly lower to that obtained for the indole macrocycle (docking score = -10.241), suggesting that this macrocycle is potentially able to bind to the PBD surface (Figure 56).

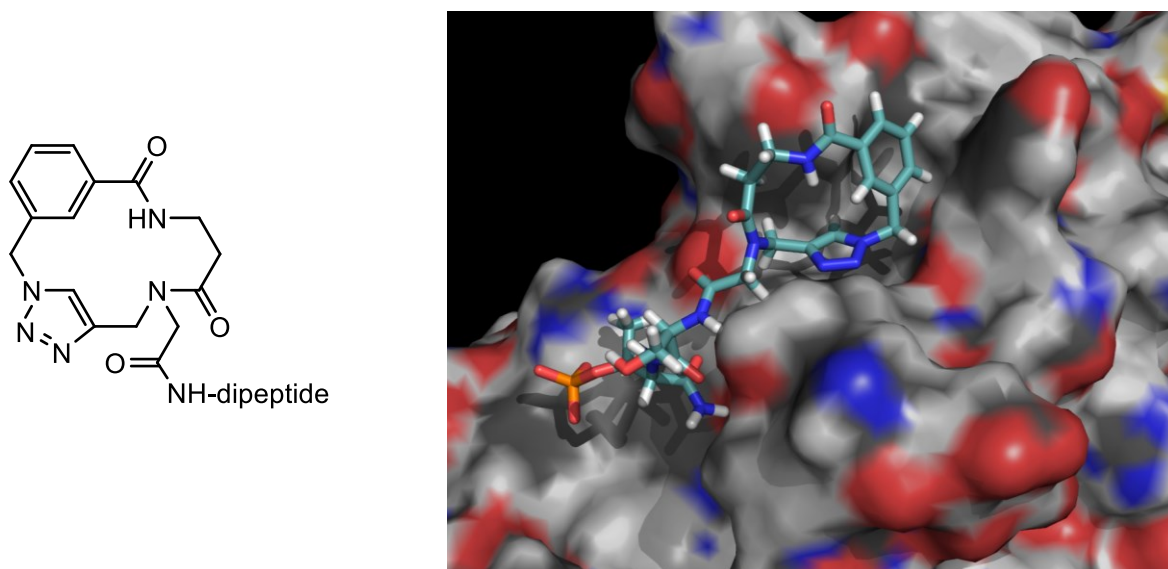


Figure 56. Docking pose for the benzyl derivative.

Another well-ranked molecule, the *m*-coumaric acid derivative, achieved a docking score of -11.811 with a sensible docking pose (Figure 57). As for the indole macrocycle, the side chain resided at the

tyrosine pocket binding site. It also appeared to fit well, spatially, within the phosphopeptide binding groove.

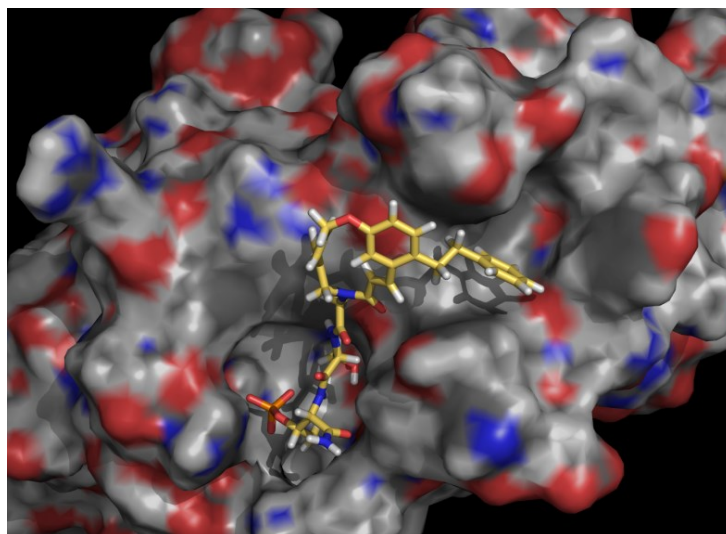
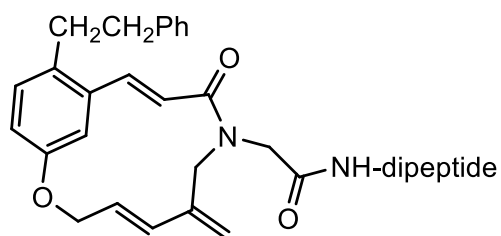


Figure 57. Docking pose for *m*-coumaric derivative.

Finally, the docking analysis of the tetrazolidinone derivative revealed that it seemed to bind with a reasonable pose to the PBD (docking score = -10.052) (Figure 58).

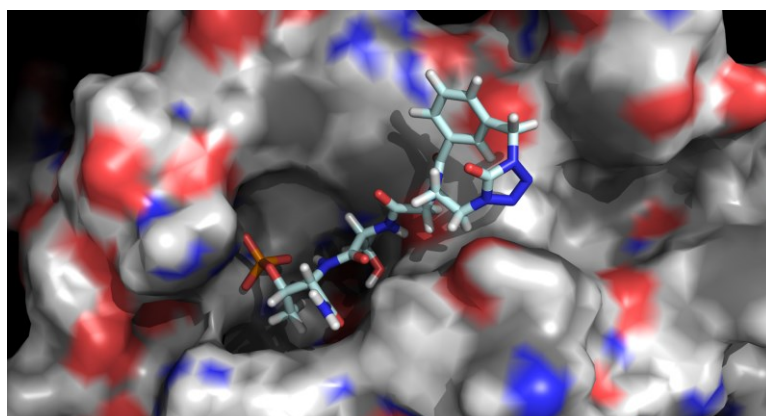
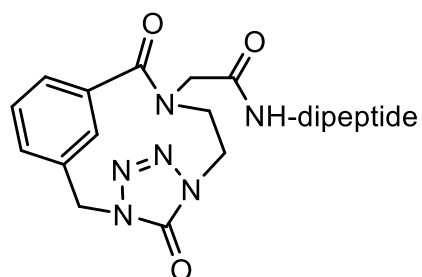


Figure 58. Docking pose for tetrazolidinone derivative.

Also in this case, the insertion of a side chain enhanced PBD binding affinity by hydrophobic interactions formed with the tyrosine pocket (docking score = -11.948) (Figure 59).

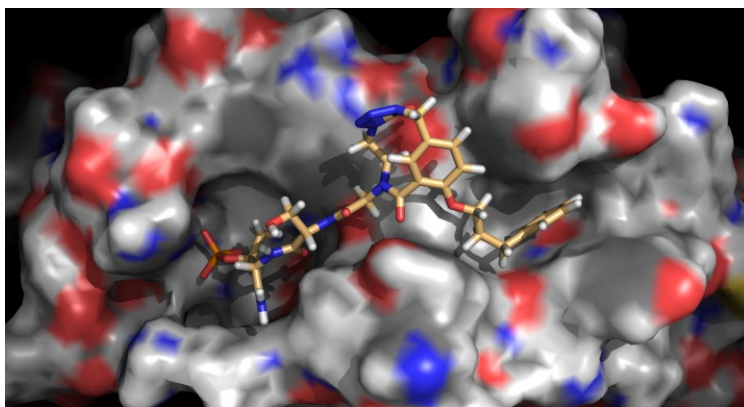
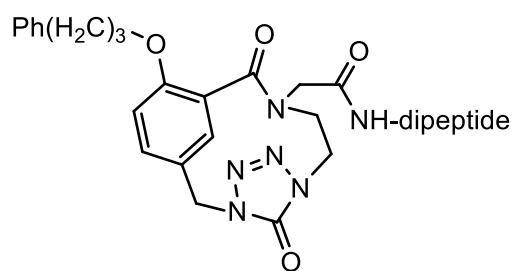
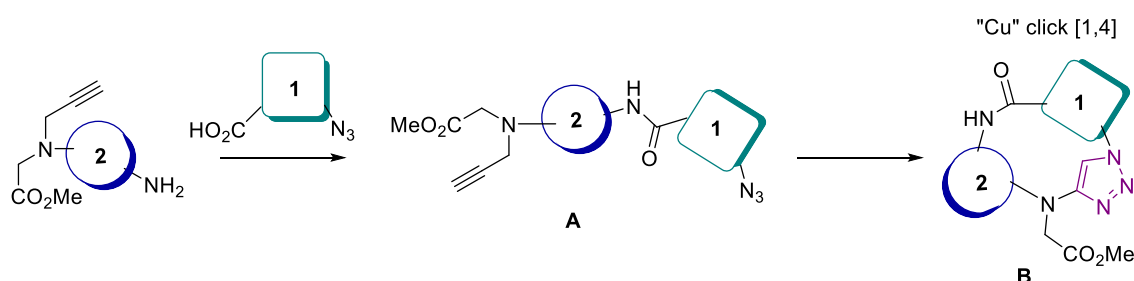


Figure 59. Docking pose for tetrazolidinone derivative with a side chain.

On the basis of computational docking experiments, the designed molecules were potential plk1-PBD inhibitors. Retrosynthetic analysis was carried out for each compound to ensure a reasonable synthetic route could be determined. Macrocycles were prepared according to the synthetic route proposed in ‘Paragraph 5.4’.

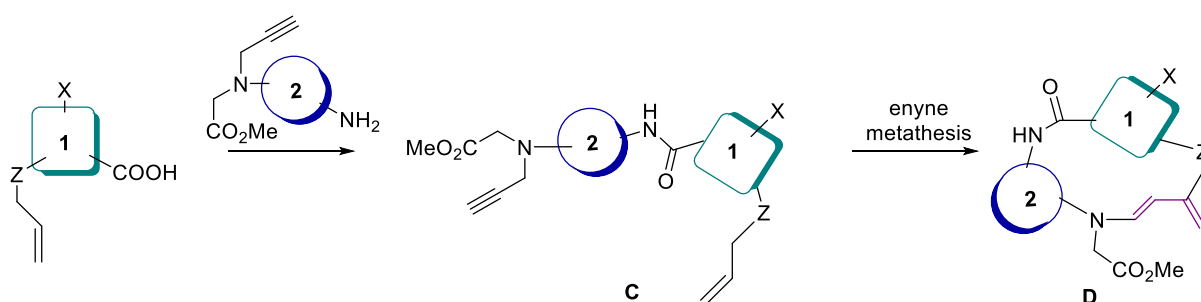
5.4 General chemistry

The construction of the macrocyclic compounds was based on a strategy previously developed in the Spring group and on new key reactions that allowed to introduce the desired functionalities. In the proposed strategy the structural diversity was achieved by exploiting the chemistry of the azide group (Scheme 9). Different starting units, synthesized with conventional chemistry, contributed to increase the diversity among the structures. In the first stage, structural diversity was introduced by varying the amine and the azide-bearing carboxylic acid. With a triple bond installed on the amine compound, intramolecular azide-alkyne cycloaddition with the "click" reaction furnished the corresponding 1,4-isomers (**B**) using Cu-catalysis for the cyclization.



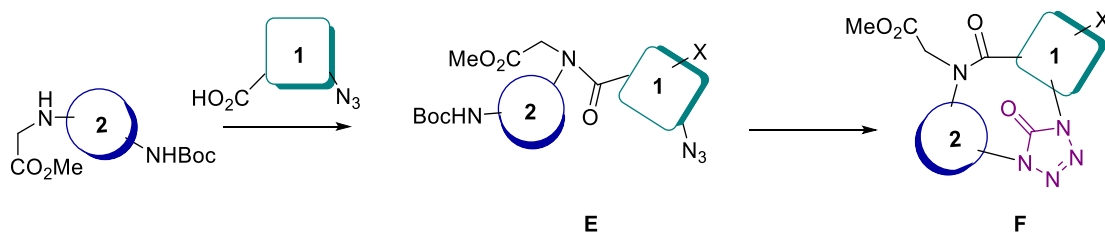
Scheme 9.

Beyond the copper-catalysed cycloaddition, enyne metathesis was also used for the cyclization (**D**) (Scheme 10).



Scheme 10.

Moreover, a new one-pot reaction carried out in mild conditions, and without the use of any metal catalyst, was employed for the synthesis of tetrazolone derivatives (**F**) (Scheme 11).

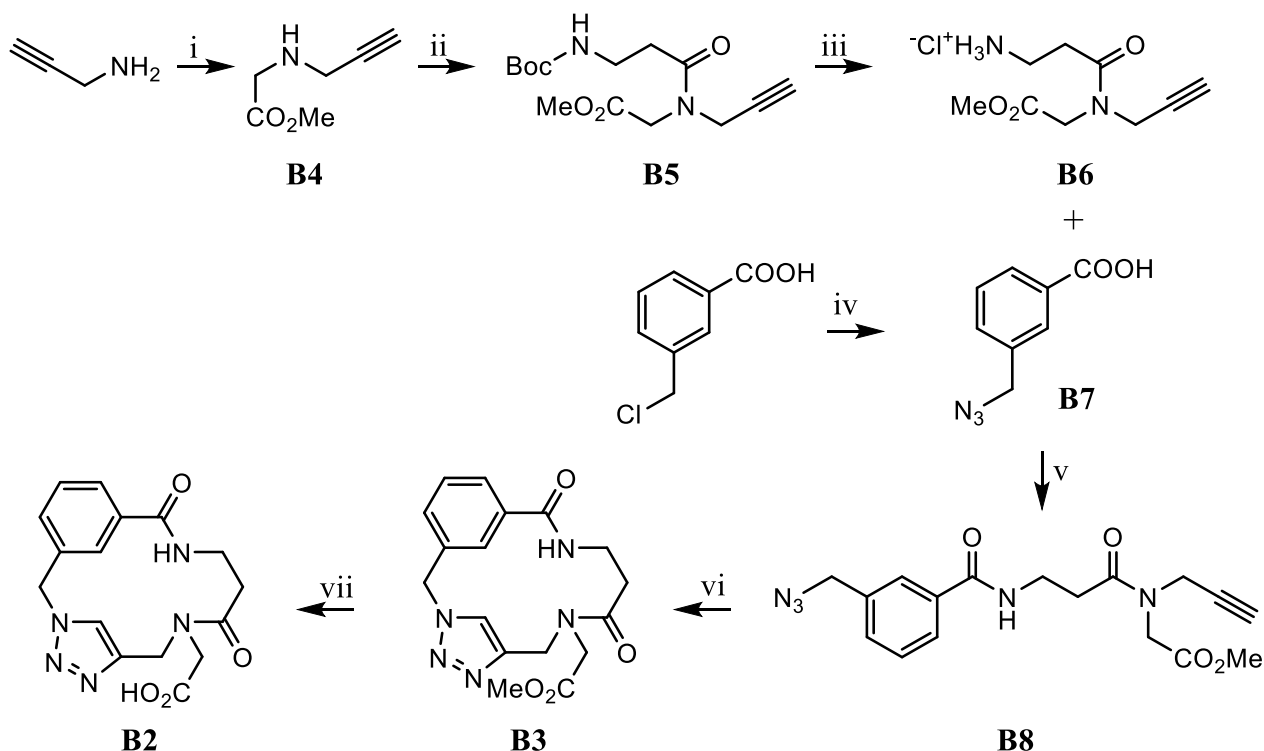


Scheme 11.

The proposed synthetic methodologies are appropriate for the obtainment of the macrocycle compounds as for the following key characteristics: i) the desired frameworks were rapidly obtained from easily accessible starting materials, ii) the building blocks are commercially available or easily synthesized and were combined in one or more synthetic iteration steps which allowed the generation of products with the desired features. The final compounds present natural product-like motifs with significantly structural diversity to increase the chances of getting new hits.

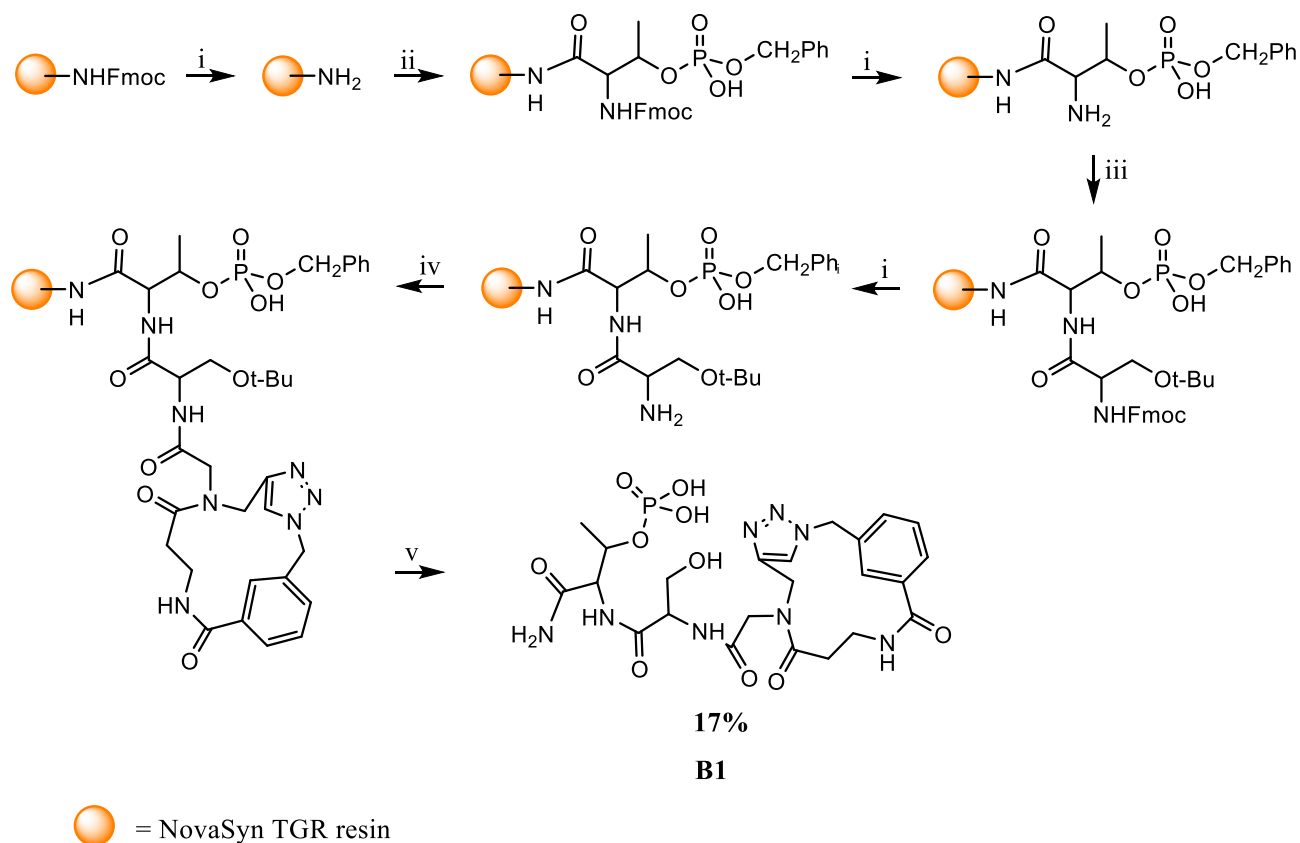
5.4.1 Synthesis of benzyl macrocycle

The final benzyl macrocycle **B2** was synthesized as shown in Scheme 12. The starting unit **B6** was prepared in two step from the commercially available propargyl amine. Alkylation with methyl bromoacetate led to *N*-propargyl glycine methyl ester **B4** which was reacted with *N*-Boc β -alanine in the presence of the coupling agent 1-[Bis(dimethylamino)methylene]-1*H*-1,2,3-triazolo[4,5-*b*]pyridinium 3-oxid hexafluorophosphate (HATU) and *N*-methylmorpholine (NMM) to afford the amido compound **B5**. Its Boc-protecting group was then hydrolysed with a 4*N* solution of HCl in dioxane to obtain the building block unit **B6**. Azido building block **B7** was synthesized from the commercially available 3-chloromethyl benzoic acid which underwent a nucleophilic substitution with sodium azide in DMSO. The amidic coupling between compound **B6** and **B7** led to the formation of the linear precursor **B8** which were subsequently macrocyclized using copper-catalysed cycloadditions (CuAAC) providing the 1,4-isomers **B3**. A basic hydrolysis of the ester group was then performed and this led to the formation of the corresponding acid **B2** (40% yield).



Scheme 12. Reagents and conditions: i) methyl bromoacetate, DIPEA, dry DCM, rt, overnight; ii) *N*-Boc β-alanine, NMM, HATU, dry DCM, rt, overnight; iii) HCL-dioxane 4N, dry DCM, rt, 3h; iv) NaN₃, DMSO, 30°C, 5h; v) NMM, HATU, dry DCM, rt, overnight; vi) CuI, DIPEA, dry THF, reflux, 120h (*C*=0.00075M); vii) LiOH, THF/water (2:1), rt, 4h, then HCl-dioxane 4 N, 10min, rt.

NovaSyn TGR resin was used to prepare peptide amides utilizing Fmoc chemistry (Scheme 13). The resin was pre-swelled in DCM and washed with DMF, then de-protected with 20% piperidine in DMF. The peptide sequence is assembled using the standard coupling procedure with HATU as the coupling agent and DIPEA as a base. To check if the coupling step had proceed to completion, the chloranyl test was performed for the identification of unreacted amines. Finally the completed macrocyclic dipeptide **B1** is cleaved from the resin under acidic conditions.

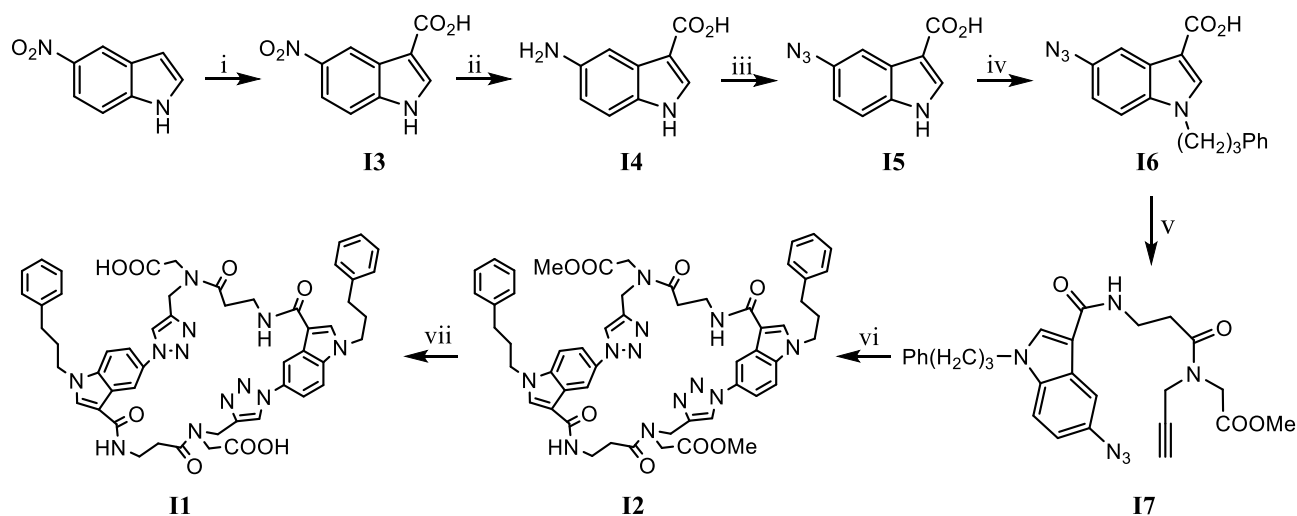


Scheme 13. Reagents and conditions: i) 20% piperidine in DMF, 2 x 10 min, rt; ii) Fmoc-Thr(HPO₃Bzl)-OH, DIPEA, HATU, DMF, rt, 2h; iii) NH-Fmoc-*tert*-Bu-serine, DIPEA, HATU, DMF, rt, 2h; iv) Macrocycle, DIPEA, HATU, DMF, rt, 2h; v) 95% TFA, 2.5% TIPS, 2.5% H₂O, rt, 2h.

5.4.2 Synthesis of indole macrocycle

The synthesis of compounds **I1** and **I2** is shown in Scheme 14. The commercially available 5-nitroindole was carboxylated with trifluoroacetic anhydride and following hydrolysis with 1 M NaOH to obtain the 5-nitro-*1H*-indole 3-carboxylic acid **I3**. The subsequent hydrogenation of the nitro group provided the amine **I4** which underwent a nucleophilic substitution on the diazonium intermediate with sodium azide to afford the azido unit **I5**. This latter was reacted with the 3-bromo-1-phenylpropane in the presence of sodium hydride as a base providing compound **I6** in moderate yield. Then the carboxylic group was condensed with the previously described intermediate **B6** to obtain the amide **I7**. This reaction was performed with HATU in the presence of *N*-methylmorpholine at room temperature for 16 h. The subsequent macrocyclization using copper-catalysed cycloadditions (CuAAC) provided the final compound **I2**. Unfortunately, the desired macrocycle could not be obtained, likely due to its highly strained nature, and only the dimer **I2** was

found. The basic hydrolysis of esters with lithium hydroxide led to the formation of the corresponding carboxylic acid **11**.

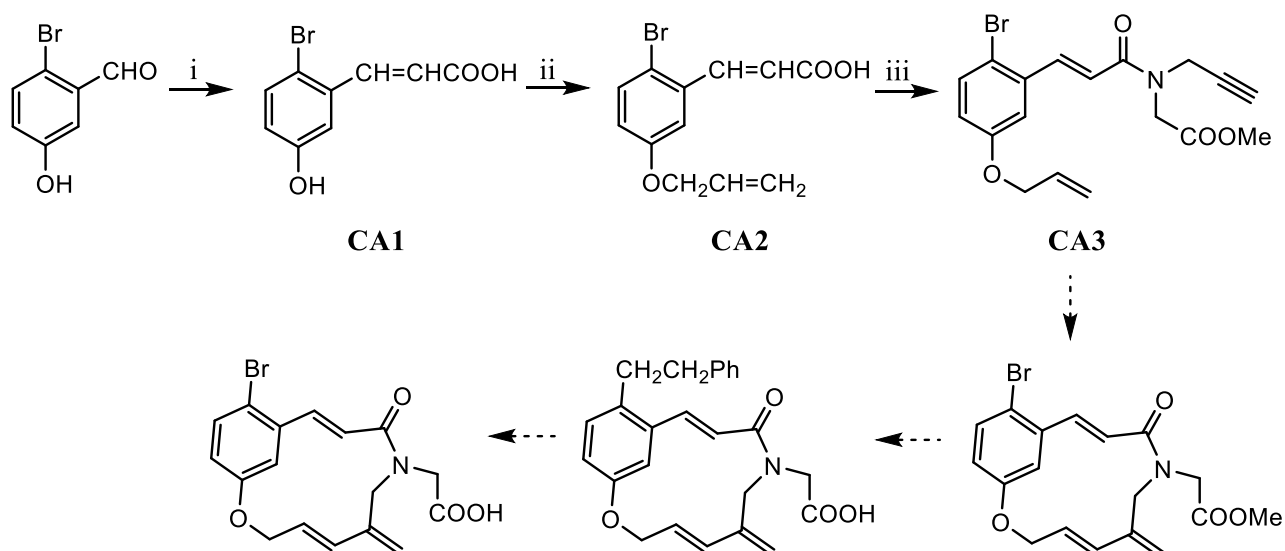


Scheme 14. Reagents and conditions: i) 1) TFAA, dry DMF, reflux, overnight; 2) NaOH 25%, reflux, overnight; ii) H₂, Pd/C, MeOH, rt, overnight; iii) NaNO₂, NaN₃, rt, 2h; iv) 3-Br-1-phenylpropane, NaH (60% mineral oil), dry THF, rt, 24h. v) **B6**, NMM, HATU, dry DCM, rt, overnight; vi) CuI, DIPEA, dry THF, reflux, 168h (C=0.00075M); vii) LiOH, THF/water (2:1), rt, 4h, then HCl-dioxane 4 N, 10min, rt.

5.4.3 Synthesis of the coumaric acid macrocycle

As shown in Scheme 15, the precursor of the coumaric acid macrocycle was selected as the commercially available 5-bromo-2-hydroxy benzaldehyde. 5-bromo-2-hydroxy *m*-coumaric acid **CA1** was synthesized through a one-pot reaction with malonic acid in pyridine. **CA1** was then treated with allyl bromide and potassium carbonate to obtain the diallyl derivative, which was hydrolyzed in basic conditions to afford the allyl ether **CA2**. The amidic coupling with the intermediate **B4** allowed the formation of the linear precursor **CA3**. The subsequent macrocyclization using enyne metathesis in the presence of Grubbs second-generation catalyst should have led to the coumaric acid macrocycle. Unfortunately, this reaction failed to proceed likely due to the interference of the internal double bond of the coumaric scaffold.

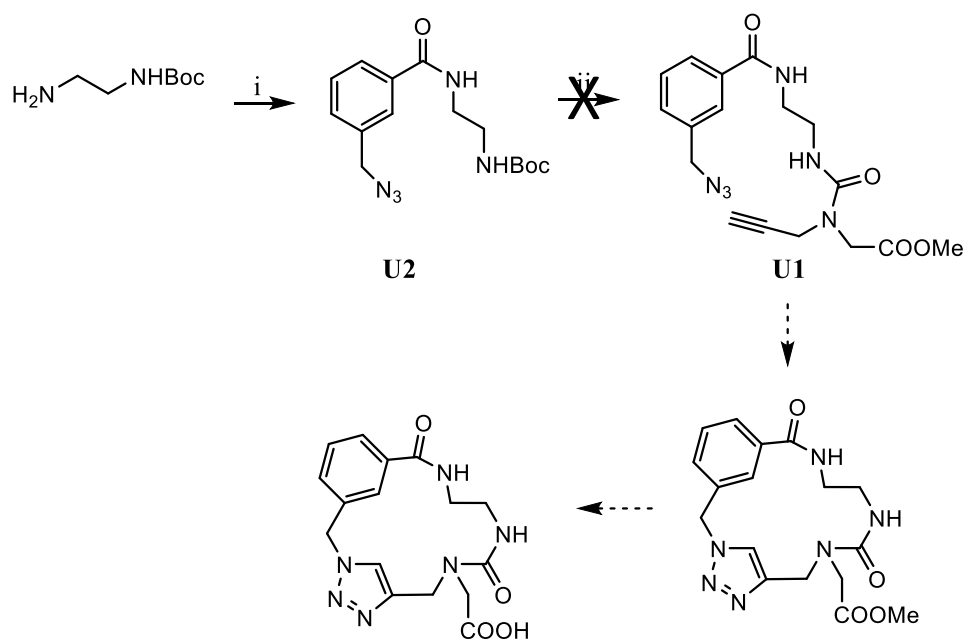
Different reaction conditions were attempted providing in most cases undesired byproducts. The synthesis should have been completed by a Suzuki coupling and the final hydrolysis of the ester group.



Scheme 15. Reagents and conditions: i) malonic acid, piperidine (cat.), dry Py, reflux, 4h; ii) 1) allyl bromide, K_2CO_3 , acetone, reflux, 20h; 2) 1 M NaOH, EtOH, reflux, 1h; iii) **B4**, NMM, HATU, dry DCM, rt, overnight;

5.4.4 Synthesis of the urea macrocycle

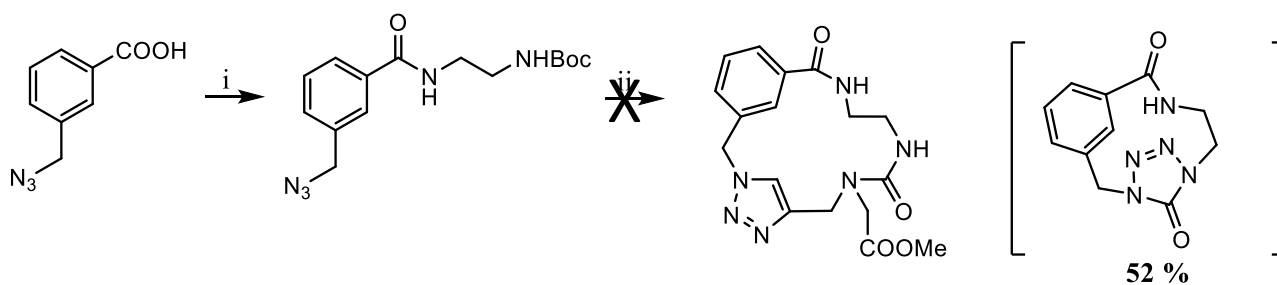
In order to synthesize the urea macrocycle, I followed a one-pot procedure described by Spyropoulos and Kokotos [156] to obtain the urea containing linear precursor **U1** (Scheme 16). According to this procedure, the Boc-protected amine **U2**, obtained from the coupling reaction between the commercially available *N*-Boc ethylenediamine and the intermediate **B7**, could be transformed into a trisubstituted urea through *in situ* generation of the isocyanate with 2-chloropyridine and triflic anhydride. Despite the screening of several reaction conditions (See Table “Reagents and conditions”), I obtained the linear precursor **U2** only as traces.



Scheme 16. Reagents and conditions: i) NMM, HATU, dry DCM, rt, overnight; ii) 1. Tf_2O , 2-CIPy, 50min, rt; 2. **B4**, see Table.

Starting material	B4	Tf_2O	NEt_3	2-CIPy	Solvent	Time	T
1	3	1,5	0	3	DCM	20h	rt
1	3	2,5	0	5	DCM	20h	rt
1	3	1,5	6	3	DCM	20h	rt
1	3	1,5	0	3	toluene	20h	reflux

The main product I've obtained using toluene as solvent under reflux was the cyclic tetrazolone (Scheme 17).



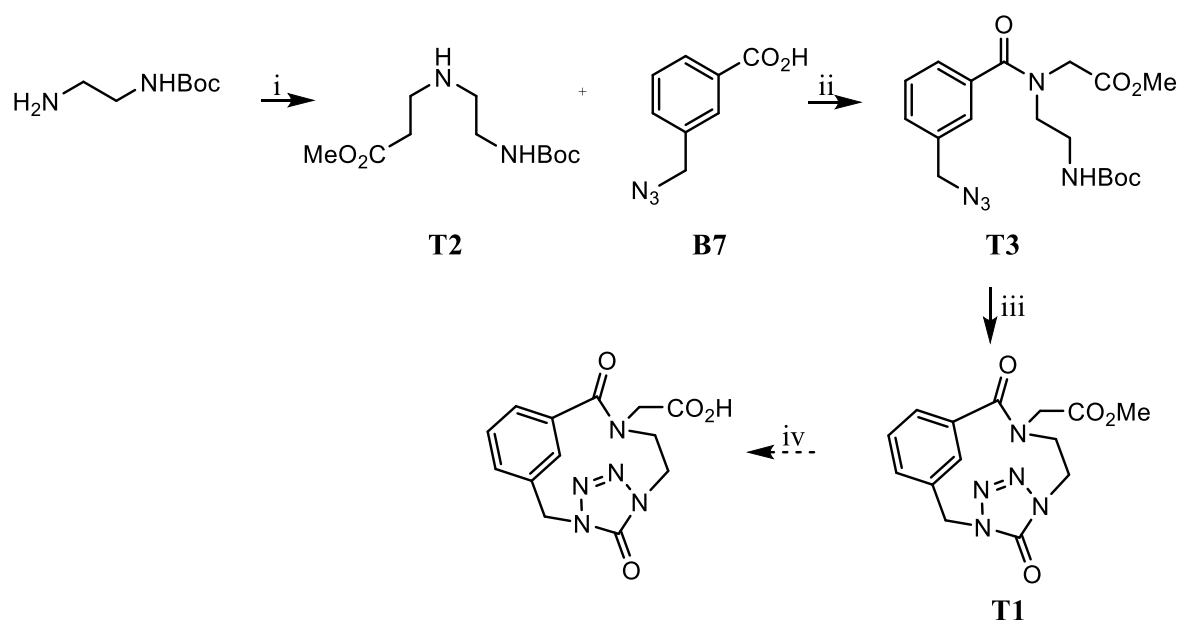
Scheme 17. Reagents and conditions: i) NMM, HATU, dry DCM, rt, overnight; ii) 1. Tf_2O , 2-CIPy, toluene, 50min, rt; 2. **B5**, 20h, reflux.

This reaction was interesting since it could be a new method to cyclise linear scaffold in one-pot reaction without using any metal catalyst and could be applied to several starting building blocks

with different chain lengths in order to provide macrocycle of different sizes. Indeed, this reaction was employed for the synthesis of the following tetrazolone derivative **T1**.

5.4.5 Synthesis of the tetrazolone macrocycle **T1**

As depicted in Scheme 18, the synthesis of tetrazolone macrocycle **T1** started from the commercially available *N*-Boc diethylamine which was alkylated with methyl bromoacetate to afford compound **T2**. Then this latter was coupled with the previously synthesized benzyl azide **B7** to provide compound **T3**. Also in this case, different conditions to obtain the final tetrazolone **T1** were performed (See Table “Reagents and conditions”): reactions carried out at room temperature led to the starting material, while changing the solvent and increasing the temperature **T1** was obtained unfortunately only in low yield.



Scheme 18. Reagents and conditions: i) methyl bromoacetate, DIPEA, dry DCM, rt, overnight; ii) NMM, HATU, dry DCM, rt, overnight; iii) see Table; iv) LiOH, THF/water (2:1), rt, 4h.

Starting material	Tf ₂ O	NEt ₃	2-CIPy	Solvent	Time	T	Yield
1	1,5	0	3	DCM	20h	rt	SM
1	1,5	3	3	toluene	20h	rt	SM
1	1,5	0	3	DCE	20h	60°C	traces
1	1,5	0	3	toluene	20h	70°C	15%

5.5 Experimental Session

5.5.1 Materials and methods

Except as otherwise indicated, reactions were carried out using oven-dried glassware under nitrogen with dry, freshly distilled solvents. Tetrahydrofuran was distilled from calcium hydride and LiAlH_4 in the presence of triphenyl methane. Diethyl ether was distilled from calcium hydride and LiAlH_4 . CH_2Cl_2 , MeOH, toluene, MeCN and hexane were distilled from calcium hydride. Petroleum ether refers to the 40-60 °C fractions. All other reagents were used as obtained from commercial sources.

Thin layer chromatography was carried out on glass Merck Kieselgel 60 F254 plates, visualised by ultraviolet irradiation (254 and 365 nm) or stains as ninhydrin and potassium permanganate, prepared by standard procedures. Retention factors (R_f) are quoted to 0.01. Flash column chromatography was carried out using slurry-packed Merck 9385 Kieselgel 60 silica gel under a positive pressure of air or nitrogen.

Preparative HPLC purification was performed on an Agilent 1260 Infinity system fitted with a Supelcosil ABZ+Plus column (250 mm x 21.2 mm, 5 μm) using linear gradient systems (solvent A: 0.1% (v/v) TFA in water, solvent B: 0.05% (v/v) TFA in acetonitrile) at a flow rate of 20 mL min^{-1} . Analytical HPLC analysis was performed on an Agilent 1260 Infinity system fitted with a Supelcosil ABZ+Plus column (150 mm x 4.6 mm, 3 μm) using linear gradient systems (solvent A: 0.05% (v/v) TFA in water, solvent B: 0.05% (v/v) TFA in acetonitrile) over 15 min at a flow rate of 1 mL min^{-1} . Retention times (t_r) are reported to the nearest 0.01 min. Peak area percentages are calculated for the UV absorbance at 220 nm and reported to the nearest 1%

Nuclear magnetic resonance (NMR) spectra were recorded using an internal deuterium lock on Bruker DPX 400 (400MHz), Bruker Avance 400 QNP Ultrashield (400 MHz), Bruker Avance 500 BB ATM (500 MHz) and Bruker Avance 500 Cryo Ultrashield (500 MHz) spectrometers. Chemical shifts (δ) are referenced to the solvent signal and are quoted in ppm to the nearest 0.01 ppm for δ_{H} and to the nearest 0.1 ppm for δ_{C} . Coupling constants (J) are reported in Hertz to the nearest 0.1 Hz. Assignments are supported by DEPT-135, ^1H - ^1H COSY, HMQC, HMBC and NOESY spectra where necessary. Data are reported as follows: chemical shift, multiplicity (br, broad; s, singlet; d, doublet; t, triplet; q, quartet; quint, quintet; m, multiplet; or as a combination of these), integration, assignment and coupling constant(s). Low resolution mass spectra (ESI) were recorded using an LCMS system (Agilent 1200

series LC with an ESCi Multi-Mode Ionization Waters ZQ spectrometer using MassLynx 4.0 software). High resolution mass spectrometry (HRMS) was carried out with a Micromass Q-TOF or a Waters LCT Premier Mass Spectrometer using electrospray ionisation [ESI] or electron ionisation [EI]. The dipeptide was synthesized on NovaSyn TGR resin (0.25mmol x g) using standard Fmoc-solid phase protocol. Fmoc-phosphothreonine and Fmoc tert butyl-serine were purchase from Novabiochem and used without any further purification.

5.5.2 General procedures

5.5.2.1 GP1- Amide formation

At 0 °C, the appropriate carboxylic acid (1 eq) was dissolved in dry DCM (0.6 M) followed by addition of *N*-methyldmorpholine (1.2 eq) and HATU (1.2 eq). The reaction mixture was stirred for 20 min at 0 °C then the amine (1.2 eq), dissolved in the minimum amount of solvent, was added. The reaction was stirred at room temperature for 16 h. Then the mixture was diluted with water (20 mL) and extracted with dichloromethane (3 × 10 mL). The organic layers were washed with a 10 % solution of citric acid (3 x 10 mL), dried over MgSO₄ and concentrated *in vacuo*. Purification conditions are specified in the description of each product.

5.5.2.2. GP2 – CuAAC macrocyclization

The linear precursor (1.0 eq) was dissolved in dry THF (0.75 mM) and DIPEA (3 eq) was added. After bubbling argon through the solution for 20 min, CuI (2 eq) was added and the mixture was heated to reflux until HPLC analysis indicated complete turnover. Subsequently, the solvent was removed and the residue was dissolved in CH₂Cl₂/MeOH (9:1), filtered through a pad of SiO₂ and further purified as indicated.

5.5.2.3 GP3 - Metathesis macrocyclization

The linear precursor (1.0 eq) was dissolved in dry CH₂Cl₂ (1 mM) and ethylene was bubbled through the solution for 10 min. Grubbs 2nd generation catalyst (0.2 eq) was added and the reaction was heated to reflux under an ethylene atmosphere. When HPLC indicated complete formation of the diene intermediate (typically after 4 h), the atmosphere was changed to argon. Refluxing was continued until HPLC indicated reaction completion; if an incomplete conversion was observed, additional catalyst

was added in portions of 0.1 eq. The solvent was removed under reduced pressure and the crude product was purified as indicated.

5.5.2.4 GP4 – Hydrolysis

The suitable macrocycle (1.0 eq) was dissolved in THF (20 mM) and a solution of LiOH (2.0 eq) in water (half of the THF volume) was added at 0 °C. After stirring at room temperature until TLC indicated complete reaction (~2 h), the reaction was quenched by the addition of HCl in dioxane (4 M; 2.5 eq) and stirred for another 10 minutes. The solvent was removed under a stream of nitrogen and the residue was purified using preparative HPLC.

5.5.2.5 GP5 - Coupling with dipeptide

Activation of resin

The NovaSyn TGR resin (0.25 mmol x g, 1eq) was swelled in dichloromethane (3 x 1 mL) and washed with DMF (3 x 1 mL). the Fmoc protecting group is removed by treatment with 20% piperidine in DMF under continuous stirring (x 1 min) and then under mild stirring (2 x 10 min). Finally, the resin was washed with DMF (3 x 1 mL).

Chloranil test [157]

This sensitive test has been developed for reliable detection of primary and secondary amino groups. The solution consists of 50 µL chloranil in toluene and 200 µL acetaldehyde. A few beads of resin are placed in a small test tube and 2-5 drops of solution are added. After a short mixing the mixture is left at room temperature for 5 min and the beads inspected.

Results:

colourless to yellowish beads: negative (absence of free amine in the mixture);

dark blue to green beads: positive, the coupling should be repeated.

Coupling of aminoacids to the resin

NH-Fmoc-phosphothreonine was dissolved in the minimum amount of DMF (1 mL) and HATU (2.25 eq) and DIPEA (4.5 eq) were added. The mixture was stirred at room temperature for 10 min. Then the solution was added to the activated resin and stirred for 2 hours at room temperature.

The coupling was monitored by chloranil test until completion. The resin was washed with DCM (3 x 1 mL) and dried before the test.

The Fmoc protecting group was removed by treatment with 20% piperidine in DMF as described in ‘Activation of resin’.

Fmoc tert-butyl serine (4 eq) was coupled to the resin in the presence of HATU (4 eq) and DIPEA (8 eq) with the same procedure used for NH-Fmoc-pThr. The chloranil color test was performed before proceeding to the next step.

Coupling of macrocycle to the resin.

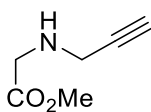
The resin was washed with DMF (3 x 1 mL) and the coupling with macrocycle was performed. A solution of suitable macrocycle (1 eq), HATU (1 eq) and DIPEA (2 eq) in DMF (1 mL) was added to the peptide resin. The mixture was stirred at room temperature for 16 h. If the chloranil color test has been positive, the functionalized resin was washed with DMF (3 x 1 mL), dried with DCM (3 x 1 mL) and the TFA cleavage was carried out.

Cleavage from the resin

The dipeptide macrocycle was cleaved from the resin by treatment with 2 mL of trifluoroacetic acid: triisopropylsilane:H₂O (95:2.5:2.5) for 4 h at room temperature. The resin was filtered off and the filtrate was concentrated under *vacuo*. After the addition of cold Et₂O, a precipitation of a white solid occurred. The precipitate was washed with diethyl ether (3 x 1 mL). The resulting solid was dissolved in DMSO and purified with a reverse phase preparative HPLC to afford the final product.

5.5.3 Synthesis of benzyl derivatives (B1-9)

Synthesis of *N*-propargyl-glycine methyl ester **B4**

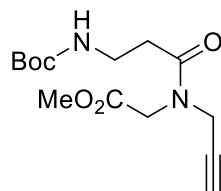


DIPEA (570 μ L, 3.27 mmol) and methyl bromoacetate (309 μ L, 3.27 mmol) were added dropwise to a solution of propargyl amine (418 μ L, 6.54 mmol, 2.00 eq) in dry CH₂Cl₂ (11.6 mL). The reaction mixture was stirred at room temperature for 16 h and then the solvent was removed. After purification by flash column chromatography (petroleum ether/EtOAc 8:2 to 6:4) the title compound **B4** was isolated.

Yield: 77 %. Yellow pale oil. R_f = 0.25 (Petroleum ether/ EtOAc 5:5). ¹H NMR (500 MHz, CDCl₃) δ = 3.76 (s, 3H, CH₃), 3.55 (s, 2H, CH₂), 3.51 (d, 2H, CH₂, J=2.4 Hz), 2.25 (t, 1H, CH, J = 2.4), 1.55 (br s,

1H, NH). ^{13}C NMR (125 MHz, CDCl_3) δ = 172.3, 81.0, 72.0, 51.9, 49.0, 37.6. HRMS consistent with literature data.

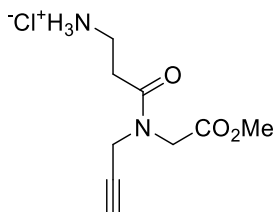
Synthesis of *N-tert*-Butoxycarbonyl-L-alanyl-N-propargyl-L-glycine methyl ester **B5**



At 0 °C, to a solution of Boc β -alanine (572 mg, 3.02 mmol) in dry DCM (41 mL) *N*-methylmorpholine (322 μL , 3.02 mmol) was added, followed by HATU (931 mg, 3.02 mmol). The reaction mixture was stirred for 20 min at 0 °C whereupon **B4** (320 mg, 2.52 mmol), dissolved in the minimum amount of solvent, was added. The reaction was stirred at room temperature for 16 h. Then the mixture was diluted with water (20 mL) and extracted with dichloromethane (3 \times 10 mL). The organic layers were washed with a 10 % solution of citric acid (3 \times 10 mL), dried over MgSO_4 and concentrated *in vacuo*. The crude product was purified by flash chromatography (petroleum ether/EtOAc 8:2 to 6:4) to afford compound **B5** as a mixture of two rotamers (**B5a**, **B5b**) (80 % yield, 1:1.5 ratio).

Colourless oil. R_f = 0.54 (DCM/MeOH 9:1). ^1H NMR (400 MHz, CDCl_3) (**B5a**) δ = 4.35 (d, 2H, CH_2 , J = 2.4), 4.22 (s, 2H, CH_2), 3.79 (s, 3H, CH_3), 3.49 - 3.42 (m, 2H, CH_2), 2.46 (t, 2H, CH_2 , J = 5.6), 2.27 (t, 1H, CH, J = 2.4), 1.59 (s, 9H, 3 CH_3); (**B5b**) δ = 4.25 (s, 2H, CH_2), 4.17 (d, 2H, CH_2 , J = 2.4), 3.76 (s, 3H, CH_3), 3.49 - 3.42 (m, 2H, CH_2), 2.67 (t, 2H, CH_2 , J = 5.6), 2.35 (t, 1H, CH, J = 2.4), 1.45 (s, 9H, 3 CH_3); ^{13}C NMR (125 MHz, CDCl_3) (**B5a**) δ = 172.1, 169.5, 155.9, 79.2, 73.5, 52.6, 47.6, 38.1, 33.3, 28.4. (**B5b**) δ = 171.9, 169.2, 155.9, 78.0, 73.0, 52.2, 46.3, 35.1, 33.2, 28.4. HRMS (ESI+) found m/z = 299.1606 $[\text{M-H}]^+$, $\text{C}_{14}\text{H}_{23}\text{N}_2\text{O}_5^+$ required 299.1607.

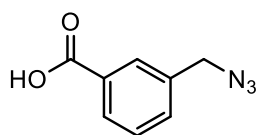
Synthesis of L-alanyl-N-propargyl-L-glycine methyl ester hydrochloride **B6**



A solution of Boc-protected methyl ester **B5** (605 mg, 2.2 mmol) in dry CH_2Cl_2 (1.8 mL) was cooled to $0\text{ }^\circ\text{C}$ and 4 M HCl in 1,4-dioxane (2 mL) was added dropwise. The reaction was stirred for 5 h at room temperature. The solvent was removed under a stream of N_2 to yield amine **B6** as a mixture of two rotamers (**B6a**, **B6b**) (90 % yield, 1:1.5 ratio) used in the next step without any further purification.

Orange foam. $R_f = 0.12$ (DCM/MeOH 9:1). $^1\text{H NMR}$ (400 MHz, MeOD) (**B6a**) $\delta = 4.37$ (s, 2H, CH_2), 4.33 – 4.31 (m, 2H, CH_2), 3.80 (s, 3H, CH_3), 3.26 – 3.20 (m, 2H, CH_2), 2.90 (t, 1H, CH, $J = 2.4$), 2.76 – 2.72 (m, 2H, CH_2). (**B6b**) $\delta = 4.33$ – 4.31 (m, 2H, CH_2), 4.27 (s, 2H, CH_2), 3.75 (s, 3H, CH_3), 3.26 – 3.20 (m, 2H, CH_2), 2.97 (t, 1H, CH, $J = 6.5$), 2.76 – 2.72 (m, 1H, CH). $^{13}\text{C NMR}$ (100 MHz, MeOD) (**B6a**) $\delta = 172.3$, 171.1, 78.7, 74.4, 53.0, 39.1, 36.9, 36.6, 30.8. (**B6b**) $\delta = 172.3$, 171.2, 78.4, 75.2, 52.7, 38.9, 36.8, 36.3, 30.8. HRMS (ESI+) found $m/z = 199.1081$ $[\text{M-H}]^+$, $\text{C}_9\text{H}_{15}\text{N}_2\text{O}_3^+$ required 199.1083.

Synthesis of 3-(Azidomethyl)benzoic acid **B7** [158]

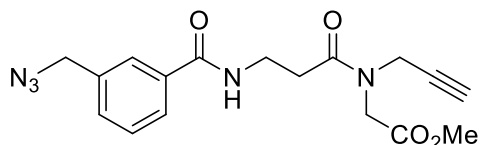


3-(Chloromethyl)benzoic acid (500 mg, 2.93 mmol) was dissolved in DMSO (10 mL, $C = 0.3\text{M}$), and sodium azide (230 mg, 3.52 mmol) was added. After stirring at $30\text{ }^\circ\text{C}$ for 5 h, the reaction mixture was diluted with water (10 mL) and extracted with EtOAc (4×3 mL). The combined organic layers were washed with water and brine and dried over Mg_2SO_4 . The solvent was removed under reduced pressure to give the crude azide **B7**.

Yield: 86 %. White solid. $R_f = 0.42$ (Hexane/ EtOAc 5:5); **m.p.** $68\text{--}69\text{ }^\circ\text{C}$. $^1\text{H NMR}$ (500 MHz, CDCl_3) $\delta = 8.10$ (dt, 1H, ArH, $J = 7.7$, $J = 1.5$), 8.07 (s, 1H, ArH), 7.60 (dt, 1H; ArH, $J = 7.7$, $J = 1.4$), 7.52 (t, 1H, ArH, $J = 7.7$), 4.44 (s, 2H, CH_2). $^{13}\text{C NMR}$ (125 MHz, CDCl_3 , $27\text{ }^\circ\text{C}$) $\delta = 170.9$, 136.5, 133.8,

130.5, 130.2, 130.1, 129.6, 54.7. **HRMS** (ESI-) found $m/z = 176.0465$ $[M-H]^-$, $C_8H_6N_3O_2^-$ required 176.0465.

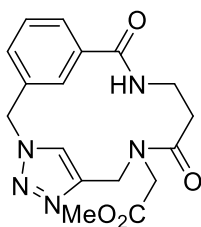
Synthesis of the linear benzyl amide **B8**



GP1 was followed to prepare the linear compound **B8** from intermediates **B6** and **B7**. The crude product was purified by flash chromatography (petroleum ether/EtOAc 8:2 to 5:5) as a mixture of two rotamers (**B8a**, **B8b**) (88 % yield, 1.5:1 ratio).

Colourless oil. $R_f = 0.28$ (Hexane/EtOAc 3:7). **HPLC** $t_r = 12.52$ min (10-60 % B). 1H NMR (400 MHz, $CDCl_3$) (**B8a**) $\delta = 7.77 - 7.71$ (m, 2H, ArH), 7.48 – 7.45 (m, 2H, ArH), 7.12 (br s, 1H, NH), 4.42 (s, 2H, CH_2), 4.36 (d, 1H, CH_2 , $J = 2.4$), 4.18 (t, 1H, CH_2 , $J = 2.4$), 3.87 – 3.79 (m, 2H, CH_2), 3.77 (s, 3H, CH_3), 2.82 (t, 2H, CH_2 , $J = 5.6$), 2.33 (t, 1H, CH, $J = 2.4$); (**B8b**) $\delta = 7.77 - 7.71$ (m, 2H, ArH), 7.48 – 7.45 (m, 2H, ArH), 7.12 (br s, 1H, NH), 4.27 (s, 2H, CH_2), 4.23 (d, 1H, CH_2 , $J = 2.4$), 4.18 (d, 1H, CH_2 , $J = 2.4$), 4.15 (s, 1H, CH_2), 4.13 (s, 1H, CH_2), 3.78 (s, 3H, CH_3), 2.60 (t, 2H, CH_2 , $J = 5.6$), 2.27 (t, 1H, CH, $J = 2.4$). ^{13}C NMR (125 MHz, $CDCl_3$) (**B8a**) $\delta = 172.3, 169.5, 166.8, 136.0, 135.1, 131.0, 129.0, 126.9, 126.7, 77.8, 73.8, 54.4, 52.3, 46.7, 38.3, 35.4, 32.6$; (**B8b**) $\delta = 172.0, 169.1, 166.8, 135.9, 135.1, 131.0, 129.0, 126.9, 126.7, 77.8, 73.2, 54.4, 52.6, 47.7, 35.4, 35.3, 32.7$. **HRMS** (ESI+) found $m/z = 358.1515$ $[M-H]^+$, $C_{17}H_{20}N_5O_4^+$ required 358.1508.

Synthesis of benzyl macrocycle ester **B3**



The linear precursor **B8** (50 mg, 0.140 mmol) was reacted according to general procedure **GP2** for 120 h. The reaction progress was monitored by analytical HPLC (Figure 60). After purification by preparative HPLC (10-60 % B), title compound **B3** was isolated.

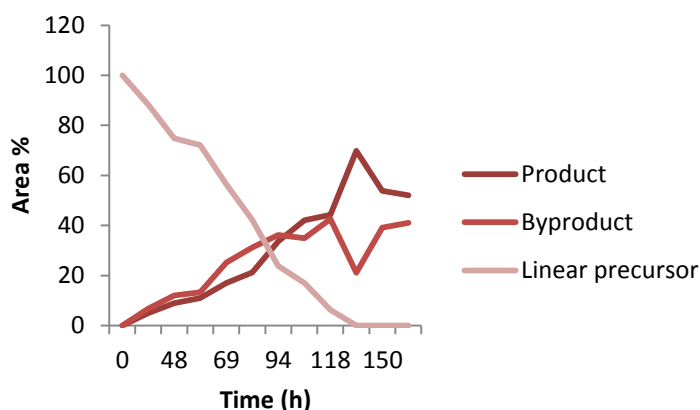
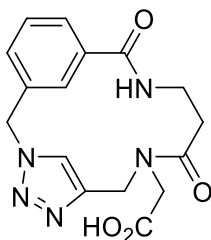


Figure 60. Reaction progress.

Yield: 50 %. White foam. $R_f = 0.20$ (DCM/MeOH 9:1). HPLC $t_r = 6.13$ min (10-60 % B); $^1\text{H NMR}$ (400 MHz, MeOD) $\delta = 8.27$ (s, 1H, ArH_{tetrazole}), 7.56 (d, 2H, ArH, $J = 7.6$), 7.48 (t, 1H, ArH, $J = 7.6$), 6.14 (s, 1H, ArH), 5.90 (d, 1H, CH₂, $J = 16.8$), 5.75 (d, 1H, CH₂, $J = 16.8$), 5.41 (d, 1H, CH₂, $J = 14.4$), 4.60 (d, 1H, CH₂, $J = 18.6$), 4.38 (d, 1H, CH₂, $J = 18.6$), 4.07 (d, 1H, CH₂, $J = 14.4$), 3.70 (dd, 1H, CH₂, $J = 2.8$, $J = 13.2$), 3.48 (td, 1H, CH₂, $J = 2.8$, $J = 13.2$), 3.60 (s, 3H, CH₃), 2.77 – 2.68 (m, 1H, CH₂), 2.44 (d, 1H, CH₂, $J = 15.2$). $^{13}\text{C NMR}$ (125 MHz, MeOD) $\delta = 173.6$, 171.7, 171.4, 145.4, 138.2, 138.0, 130.3, 129.5, 128.8, 127.0, 125.4, 53.6, 53.0, 52.4, 45.1, 36.7, 33.0. HRMS (ESI+) found $m/z = 358.1512$ $[\text{M-H}]^+$, $\text{C}_{17}\text{H}_{20}\text{N}_5\text{O}_4^+$ required 358.1515.

Synthesis of benzyl macrocycle carboxylic acid **B2**

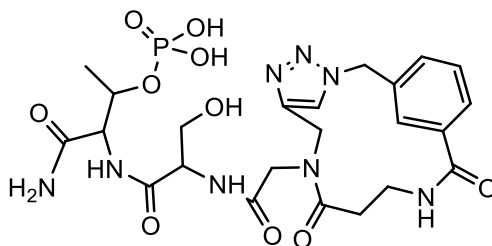


Benzyl macrocyclic ester **B3** (50 mg, 0.140 mmol) was reacted according to general procedure **GP4**. After purification by preparative HPLC (2.5-50 % B) title compound **B2** was isolated.

Yield: 49 %. White foam. HPLC $t_r = 7.88$ min (2.5-50 % B). $^1\text{H NMR}$ (400 MHz, MeOD) $\delta = 8.24$ (s, 1H, CH), 7.54 (d, 2H, ArH, $J = 7.6$), 7.47 (t, 1H, ArH, $J = 7.6$), 6.10 (s, 1H, ArH), 5.82 (q, 1H, CH₂, $J =$

16.8), 5.40 (d, 1H, CH₂, J = 14.8), 4.38 (d, 1H, CH₂, J = 16.8), 4.08 (d, 1H, CH₂, J = 14.8), 3.50 (td, 1H, CH₂, J = 2.8, J = 13.6), 3.49 (dd, 1H, CH₂, J = 2.8, J = 13.6), 2.87 – 2.78 (m, 1H, CH₂), 2.40 (d, 1H, CH₂, J = 16.8). ¹³C NMR (125 MHz, MeOD) δ = 172.1, 171.5, 170.2, 144.1, 136.9, 136.4, 128.8, 128.5, 127.9, 127.5, 125.6, 124.4, 52.3, 44.3, 36.3, 30.7. HRMS (ESI+) found m/z = 344.1344 [M-H]⁺, C₁₆H₁₈N₅O₄⁺ required 344.1353.

Synthesis of dipeptidic benzyl macrocycle **B1**

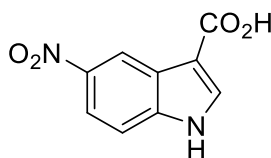


The dipeptidic benzyl macrocycle **B1** was synthesized according to **GP5** using standard Fmoc-solid phase protocol. Purification was performed by preparative HPLC (2.5-20 % B).

Yield: 17 %. White foam. HPLC t_r = 8.025 min (2.5-50 % B). HRMS (ESI+) found m/z = 611.1956 [M-H]⁺, C₂₃H₃₂N₈O₁₀P₁⁺ required 611.1974.

5.5.4 Synthesis of indole derivatives (I1-7)

Synthesis of 5-nitro-1*H*-indole 3-carboxylic acid **I3** [159]

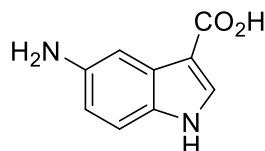


5-Nitroindole (2 g, 12.33 mmol) was dissolved in dry DMF (30.8 mL) under an atmosphere of nitrogen. At 0 °C trifluoroacetic anhydride (3.43 mL, 24.66 mmol) was added dropwise and the reaction mixture was stirred at reflux for 16 h. DMF was then removed under reduced pressure and 25 % NaOH was added. The resulting solution was stirred at reflux for another 16 h. After the completion of the reaction monitored by TLC, the black solid was filtered off and the solution was cooled to 0°C

and adjusted to pH = 2 by the careful addition of concentrated hydrochloric acid. The precipitate was collected by filtration and dried.

Yield: 90 %. Brown solid. $R_f = 0.50$ (Hexane/EtOAc 1:1). $^1\text{H NMR}$, $^{13}\text{C NMR}$, **HRMS** consistent with literature data.

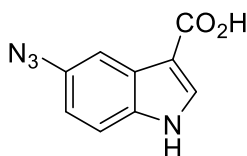
Synthesis of 5-nitro-1H-indole 3-carboxylic acid **I4** [158]



5-Nitro-1H-indole-3-carboxylic acid **I3** (900 mg, 4.36 mmol) and Pd/C (180 mg, 0.2 eq) were suspended in dry MeOH (30 mL) and stirred vigorously under an atmosphere of hydrogen at room temperature overnight. The catalyst was removed by filtration through a pad of Celite and the solvent removed under reduced pressure affording 5-amino-1H-indole-3-carboxylic acid **I4**.

Yield: 97 %. Dark brown solid. $R_f = 0.16$ ($\text{CH}_2\text{Cl}_2/\text{MeOH}$ 9:1); **mp** 155 °C; $^1\text{H NMR}$ (400 MHz, DMSO- d_6) $\delta = 11.30$ (s, 1H; NH), 7.71 (s, 1H, CH), 7.26 (d, 1H, ArH, $J = 2.0$), 7.10 (d, 1H, ArH, $J = 8.5$), 6.52 (dd, 1H, ArH, $J = 8.5$, $J = 2.0$), 4.63 (br s, 2H, NH_2); $^{13}\text{C NMR}$ (100 MHz, DMSO- d_6) $\delta = 167.4$, 143.0, 131.0, 129.9, 127.6, 112.1, 112.0, 107.5, 104.2; **HRMS** (ESI+) $m/z = 132.0685$ [M-CO_2] $^+$ found, $\text{C}_8\text{H}_8\text{N}_2^+$ required 132.0682.

Synthesis of 5-Azido-1H-indole-3-carboxylic acid **I5**

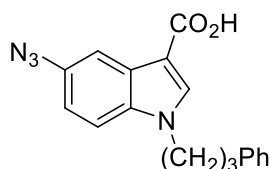


5-Amino-1H-indole-3-carboxylic acid **I4** (750 mg, 4.26 mmol) was dissolved in 2 M HCl (13.3 mL) at -10 °C (ice/NaCl bath). Then NaNO_2 (308 g, 4.47 mmol, dissolved in 13 mL of water) was added dropwise and the solution was stirred for 20 min at -10 °C. The mixture was added to a solution of NaN_3 (290 mg, 4.47 mmol) in ice water (13 mL). The reaction was warmed to room temperature and stirred for 2 h. Then concentrated HCl (2.7 mL) was added and the mixture was filtered. The resulting

solid was washed with water (10 mL) and petroleum ether (10 mL) and subsequently dried *in vacuo* affording 5-azido-1H-indole-3-carboxylic acid **I5**.

Yield: 66 %. Brown solid. $R_f = 0.34$ ($\text{CH}_2\text{Cl}_2/\text{MeOH}$ 9:1); **mp** 160 °C decomposition; $^1\text{H NMR}$ (400 MHz, DMSO-d_6) $\delta = 12.05$ (br s, 1H; CO_2H), 11.93 (br s, 1H; NH), 8.05 (d, 1H, CH, $J = 3.0$), 7.69 (d, 1H, ArH, $J = 2.3$), 7.50 (d, 1H, ArH, $J = 8.6$), 6.93 (dd, 1H, ArH, $J = 8.6$, $J = 2.3$); $^{13}\text{C NMR}$ (100 MHz, DMSO-d_6) $\delta = 165.6$, 134.1, 133.5, 132.5, 126.9, 114.2, 113.7, 109.7, 107.0; **HRMS** (ESI+) $m/z = 174.0423$ $[\text{M-N}_2]^+$ found, $\text{C}_9\text{H}_6\text{N}_2\text{O}_2^+$ required 174.0424.

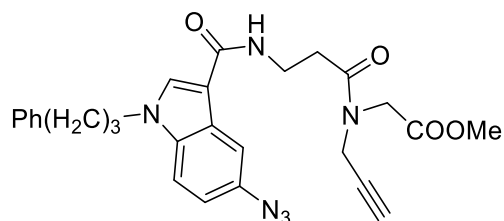
Synthesis of 5-azido-1-(3-phenylpropyl)-indole-3-carboxylic acid **I6**



To a solution of **I5** (200 mg, 0.99 mmol) in dry THF (1.6 mL), NaH (60% in mineral oil, 60 mg, 2.47 mmol) and a 3 M solution of 3-bromo-1-phenyl propane (165 μL , 1.08 mmol) in THF were added. The mixture was stirred at room temperature for 24 h. The solvent was evaporated under reduced pressure and the residue was diluted with 2 M HCl and extracted with ethyl acetate (3 x 4 mL). The organic layers were collected, dried over anhydrous MgSO_4 and evaporated under reduced pressure. Upon purification by flash chromatography ($\text{CH}_2\text{Cl}_2/\text{MeOH}$ from 98:2 to 95:5) the final product **I6** was obtained.

Yield: 25 %. Brown solid. $R_f = 0.30$ (Hexane/EtOAc 4:6). $^1\text{H NMR}$ (400 MHz, CDCl_3) $\delta = 7.94$ (d, 1H, CH, $J = 1.6$), 7.33 (t, 1H, ArH, $J = 7.2$), 7.18 (d, 1H, ArH, $J = 5.6$), 6.96 (dd, 1H, ArH, $J = 7.2$, $J = 1.6$), 4.17 (t, 2H, CH_2 , $J = 6.0$), 2.69 (t, 2H, CH_2 , $J = 6.0$), 2.26 (t, 2H, CH_2 , $J = 6$). $^{13}\text{C NMR}$ (125 MHz, CDCl_3) $\delta = 202.3$, 168.7, 140.0, 136.1, 134.8, 134.2, 128.7, 128.3, 127.9, 126.4, 115.1, 111.4, 111.2, 105.8, 53.4, 46.5, 32.7, 31.0. **HRMS** (ESI+) found $m/z = 321.1354$ $[\text{M-H}]^+$, $\text{C}_{18}\text{H}_{17}\text{N}_4\text{O}_2^+$ required 321.1352.

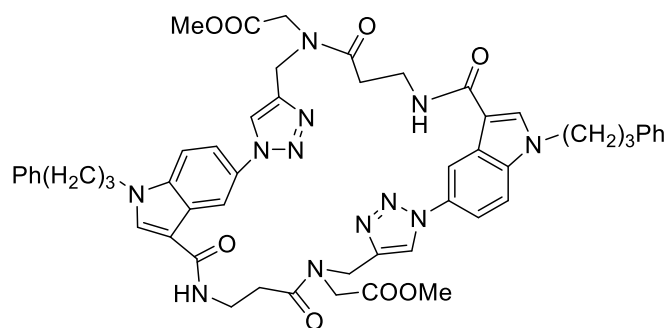
Synthesis of the linear azido indole **I7**



GP1 was followed to prepare the linear compound **I7** from intermediates (**I6**, **B6**). The crude product was purified by flash chromatography (petroleum ether/EtOAc 8:2 to 2:8).

Yield: 55 %. Jelly-like orange solid. $R_f = 0.25$ (Hexane/EtOAc 2:8). $^1\text{H NMR}$ and $^{13}\text{C NMR}$ Appropriate NMR data could not be obtained for this compound due to the existence of rotamers (**I7a**, **I7b**) at a temperature range of 25-120 °C. The purity of the final compound was determined by HPLC analysis and were > 95 %. **HRMS** (ESI+) found $m/z = 501.2290$ $[\text{M}-\text{H}]^+$, $\text{C}_{27}\text{H}_{29}\text{N}_6\text{O}_4^+$ required 501.2250.

Synthesis of indole macrocycle ester **I2**



The linear precursor **I7** (50 mg, 0.10 mmol) was reacted according to **GP2** for 150 h (Figure 61). After purification by preparative HPLC (50-100 % B), title compound **I2** was isolated.

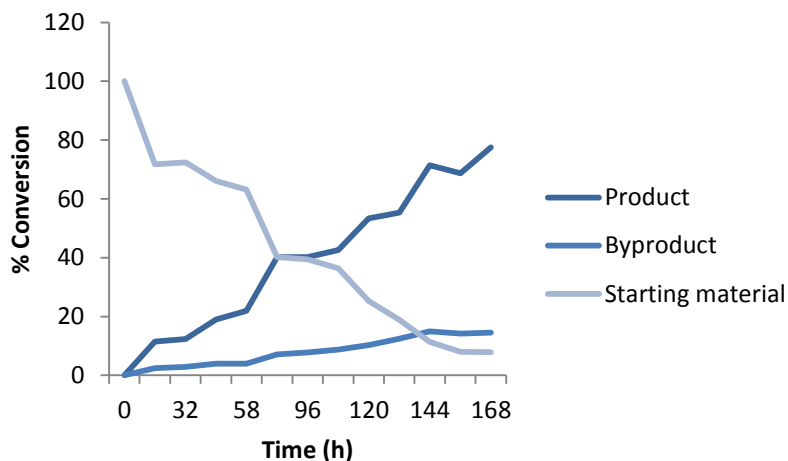
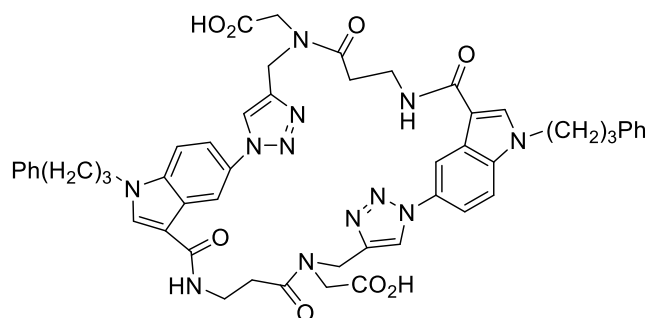


Figure 61. Reaction progress.

Dimer formation as a result of an intermolecular cyclization was mainly observed (for details see ‘Chapter 5.4.2’).

Yield: 20%. Yellow foam. $R_f = 0.33$ (DCM/MeOH 9:1). **HPLC** $t_r = 6.641$ min (50-100 % B); **1H LCMS** (ESI+) $m/z = 1001.6$ $[M+H]^+$.

Synthesis of indole macrocycle carboxylic acid **I1**

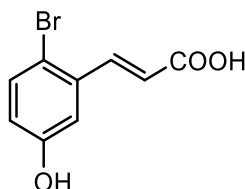


Indole macrocycle ester **I2** (20 mg, 0.04 mmol) was reacted according to **GP4**. After purification by preparative HPLC (40-70 % B), title compound **I1** was isolated.

Yield: 20 %. White foam. **HPLC** $t_r = 8.681$ min (40-70 % B). **HRMS** (ESI-) found $m/z = 971.4005$ $[M-H]^-$, $C_{16}H_{18}N_5O_4^+$ required 971.3953.

5.5.5 Synthesis of *m*-coumaric acid derivatives (CA1-3)

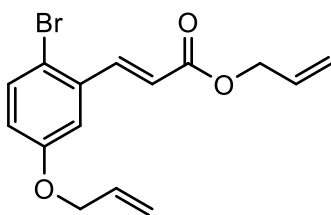
Synthesis of 2-bromo-5-hydroxy cinnamic acid CA1



To a solution of 2-bromo-5-hydroxybenzaldehyde (1 g, 4.97 mmol) in pyridine (6.6 mL), malonic acid (1.139 g, 10.95 mmol) and piperidine (86 μ L, 0.99 mmol) were added. The reaction mixture was stirred under reflux for 4 h and then cooled to room temperature. The solution was poured into 2N ice-cold aqueous HCl (2 mL) and the precipitate was collected by filtration, washed with water and dried under vacuum.

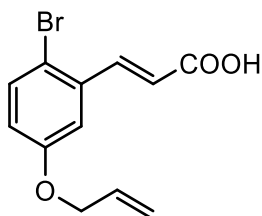
Yield: 69 %. White solid. R_f = 0.39 (DCM/MeOH 9:1). $^1\text{H NMR}$ (400 MHz, MeOD) δ = 7.94 (d, 1H, CH, J = 16), 7.42 (d, 1H, ArH, J = 8.8), 7.13 (d, 1H, ArH, J = 2.8), 6.75 (dd, 1H, ArH, J = 2.8, J = 8.8), 6.36 (d, 1H, CH, J = 16). $^{13}\text{C NMR}$ (125 MHz, MeOD) δ = 158.6, 144.3, 136.1, 135.1, 120.3, 115.1, 115.0. **HRMS** (ESI+) found m/z = 264.9466 $[\text{M}-\text{Na}]^+$, $\text{C}_9\text{H}_7\text{O}_3$ $^{79}\text{Br}^{23}\text{Na}^+$ required 264.9471.

Synthesis of 2-bromo-5-sallyloxy-cinnamic acid CA2



Allyl bromide (21.3 μ L, 0.246 mmol) and potassium carbonate (57 mg, 0.410 mmol) were added to a solution of 2-bromo-5-hydroxy cinnamic acid **CA1** (50 mg, 0.205 mmol) in acetone (5 mL). The resulting mixture was stirred under reflux for 18 h. Then the solvent was removed *in vacuo* and the remaining residue was poured into water and extracted with ethyl acetate (1 x 3 mL). Flash chromatography (eluent: petroleum ether/ethyl acetate from 10 to 9:1) of the crude product gave the diallyl compound.

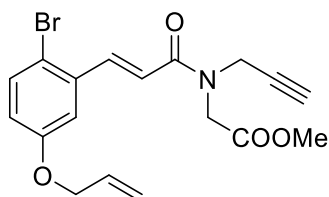
Yield: 85 %. White solid. $R_f = 0.47$ (Hexane/EtOAc 8:2). $^1\text{H NMR}$ (400 MHz, CDCl_3) $\delta = 8.05$ (d, 1H, CH, $J = 16$), 7.50 (d, 1H, ArH, $J = 8.8$), 7.16 (d, 1H, ArH, $J = 2.8$), 6.85 (dd, 1H, ArH, $J = 2.8$, $J = 8.8$), 6.40 (d, 1H, CH, $J = 16$), 6.06 – 5.99 (m, 2H, CH), 5.43 (ddd, 2H, CH_2 , $J = 1.6$, $J = 2.8$, $J = 10$), 5.32 (ddd, 2H, CH_2 , $J = 1.6$, $J = 2.8$, $J = 10$), 4.75 (dt, 2H, CH_2 , $J = 1.2$, $J = 5.6$), 4.57 (dt, 2H, CH_2 , $J = 1.2$, $J = 5.6$). $^{13}\text{C NMR}$ (125 MHz, CDCl_3) $\delta = 165.9$, 157.9, 143.4, 135.0, 134.0, 132.5, 132.1, 120.7, 118.4, 118.3, 118.1, 116.1, 113.5, 69.1, 65.4. **HRMS** (ESI+) found $m/z = 345.0083$ $[\text{M}-\text{Na}]^+$, $\text{C}_{15}\text{H}_{15}\text{O}_3$ $^{79}\text{Br}^{23}\text{Na}^+$ required 245.0097.



The allyl 2-bromo-5-allyloxy cinnamate (56 mg, 0.173 mmol) was dissolved in ethanol (1 mL) and an aqueous solution of 1 N NaOH (0.259 mL, 1.5 eq) was added. The solution was stirred at reflux for 1 h. Then the solvent was removed under reduced pressure and the residue was diluted with water (5 mL) and extracted with ethyl acetate (1 x 2 mL). The aqueous layer was acidified with 2 N HCl (1 mL) and extracted with ethyl acetate (3 x 2 mL). The organic layer was dried over MgSO_4 anhydrous and evaporated under reduced pressure to afford 2-bromo-5-allyloxy cinnamic acid **CA2** which was used in the next step without any further purification.

Yield: quantitative. Brown solid. $R_f = 0.57$ (DCM/MeOH 8.5:1.5). $^1\text{H NMR}$ (400 MHz, MeOD) $\delta = 7.99$ (d, 1H, CH, $J = 16$), 7.54 (d, 1H, ArH, $J = 8.8$), 7.30 (d, 1H, ArH, $J = 2.8$), 6.94 (dd, 1H, ArH, $J = 2.8$, $J = 8.8$), 6.47 (d, 1H, CH, $J = 16$), 6.11 – 6.07 (m, 1H, CH), 5.44 (dd, 1H, CH_2 , $J = 1.2$, $J = 17.6$), 5.29 (dd, 1H, CH_2 , $J = 1.2$, $J = 17.6$), 4.61 (dt, 2H, CH_2 , $J = 1.2$, $J = 5.2$). $^{13}\text{C NMR}$ (125 MHz, MeOD) $\delta = 169.7$, 159.7, 144.2, 136.3, 135.1, 134.4, 122.6, 119.8, 117.9, 116.7, 114.6, 70.1. **HRMS** (ESI+) found $m/z = 304.9780$ $[\text{M}-\text{Na}]^+$, $\text{C}_{12}\text{H}_{11}\text{O}_3$ $^{79}\text{Br}^{23}\text{Na}^+$ required 304.9784.

Synthesis of linear methyl 2-(3-(5-(allyloxy)-2-bromophenyl)-N-(prop-2-ynyl)acrylamido)acetate CA3

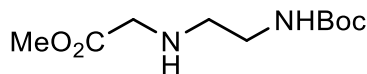


GP1 was followed to prepare the linear compound **CA3** from intermediates **CA2** and **B4**. The crude product was purified by flash chromatography (petroleum ether/EtOAc 8:2 to 6:4) and linear compound **CA3** was isolated as a mixture of two rotamers (**CA3a**, **CA3b**) (88 % yield, 1.6:1 ratio).

Colourless oil. $R_f = 0.36$ (Hexane/EtOAc 6:4). **HPLC** $t_r = 8.802$ min (60-100 % B); **$^1\text{H NMR}$** (500 MHz, CDCl_3) (**CA3a**) $\delta = 7.92$ (d, 1H, CH, $J = 16$), 7.48 (d, 1H, ArH, $J = 8.8$), 7.06 (s, 1H, ArH), 6.83 – 6.79 (m, 1H, ArH), 6.55 (d, 1H, CH, $J = 15$), 6.08 – 6.00 (m, 1H, CH), 5.43 (d, 1H, CH_2 , $J = 17.5$), 5.33 (d, 1H, CH_2 , $J = 10.5$), 4.56 (d, 2H, CH_2 , $J = 5$), 4.44 (s, 2H, CH_2), 4.32 (s, 3H, CH_3), 3.77 (d, 2H, CH_2 , $J = 13.5$), 2.28 (s, 1H, CH); (**CA3b**) $\delta = 7.97$ (d, 1H, CH, $J = 16$), 7.48 (d, 1H, ArH, $J = 8.8$), 7.15 (d, 1H, ArH, $J = 2.5$), 6.83 – 6.79 (m, 2H, CH, ArH), 6.08 – 6.00 (m, 1H, CH), 5.43 (d, 1H, CH_2 , $J = 17.5$), 5.33 (d, 1H, CH_2 , $J = 10.5$), 4.56 (d, 2H, CH_2 , $J = 5$), 4.35 (s, 2H, CH_2), 4.32 (dd, 2H, CH_2 , $J = 2.5$, $J = 10.5$), 3.77 (s, 3H, CH_3), 2.39 (s, 1H, CH). **$^{13}\text{C NMR}$** (125 MHz, CDCl_3) (**CA3a**) $\delta = 169.3$, 166.2, 157.9, 142.4, 135.8, 134.0, 132.6, 119.9, 118.3, 177.2, 115.8, 114.4, 78.0, 73.1, 69.2, 52.6, 48.1, 35.7; (**CA3b**) $\delta = 169.6$, 166.3, 157.9, 142.4, 135.8, 134.0, 132.6, 119.6, 118.3, 177.4, 115.9, 114.2, 77.8, 73.7, 69.2, 52.3, 47.1, 38.6. **HRMS** (ESI+) found $m/z = 392.0519$ $[\text{M-H}]^+$, $\text{C}_{18}\text{H}_{19}\text{NO}_4\text{Br}^+$ required 392.0497.

5.5.5 Synthesis of tetrazolone derivatives (T1-3)

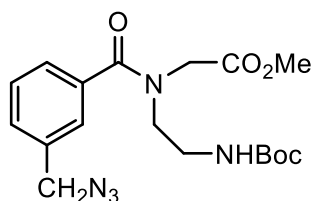
Synthesis of methyl 2-(2-(tert-butoxycarbonylamino)ethylamino)acetate T2



DIPEA (114 μ L, 0.654 mmol) and methyl bromoacetate (62 μ L, 0.654 mmol) were added dropwise to a solution of *N*-Boc ethylenediamine (207 μ L, 1.30 mmol) in dry CH_2Cl_2 (2.32 mL). The reaction mixture was stirred at room temperature for 16 h and then the solvent was removed. After purification by flash column chromatography (petroleum ether/EtOAc 8:2 to 1:9), the title compound **T2** was isolated.

Yield: 57 %. Yellow pale oil. $R_f = 0.44$ (DCM/MeOH 9:1). $^1\text{H NMR}$ (400 MHz, CDCl_3) $\delta = 5.02$ (br s, 1H, NH), 3.70 (s, 3H, CH_3), 3.46 (s, 2H, CH_2), 3.25 (q, 2H, CH_2 , $J = 5.6$), 2.79 (t, 2H, CH_2 , $J = 5.6$), 1.86 (br s, 1H, NH), 1.47 (t, 9H, 3 CH_3). $^{13}\text{C NMR}$ (125 MHz, CDCl_3) $\delta = 172.7$, 156.1, 79.3, 51.9, 50.2, 48.8, 40.0. **HRMS** (ESI⁺) found $m/z = 233.1505$ [$\text{M}-\text{H}$]⁺, $\text{C}_{10}\text{H}_{21}\text{N}_2\text{O}_4$ ⁺, required 233.1501.

Synthesis of the linear methyl 2-(3-(azidomethyl)-*N*-(2-(tert-butoxycarbonylamino)ethylbenzamido) acetate T3

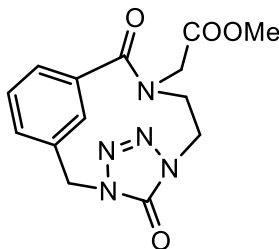


GP1 was followed to prepare the linear compound **T3** from intermediates **T2**, **B7**). The crude product was purified by flash chromatography (petroleum ether/EtOAc 8:2 to 4:6) as a mixture of two rotamers (**T3a**, **T3b**) (61 % yield, 1:1.5 ratio)

Colourless oil. $R_f = 0.25$ (Petroleum ether/ EtOAc 1:1). $^1\text{H NMR}$ (400 MHz, CDCl_3) (**T3a**) $\delta = 7.43$ (t, 2H, ArH, $J = 8$), 7.39 (dd, 1H, ArH, $J = 2$, $J = 8$), 7.38 (s, 1H, ArH), 4.40 (s, 2H, CH_2), 4.25 (s, 2H, CH_2), 3.84 (s, 3H, CH_3), 3.48 – 3.46 (m, 2H, CH_2), 3.20 (d, 2H, CH_2 , $J = 5$), 1.41 (s, 9H, 3 CH_3); (**T3b**) $\delta = 7.43$ (t, 2H, ArH, $J = 8$), 7.39 (dd, 1H, ArH, $J = 2$, $J = 8$), 7.38 (s, 1H, ArH), 4.35 (s, 2H, CH_2), 4.03

(s, 2H, CH₂), 3.72 (s, 3H, CH₃), 3.68 (s, 2H, CH₂), 3.48 – 3.46 (m, 2H, CH₂), 1.43 (s, 9H, 3 CH₃). ¹³C NMR (125 MHz, CDCl₃) (**T3a**) δ = 172.0, 170.3, 155.6, 136.0, 129.2, 126.8, 126.5, 79.6, 54.3, 52.5, 50.7, 47.6, 38.6, 28.4; (**T3b**) δ = 172.2, 170.0, 155.9, 136.0, 129.6, 126.4, 126.3, 79.6, 54.3, 52.5, 51.4, 46.8, 38.5, 28.4. HRMS (ESI+) found m/z = 392.1957 [M-H]⁺, C₁₈H₂₆N₅O₅⁺, required 392.1934.

Synthesis of methyl ester tetrazolone macrocycle **T1**



Boc-protected amine **T3** (100 mg, 0.255 mmol) was dissolved in dry toluene (10.5 mL) and 2-chloropyridine (72 μL, 0.762 mmol) and trifluoromethanesulfonic anhydride (64 μL, 0.384 mmol) were added. The reaction mixture was stirred at room temperature for 2 hours. After the formation of the isocyanate intermediate, the reaction was heated at 70 °C for 1 hours. Then the solvent was evaporated, the residue diluted with CH₂Cl₂ (10 mL) and washed with a solution of 10 % citric acid (3 x 3 mL). The organic phase was dried over Mg₂SO₄, filtered and evaporated under reduced pressure. The crude was purified by flash column chromatography (petroleum ether/EtOAc 5:5 to 4:6) to afford the final product **T1**.

Yield: 15 %. Colourless oil. R_f = 0.33 (Petroleum ether/ EtOAc 3:7). ¹H NMR (400 MHz, CDCl₃) δ = 7.59 (dd, 1H, ArH, J = 2, J = 8), 7.57 (s, 1H, ArH), 7.48 – 7.41 (m, 2H, ArH), 4.42 (s, 2H, CH₂), 4.10 (t, 2H, CH₂, J = 7.2), 4.05 (s, 2H, CH₂), 3.79 (s, 3H, CH₃), 3.67 (t, 2H, CH₂, J = 7.6). ¹³C NMR (125 MHz, CDCl₃) δ = 169.7, 168.8, 154.5, 135.0, 134.9, 130.8, 128.6, 128.3, 128.0, 54.4, 52.4, 44.9, 41.7, 40.8. HRMS (ESI+) found m/z = 318.1210 [M-H]⁺, C₁₄H₁₆N₅O₄⁺, required 318.1202.

5.6 Final remarks

In conclusion, during my experience abroad several derivatives, potentially targeting the Plk1 polo-box like domain and the tyrosine pocket were designed and synthesized. This work is a part of a wider research project, in which various classes of derivatives will be investigated in order to identify lead compounds to further develop as Plk1 inhibitors. Several techniques will be exploited to assess the *in vitro* biological activity of the synthesized compounds. Fluorescent Polarization (FP) will be used to test not only the final compounds, but also the linear precursors and the key fragments in order to investigate the importance of the macrocyclic scaffold. Isothermal Titration Calorimetry (ITC), Mass Spectroscopy (MS) and Surface Plasmon Resonance (SPR) will also be used for the most powerful hits to identify compounds that bind to the targeted protein interface, followed by X-ray crystallography to define the precise location and orientation of binding.

6. APPENDIX

APPENDIX 1a

Zosteric acid derivatives

Cmp	Conc. (µM)	Planktonic growth						Cells adhesion					
		Average (OD600/min)	St.dev (OD600/min)	err%	ANOVA	diff cont %	Level	Average (n°cell)	St.dev (n°cell)	err%	ANOVA	diff cont %	Level
ZA	0	1,28E-03	2,54E-05	1,98	a	0,00	0	1,92E+07	1,82E+06	9,49	b	0,00	0
	0,183	1,32E-03	6,23E-05	4,72	a	2,86	0	2,77E+07	1,68E+06	6,08	d	44,59	+
	1,83	1,31E-03	3,80E-05	2,91	a	1,76	0	1,54E+07	2,91E+06	18,91	c	-19,76	0
	18,3	1,29E-03	3,92E-05	3,05	a	0,11	0	1,55E+07	1,92E+06	12,44	c	-19,34	0
	183	1,30E-03	4,12E-05	3,17	a	1,07	0	1,39E+07	1,33E+06	9,59	c	-27,67	-
	1830	1,30E-03	4,35E-05	3,35	a	1,21	0	5,64E+06	1,16E+06	20,51	a	-70,56	---
2	0	1,28E-03	2,54E-05	1,98	abc	0,00	0	1,92E+07	1,82E+06	9,49	b	0,00	0
	0,183	1,31E-03	2,54E-05	1,94	ab	2,06	0	2,29E+07	1,62E+06	7,09	b	19,37	0
	1,83	1,26E-03	4,50E-05	3,56	abc	-1,72	0	1,03E+07	1,35E+06	13,08	ce	-46,05	---
	18,3	1,23E-03	1,50E-05	1,22	abc	-3,99	0	1,42E+07	2,42E+06	17,00	de	-25,80	-
	183	1,23E-03	6,03E-05	4,88	abc	-3,87	0	1,49E+07	1,43E+06	9,60	de	-22,36	-
	1830	9,74E-04	3,80E-05	3,91	e	-24,17	--	1,22E+07	2,67E+06	21,92	cde	-36,38	--
3	0	1,28E-03	2,54E-05	1,98	abc	0,00	0	1,92E+07	1,82E+06	9,49	bef	0,00	0
	0,183	1,24E-03	4,33E-05	3,49	abcd	-3,32	0	1,25E+07	4,29E+06	34,40	cdef	-34,95	--
	1,83	1,22E-03	9,79E-06	0,80	abcdef	-4,74	0	1,17E+07	1,67E+06	14,20	cdf	-38,77	--
	18,3	1,19E-03	4,10E-05	3,46	bcdef	-7,58	0	1,78E+07	1,04E+06	5,85	bcef	-7,37	0
	183	1,14E-03	4,83E-05	4,25	def	-11,37	-	1,44E+07	1,54E+06	10,75	bcdef	-25,03	-
	1830	8,33E-04	2,11E-05	2,53	h	-35,10	---	1,32E+07	2,77E+06	20,95	cdef	-31,11	--
4	0	1,28E-03	2,54E-05	1,98	abc	0,00	0	1,92E+07	1,82E+06	9,49	bceh	0,00	0
	0,183	1,24E-03	2,45E-05	1,97	ac	-3,14	0	1,92E+07	2,64E+06	13,73	bcefhg	0,37	0

	1,83	1,23E-03	3,23E-05	2,62	ac	-4,12	0	1,17E+07	1,10E+06	9,47	defl	-39,15	--
	18,3	1,14E-03	8,20E-06	0,72	df	-11,53	-	1,58E+07	1,26E+06	7,97	bcdefghl	-17,47	0
	183	1,15E-03	6,23E-05	5,42	de	-10,43	-	1,36E+07	2,44E+06	17,90	bcdefghl	-28,79	-
	1830	9,42E-04	4,27E-05	4,54	g	-26,65	--	1,14E+07	2,55E+06	22,35	df	-40,52	---
5	0	1,28E-03	2,54E-05	1,98	ab	0,00	0	1,92E+07	1,82E+06	9,49	bc	0,00	0
	0,183	1,34E-03	7,14E-05	5,33	ab	4,38	0	1,82E+07	4,40E+06	24,16	bcd	-4,88	0
	1,83	1,29E-03	5,23E-05	4,06	abc	0,19	0	1,82E+07	1,14E+06	6,26	bcd	-5,16	0
	18,3	1,22E-03	5,23E-05	4,28	bc	-4,95	0	1,63E+07	2,90E+06	17,75	bcd	-14,70	0
	183	1,21E-03	2,90E-05	2,39	c	-5,56	0	1,54E+07	2,97E+06	19,36	cd	-19,83	0
	1830	9,87E-04	2,77E-05	2,80	d	-23,12	--	1,30E+07	3,33E+06	25,60	d	-32,21	--
6	0	1,28E-03	2,54E-05	1,98	a	0,00	0	1,92E+07	1,82E+06	9,49	bc	0,00	0
	0,183	1,25E-03	4,30E-05	3,44	a	-2,79	0	1,75E+07	2,13E+06	12,19	bcd	-8,89	0
	1,83	1,27E-03	2,98E-05	2,34	a	-0,79	0	1,43E+07	2,46E+06	17,30	cde	-25,63	-
	18,3	1,30E-03	4,51E-05	3,48	a	1,06	0	1,18E+07	3,11E+06	26,45	de	-38,64	--
	183	1,12E-03	2,07E-06	0,18	b	-12,86	-	1,40E+07	3,07E+06	21,98	cde	-27,19	-
	1830	8,31E-04	2,10E-05	2,52	c	-35,27	---	1,14E+07	2,18E+06	19,06	de	-40,36	---
7	0	1,28E-03	2,54E-05	1,98	a	0,00	0	1,92E+07	1,82E+06	9,49	b	0,00	0
	0,183	1,30E-03	4,13E-05	3,18	a	1,24	0	1,84E+07	2,97E+06	16,13	b	-3,87	0
	1,83	1,27E-03	3,05E-05	2,40	a	-0,96	0	1,82E+07	1,60E+06	8,81	b	-5,10	0
	18,3	1,24E-03	4,17E-05	3,35	a	-3,05	0	1,13E+07	7,40E+05	6,57	c	-41,17	---
	183	1,29E-03	1,80E-05	1,39	a	0,38	0	7,85E+06	1,06E+06	13,45	a	-59,02	---
	1830	7,73E-04	1,98E-05	2,57	c	-39,82	---	1,09E+07	1,77E+06	16,19	c	-43,00	---
8	0	1,28E-03	2,54E-05	1,98	a	0,00	0	1,92E+07	1,82E+06	9,49	bc	0,00	0
	0,183	1,26E-03	4,50E-05	3,57	a	-1,86	0	1,81E+07	1,82E+06	10,06	bcdf	-5,41	0
	1,83	1,24E-03	2,10E-05	1,69	a	-3,08	0	1,47E+07	1,73E+06	11,83	cdef	-23,51	-
	18,3	1,24E-03	2,28E-05	1,83	a	-3,14	0	1,19E+07	2,25E+06	18,92	deg	-37,94	--
	183	1,25E-03	5,88E-05	4,70	a	-2,43	0	1,57E+07	1,81E+06	11,54	cdf	-18,09	0
	1830	8,68E-04	2,46E-05	2,83	d	-32,40	---	1,10E+07	2,81E+06	25,41	deg	-42,38	---
9	0	1,28E-03	2,54E-05	1,98	a	0,00	0	1,92E+07	1,82E+06	9,49	bc	0,00	0

	0,183	1,29E-03	2,82E-05	2,19	a	0,12	0	1,73E+07	3,18E+06	18,34	bcd	-9,57	0
	1,83	1,26E-03	1,80E-05	1,43	a	-1,99	0	1,75E+07	3,70E+06	21,10	bc	-8,60	0
	18,3	1,31E-03	3,99E-07	0,03	a	1,90	0	1,88E+07	4,12E+06	21,95	bc	-1,95	0
	183	1,28E-03	4,72E-05	3,69	a	-0,41	0	1,56E+07	2,04E+06	13,06	bcd	-18,67	0
	1830	9,65E-04	4,19E-05	4,35	c	-24,88	--	1,18E+07	2,26E+06	19,18	cd	-38,63	--
10	0	1,28E-03	2,54E-05	1,98	abc	0,00	0	1,92E+07	1,82E+06	9,49	b	0,00	0
	0,183	1,25E-03	3,64E-05	2,92	abc	-2,93	0	2,26E+07	1,58E+06	6,99	b	18,06	0
	1,83	1,24E-03	2,43E-05	1,95	abc	-3,19	0	1,53E+07	1,70E+06	11,07	d	-20,05	-
	18,3	1,31E-03	1,21E-05	0,93	ab	2,04	0	1,43E+07	2,78E+06	19,49	d	-25,44	-
	183	1,24E-03	3,54E-05	2,86	ac	-3,38	0	3,98E+06	6,49E+05	16,31	a	-79,23	---
	1830	8,66E-04	9,35E-06	1,08	f	-32,56	---	4,82E+06	3,41E+05	7,08	a	-74,86	---
11	0	1,28E-03	2,54E-05	1,98	a	0,00	0	1,92E+07	1,82E+06	9,49	b	0,00	0
	0,183	1,30E-03	4,49E-05	3,45	a	1,13	0	1,63E+07	3,66E+06	22,45	b	-14,90	0
	1,83	1,26E-03	5,01E-05	3,97	a	-1,68	0	1,14E+07	1,95E+06	17,03	c	-40,28	---
	18,3	1,27E-03	2,54E-05	2,00	a	-1,14	0	1,06E+07	1,75E+06	16,61	c	-44,92	---
	183	1,28E-03	4,65E-05	3,64	a	-0,51	0	1,14E+07	1,08E+06	9,49	c	-40,73	---
	1830	1,11E-03	9,30E-06	0,83	b	-13,24	-	2,19E+07	2,82E+06	12,86	d	14,29	0
12	0	1,28E-03	2,54E-05	1,98	abc	0,00	0	1,92E+07	1,82E+06	9,49	b	0,00	0
	0,183	1,23E-03	6,43E-05	5,24	abd	-4,42	0	1,26E+07	1,45E+06	11,57	ce	-34,41	-
	1,83	1,33E-03	2,80E-05	2,11	ac	3,46	0	7,30E+06	6,92E+05	9,49	ade	-61,92	---
	18,3	1,32E-03	3,01E-05	2,27	ac	3,08	0	1,04E+07	2,27E+06	21,90	cde	-45,97	---
	183	1,28E-03	4,79E-05	3,73	abc	-0,03	0	1,17E+07	2,79E+06	23,90	ce	-39,12	--
	1830	1,02E-03	9,59E-06	0,94	e	-20,44	--	1,33E+07	7,73E+05	5,82	ce	-30,69	--
13	0	1,28E-03	2,54E-05	1,98	a	0,00	0	1,92E+07	1,82E+06	9,49	b	0,00	0
	0,183	1,30E-03	6,78E-05	5,22	a	1,21	0	2,30E+07	6,19E+06	26,94	b	19,90	0
	1,83	1,25E-03	4,56E-05	3,64	a	-2,36	0	2,05E+07	1,97E+06	9,59	b	7,00	0
	18,3	1,31E-03	1,00E-05	0,76	a	2,38	0	1,12E+07	2,08E+06	18,55	c	-41,44	---
	183	1,16E-03	3,06E-05	2,65	b	-10,03	-	1,25E+07	2,49E+06	20,02	c	-34,97	--
	1830	8,51E-04	2,53E-05	2,97	d	-33,69	---	1,39E+07	2,26E+06	16,24	c	-27,4594	-

14	0	1,28E-03	2,54E-05	1,98	a	0,00	0	1,92E+07	1,82E+06	9,49	bc	0,00	0
	0,183	1,33E-03	2,65E-05	1,99	a	3,41	0	1,86E+07	2,31E+06	12,43	bcd	-3,15	0
	1,83	1,32E-03	3,12E-05	2,37	a	2,66	0	4,71E+06	9,06E+05	19,22	a	-75,40	- - -
	18,3	1,26E-03	6,50E-05	5,18	a	-2,23	0	1,50E+07	1,83E+06	12,20	cde	-21,94	-
	183	1,28E-03	6,93E-05	5,42	a	-0,48	0	1,39E+07	3,16E+06	22,71	de	-27,44	-
	1830	8,66E-04	3,24E-05	3,75	b	-32,54	- - -	1,40E+07	2,81E+06	20,10	de	-27,01	-
15	0	1,28E-03	2,54E-05	1,98	a	0,00	0	1,92E+07	1,82E+06	9,49	bc	0,00	0
	0,183	1,32E-03	3,89E-05	2,94	a	2,92	0	1,71E+07	1,56E+06	9,10	bcd	-10,57	0
	1,83	1,30E-03	1,36E-05	1,05	a	0,95	0	1,60E+07	1,78E+06	11,14	cde	-16,42	0
	18,3	1,30E-03	4,55E-05	3,48	a	1,62	0	1,72E+07	2,26E+06	13,18	bcd	-10,51	0
	183	1,32E-03	5,18E-07	0,04	a	2,52	0	1,34E+07	1,82E+06	13,59	def	-30,22	- -
	1830	1,03E-03	3,59E-05	3,50	b	-20,07	- -	1,24E+07	1,56E+06	12,58	def	-35,24	- -
16	0	1,28E-03	2,54E-05	1,98	abc	0,00	0	1,92E+07	1,82E+06	9,49	bcef	0,00	0
	0,183	1,21E-03	1,78E-05	1,47	abcde	-5,68	0	1,93E+07	6,07E+05	3,15	bcefg	0,68	0
	1,83	1,27E-03	1,13E-05	0,89	abc	-1,20	0	1,70E+07	1,39E+06	8,18	bcef	-11,20	0
	18,3	1,23E-03	4,45E-05	3,61	abcd	-3,89	0	1,33E+07	2,12E+06	15,93	abcef	-30,56	- -
	183	1,30E-03	2,20E-05	1,69	abc	1,57	0	2,29E+07	5,05E+06	22,02	bcef	19,62	0
	1830	1,14E-03	3,39E-05	2,97	bde	-10,95	-	4,25E+07	1,35E+07	31,90	hi	121,57	+
17	0	1,28E-03	2,54E-05	1,98	abc	0,00	0	1,92E+07	1,82E+06	9,49	bd	0,00	0
	0,183	1,28E-03	2,84E-05	2,22	abcd	-0,29	0	3,62E+07	3,74E+06	10,33	c	88,79	+
	1,83	1,30E-03	6,57E-05	5,07	abcd	0,87	0	1,76E+07	7,52E+05	4,27	bdf	-8,09	0
	18,3	1,33E-03	3,87E-05	2,91	ab	3,62	0	1,37E+07	1,40E+06	10,18	ef	-28,33	-
	183	1,29E-03	2,13E-05	1,65	abc	0,68	0	1,49E+07	1,95E+06	13,06	def	-22,26	-
	1830	1,05E-03	3,50E-05	3,32	ef	-17,95	-	1,08E+07	1,55E+06	14,34	h	-43,68	- - -
18	0	1,28E-03	2,54E-05	1,98	ac	0,00	0	1,92E+07	1,82E+06	9,49	bc	0,00	0
	0,183	1,29E-03	1,68E-05	1,30	ac	0,41	0	1,78E+07	4,71E+05	2,64	bce	-7,13	0
	1,83	1,22E-03	7,55E-05	6,16	ab	-4,66	0	1,75E+07	1,89E+06	10,81	bce	-8,79	0
	18,3	1,31E-03	1,58E-05	1,20	ac	2,40	0	1,31E+07	2,37E+06	17,99	cdef	-31,41	- -
	183	1,25E-03	2,65E-05	2,12	abc	-2,47	0	1,59E+07	1,82E+06	11,44	de	-17,14	0

	1830	9,96E-04	1,83E-05	1,84	d	-22,39	--	1,19E+07	2,42E+06	20,32	df	-37,93	--
19	0	1,28E-03	2,54E-05	1,98	ab	0,00	0	1,92E+07	1,82E+06	9,49	bcd	0,00	0
	0,183	1,28E-03	2,30E-05	1,79	ab	0,07	0	2,16E+07	1,48E+06	6,85	bc	12,75	0
	1,83	1,26E-03	3,81E-05	3,02	abc	-1,68	0	1,89E+07	1,88E+06	9,94	bcd	-1,22	0
	18,3	1,31E-03	4,07E-05	3,11	ab	1,79	0	1,61E+07	2,28E+06	14,19	bd	-16,05	0
	183	1,20E-03	2,64E-05	2,21	bc	-6,82	0	1,95E+07	2,49E+06	12,78	bcd	1,50	0
	1830	1,00E-03	5,16E-05	5,16	c	-22,04	--	2,79E+07	4,58E+06	16,42	e	45,65	+
20	0	1,28E-03	2,54E-05	1,98	a	0,00	0	1,92E+07	1,82E+06	9,49	bc	0,00	0
	0,183	1,30E-03	5,77E-05	4,45	a	0,88	0	1,93E+07	4,39E+06	22,72	bcd	0,81	0
	1,83	1,29E-03	4,61E-05	3,57	a	0,50	0	1,67E+07	1,18E+06	7,04	bcd	-12,94	0
	18,3	1,30E-03	1,15E-05	0,88	a	1,58	0	1,65E+07	1,86E+06	11,30	cd	-13,94	0
	183	1,32E-03	4,13E-05	3,13	a	2,69	0	1,80E+07	2,77E+06	15,40	bcd	-6,18	0
	1830	1,05E-03	3,95E-05	3,75	b	-18,13	-	1,61E+07	1,39E+06	8,61	cd	-15,75	0
21	0	1,28E-03	2,54E-05	1,98	a	0,00	0	1,92E+07	1,82E+06	9,49	bf	0,00	0
	0,183	1,29E-03	3,87E-05	3,01	a	0,21	0	3,59E+07	3,71E+06	10,33	c	87,42	+
	1,83	1,31E-03	5,42E-05	4,14	a	2,05	0	1,46E+07	1,87E+06	12,79	def	-23,68	-
	18,3	1,28E-03	3,80E-05	2,97	a	-0,29	0	1,36E+07	1,93E+06	14,12	de	-28,82	-
	183	1,29E-03	5,08E-05	3,95	a	0,13	0	1,74E+07	1,15E+06	6,58	bdf	-8,95	0
	1830	1,03E-03	4,71E-05	4,59	d	-20,16	--	1,33E+07	1,70E+06	12,78	de	-30,57	--
22	0	1,28E-03	2,54E-05	1,98	a	0,00	0	1,92E+07	1,82E+06	9,49	bc	0,00	0
	0,183	1,31E-03	4,76E-05	3,64	a	1,90	0	1,76E+07	7,64E+05	4,33	bce	-7,98	0
	1,83	1,27E-03	5,49E-05	4,33	a	-1,23	0	1,72E+07	1,78E+06	10,34	bce	-10,36	0
	18,3	1,30E-03	1,43E-05	1,10	a	1,46	0	1,41E+07	1,36E+06	9,61	de	-26,16	-
	183	1,29E-03	2,68E-05	2,07	a	0,63	0	1,53E+07	2,29E+06	14,93	cde	-19,96	0
	1830	8,64E-04	2,05E-05	2,37	b	-32,67	---	1,58E+07	2,59E+06	16,36	cde	-17,47	0
23	0	1,28E-03	2,54E-05	1,98	a	0,00	0	1,92E+07	1,82E+06	9,49	bc	0,00	0
	0,183	1,30E-03	2,88E-05	2,21	a	1,40	0	1,91E+07	3,34E+06	17,48	bcd	-0,13	0
	1,83	1,31E-03	2,52E-05	1,92	a	2,18	0	1,58E+07	1,04E+06	6,55	cde	-17,44	0
	18,3	1,30E-03	4,25E-05	3,27	a	1,14	0	1,52E+07	2,26E+06	14,88	de	-20,60	-

24	183	1,29E-03	3,61E-05	2,81	a	0,12	0	5,96E+06	4,46E+05	7,48	a	-68,90	---
	1830	1,13E-03	1,57E-05	1,38	b	-11,61	-	7,22E+06	1,30E+06	17,96	a	-62,34	---
	0	1,28E-03	2,54E-05	1,98	acd	0,00	0	1,92E+07	1,82E+06	9,49	b	0,00	0
	0,183	1,21E-03	1,34E-05	1,10	bcd	-5,58	0	3,07E+07	1,70E+06	5,54	c	60,29	+
	1,83	1,29E-03	3,26E-05	2,52	acd	0,75	0	2,66E+07	2,31E+06	8,66	ce	38,91	+
	18,3	1,29E-03	1,98E-05	1,54	acd	0,43	0	1,37E+07	6,17E+05	4,50	deg	-28,42	-
	183	1,24E-03	7,21E-06	0,58	abcd	-3,61	0	1,18E+07	3,28E+06	27,88	df	-38,53	--
25	1830	1,17E-03	6,13E-05	5,25	bcd	-9,14	0	9,94E+06	4,33E+05	4,36	degh	-48,14	---
	0	1,28E-03	2,54E-05	1,98	a	0,00	0	1,92E+07	1,82E+06	9,49	b	0,00	0
	0,183	1,32E-03	1,73E-05	1,31	a	2,93	0	2,26E+07	2,25E+06	9,96	c	17,80	0
	1,83	1,29E-03	7,38E-05	5,73	a	0,37	0	1,22E+07	1,54E+06	12,57	d	-36,25	--
	18,3	1,31E-03	5,72E-05	4,35	a	2,26	0	1,50E+07	1,64E+06	10,96	d	-21,75	-
	183	1,12E-03	2,66E-05	2,37	b	-12,66	-	1,24E+07	1,46E+06	11,78	d	-35,24	--
26	1830	5,61E-04	1,66E-05	2,96	c	-56,28	---	1,47E+07	2,29E+06	15,56	d	-23,17	-
	0	1,28E-03	2,54E-05	1,98	ab	0,00	0	1,92E+07	1,82E+06	9,49	bc	0,00	0
	0,183	1,31E-03	2,41E-05	1,84	ab	2,18	0	1,63E+07	1,27E+06	7,84	bcd	-15,20	0
	1,83	1,27E-03	3,99E-05	3,15	abc	-1,37	0	1,58E+07	1,67E+06	10,57	cd	-17,76	0
	18,3	1,26E-03	5,97E-05	4,74	abc	-1,92	0	1,52E+07	2,46E+06	16,18	cd	-20,80	-
	183	1,25E-03	3,01E-05	2,41	abc	-2,92	0	1,47E+07	1,06E+06	7,21	cd	-23,44	-
27	1830	8,08E-04	2,57E-05	3,18	e	-37,06	---	1,62E+07	2,03E+06	12,53	cd	-15,63	0
	0	1,28E-03	2,54E-05	1,98	a	0,00	0	1,92E+07	1,82E+06	9,49	b	0,00	0
	0,183	1,26E-03	3,10E-05	2,45	a	-1,69	0	4,77E+07	4,72E+06	9,90	c	148,78	+
	1,83	1,29E-03	1,36E-05	1,05	a	0,37	0	1,83E+07	2,16E+06	11,86	b	-4,76	0
	18,3	1,31E-03	1,28E-05	0,97	a	2,32	0	1,96E+07	1,21E+06	6,15	b	2,38	0
	183	1,15E-03	3,39E-05	2,95	b	-10,36	-	4,16E+07	5,39E+06	12,96	c	117,10	+
28	1830	1,09E-03	1,01E-05	0,93	b	-15,26	-	9,52E+07	1,19E+07	12,52	e	396,86	+
	0	1,28E-03	2,54E-05	1,98	a	0,00	0	1,92E+07	1,82E+06	9,49	b	0,00	0
	0,183	1,31E-03	2,29E-05	1,76	a	1,67	0	1,94E+07	1,48E+05	0,76	b	1,10	0
	1,83	1,28E-03	1,77E-05	1,38	a	-0,20	0	1,99E+07	1,46E+06	7,35	b	3,77	0

	18,3	1,28E-03	2,93E-05	2,30	a	-0,61	0	1,76E+07	9,69E+05	5,50	b	-8,15	0
	183	1,28E-03	5,05E-05	3,93	a	0,01	0	1,26E+07	1,83E+06	14,57	c	-34,39	--
	1830	8,60E-04	1,56E-05	1,81	c	-33,01	---	9,20E+06	1,37E+06	14,85	d	-52,00	---
29	0	1,28E-03	2,54E-05	1,98	a	0,00	0	1,92E+07	1,82E+06	9,49	bde	0,00	0
	0,183	1,28E-03	3,81E-05	2,98	a	-0,57	0	2,52E+07	4,53E+06	17,96	c	31,74	+
	1,83	1,29E-03	5,70E-05	4,43	a	0,23	0	1,99E+07	2,26E+06	11,33	bd	4,07	0
	18,3	1,29E-03	4,59E-05	3,57	a	0,20	0	1,95E+07	1,06E+06	5,41	bd	1,79	0
	183	1,29E-03	2,31E-05	1,79	a	0,60	0	1,67E+07	1,78E+06	10,64	be	-12,90	0
	1830	1,15E-03	2,87E-05	2,50	b	-10,65	-	1,71E+07	1,57E+06	9,22	be	-10,97	0
30	0	1,28E-03	2,54E-05	1,98	a	0,00	0	1,92E+07	1,82E+06	9,49	b	0,00	0
	0,183	1,27E-03	1,18E-05	0,92	a	-0,72	0	2,60E+07	1,54E+06	5,92	c	35,59	+
	1,83	1,29E-03	2,37E-05	1,83	a	0,83	0	1,73E+07	1,62E+06	9,36	b	-9,71	0
	18,3	1,24E-03	5,06E-05	4,08	a	-3,48	0	1,67E+07	7,99E+05	4,79	b	-12,95	-
	183	1,12E-03	4,35E-05	3,87	b	-12,58	-	1,64E+07	2,41E+06	14,67	b	-14,33	-
	1830	5,53E-04	1,03E-05	1,86	c	-56,89	---	1,12E+07	1,46E+06	13,04	d	-41,78	---
31	0	1,28E-03	2,54E-05	1,98	a	0,00	0	1,92E+07	1,82E+06	9,49	bd	0,00	0
	0,183	1,29E-03	5,32E-05	4,13	a	0,29	0	2,56E+07	2,58E+06	10,06	c	33,75	+
	1,83	1,29E-03	4,10E-05	3,18	a	0,23	0	1,79E+07	1,07E+06	5,97	bd	-6,83	0
	18,3	1,31E-03	5,95E-05	4,56	a	1,72	0	1,93E+07	2,42E+06	12,53	bd	0,73	0
	183	1,28E-03	4,88E-05	3,81	a	-0,43	0	2,14E+07	1,48E+06	6,95	bcd	11,51	0
	1830	7,64E-04	2,17E-05	2,84	b	-40,52	---	1,42E+07	2,75E+06	19,32	d	-25,78	-
32	0	1,28E-03	2,54E-05	1,98	a	0,00	0	1,92E+07	1,82E+06	9,49	be	0,00	0
	0,183	1,23E-03	1,22E-05	0,99	a	-3,95	0	2,38E+07	2,11E+06	8,88	ce	24,26	+
	1,83	1,29E-03	2,47E-05	1,92	a	0,31	0	1,82E+07	1,76E+06	9,68	be	-5,29	0
	18,3	1,32E-03	2,96E-05	2,24	a	2,86	0	1,97E+07	1,93E+06	9,80	be	2,99	0
	183	1,26E-03	4,72E-05	3,75	a	-2,10	0	2,06E+07	2,17E+06	10,57	bce	7,33	0
	1830	8,28E-04	2,75E-05	3,32	b	-35,51	---	1,40E+07	1,59E+06	11,39	f	-26,98	-
33	0	1,28E-03	2,54E-05	1,98	a	0,00	0	1,92E+07	1,82E+06	9,49	b	0,00	0
	0,183	1,23E-03	3,27E-05	2,65	a	-3,94	0	2,85E+07	4,28E+06	15,02	c	48,69	+

	1,83	1,26E-03	4,71E-06	0,37	a	-2,14	0	1,58E+07	2,89E+06	18,31	b	-17,68	0
	18,3	1,29E-03	1,43E-05	1,11	a	0,61	0	1,99E+07	4,27E+06	21,44	b	4,02	0
	183	1,24E-03	4,07E-05	3,28	a	-3,25	0	1,85E+07	2,23E+06	12,03	b	-3,23	0
	1830	8,19E-04	1,93E-05	2,36	d	-36,19	---	9,43E+06	1,87E+06	19,87	e	-50,79	---
34	0	1,28E-03	2,54E-05	1,98	a	0,00	0	1,92E+07	1,82E+06	9,49	bd	0,00	0
	0,183	1,26E-03	4,07E-05	3,24	a	-2,04	0	3,21E+07	3,89E+06	12,11	cd	67,46	+
	1,83	1,24E-03	2,69E-05	2,16	a	-3,05	0	1,90E+07	2,02E+06	10,64	bcd	-0,85	0
	18,3	1,29E-03	5,44E-05	4,22	a	0,56	0	1,92E+07	1,57E+06	8,15	bcd	0,24	0
	183	1,31E-03	2,61E-05	1,99	a	2,23	0	1,93E+07	2,81E+06	14,58	bcd	0,60	0
	1830	8,18E-04	2,53E-05	3,09	b	-36,31	---	1,39E+07	2,44E+06	17,56	bd	-27,57	-
35	0	1,28E-03	2,54E-05	1,98	ab	0,00	0	1,92E+07	1,82E+06	9,49	b	0,00	0
	0,183	1,29E-03	1,11E-05	0,87	abc	0,16	0	3,30E+07	5,29E+06	16,02	c	72,26	+
	1,83	1,31E-03	4,72E-05	3,61	abc	1,96	0	1,84E+07	1,46E+06	7,93	b	-3,76	0
	18,3	1,33E-03	1,47E-05	1,10	bc	3,53	0	1,78E+07	1,76E+06	9,88	b	-7,28	0
	183	1,30E-03	1,00E-05	0,77	abc	1,04	n.b.	1,68E+07	2,86E+06	16,98	b	-12,13	0
	1830	1,03E-03	1,76E-05	1,70	d	-19,39	-	2,23E+07	3,77E+06	16,90	d	16,50	0
36	0	1,28E-03	2,54E-05	1,98	a	0,00	0	1,92E+07	1,82E+06	9,49	b	0,00	0
	0,183	1,29E-03	3,40E-05	2,64	a	0,31	0	1,86E+07	3,49E+06	18,80	b	-3,07	0
	1,83	1,27E-03	3,51E-05	2,76	a	-0,89	0	1,94E+07	3,36E+06	17,34	b	1,04	0
	18,3	1,26E-03	5,95E-05	4,74	a	-2,16	0	1,98E+07	2,45E+06	12,33	b	3,58	0
	183	1,27E-03	1,87E-05	1,48	a	-1,39	0	2,10E+07	5,01E+06	23,91	b	9,41	0
	1830	9,54E-04	4,57E-05	4,79	b	-25,66	--	1,83E+07	1,94E+06	10,60	b	-4,37	0
37	0	1,28E-03	2,54E-05	1,98	ac	0,00	0	1,92E+07	1,82E+06	9,49	b	0,00	0
	0,183	1,27E-03	3,52E-05	2,77	abc	-0,89	0	2,09E+07	4,03E+06	19,24	b	9,15	0
	1,83	1,24E-03	3,65E-05	2,94	ab	-3,19	0	1,63E+07	2,14E+06	13,18	d	-15,16	0
	18,3	1,24E-03	2,74E-05	2,21	ab	-3,45	0	1,87E+07	2,03E+06	10,84	bd	-2,50	0
	183	1,33E-03	3,00E-05	2,25	ac	3,88	0	1,13E+07	3,81E+06	33,76	ae	-41,15	---
	1830	1,16E-03	3,19E-05	2,76	d	-9,88	0	7,03E+06	7,53E+05	10,70	ae	-63,30	---
38	0	1,28E-03	2,54E-05	1,98	a	0,00	0	1,92E+07	1,82E+06	9,49	bd	0,00	0

	0,183	1,31E-03	1,31E-04	9,96	a	2,28	0	3,79E+07	6,05E+06	15,95	c	98,02	+
	1,83	1,31E-03	1,40E-05	1,07	a	1,66	0	3,69E+07	4,08E+06	11,06	c	92,49	+
	18,3	1,31E-03	2,70E-05	2,05	a	2,24	0	3,54E+07	2,01E+06	5,68	c	84,50	+
	183	1,24E-03	3,32E-05	2,68	a	-3,39	0	2,11E+07	1,45E+06	6,88	bd	9,90	0
	1830	1,22E-03	3,40E-05	2,79	a	-4,98	0	4,30E+07	1,01E+07	23,51	c	124,16	+
39	0	1,28E-03	2,54E-05	1,98	ab	0,00	0	1,92E+07	1,82E+06	9,49	b	0,00	0
	0,183	1,32E-03	4,49E-05	3,41	ab	2,71	0	2,46E+07	1,71E+06	6,93	b	28,52	+
	1,83	1,28E-03	7,43E-05	5,82	ab	-0,56	0	2,36E+07	2,59E+06	10,98	b	23,00	+
	18,3	1,30E-03	3,17E-05	2,44	ab	1,27	0	1,35E+07	2,84E+06	21,08	b	-29,61	-
	183	1,24E-03	4,70E-05	3,78	a	-3,17	0	5,08E+07	5,26E+06	10,36	c	164,82	+
	1830	8,78E-04	2,41E-05	2,74	c	-31,64	- - -	5,43E+07	7,58E+06	13,97	c	183,29	+
40	0	1,28E-03	2,54E-05	1,98	a	0,00	0	1,92E+07	1,82E+06	9,49	bc	0,00	0
	0,183	1,29E-03	7,27E-05	5,64	a	0,30	0	1,39E+07	1,53E+06	11,00	abc	-27,34	-
	1,83	1,27E-03	5,23E-05	4,11	a	-0,88	0	1,64E+07	1,11E+06	6,80	bc	-14,39	0
	18,3	1,27E-03	3,63E-05	2,87	a	-1,26	0	1,83E+07	1,44E+06	7,84	bc	-4,30	0
	183	1,28E-03	6,25E-05	4,87	a	-0,16	0	1,62E+07	1,88E+06	11,59	bc	-15,26	0
	1830	1,25E-03	1,54E-05	1,23	a	-2,25	0	5,45E+07	9,96E+06	18,28	e	184,36	+
41	0	1,28E-03	2,54E-05	1,98	a	0,00	0	1,92E+07	1,82E+06	9,49	b	0,00	0
	0,183	1,26E-03	2,54E-05	2,03	a	-2,19	0	5,75E+07	3,24E+06	5,63	e	199,95	+
	1,83	1,28E-03	5,09E-05	3,96	a	0,08	0	1,93E+07	1,64E+06	8,48	bc	0,83	0
	18,3	1,29E-03	4,08E-05	3,16	a	0,64	0	1,14E+07	8,92E+05	7,81	bc	-40,43	- - -
	183	1,10E-03	1,97E-05	1,79	b	-14,41	-	3,02E+07	1,19E+06	3,95	d	57,49	+
	1830	9,98E-04	3,95E-05	3,96	c	-22,27	- -	2,64E+07	3,14E+06	11,89	d	37,76	+
42	0	1,28E-03	2,54E-05	1,98	a	0,00	0	1,92E+07	1,82E+06	9,49	bcd	0,00	0
	0,183	1,26E-03	4,54E-05	3,61	a	-2,19	0	2,87E+07	5,60E+06	19,53	bc	49,69	+
	1,83	1,25E-03	6,63E-05	5,30	a	-2,61	0	1,72E+07	1,86E+06	10,78	bd	-10,13	0
	18,3	1,16E-03	3,10E-05	2,68	b	-9,96	0	1,12E+07	1,38E+06	12,33	e	-41,80	- - -
	183	9,20E-04	5,21E-05	5,66	c	-28,33	- -	2,85E+07	3,12E+06	10,94	f	48,83	+
	1830	5,53E-04	1,58E-05	2,85	d	-56,93	- - -	5,72E+07	2,53E+06	4,42	h	198,51	+

43	0	1,28E-03	2,54E-05	1,98	a	0,00	0	1,92E+07	1,82E+06	9,49	b	0,00	0
	0,183	1,25E-03	5,90E-05	4,73	a	-2,75	0	3,90E+07	2,73E+06	7,00	c	103,54	+
	1,83	1,26E-03	3,38E-05	2,67	a	-1,49	0	1,88E+07	8,81E+05	4,69	b	-1,99	0
	18,3	1,32E-03	2,38E-05	1,81	a	2,61	0	1,45E+07	1,90E+06	13,07	d	-24,08	-
	183	1,13E-03	2,97E-05	2,63	b	-12,31	-	1,31E+07	2,36E+06	17,98	d	-31,43	--
	1830	7,41E-04	2,27E-05	3,06	de	-42,25	---	1,51E+07	1,64E+06	10,90	d	-21,25	-
44	0	1,28E-03	2,54E-05	1,98	ab	0,00	0	1,92E+07	1,82E+06	9,49	bdf	0,00	0
	0,183	1,23E-03	1,65E-05	1,34	abc	-4,03	0	2,87E+07	5,60E+06	19,53	c	49,69	+
	1,83	1,24E-03	1,93E-05	1,56	abc	-3,79	0	1,78E+07	2,36E+06	13,28	bd	-7,38	0
	18,3	1,21E-03	3,31E-05	2,74	bcd	-5,71	0	1,13E+07	1,68E+06	14,81	e	-40,87	---
	183	1,15E-03	4,22E-05	3,68	cd	-10,75	-	2,27E+07	1,68E+06	7,40	bf	18,70	0
	1830	1,08E-03	2,24E-05	2,07	d	-15,57	-	5,60E+07	6,49E+06	11,59	h	192,07	+
45	0	1,28E-03	2,54E-05	1,98	a	0,00	0	1,92E+07	1,82E+06	9,49	bd	0,00	0
	0,183	1,28E-03	4,46E-05	3,49	a	-0,38	0	2,67E+07	4,51E+06	16,91	cd	39,31	+
	1,83	1,29E-03	4,54E-05	3,51	a	0,55	0	2,00E+07	2,76E+06	13,78	bcd	4,48	0
	18,3	1,30E-03	2,32E-05	1,78	a	1,61	0	1,99E+07	3,30E+06	16,55	bd	4,03	0
	183	1,27E-03	2,71E-05	2,14	a	-1,19	0	1,95E+07	3,44E+06	17,61	bcd	1,86	0
	1830	1,03E-03	4,01E-05	3,89	b	-19,67	-	1,66E+07	3,32E+06	19,98	bd	-13,31	0

Appendix 1a. Planktonic growth and cells adhesion in the presence of each ZA related compound. Percentage reduction respect to the negative control is reported. a) Percentage reduction of the maximum specific growth rate: code (0) $x > -10\%$; code (-) $-10\% \leq x < -20\%$; code (--) $-20\% \leq x < -30\%$; code (---) $x \leq -30\%$; b) Percentage reduction of the number of adhered cells: code (+) $x > +20\%$; code (0) $+20\% \leq x < -20\%$; code (-) $-20\% \leq x < -30\%$; code (--) $-30\% \leq x < -40\%$; code (---) $x \leq -40\%$. According to post hoc analysis (Tukey's HSD, $p < 0.05$), data sharing the same letter indicates no significant difference.

APPENDIX 1b

Salicylic acid derivatives

Cmp	Conc. (µM)	Planktonic growth						Cells adhesion					
		Average (OD600/min)	St.dev (OD600/min)	err%	ANOVA	diff cont %	Level	Average (n°cell)	St.dev (n°cell)	err%	ANOVA	diff cont %	Level
SA	0	1,28E-03	2,54E-05	1,98	0,00	0	1,92E+07	1,82E+06	9,49	b	0,00	0	
	0,183	1,27E-03	4,56E-05	3,59	-1,08	0	1,37E+07	2,43E+06	17,79		-28,76	-	
	1,83	1,29E-03	6,33E-05	4,92	0,28	0	1,31E+07	2,56E+06	19,54		-31,57	--	
	18,3	1,32E-03	1,16E-05	0,88	2,75	0	1,02E+07	2,34E+06	23,02		-46,99	---	
	183	1,28E-03	4,16E-05	3,25	-0,18	0	6,24E+06	9,21E+05	14,75		-67,42	---	
	1830	7,19E-04	1,26E-05	1,75	-44,02	---	9,59E+06	1,54E+06	16,06		-49,97	---	
47	0	1,28E-03	2,54E-05	1,98	0,00	0	1,92E+07	1,82E+06	9,49	b	0,00	0	
	0,183	1,24E-03	3,30E-05	2,66	-3,37	0	2,21E+07	2,93E+06	13,22		15,57	0	
	1,83	1,27E-03	5,96E-05	4,68	-0,88	0	5,61E+06	6,43E+05	11,45		-70,71	---	
	18,3	1,30E-03	3,74E-05	2,87	1,32	0	5,28E+06	1,22E+06	23,09		-72,47	---	
	183	1,31E-03	7,41E-05	5,64	2,29	0	8,50E+06	4,65E+05	5,47		-55,63	---	
	1830	9,89E-04	1,27E-05	1,28	-22,93	--	1,51E+07	3,04E+06	20,16		-21,21	-	
48	0	1,28E-03	2,54E-05	1,98	0,00	0	1,92E+07	1,82E+06	9,49	b	0,00	0	
	0,183	1,28E-03	1,18E-04	9,19	-0,05	0	3,22E+07	3,87E+06	12,05		67,79	+	
	1,83	1,30E-03	7,41E-06	0,57	1,38	0	1,12E+07	1,18E+06	10,53		-41,31	---	
	18,3	1,28E-03	6,66E-05	5,18	0,00	0	1,12E+07	1,41E+06	12,59		-41,42	---	
	183	1,21E-03	2,43E-05	2,01	-5,66	0	1,17E+07	2,45E+06	20,99		-38,98	--	
	1830	1,05E-03	2,70E-05	2,56	-18,03	--	8,69E+06	1,53E+06	17,56		-54,65	---	






Appendix 1b. Planktonic growth and cells adhesion in the presence of each SA related compound. Percentage reduction respect to the negative control is reported. a) Percentage reduction of the maximum specific growth rate: code (0) $x > -10\%$; code (-) $-10\% \leq x < -20\%$; code (--) $-20\% \leq x < -30\%$; code (---) $x \leq -30\%$; b) Percentage reduction of the number of adhered cells: code (+) $x > +20\%$; code (0) $+20\% \leq x < -20\%$; code (-) $-20\% \leq x < -30\%$; code (--) $-30\% \leq x < -40\%$; code (---) $x \leq -40\%$. According to post hoc analysis (Tukey's HSD, $p < 0.05$), data sharing the same letter indicates no significant difference.

APPENDIX 2

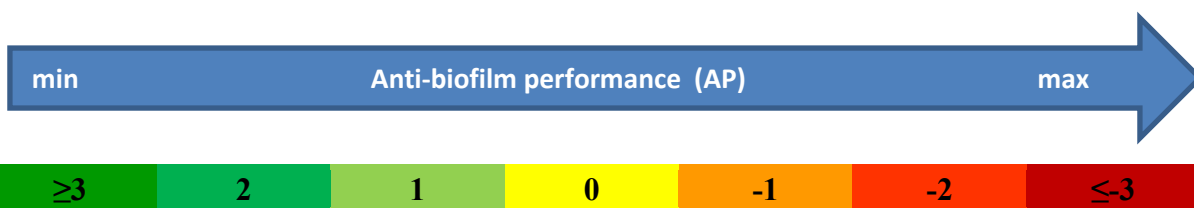
Cmp	0 μM	0.183 μM	1.83 μM	18.3 μM	183 μM	1830 μM	TREND
5	Yellow	Yellow	Yellow	Yellow	Yellow	Red	1
9	Yellow	Yellow	Yellow	Yellow	Yellow	Red	
19	Yellow	Yellow	Yellow	Yellow	Yellow	Green	
20	Yellow	Yellow	Yellow	Yellow	Yellow	Green	
36	Yellow	Yellow	Yellow	Yellow	Yellow	Green	
27	Yellow	Blue	Yellow	Yellow	Green	Green	2
29	Yellow	Blue	Yellow	Yellow	Yellow	Green	
35	Yellow	Blue	Yellow	Yellow	Yellow	Green	
45	Yellow	Blue	Yellow	Yellow	Yellow	Green	
31	Yellow	Blue	Yellow	Yellow	Yellow	Red	
32	Yellow	Blue	Yellow	Yellow	Yellow	Red	
33	Yellow	Blue	Yellow	Yellow	Yellow	Red	
34	Yellow	Blue	Yellow	Yellow	Yellow	Red	3
37	Yellow	Yellow	Yellow	Yellow	Orange	Orange	
11	Yellow	Yellow	Orange	Orange	Orange	Green	
16	Yellow	Yellow	Yellow	Orange	Yellow	Green	
22	Yellow	Yellow	Yellow	Orange	Yellow	Green	
26	Yellow	Yellow	Yellow	Orange	Orange	Green	
2	Yellow	Yellow	Orange	Orange	Orange	Red	
3	Yellow	Orange	Orange	Yellow	Red	Red	
4	Yellow	Orange	Orange	Green	Red	Red	
6	Yellow	Orange	Orange	Orange	Red	Red	
7	Yellow	Yellow	Orange	Orange	Red	Red	
8	Yellow	Orange	Orange	Yellow	Red	Red	
10	Yellow	Orange	Orange	Orange	Red	Red	
12	Yellow	Orange	Orange	Orange	Red	Red	
13	Yellow	Yellow	Orange	Red	Red	Red	
14	Yellow	Orange	Orange	Orange	Red	Red	
15	Yellow	Yellow	Yellow	Yellow	Orange	Red	
18	Yellow	Yellow	Yellow	Orange	Yellow	Red	
23	Yellow	Yellow	Yellow	Orange	Orange	Red	

25	no biological activity	anti-biofilm activity	biocidal effect			
28	no biological activity	anti-biofilm activity	biocidal effect			
SA	no biological activity	anti-biofilm activity	biocidal effect			
47	no biological activity	anti-biofilm activity	biocidal effect			
ZA	no biological activity	increased biofilm formation	anti-biofilm activity	4		
24	no biological activity	increased biofilm formation	anti-biofilm activity			
41	no biological activity	increased biofilm formation	no biological activity		transition from planktonic to biofilm mode of life	
42	no biological activity	increased biofilm formation	no biological activity		transition from planktonic to biofilm mode of life	
44	no biological activity	increased biofilm formation	no biological activity		transition from planktonic to biofilm mode of life	
17	no biological activity	increased biofilm formation	anti-biofilm activity		biocidal effect	
21	no biological activity	increased biofilm formation	anti-biofilm activity		no biological activity	biocidal effect
30	no biological activity	increased biofilm formation	no biological activity		transition from planktonic to biofilm mode of life	biocidal effect
43	no biological activity	increased biofilm formation	anti-biofilm activity		biocidal effect	biocidal effect
48	no biological activity	increased biofilm formation	anti-biofilm activity		biocidal effect	biocidal effect
38	no biological activity	increased biofilm formation	no biological activity	increased biofilm formation	5	
39	no biological activity	increased biofilm formation	anti-biofilm activity	increased biofilm formation		transition from planktonic to biofilm mode of life
40	no biological activity	anti-biofilm activity	no biological activity	increased biofilm formation		

Appendix 2. Biological activity of each ZA related compound at different concentrations.

	no biological activity
	anti-biofilm activity
	increased biofilm formation
	transition from planktonic to biofilm mode of life
	biocidal effect

APPENDIX 3



Cmpd	0 μ M	0.183 μ M	1.83 μ M	18.3 μ M	183 μ M	1830 μ M	AP
ZA	0	1	0	-1	-2	-3	-3
2	0	-1	-2	-3	-4	-5	-5
3	0	-2	-3	0	1	2	-3
4	0	-1	-2	1	0	-1	-2
5	0	0	0	0	0	0	0
6	0	-1	-2	-3	0	1	-3
7	0	0	-1	-2	-3	0	-6
8	0	-1	-2	-3	0	1	-3
9	0	0	0	0	0	0	0
10	0	-1	-2	-3	-4	0	-5
11	0	-1	-2	-3	-4	1	-8
12	0	-1	-2	-3	-4	0	-9
13	0	0	0	-1	-2	1	-2
14	0	-1	-2	-3	-4	1	-3
15	0	0	0	0	-1	0	-2
16	0	0	0	-1	0	1	0
17	0	1	0	-1	-2	-3	-3
18	0	0	0	-1	0	1	-2
19	0	0	0	0	0	2	3
20	0	0	0	0	0	1	1
21	0	-1	-2	-3	0	1	-1
22	0	0	0	-1	0	1	2
23	0	0	0	-1	-2	-3	-6
24	0	1	0	-1	-2	-3	-4
25	0	-1	-2	-3	-4	1	-2
26	0	0	0	-1	-2	2	1

27						5
28						-2
29						2
30						2
31						3
32						3
33						3
33						1
35						2
36						2
37						-6
38						4
39						6
40						0
41						3
42						5
43						1
44						1
45						2
SA						-9
47						-8
48						-8

Appendix 3. Anti-biofilm performance of each ZA related compound. Total and related to each concentration values are reported.

7. REFERENCES

- [1] J. W. Costerton. Introduction to biofilm. *International Journal of Antimicrobial Agents*. (1999) 11, 217–221.
- [2] L. Hall-Stoodley, J. W. Costerton and P. Stoodley. Bacterial biofilms: From the natural environment to infectious diseases. *Nature Reviews Microbiology*. (2004) 2, 95-108.
- [3] R. M. Donlan and J. W. Costerton. Biofilms: Survival Mechanisms of Clinically Relevant Microorganisms. *Clinical Microbiology Reviews*. (2002) 15(2), 167-193.
- [4] D. Davies. Understanding biofilm resistance to antibacterial agents. *Nat. Rev. Drug discovery*. (2003) 2, 114-122.
- [5] D. A. Rasko and V. Sperandio. Anti-virulence strategies to combat bacteria-mediated disease. *Nature Reviews Drug Discovery*. (2010) 9(2), 117-128.
- [6] F. Villa and F. Cappitelli. Plant-derived bioactive compounds at sub-lethal concentrations: towards smart biocide-free antibiofilm strategies. *Phytochem Rev*. (2013) 12, 245-254.
- [7] F. Villa, G. Borgonovo, F. Cappitelli, B. Giussani and A. Bassoli. Sub-lethal concentrations of *Muscari comosum* bulb extract suppress adhesion and induce detachment of sessile yeast cells. *Biofouling*. (2012) 28, 1107-1117.
- [8] D. J. Musk and P. J. Hergenrother. Chemical countermeasures for the control of bacterial biofilms: effective compounds and promising targets. *Curr. Med. Chem*. (2006) 13, 2163-2177.
- [9] I. Francolini and G. Donelli. Prevention and control of biofilm-based medical-device-related infections. *FEMS Immunology and Medical Microbiology*. (2010) 59, 227-238.
- [10] P. Stoodley, K. Sauer, D. G. Davies and J. W. Costerton. Biofilms as complex differentiated communities. *Annu. Rev. Microbiol*. (2002) 56, 187–209.
- [11] E. Karatan and P. Watnick. Signals, Regulatory Networks, and Materials That Build and Break
- [12] H. C. Flemming and J. Wingender. The biofilm matrix. *Nature Reviews Microbiology*. (2004) 2, 623-633.
- [13] H. C. Flemming, T. R. Neu and D. Wozniak. The EPS matrix: the house of biofilm cells. *J. Bacteriol*. (2007) 189, 7945–7947.
- Bacterial Biofilms. *Microbiology and Molecular Biology Reviews*. (2009) 310–347.

- [14] T. T. More, J. S. S. Yadav, S. Yan, R. D. Tyagi and R. Y. Surampalli. Extracellular polymeric substances of bacteria and their potential environmental applications. *Journal of Environmental Management*. (2014) 144, 1-25.
- [15] Y. Chen, H. J. Busscher, H. C. van der Mei and W. Norde. Statistical analysis of long- and short-range forces involved in bacterial adhesion to substratum surfaces as measured using atomic force microscopy. *Appl. Environ. Microbiol.* (2011) 77, 5065-5070.
- [16] J. Palmer, S. Flint and J. Brooks. Bacterial cell attachment, the beginning of a biofilm. *J Ind Microbiol Biotechnol.* (2007) 34(9), 577-88.
- [17] A. Svensson, A. Larsson, H. Emtenäs, M. Hedenström, T. Fex, S. J. Hultgren, J. S. Pinkner, F. Almqvist and J. Kihlberg. Design and evaluation of pilicides: potential novel antibacterial agents directed against uropathogenic *Escherichia coli*. *Chembiochem.* (2001) 2(12), 915-918.
- [18] W. M. Dunne. Bacterial Adhesion: Seen any Good Biofilms Lately? *Clin. Microbiol. Rev.* (2002) 15, 155–166.
- [19] G. Laverty, S. P. Gorman and B. F. Gilmore. Biomolecular mechanisms of staphylococcal biofilm formation. *Future Microbiol.* (2013) 8, 509-524.
- [20] E. Karatan and P. Watnick. Signals, Regulatory Networks, and Materials That Build and Break Bacterial Biofilms. *Microbiol Mol Biol Rev.* (2009) 73(2), 310-347.
- [21] B. R. Boles and A. R. Horswill. Agr-mediated dispersal of *Staphylococcus aureus* biofilms. *PLoS Pathog.* (2008) 4(4), 1-13.
- [22] D. W. Jackson, K. Suzuki, L. Oakford, J. W. Simecka, M. E. Hart and T. Romeo. Biofilm formation and dispersal under the influence of the global regulator CsrA of *Escherichia coli*. *J. Bacteriol.* (2002) 184, 290-301.
- [23] B. R. Boles, M. Thoendel and P. K. Singh. Rhamnolipids mediate detachment of *Pseudomonas aeruginosa* from biofilms. *Mol. Microbiol.* (2005) 57, 1210-1223.
- [24] J. Azeredo and I. W. Sutherland. The use of phages for the removal of infectious biofilms. *Curr. Pharm. Biotechnol.* (2008) 9, 261-266.
- [25] P. Landini, D. Antoniani, J. G. Burgess and R. Nijland. Molecular mechanisms of compounds affecting bacterial biofilm formation and dispersal. *Applied Microbiology and Biotechnology.* (2010) 86, 813-823.

- [26] S. R. Chhabra, B. Philipp, L. Eberl, M. Givskov, P. Williams and M. Camara. Extracellular communication in bacteria. In *Chemistry of Pheromones and Other Semiochemicals II* (Springer Berlin: Heidelberg, Germany). (2005) 240, 279-317.
- [27] W. R. J. D. Galloway, J. T. Hodgkinson, S. D. Bowden, M. Welch and D. R. Spring. Quorum Sensing in Gram-Negative Bacteria: Small-Molecule Modulation of AHL and AI-2 Quorum Sensing Pathways. *Chem. Rev.* (2011) 111, 28-67.
- [28] B. Michael, J. N. Smith, S. Swift, F. Heffron and B. M. Ahmer. SdiA of *Salmonella enterica* is a LuxR Homolog that Detects Mixed Microbial Communities. *J. Bacteriol.* (2001) 183, 5733-5742.
- [29] G. Laverty, S. P. Gorman and B. F. Gilmore. Biomolecular Mechanisms of *Pseudomonas aeruginosa* and *Escherichia coli* Biofilm Formation. *Pathogens.* (2014) 3(3), 596-632.
- [30] J. W. Costerton, L. Montanaro and C. R. Arciola. Bacterial communications in implant infections: a target for an intelligence war. *International Journal of Artificial Organs.* (2007) 30, 757-763.
- [31] B. Gray, P. Hall and H. Gresham. Targeting *agr*- and *agr*-like quorum sensing systems for development of common therapeutics to treat multiple Gram-positive bacterial infections. *Sensors.* (2013) 13, 5130-5166.
- [32] L. Cegelski, G. R. Marshall, G. R. Eldridge and S. J. Hultgren. The biology and future prospects of antivirulence therapies. *Nature Reviews Microbiology.* (2008) 6, 17-27.
- [33] M. Guo, S. Gamby, Y. Zheng and H.O. Sintim. Small molecule inhibitors of AI-2 signaling in bacteria: state-of-the-art and future perspectives for anti-quorum sensing agents. *International Journal of Molecular Sciences.* (2013) 14, 17694-17728.
- [34] D. I. Andersson and D. Hughes. Antibiotic resistance and its cost: is it possible to reverse resistance? *Nat Rev Microbiol.* (2010) 8, 260-271.
- [35] H. Nikaido. Multidrug resistance in bacteria. *Annu. Rev. Biochem.* (2009) 78, 119-146.
- [36] X. Z. Li and H. Nikaido. Efflux-mediated drug resistance in bacteria: an update. *Drugs.* (2009) 69, 1555–1623.
- [37] P.S. Stewart. Diffusion in biofilms. *Journal of Bacteriology.* (2003) 185, 1485-1491.
- [38] T. Bottcher, I. Kolodkin-Gal, R. Kolter, R. Losick and J. Clardy. Synthesis and activity of biomimetic biofilm disruptors. *Journal of the American Chemical Society.* (2013) 135, 2927-2930.

- [39] A. Davin-Regli, J. M. Bolla, C.E. James, J. P. Lavigne, J. Chevalier, E. Garnotel, A. Molitor and J.-M. Pagés. Membrane permeability and regulation of drug “influx and efflux” in enterobacterial pathogens. *Current Drug Targets*. (2008) 9, 750-759.
- [40] J. W. Costerton, B. Ellis, K. Lam, F. Johnson and A. Khoury. Mechanism of electrical enhancement of efficacy of antibiotics in killing biofilm bacteria. *Antimicrobial Agents and Chemotherapy*. (1994) 38, 2803-2809.
- [41] K. Lewis. Multidrug tolerance of biofilms and persister cells. *Current Topics in Microbiology and Immunology*. (2008) 322, 107-131.
- [42] S. Lee, A. Hinz, E. Bauerle, A. Angermeyer, K. Juhaszova, Y. Kaneko, P.K. Singh and C. Manoil. Targeting a bacterial stress response to enhance antibiotic action. *Proceedings of the National Academy of Sciences USA*. (2009) 106, 14570-14575.
- [43] F. Villa, S. Villa, A. Gelain and F. Cappitelli. Sub-lethal activity of small molecules from natural sources and their synthetic derivatives against biofilm forming nosocomial pathogens. *Current Topics in Medicinal Chemistry*. (2013) 13(24), 3184-3204.
- [44] R. J. Worthington, J. J. Richards and C. Melander. Small molecule control of bacterial biofilm. *Org. Biomol. Chem*. (2012) 10, 7457-7474.
- [45] N. Amara, R. Mashlach, D. Amar, P. Krief, S. A. H. Spieser, M. J. Bottomley, A. Aharoni and M. M. Meijler. Covalent Inhibition of Bacterial Quorum Sensing. *J. Am. Chem. Soc.* (2009) 131, 10610-10619.
- [46] G. D. Geske, R. J. Wezeman, A. P. Siegel and H. E. Blackwell. Small Molecule Inhibitors of Bacterial Quorum Sensing and Biofilm Formation. *J. Am. Chem. Soc.* (2005) 127, 12762-12763.
- [47] K. M. Smith, Y. G. Bu and H. Suga. Library Screening for Synthetic Agonists and Antagonists of a *Pseudomonas aeruginosa* Autoinducer. *Chem. Biol.* (2003) 10, 563-571.
- [48] F. G. Glansdorp, G. L. Thomas, J. J. Lee, J. M. Dutton, G. P. Salmond, M. Welch and D. R. Spring. Synthesis and stability of small molecule probes for *Pseudomonas aeruginosa* quorum sensing modulation. *Org. Biomol. Chem*. (2004) 2, 3329-3336.
- [49] C. E. McInnis and H. E. Blackwell. Thiolactone modulators of quorum sensing revealed through library design and screening. *Bioorg. Med. Chem.* (2011) 19, 4820–4828.

- [50] D. Ren, R. Zuo, A. F. Gonzalez, L. A. Bedzyk, G. R. Eldridge, M. E. Pasmore and T. K Wood. Differential gene expression for investigation of *Escherichia coli* biofilm inhibition by plant extract ursolic acid. *Appl. Environ. Microbiol.* (2005) 71, 4022-4034.
- [51] L. M. Junker and J. Clardy. High-throughput screens for small-molecule inhibitors of *Pseudomonas aeruginosa* biofilm development. *Antimicrob. Agents Chemother.* (2007), 51, 3582-3590.
- [52] L. Rasmussen, E. L. White, A. Pathak, J. C. Ayala, H. Wang, J. H. Wu, J. A. Benitez and A. J. Silva. A high-throughput screening assay for inhibitors of bacterial motility identifies a novel inhibitor of the Na⁺-driven flagellar motor and virulence gene expression in *Vibrio cholerae*. *Antimicrob Agents Chemother.* (2011) 55, 4134-4143.
- [53] Z. Zeng, L. Qian, L. Cao, H. Tan, Y. Huang, X. Xue, Y. Shen and S. Zhou. Virtual screening for novel quorum sensing inhibitors to eradicate biofilm formation of *Pseudomonas aeruginosa*. *Appl. Microbiol. Biotechnol.* (2008) 79, 119-126.
- [54] L. Yang, M. T. Rybtke, T. H. Jakobsen, M. Hentzer, T. Bjarnsholt, M. Givskov and T. Nielsen. Computer-aided identification of recognized drugs as *Pseudomonas aeruginosa* quorum-sensing inhibitors. *Antimicrob. Agents Chemother.* (2009) 53, 2432-2443.
- [55] K. C. Peach, W. M. Bray, N. J. Shikuma, N. C. Gassner, R. S. Lokey, F. H. Yildiz and R. G. Linnington. An image-based 384-well high-throughput screening method for the discovery of biofilm inhibitors in *Vibrio cholerae*. *Mol. BioSyst.* (2011) 7, 1176-1184.
- [56] C. L. Quave, M. Estevez-Carmona, C. M. Compadre, G. Hobby, H. Hendrickson, K. E. Beenken and M. S. Smeltzer. Ellagic acid derivatives from *Rubus ulmifolius* inhibit *Staphylococcus aureus* biofilm formation and improve response to antibiotics. *PLoS One* (2012) 7, e28737.
- [57] A. Vikram, G. K. Jayaprakasha, P. R. Jesudhasan, S. D. Pillai and B. S. Patil. Suppression of bacterial cell-cell signaling, biofilm formation and type III secretion system by citrus flavonoids. *J. Appl. Microbiol.* (2010) 109, 515-527.
- [58] F. Ali, P. L. Sangwan, S. Koul, A. Pandey, S. Bani, S. T. Abdullah, P. R. Sharma, S. Kitchlu and I. A. Khan. 4-epi-Pimaric acid: a phytomolecule as a potent antibacterial and anti-biofilm agent for oral cavity pathogens. *Eur. J. Clin. Microbiol. Infect. Dis.* (2012) 31, 149-159.

- [59] S. Chursi, P.N. Phatthalung and S.P. Voravuthikunchai. Anti-biofilm activity of *Quercus infectoria* G. Olivier against methicillin-resistant *Staphylococcus aureus*. *Lett. Appl. Microbiol.* (2012) 54, 511-517.
- [60] Y. Han, S. Hou, K. A. Simon, D. Ren and Y. Y. Luk. Identifying the important structural elements of brominated furanones for inhibiting biofilm formation by *Escherichia coli*. *Bioorg. Med. Chem. Lett.* (2008) 18, 1006-1010.
- [61] C. Kim, J. Kim, H. Y. Park, H. J. Park, J. H. Lee, C. K. Kim and J. Yoon. Furanone derivatives as quorum-sensing antagonists of *Pseudomonas aeruginosa*. *Appl. Microbiol. Biotechnol.* (2008) 80, 37-47.
- [62] B. K. Sharma-Kuinkel, E. E. Mann, J. Ahn, L. J. Kuechenmeister, P. M. Dunman and K. W. Bayles. The *Staphylococcus aureus* LytSR two-component regulatory system affects biofilm formation. *J. Bacteriol.* (2009) 191, 4767-4775.
- [63] R.W. Huigens, J. J. Richards, G. Parise, T. E. Ballard, W. Zeng, R. Deora and C. Melander. Inhibition of *Pseudomonas aeruginosa* biofilm formation with bromoageliferin analogues. *J. Am. Chem. Soc.* (2007) 129, 6966-6967.
- [64] J. J. Richards, R. W. Huigens, T. E. Ballard, A. Basso, J. Cavanagh and C. Melander. Inhibition and dispersion of proteobacterial biofilms. *Chem. Comm.* (2008) 14, 1698-1700.
- [65] S. A. Rogers, R.W. Huigens, J. Cavanagh and C. Melander. Synergistic effects between conventional antibiotics and 2-aminoimidazole-derived antibiofilm agents. *Antimicrob. Agents Chemother.* (2010) 54, 2112-2118.
- [66] E. A. Lindsey, R.J. Worthington, C. Alcaraz and C. Melander. 2-Aminopyrimidine as a novel scaffold for biofilm modulation. *Org. Biomol. Chem.* (2012) 10, 2552-2561.
- [67] T. Harder. Marine epibiosis: concepts, ecological consequences and host defence. In Hans-Curt Flemming, P. Sriyutha Murthy, R. Venkatesan, K. E. Cooksey (eds) *Marine and industrial biofouling* (Springer Series on Biofilms), edn. First, Springer, Berlin, (2008) 219-232.
- [68] S. Engel, P. R. Jensen and W. Fenical. Chemical ecology of marine microbial defense. *J Chem Ecol.* (2002) 28, 1971-1985.
- [69] F. Villa, D. Albanese, B. Giussani, P. S. Stewart, D. Daffonchio and F. Cappitelli. Hindering biofilm formation with zosteric acid. *Biofouling.* (2010) 26(6), 739-752.

- [70] F. Villa, B. Pitts, P. S. Stewart, B. Giussani, S. Roncoroni, D. Albanese, C. Giordano, M. Tunesi and F. Cappitelli. Efficacy of Zosteric Acid Sodium Salt on the Yeast Biofilm Model *Candida albicans*. *Microbial Ecology*. (2011) 62(3), 584-598.
- [71] F. Villa, W. Remelli, F. Forlani, A. Vitali and F. Cappitelli. Altered expression level of *Escherichia coli* proteins in response to treatment with the antifouling agent zosteric acid sodium salt. *Environmental Microbiology*. (2012) 14(7), 1753-1176.
- [72] M. S. Stanley, M. E. Callow, R. Perry, R. S. Alberte, R. Smith and J. A. Callow. Inhibition of fungal spore adhesion by zosteric acid as the basis for a novel, non-toxic crop protection technology. *Phytopathology*. (2002) 92, 378-383.
- [73] W. Szymanski, B. Wu, B. Weiner, S. de Wildeman, B. L. Feringa and D. B. Janssen. Phenylalanine aminomutase-catalyzed addition of ammonia to substituted cinnamic acids: a route to enantiopure alpha- and beta-amino acids. *J Org Chem*. (2009) 74(23), 9152-9157.
- [74] S. Ueda, T. Okada and H. Nagasawa. Oxindole synthesis by palladium-catalysed aromatic C-H alkenylation. *Chem Commun*. (2010) 46(14), 2462-2464.
- [75] P. De, Y. G. Koumba, P. Constant, F. Bedos-Belval, H. Duran, N. Saffon, M. Daffé and M. Baltas. Design, synthesis, and biological evaluation of new cinnamic derivatives as antituberculosis agents. *J Med Chem*. (2011) 54(5), 1449-1461.
- [76] P.J. Nowatzki, R.R. Koepsel, P. Stoodley, K. Min, A. Harper, H. Murata, J. Donfack, E.R. Hortelano, G.D. Ehrlich and A.J. Russell. Salicylic acid-releasing polyurethane acrylate polymers as anti-biofilm urological catheter coatings. *Acta Biomater*. (2012) 8(5), 1869-1880.
- [77] S. L. A. Andrade, E. V. Patridge, J. G. Ferry and O. Einsle. Crystal Structure of the NADH: Quinone Oxidoreductase WrbA from *Escherichia coli*. *Journal of Bacteriology*. (2007) 189, 9101-9107.
- [78] E. V. Patridge and J. G. Ferry. WrbA from *Escherichia coli* and *Archaeoglobus fulgidus* is an NAD(P)H: quinone oxidoreductase. *Journal of Bacteriology*. (2006) 188, 3498-3506.
- [79] M. A. Adams and Z. Jia. Structural and biochemical evidence for an enzymatic quinone redox cycle in *Escherichia coli*: identification of a novel quinol monooxygenase. *The Journal of Biological Chemistry*. (2005) 280, 8358-8363.
- [80] M. Čáp, L. se Váchová and Z. Palková. Reactive oxygen species in the signaling and adaptation of multicellular microbial communities. *Oxidative Medicine and Cellular Longevity*. (2012), ID 976753.

- [81] R. Grandori and J. Carey. Six new candidate members of the α/β twisted open-sheet family detected by sequence similarity to flavodoxin. *Protein Science*. (1994) 3, 2185-2193.
- [82] M. Hu, C. Zhang, Y. Mu, Q. Shen and Y. Feng. Indole Affects Biofilm Formation in Bacteria. *Indian journal of Microbiololy*. (2010) 50, 362-368.
- [83] G. Li and K. D. Young. Indole production by the tryptophanase TnaA in *Escherichia coli* is determined by the amount of exogenous tryptophan. *Microbiology*. (2013) 159, 402-410.
- [84] S. Lacour and P. Landini. σ S-Dependent gene expression at the onset of stationary phase in *Escherichia coli*: function of σ s-dependent genes and identification of their promoter sequences. *Journal of Bacteriology*. (2004) 186, 7186-7195.
- [85] A. Collet, S. Vilain, P. Cosette, G. A. Junter, T. Jouenne, R. S. Phillips and P. Di Martino. Protein expression in *Escherichia coli* S17-1 biofilms: impact of indole. *Antonie van Leeuwenhoek*. (2007) 91, 71-85.
- [86] A. Polo, P. Foladori, B. Ponti, R. Bettinetti, M. Gambino, F. Villa and F. Cappitelli. Evaluation of zosteric acid for mitigating biofilm formation of *Pseudomonas putida* isolated from a membrane bioreactor system International Journal of Molecular Sciences. (2014) 15, 9497-9518.
- [87] F. A. Saul, J.-P. Arié, B. Vulliez-le Normand, R. Kahn, J-M. Betton and Bentley G.A. Structural and functional studies of Fkpa from *Escherichia coli*, a *cis/trans* peptidyl-prolyl isomerase with chaperone activity. *Journal of Molecular Biology*. (2004) 335, 595-608.
- [88] B. R. Epperly and E. E. Dek. L-threonine dehydrogenase from *Escherichia coli*. Identification of an active site cysteine residue and metal ion studies. *The Journal of Biological Chemistry*. (1990) 266, 6086-6092.
- [89] S. N. Goh. Effects of different amino acids on biofilm growth, swimming motility and twitching motility in *Escherichia coli* BL21. *Journal of Biology and Life Science*. (2013) 4, 103-115.
- [90] E. J Calabrese and L. A. Baldwin. Applications of hormesis in toxicology, risk assessment, and chemotherapeutics. *Trends in Pharmacological Sciences* (2002) 23(7), 331-337.
- [91] L. Migliore, A. Rotini and M. C. Thaller. Low Doses of Tetracycline Trigger the *E. coli* Growth: A Case of Hormetic Response. *Dose Response*. (2013) 28(11), 550-7
- [92] M. Salta, A. J. Wharton, S. P. Dennington, P. Stoodley and K. R. Stokes. Anti-Biofilm Performance of Three Natural Products against Initial Bacterial Attachment. *Int. J. Mol. Sci.* (2013) 14, 21757-21780.

- [93] L. R. Hoffman, D. A. D'Argenio, M. J. MacCoss, Z. Zhang, R. A. Jones, S. I. Miller. Aminoglycoside antibiotics induce bacterial biofilm formation. *Nature*. (2005) 436, 1171–1175.
- [94] V. A. Plyuta, V. A. Lipasovaa, A. E. Kuznetsov and I. A. Khmela. Effect of salicylic, indole-3-acetic, gibberellic, and abscisic acids on biofilm formation by *Agrobacterium tumefaciens* C58 and *Pseudomonas aeruginosa* PAO1. *Applied Biochemistry and Microbiology*. (2013) 49, 706-710.
- [95] W. Zhang, P.K. Chu, J. Ji, Y. Zhang, R.K.Y. Fu and Q. Yan. Antibacterial properties of plasma-modified and triclosan or bronopol coated polyethylene. *Polymer*. (2006) 47, 931–936.
- [96] G. Subbiahdoss, R. Kuijter, D.W. Grijpma, H.C. van der Mei and H.J. Busscher. Microbial biofilm growth vs. tissue integration: "the race for the surface" experimentally studied. *Acta Biomater*. (2009) 5, 1399-1404.
- [97] A. B. Estrela, M.G. Heck and W.R. Abraham. Novel approaches to control biofilm infections. *Current Med. Chem*. (2009) 16, 1512-1530.
- [98] C. A. Barrios, Q. Xu, T. Cutright and B. Z. Newby. Incorporating zosteric acid into silicone coatings to achieve its slow release while reducing fresh water bacterial attachment. *Colloids Surf B*. (2005) 41, 83-93.
- [99] G. Lu, D. Wu and R. Fu. Studies on the synthesis and antibacterial activities of polymeric quaternary ammonium salts from dimethylaminoethyl methacrylate. *Reactive and Functional Polymers*. (2007) 67, 355–366.
- [100] J. M. Goddard and J. H. Hotchkiss. Polymer surface modification for the attachment of bioactive compounds. *Progress in Polymer Science*. (2007) 32(7), 698–725.
- [101] T. R. Hoare and D.S. Kohane. Hydrogels in drug delivery: Progress and challenges. *Polymer*. (2008) 49, 1993.
- [102] R. O. Darouiche. Prevention of infections associated with vascular catheters. *Int. J. Artif. Organs*. (2008) 31, 810–819.
- [103] P. Wu and D.W. Grainger. Drug/device combinations for local drug therapies and infection prophylaxis. *Biomaterials*. (2006) 27, 2450-2467.
- [104] G. D. Wright and A. D. Sutherland. New strategies for combating multidrug-resistant bacteria. *Trends Mol. Med*. (2007) 13, 260-267.
- [105] S. Minko. Grafting on Solid Surfaces: "Grafting to" and "Grafting from" Methods. *Polymer Surfaces and Interfaces*. (2008) 215-234.

- [106] K. Glinel, P. Thebault, V. Humblot, C.M. Pradier and T. Jouenne. Antibacterial surfaces developed from bio-inspired approaches. *Acta Biomaterialia*. (2012) 8, 1670–1684.
- [107] M. Charnley, M. Textor and C. Acikgoz. Designed polymer structures with antifouling-antimicrobial properties. *Reactive & Functional Polymers*. (2011) 71, 329-334.
- [108] K. Yoshimoto, M. Nishio, H. Sugawara and Y. Nagasaki. Direct observation of adsorption-induced inactivation of antibody fragments surrounded by mixed-PEG layer on a gold surface. *J. Am. Chem. Soc.* (2010) 132, 7982-7989.
- [109] J.-P. Maréchal and C. Hellio. Challenges for the development of new non-toxic antifouling solutions. *Int. J. Mol. Sci.* (2009) 10, 4623-4637.
- [110] A. Caro, V. Humblot, C. Me'thivier, M. Minier, M. Salmain and C. Pradier. Grafting of lysozyme and/or poly(ethylene glycol) to prevent biofilm growth on stainless steel surfaces. *J. Phys. Chem. B.* (2009) 113, 2101–2109.
- [111] R. Mendelsohn, J. W. Brauner and A. Gericke. External Infrared Reflection Absorption Spectrometry of Monolayer Films at the Air-Water Interface. *Annual Review of Physical Chemistry*. (1995) 46, 305-334.
- [112] R. G. Kraus, E. D. Emmons, J. S. Thompson and A. M. Covington. Infrared Absorption Spectroscopy of Polycarbonate at High Pressure. *Journal of Polymer Science: Part B: Polymer Physics*. (2008) 46(7), 734-742.
- [113] J. N. Anderl, M. J. Franklin and P. S. Stewart. Role of antibiotic penetration limitation in *Klebsiella pneumoniae* biofilm resistance to ampicillin and ciprofloxacin. *Antimicrob. Agents Chemother.* (2000) 44, 1818-1824.
- [114] E.R. Kenawy, S.D. Worley and R. Broughton. The chemistry and applications of antimicrobial polymers: a state-of-the-art review. *Biomacromolecules*. (2007) 8, 1359-1384.
- [115] A. M. Carmona-Ribeiro and L. Dias de Melo Carrasco. Cationic Antimicrobial Polymers and Their Assemblies. *Int. J. Mol. Sci.* (2013) 14(5), 9906-9946.
- [116] J.K. Baveja, M.D.P. Willcox, E.B.H. Hume, N. Kumar, R. Odell and L.A. Poole-Warren. Furanones as potential anti-bacterial coatings on biomaterials. (2004) 25, 5003-5012.
- [117] R. Kuehl, S. Al-Bataineh, O. Gordon, R. Luginbuehl, M. Otto, M. Textor and R. Landmann. Furanone at subinhibitory concentrations enhances staphylococcal biofilm formation by *luxS* repression. *Agents Chemother.* (2009) 53, 4159-4166.

- [118] F. Cappitelli and C. Sorlini. Microorganisms attack synthetic polymers in items representing our cultural heritage. *Appl. Environ. Microb.* (2008) 74, 564–569.
- [119] N. Maraschin. Polyethylene, Low Density. *Kirk-Othmer Encyclopedia of Chemical Technology.* (2005) 3-39.
- [120] M. Lehocky, H. Drnovska, B. Lapciková, A.M. Barros-Timmons, T. Trindade, M. Zembala and L. Jr. Lapcik. Plasma surface modification of polyethylene. *Colloids and Surfaces A: Physicochem. Eng. Aspects.* (2003) 222, 125-131.
- [121] T. Govindarajan and R. Shandas. A Survey of Surface Modification Techniques for Next-Generation Shape Memory Polymer Stent Devices. *Polymers.* (2014) 6, 2309-2331.
- [122] S. Yoshida, K. Hagiwara, T. Hasebe and A. Hotta. Surface modification of polymers by plasma treatments for the enhancement of biocompatibility and controlled drug release. *Surface & Coatings Technology.* (2013) 233, 99-107.
- [123] K. S. Siow, L. Britcher, S. Kumar and H. J. Griesser. Plasma Methods for the Generation of Chemically Reactive Surfaces for Biomolecule Immobilization and Cell Colonization - A Review. *Plasma Process. Polym.* (2006) 3, 392-418.
- [124] Y. Wei, X. Wang, J. Gao and Y. Chen. Plasma-Induced Graft Polymerization of Poly(ethylene glycol) on Poly(methyl methacrylate) Surfaces for Improving Antistatic Property. *Journal of Applied Polymer Science.* (2010) 118, 943-949.
- [125] S. Guruvenketa, G. M. RAO, M. Komath and A. M. Raichur. Plasma surface modification of polystyrene and polyethylene. *Applied Surface Science.* (2004) 236, 278-284.
- [126] J. G. A. Terlingen, H. F. C. Gerritsen, A. S. Hoffman and J. Feijen. Introduction of Functional Groups on Polyethylene Surfaces by a Carbon Dioxide Plasma Treatment. *Journal of Applied Polymer Science.* (1995) 57, 969-982.
- [127] E. F. C. Vidaurre, C. A. Achete, F. Gallo, D. Garcia, R. Simão and A. C. Habert. Surface Modification of Polymeric Materials by Plasma Treatment. *Materials Research.* (2002) 5(1), 37-41.
- [128] S. Zanini, E. Grimoldi and C. Riccardi. Development of controlled releasing surfaces by plasma deposited multilayers. *Materials Chemistry and Physics.* (2013) 138, 850-855.
- [129] S. Zanini, C. Riccardi, M. Orlandi, C. Colombo and F. Croccolo. Plasma-induced graft-polymerisation of ethylene glycol methacrylate phosphate on polyethylene films. *Polymer Degradation and Stability.* (2008) 93(6), 1158-1163.

- [130] S. Zanini, M. Orlandi, C. Colombo, E. Grimoldi and C. Riccardi. Plasma-induced graft-polymerization of polyethylene glycol acrylate on polypropylene substrates. *Eur. Phys. J. D.* (2009) 54, 159-164.
- [131] E. Vassallo, A. Cremona, F. Ghezzi and D. Ricci. Characterization by optical emission spectroscopy of an oxygen plasma used for improving PET wettability. *Vacuum.* (2010) 84(7), 902-906.
- [132] C. K. Cho, B. K. Kim, K. Cho, C. E. Park and J. Adhesion. Investigation of the surface rearrangement of poly(imide-siloxane) using dynamic contact angle measurements. *Sci. Technol.* (2000) 14, 1071-1083.
- [133] R. Rochotzki, M. Nitschke, M. Arzt and J. Meichsner. Plasma modification of polymer films studied by eLlipsometry and infrared spectroscopy. *Physica status soLidi (a).* (1994) 145, 289-29.
- [134] P. Braun and A. C. Gingras. History of protein-protein interactions: from egg-white to complex networks. *Proteomics.* (2012) 12, 1478-1498.
- [135] D. P. Ryan and J. M. Matthews. Protein-protein interactions in human disease. *Curr. Opin. Struct. Biol.* (2005) 15, 441.
- [136] E. Cukuroglu, H. B. Engin, A. Gursoy and O. Keskin. Hot spots in protein-protein interfaces: Towards drug discovery. *Progress in Biophysics and Molecular Biology.* (2014), 1-9.
- [137] A. A. Ivanov, F. R. Khuri and H. Fu. Targeting protein-protein interactions as an anticancer strategy. *Trends Pharmacol. Sci.* (2013) 34(7), 393-400.
- [138] K. Strebhardt and A. Ullrich. Targeting polo-like kinase 1 for cancer therapy. *Nat. Rev. Cancer.* (2006), 6, 321-330.
- [139] F. A. Barr, H. H. W. Silljé and E. A. Nigg. Polo-like kinases and the orchestration of cell division. *Nat. Rev. Mol. Cell Biol.* (2004) 5, 429-430.
- [140] K. S. Lee, T. Z. Grenfell, F. R. Yarm and R. L. Erikson. Mutation of the polo-box disrupts localization and mitotic functions of the mammalian polo kinase Plk. *Proc. Natl. Acad. Sci. USA.* (1998) 95, 9301-9306.
- [141] A. Hanisch, A. Wehner, E. A. Nigg and H. H. W. Silljé. Different Plk1 functions show distinct dependencies on polo-box domain-mediated targeting. *Mol. Biol. Cell.* (2006) 17, 448-459.

- [142] Y. S. Seong, K. Kamijo, J. S. Lee, E. Fernandez, R. Kuriyama, T. Miki and K. S. Lee. A spindle checkpoint arrest and a cytokinesis failure by the dominant-negative polo-box domain of Plk1 in U-2 OS cells. *J. Biol. Chem.* (2002) 277, 32282-33293.
- [143] B. Garcia-Alvarez, G. de Carcer, S. Ibanez, E. Bragado-Nilsson and G. Montoya. Molecular and structural basis of polo-like kinase 1 substrate recognition: Implications in centrosomal localization. *Proc. Natl. Acad. Sci. USA.* (2007) 104, 3107-3112.
- [144] K. Y. Cheng, E. D. Lowe, J. Sinclair, E. A. Nigg and L. N. Johnson. The crystal structure of the human polo-like kinase-1 polo box domain and its phospho-peptide complex. *Embo J.* (2003) 22, 5757-5768.
- [145] S. M. Yun, T. Moulaei, D. Lim, J. K. Bang, J-E. Park, S. R. Shenoy, F. Liu, Y. H. Kang, C. Liao, N-K. Soung, S. Lee, D-Y. Yoon, Y. Lim, D-H. Lee, A. Otaka, E. Appella, J. B. McMahon, M. C. Nicklaus, T. R. Burke, M. B. Yaffe, A. Wlodawer and K. S. Lee. Structural and functional analyses of minimal phosphopeptides targeting the polo-box domain of polo-like kinase 1. *Nat. Struct. Mol. Biol.* (2009) 16, 876-882.
- [146] P. Śledź, C. J. Stubbs, S. Lang, Y. Q. Yang, G. J. McKenzie, A. R. Venkitaraman, M. Hyvönen and C. Abell. From crystal packing to molecular recognition: prediction and discovery of a binding site on the surface of polo-like kinase 1. *Angew. Chem. Int. Ed.* (2011) 50, 4003-4006.
- [147] L. A. Wessjohann, E. Ruijter, D. Garcia-Rivera and W. Brandt. What can a chemist learn from nature's macrocycles? A brief, conceptual view. *Mol. Diversity.* (2005) 9, 171-186.
- [148] E. Marsault and M. L. Peterson. Macrocycles are great cycles: applications, opportunities, and challenges of synthetic macrocycles in drug discovery. *J. Med. Chem.* (2004) 54 (7), 1961-2004.
- [149] J. Mallinson and I. Collins. Macrocycles in new drug discovery. *Future Med. Chem.* (2012) 4 (11), 1409-1438.
- [150] W. R. J. D. Galloway and D. R. Spring. Towards drugging the 'undruggable': enhancing the scaffold diversity of synthetic small molecule screening collections using diversity-oriented synthesis. *Div. Orient. Synth.* (2013) 1, 21-28.
- [151] Maestro, version 9.3, Schrödinger, LLC, New York, NY, 2012.
- [152] Schrödinger Suite 2012 Protein Preparation Wizard; Epik version 2.3, Schrödinger, LLC, New York, NY, 2012.
- [153] Glide, version 5.8, Schrödinger, LLC, New York, NY, 2012.

- [154] LigPrep, version 2.5, Schrödinger, LLC, New York, NY, 2012.
- [155] ConfGen, version 2.3, Schrödinger, LLC, New York, NY, 2012.
- [156] C. Spyropoulos and C. G. Kokotos. One-pot synthesis of ureas from Boc-protected amines. *J. Org. Chem.* (2014) 79 (10), 4477-83.
- [157] T. Vojkovsky. Detection of secondary amines on solid phase. *Pept. Res.* (1995) 8, 236-237.
- [158] H. S. G. Beckmann, F. Nie, C. E. Hagerman, H. Johansson, Y. S. Tan, D. Wilcke and D. R. Spring. A New Strategy for the Diversity-Oriented Synthesis of Macrocyclic Scaffolds using Multi-Dimensional Coupling. *Nature Chem.* (2013) 5, 861-867.
- [159] C. J. Swain, R. Baker, C. Kneen, R. Herbert, J. Moseley, J. Saunders, E. M. Seward, G. I. Stevenson, M. Beer, J. Stanton, K. Watling and R. G. Ball. Novel 5-HT₃ Antagonists: Indol-3-ylspiro(azabicycloalkane-3,5(4H)-oxazoles. *J. Med. Chem.* (1992) 35, 1019-1031.